From Stars to Life

− Cold Organic Chemistry and Prebiotic Insights via Matrix Isolation –

Inauguraldissertation zur Erlangung des Doktorgrades der naturwissenschaftlichen Fachbereiche

im Fachgebiet Organische Chemie (Fachbereich 08)

der Justus-Liebig-Universität Gießen

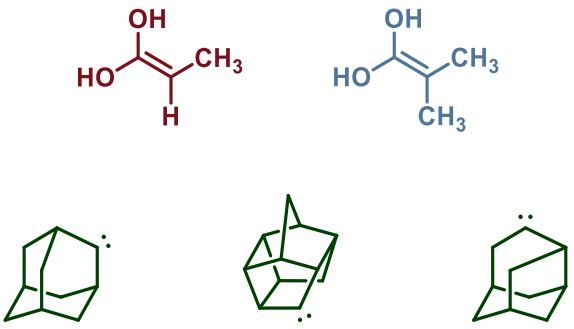

vorgelegt von

Akkad Danho

aus Pohlheim

angefertigt im Zeitraum von Februar 2022 bis März 2025

am Institut für Organische Chemie

der Justus-Liebig-Universität Gießen

Betreuer: Prof. Dr. Peter R. Schreiner, PhD

Eidesstattliche Erklärung

Hiermit versichere ich, die vorgelegte Dissertation selbständig und ohne unerlaubte fremde Hilfe und nur mit den Hilfen angefertigt zu haben, die ich in der Dissertation angegeben habe. Alle Textstellen, die wörtlich oder sinngemäß aus veröffentlichten Schriften entnommen sind, und alle Angaben, die auf mündlichen Auskünften beruhen, sind als solche kenntlich gemacht.

Bei den von mir durchgeführten und in der Dissertation erwähnten Untersuchungen habe ich die Grundsätze guter wissenschaftlicher Praxis, wie sie in der „Satzung der Justus-Liebig-Universität zur Sicherung guter wissenschaftlicher Praxis“ niedergelegt sind, eingehalten.

_____ _____

Ort, Datum Unterschrift

Dekan: Prof. Dr. Holger Zorn

Prodekan: Prof. Dr. Volker Wissemann

Studiendekan: Prof. Dr. Reinhard Dammann

Erstgutachter: Prof. Dr. Peter R. Schreiner, PhD

Zweitgutachter: Prof. Dr. Richard Göttlich

Zusammenfassung

Reaktive Intermediate sind kurzlebige, hochreaktive Moleküle, die an verschiedenen chemischen Prozessen beteiligt sind. Solche Zwischenstufen, wie Carbene und Enole, wurden unter anderem im interstellaren Raum nachgewiesen. Es wird vermutet, dass diese Verbindungen bei der Entstehung komplexer, biologisch relevanter Substanzen eine entscheidende Rolle spielen können. Um diese kurzlebigen Moleküle näher zu untersuchen, sind spezielle Methoden wie Matrixisolationsspektroskopie erforderlich, um Intermediate unter kryogenen Bedingungen zu stabilisieren und zu charakterisieren. Unter diesen Umständen beeinflussen Tunneleffekte den Ausgang einer Reaktion maßgeblich. Daher tritt neben der thermodynamischen und kinetischen Kontrolle das Prinzip der Tunnelkontrolle als drittes Prinzip der Reaktivität hervor.

In der ersten Veröffentlichung wurde erstmals Prop-1-en-1,1-diol in einer Matrix isoliert und mittels IR- und UV/Vis-Spektroskopie charakterisiert. Das Enol wird durch eine Hochvakuum-Pyrolyse ausgehend von Methylmalonsäure, erhalten. Unter UV-Bestrahlung wandelt sich das Enol in ein Isomer der Propionsäure sowie in Methylketen um. Sowohl Enol als auch Keten und Propionsäure wurden im interstellaren Medium nachgewiesen, wobei Letzteres eine grundlegende Komponente des biologischen Lebens darstellt.

2-Methylprop-1-en-1,1-diol wurde im Rahmen einer zweiten Publikation matrixisoliert und durch IR- und UV/Vis-Spektroskopie charakterisiert. Das Enol wurde ebenfalls durch eine Hochvakuum-Pyrolyse von Dimethylmalonsäure erhalten, wobei in diesem Fall auch Dimethylketen durch denselben Prozess generiert wurde. Dieses Enol weist ähnliche Reaktivität wie das zuvor isolierte Prop-1-en-1,1-diol auf und wandelt sich unter UV-Bestrahlung in Isobuttersäure um. Obwohl 2-Methylprop-1-en-1,1-diol bislang nicht im Weltraum nachgewiesen wurde, spielt die Isobuttersäure eine bedeutsame Rolle in biologischen Prozessen.

Eine dritte, bislang unveröffentlichte Studie beschäftigt sich mit der Tunnelkontrolle von Alkylcarbenen. Dabei wurde versucht, mithilfe von Wasserstoffisotopen den Ausgang zweier konkurrierender Tunnelreaktionen zu beeinflussen. Dazu wurden im Verlauf dieser Arbeit unterschiedliche Alkylcarbene auf ihre Tunnelreaktivität untersucht. Dabei wurde ein bis dato unbekanntes, unter kryogenen Bedingungen stabiles Alkylcarben, Pentacyclo[5.4.0.0^{2,6}.0^{3,10}.0^{5,9}]undecanyliden, in der Matrix isoliert und mittels IR- und UV/Vis-Spektroskopie charakterisiert. Es zeigt eine erhöhte kryogene Stabilität im Vergleich zum bereits bekannten Adamantyliden und wandelt sich erst unter Bestrahlung durch [1,2]-H-Migration zum Homohypostrophen um. Erst die Untersuchung des Protoadamantylidens, dessen Isolierung aufgrund zu kurzer Halbwertszeit nicht gelang, weist zwei konkurrierende Tunnelreaktionen auf. Sowohl das Produkt der [1,2]-H-Migration als auch das der C–H-Insertion wurden beobachtet. Anhand dieser Beobachtungen wurden Wasserstoffisotope gezielt zur Steuerung der Tunnelreaktion eingesetzt. Dieser Ansatz beeinflusste erfolgreich die Produktbildung und stellt den ersten experimentellen Nachweis für eine isotopenkontrollierte selektive Tunnelreaktion dar.

Abstract

Reactive intermediates are transient, highly reactive molecular species involved in chemical processes. It is proposed that such species might participate in the interstellar synthesis of complex molecules and in atmospheric processes. Enols and carbenes represent a class of reactive species capable of undergoing reactions under certain conditions to form prebiotic compounds. While these species have been detected in interstellar space, knowledge about their origin remains limited. Intermediates can be stabilized with the help of matrix isolation and other specialized techniques and characterized spectroscopically. Under cryogenic conditions, tunneling effects significantly impact the reactivity of molecules. In addition to the principles of thermodynamic and kinetic reaction control, tunneling control has emerged as a third fundamental paradigm of reactivity.

In the first publication, prop-1-en-1,1-diol was isolated in a matrix for the first time and characterized using IR and UV/Vis spectroscopy. The enol was obtained via high-vacuum flash pyrolysis starting from methylmalonic acid. Under UV irradiation, the enol is converted into an isomer of propionic acid as well as to methylketene. Enol, ketene, and propionic acid have previously been detected in the interstellar medium, with the latter representing a fundamental prebiotic molecule.

In a subsequent publication, 2-methylprop-1-en-1,1-diol was isolated in a matrix and identified by IR and UV/Vis spectroscopy. The enol was generated via high-vacuum flash pyrolysis of dimethylmalonic acid. In this process, dimethylketene formed as well. This enol demonstrates similar reactivity to the previously isolated prop-1-en-1,1-diol and tautomerizes to isobutyric acid under UV irradiation. Although 2-methylprop-1-en-1,1-diol has not yet been detected in space, isobutyric acid plays a significant role in biological processes.

A third, yet unpublished study dealt with quantum mechanical tunneling control of alkyl carbenes. The aim was to influence the outcome of competing tunneling reactions through the appropriate selection of alkyl carbene isotopologs with protium and deuterium. In the course of the study, various alkyl carbenes were examined for their tunneling reactivity. Among these, the previously unknown alkyl carbene pentacyclo[5.4.0.0^{2,6}.0^{3,10}.0^{5,9}]undecanylidene, was isolated and characterized. This carbene showed increased cryogenic stability compared to the known adamantylidene and only undergoes a [1,2]-H shift to homohypostrophene under irradiation. Only the study of protoadamantylidene, the isolation of which was unsuccessful due to its short half-life, revealed two competing tunneling reactions. Both the product of the [1,2]-H-shift and that of C–H insertion was observed. Based on these observations, hydrogen isotopes were selectively employed to control the tunneling reaction. This approach successfully influenced product formation, marking the first experimental evidence of an isotope-controlled tunneling reaction.

Meiner geliebten Familie in Hochachtung gewidmet.

Table of Contents

1. Introduction

1.1 Motivation and Goals

Since the beginning, humans have wondered how life originated. If life originated on Earth, one fundamental question remains: Where did the organic molecules that formed the first cell come from?[1] It is known that roughly 300 tons of organic matter are falling on Earth every year in the form of interplanetary dust.[2] In addition, large amounts of organic molecules were detected in carbonaceous meteorites[3] such as the Murchison and Murray meteorites[4-6] and in comets, for example, 67P/Churyumov-Gerasimenko, consisting of organic matter up to 45%.[7] The organic molecules found in space could have seeded primordial Earth and therefore delivered all necessary molecules for the first cell to form.[8-12] However, this does not explain how organic molecules are generated in interstellar space: In space, reactions occur under "extreme conditions" such as low temperatures (2.7 K) and at high dilution (1.46×10^{-18} Pa).[13] Reactions that occur at ambient temperatures in the laboratory may be infeasible in space. By understanding the formation and interaction of such reactions under interstellar conditions, we gain important insights into the processes that shaped the early chemical platforms of life.

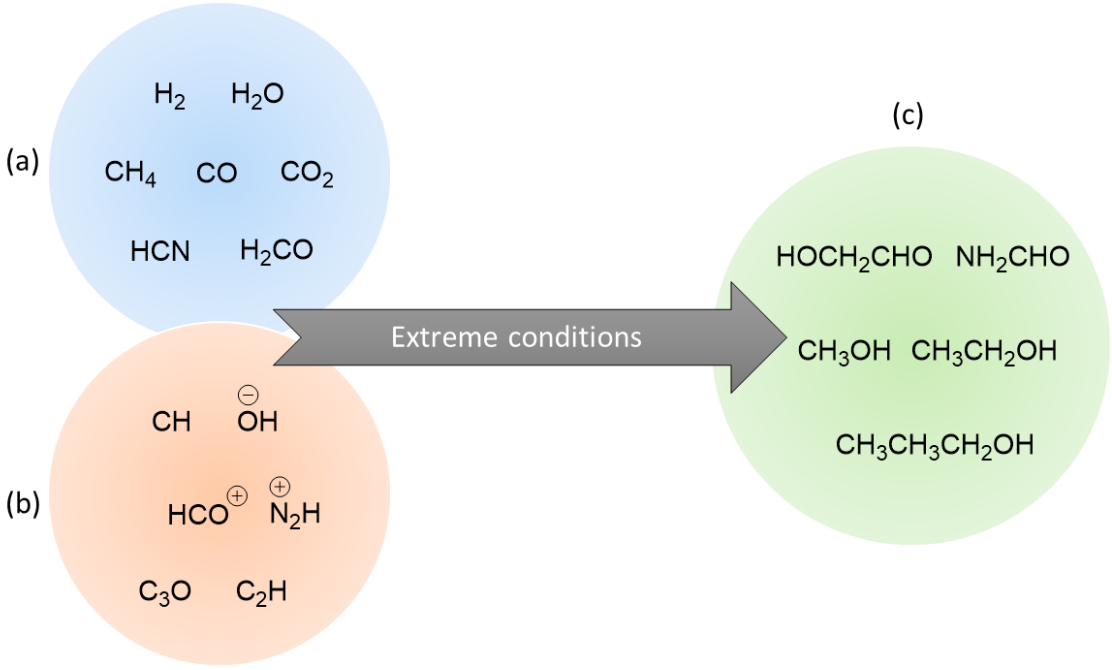

Figure 1: Examples of molecules detected in space.[14] a) Highly stable molecular building blocks. b) Highly reactive molecular building blocks. c) "Complex" organic molecules.

Complex organic molecules in interstellar space may form via small, highly reactive organic molecules. About 300 of these fleeting molecules (Figure 1b) have been detected in the interstellar medium,[1] where they remain intact due to the unique conditions of space. However, in regions such as interstellar clouds, organic reactions are thought to take place. It is argued that random energetic events such as gamma-ray bursts convert reactive intermediates into complex organic molecules (Figure 1c).[15] Despite their fleeting nature, these reactive intermediates play critical roles in biological,[16-18] atmospheric,[19-20] and combustion processes.[19, 21] Due to their reactivity, 99.9% of these reactive molecules have yet to be generated and characterized.[22]

By simulating the conditions of space, such as extremely low temperatures (2.7 K)[23] and low partial pressures (10^{-7} mbar), the matrix isolation technique is employed to capture and characterize these reactive intermediates. In a typical fashion, a volatile substance is co-deposited with an excess of an inert host gas, such as argon or nitrogen, onto a cold window (Figure 2). The captured molecule is then analyzed with IR and UV/Vis spectroscopy, requiring either a CsI (for IR) or a BaF_2 window (for UV/Vis). Depending on how the reactive species are generated *in situ*, either pyrolysis of a precursor molecule or photolysis following deposition is employed. This technique is used to investigate otherwise unobservable reactions, such as tunneling (*vide infra*).[24]

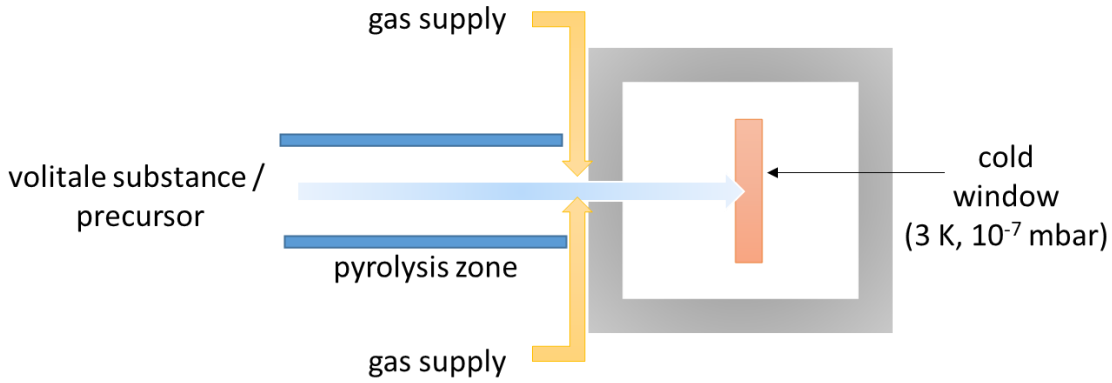

Figure 2: Schematic representation of the matrix isolation apparatus.

The subject of this work is the investigation of cryogenic organic reactions with cryo-spectroscopy in combination with density functional theory computations. The thesis is divided into two research topics: The first part deals with the potential formation of complex organic molecules, such as propionic acid, which has been confirmed to exist in space,[25] and isobutyric acid under space-like conditions. The publications suggest possible reaction pathways in which the corresponding enols can form the stable carboxylic acids. The second part investigates the formation and reactivity, mainly the tunneling behavior, of alkyl carbenes. Our strategy in this respect is to achieve controlled selective tunneling by implementing hydrogen isotopes as directing groups.

1.2 Enol Chemistry

Enols are intermediates including a carbon-carbon double bond (C=C) and at least one vinylic hydroxy group (–OH). Enols rapidly isomerize in solution to their thermodynamically more stable keto tautomer through a bimolecular acid-base reaction, as exemplified by 3-pentanone (**1**), which is more stable than its enol form **2** (Figure 3).[26]

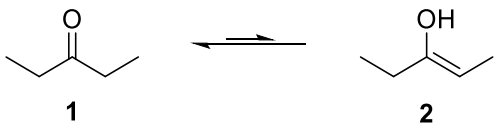

Figure 3: Keto-enol tautomerism of **1**.

Despite their highly reactive nature in solution, enols can be stabilized by changing their physicochemical properties, such as steric hindrance[27] or electronic effects,[28-29] including

resonance.[30] O'Neill and Hegarty were able to investigate enols of carboxylic acids by hydrating a range of ketenes to form their sterically hindered enols with the general formula of $Ar_2C=C(OH)_2$, (2,2-bis(2,4,6-trimethylphenyl)-1,1-ethenediol (**3**) or 1,1-ethenediol, 2,2-bis-(pentamethylphenyl) (**4**; Figure 4).[31-32] Building upon this work, Frey and Rappoport were able to generate stabilized enols of acids by the addition of water and dimethylamine to the corresponding ketenes.[33-34] Enols of carboxylic acids are more challenging to generate due to the high reactivity of the double bond and the two hydroxy groups. The authors achieved stabilization of these enols by introducing activated bulky groups, such as the Tip group, which shield the highly reactive double bond while providing additional reactive sites.[33] The authors were able to characterize these kinetically stabilized enols through NMR spectroscopy; two representative examples are **5** and **6** (Figure 4).

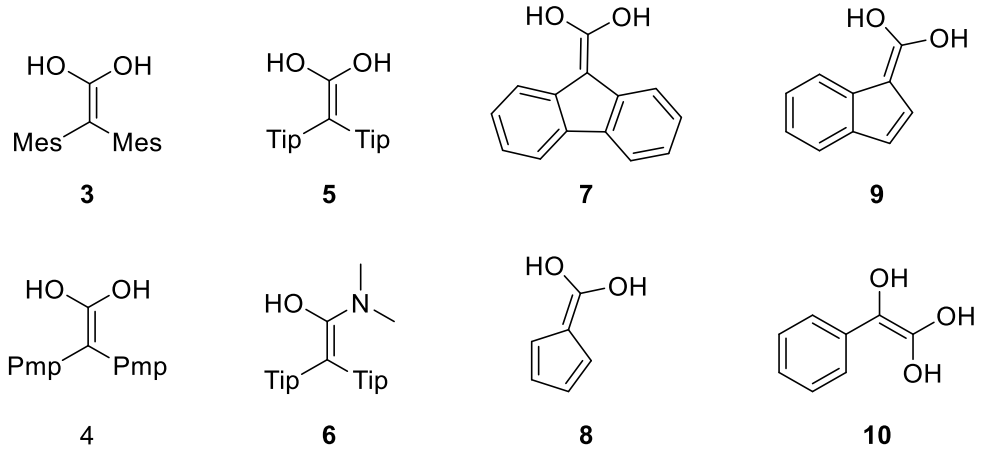

Figure 4: Examples of investigated semi-persistent (isolable) enols. (Mes = 1,3,5-trimethylbenzol, Pmp = 1,2,3,4,5-pentamethylphenyl, Tip = 2,4,6-triisopropylphenyl)

Other than changing chemical reactivity, analytical methods, such as time-resolved spectroscopy,[35-36] neutralization-reionization mass spectrometry,[37-38] NMR, IR spectroscopy,[39] and other methods[40] can be utilized for characterizing enols. Often, these methods are combined with computational chemistry to better understand structural and energetic properties.[41-44] For instance, time-resolved UV spectroscopy in combination with kinetic studies provided valuable insights into the reactivity of benzofulvene-8,8-diol (**7**),[45] fulvene-6,6-diol (**8**),[46] fluoren-9-carboxylic acid enol (**9**),[35] and 2-phenyl-1,1,2-ethenetriol (**10**) (Figure 4).[47]

Investigating simpler and smaller enols that lack steric protection remains more difficult and requires different approaches to stabilize them. Schauermann *et al*. used metal surfaces to stabilize the enol of acetophenone (**11**). By using a second acetophenone (**12**) equivalent, the authors achieved stabilization through intermolecular interactions, enabling them to investigate the formation of a keto-enol-dimer (Figure 5a).[48] Turecek *et al.* used a different approach, taking advantage of the higher stability of enols in the gas phase (*vide supra*). They were able to generate the enol of *γ*-butyrolactone (**13**) in the gas phase and characterized it using neutralization-reionization mass spectrometry (Figure 5b).[37]

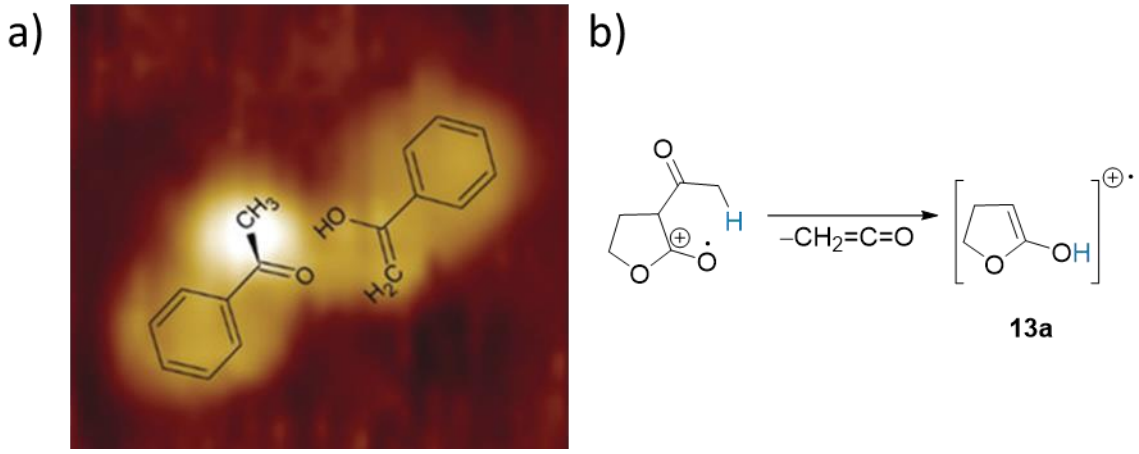

Figure 5: a) Investigation of a ketone-enol dimer by infrared reflection adsorption spectroscopy in combination with scanning tunneling microscopy. b) Generation of γ-butyrolactone radical cation (**13a**) by McLafferty rearrangement of a suitable precursor ion.

1.2.1 Enols as Potential Prebiotic Intermediates in Interstellar Space

While enols in solution are highly unstable and rapidly isomerize, they are significantly more stable in the gas phase.[49] This higher stability arises from the lack of bimolecular reactions in the gas phase and from substantial energy barriers, typically ranging from 40 to 45 kcal mol^{-1},[49-50] which hinder [1,3]H-shifts and prevent tautomerization.[37] This stability is also observed in space.[51] In 2001, ethenol was discovered in the interstellar cloud Sagittarius B2.[51] The enol was detected via microwave emissions. Furthermore, many enols were also identified in cold plasma discharges of alcohols.[52] These findings suggest that enols are abundant in the interstellar medium. Typically, they are generated through UV light and cosmic radiation of simpler molecules (Figure 1).[52] These observations may hint that enols play an important role in the chemistry of interstellar space by forming amino acids,[6] sugars,[53] and carboxylic acids,[54] which later were delivered to planets by celestial bodies.[9, 55-56]

For instance, simple amino acids could potentially have originated from amino enols. Like their hydroxy counterparts, enols of simple amides are highly unstable. These elusive molecules have the propensity to undergo fast interconversion to their more thermodynamically favorable amide isomer.[57] For example, 1-aminoethenol (**14**) is suggested as a key intermediate in the formation of acetamide (**15**),[58] which has been identified in many interstellar environments, such as Sagittarius B2 (Sgr B2)[59] and Orion KL,[60] as well as in comets[61] (*e.g.*, 67P/Churyumov–Gerasimenko).[7] In addition, it has been suggested that **15** could give rise to dipeptides (Figure 6) or larger peptides.[60] Despite their relevance for prebiotic chemistry, no direct spectroscopic evidence of **14** or other enols of amides has been presented,[62] and only a few indirect pieces of evidence are known.[63-67]

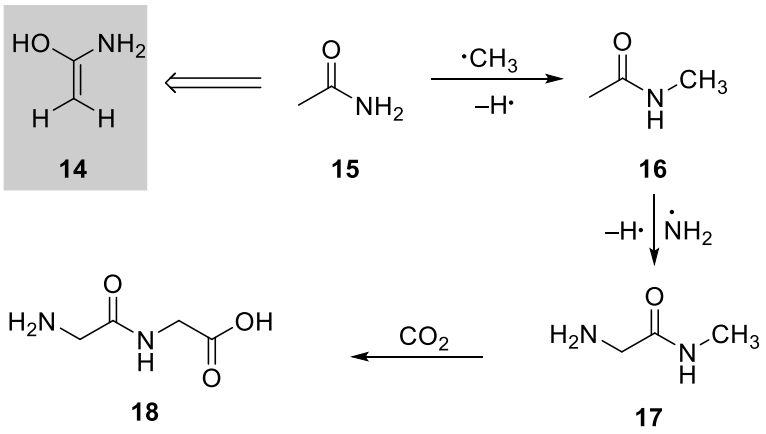

Figure 6: Possible pathway for the generation of small dipeptides with **15**. The first two steps involve neutral-neutral radical reactions, generating methylacetamide (**16**) and then methylglycinamide (**17**), with rates of 10^{-11} cm^3 s^{-1}.[68] The third step could proceed on meteorite surfaces and generate *N*-[2-(methylamino)-2-oxoethyl]carbamic acid (**18**).[60]

The enol tautomer of glycolaldehyde (**19**) could be part of the formation of carbohydrates, such as pentoses, under prebiotic conditions on primordial Earth (Figure 7).[69] Besides, **19** is the simplest sugar that has been detected in interstellar space.[70] 1,2-Ethendiol (**20**) could also be an intermediate for the formose reaction,[71] in which formaldehyde (**21**) is converted into sugars in aqueous environments, catalyzed by organic bases or minerals.[72] In 1959, Breslow suggested a series of base-catalyzed aldol reactions, with **19** acting as an autocatalyst. However, the uncatalyzed formation of **19** from formaldehyde remained unclear until 2018,[73] when it was shown to occur through a nearly barrierless carbonyl-ene reaction involving nucleophilic hydroxymethylene (**22**) (Figure 7).[74]

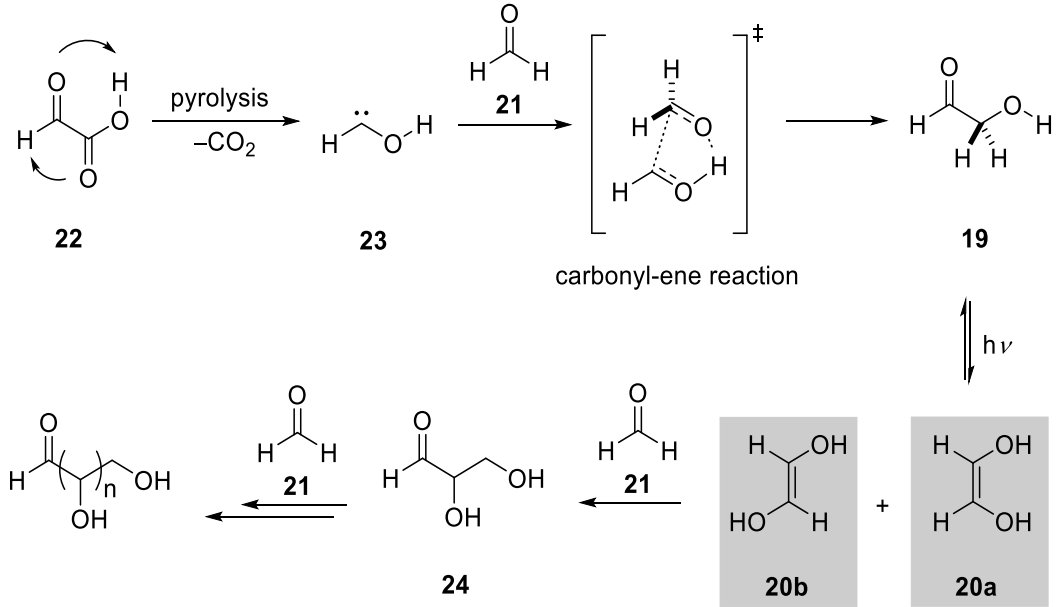

Figure 7: Gas-phase sugar formation through carbonyl-ene reaction. Decarboxylation of glyoxylic acid (**22**) forms hydroxycarbene (**23**), which undergoes a facile carbonyl-ene reaction with formaldehyde to form **19**. Photolysis generates **20a** and **20b**, which can react with formaldehyde to form glyceraldehyde (**24**) and even larger carbohydrates.

The reaction progresses through rapid enolization processes that facilitate aldol additions with formaldehyde, generating a variety of aldoses and ketoses. This makes the enols of **19**, *trans*- and especially *cis*-1,2-ethendiol (**20a** and **20b**), with the former having been detected in space,[75] important prebiotic intermediates for the formation of three- to five-carbon sugars.[69, 76,77]

Moreover, enols with additional hydroxy groups such as 1,1,2-ethentriol (**25**), could serve as intermediates for the formation of glycolic (**26**) and glyceric acid (**27**). These two compounds could potentially serve as a precursor for lipids.[78] Both are also involved in glycolysis and play a fundamental role in biochemical processes.[78] Despite **26** having been detected in meteorites such as Murchison and Bell,[79-81] its origin remains unknown.

1.2.2 Matrix Isolation Studies on Enols

Since enols are highly unstable entities, special methods such as matrix isolation are used to capture and characterize them. Notably, two research groups are investigating these small reactive intermediates, with the methods of enol generation differing significantly. The Kaiser group attempts to mimic meteorite surfaces. Typically, enriched ices are used, which are later bombarded with high-energy beams comparable to gamma-ray bursts[82] or other highly energetic phenomena in interstellar space. By using carbon dioxide (**28**) and methane-based ice (**29**) and subjecting it to high radiation, Kaiser *et al*. were able to generate 1,1-ethendiol (**30**) (Figure 8).[83-84] Changing the composition of the ice to acetone (**31**) or methanol (**32**) and treating it with high-energy radiation produced propen-2-ol (**33**) (as well as its isomer, methyl vinyl ether **34**) and **20**.[77, 85]

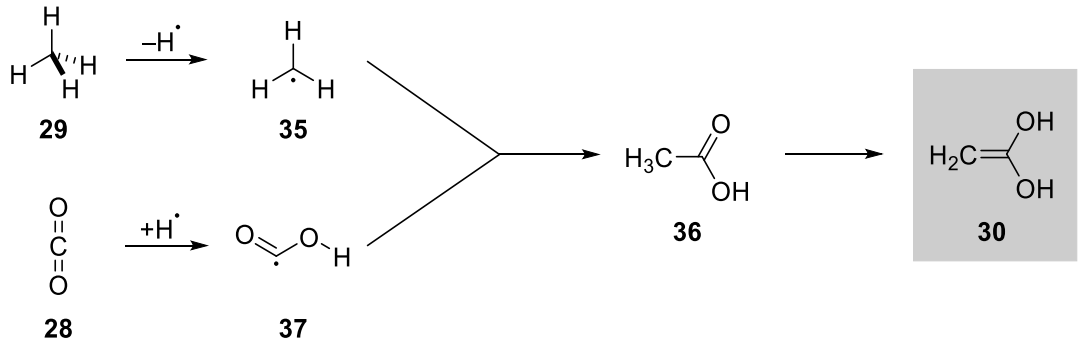

Figure 8: High-energy irradiation of methane- and carbon dioxide-based ice results in the bottom-up generation of **30**.

During sublimation of the ices, the reactive intermediates were detected, using tunable vacuum ultraviolet photoionization and reflectron time-of-flight mass spectrometry. The experiments were often conducted in conjunction with isotope labeling and isomer-selective photoionization.[86] Computational analysis reveals that the presence of water molecules, which are expected on interstellar grains, can reduce the energy barrier for keto-enol tautomerization by fifty percent. The authors demonstrated that these reactive intermediates remain intact on ice-coated nanoparticles, which are also found in molecular clouds and suggest that they persist after sublimation into the gas phase in star-forming regions, thus further exemplifying the role of these enols in interstellar chemistry.[87]

Other methods to generate enols involve the fragmentation of more complex precursors. In 1976, Saito was able to generate ethenol (**38**) by decarbonylation (pyrolysis) of ethylene glycol (**39**) (Figure 9).[40] It was not until this time that a conjugated enol had ever been produced, and few subsequent studies were conducted. The desired enol was successfully generated and confirmed using microwave spectroscopy in conjunction with isotopic labeling. However, this method produced many side products, and the outcome depended on the temperature used. At lower temperatures, the number of side products increased.

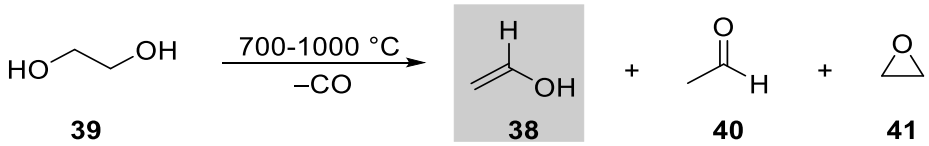

Figure 9: Generation of **38** by decarbonylation of **39**. At low temperatures, acetaldehyde (**40**) and ethylene oxide (**41**) predominantly form.

Dicarboxylic acids are more suitable as precursor molecules since their fragmentation can occur under milder conditions and only produces a CO_2. Mardyukov *et al*. were able to generate and characterize a variety of enols by fragmentation of different precursor molecules: They generated **30** by pyrolysis (decarboxylation) of malonic acid (**42**) at 400 °C and captured the enol **30** in an argon matrix (Figure 10).

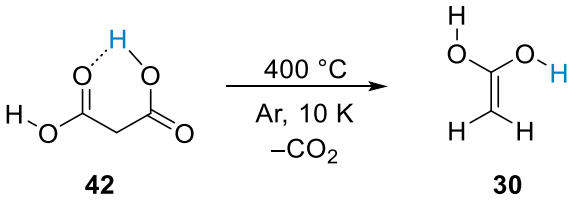

Figure 10: Generation of **30** from **42** and subsequent trapping in an argon matrix at 10 K.

By implementing the same strategy and choosing the right precursor molecule, they were able to generate **14**[57] and **25**.[88] Structures **20a** and **20b**[89] were not generated by decarboxylation, but rather by a retro-Diels-Alder reaction. The pyrolysis of *endo*,*cis*-bicyclo[2.2.1]hept-5-ene-2,3-diol (**43**) at 700 °C resulted in a retro-Diels–Alder reaction, which produced cyclopentadiene (**44**) and **20a**. By pyrolysis of *trans*-9,10-dihydro-9,10-ethanoanthracene-11,12-diol (**45**), anthracene (**46**) and **20b** formed (Figure 11).

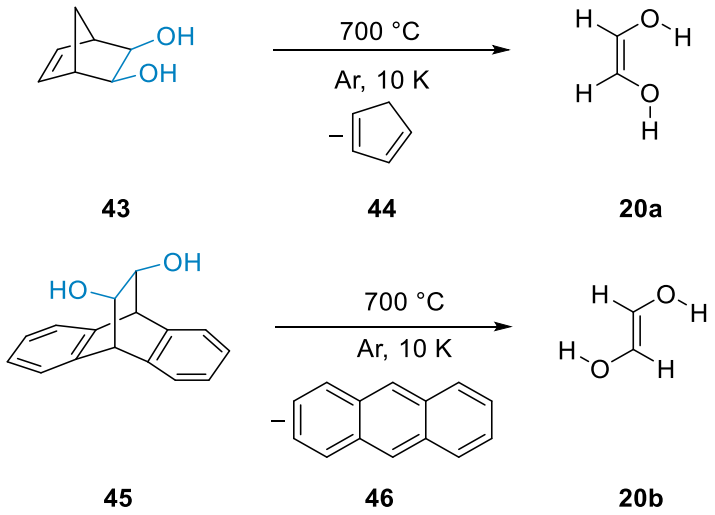

Figure 11: Generation of **20a** and **20b** from **43** and **45** and capturing all formed products in an argon matrix at 10 K.

Measuring IR spectra of the trapped molecules indicated the formation of enols and side products such as CO_2 and H_2O. Most enols show similar vibrational bands, with the C=C stretching vibration being the most common and characteristic. This vibration mode appears around 1700 cm^{-1}.[90] Attaching an amino group red-shifts the vibrational band to 1682 cm^{-1}, in comparison to a hydroxy group.[57] Conversely, attaching a third hydroxy group increases the C=C stretching vibration to 1761 cm^{-1}.[88] The IR assignments were confirmed by computed IR signals at the AE-CCSD(T)/cc-pVTZ level of theory.[90] These assignments were also confirmed by isotopic labeling experiments. For example, the deuterated 1-aminoethenol showed a significant redshift; for the C=C stretching vibration, the shift was –51 cm^{-1} (computed –59 cm^{-1}).[57]

The successful generation of **14**,[57] **30**,[88] **20a** and **20b**[89] was confirmed by UV/Vis spectra, which aligned well with the computed values. The UV/Vis spectra show a strong absorption maximum at 190 nm, which corresponds to a π-π* transition and correlates to a HOMO–LUMO+4 excitation.[90] Only **14** shows an absorption of 212 nm due to its less electron-poor character.[57] Comparing the reactivity of **14** with **30** reveals that substitution of one OH group with an NH_2 group destabilizes the HOMO, resulting in a smaller HOMO-LUMO gap in **14** (0.195 eV) compared to **30** (0.207 eV). This makes **14** more nucleophilic and prone to oxidation.[57]

By comparing the energies of the different $C_2H_4O_2$ isomers, computations at the AE-CCSD(T)/cc-pVTZ level of theory show that **20a** and **20b** are 8.6 and 12.4 kcal mol^{-1} higher than **30**[89]: Changing the position of the OH-group also changes the HOMO-LUMO gap by increasing the HOMO-energy, making **20a** and **20b** more nucleophilic than their isomeric counterpart **30**.[90]

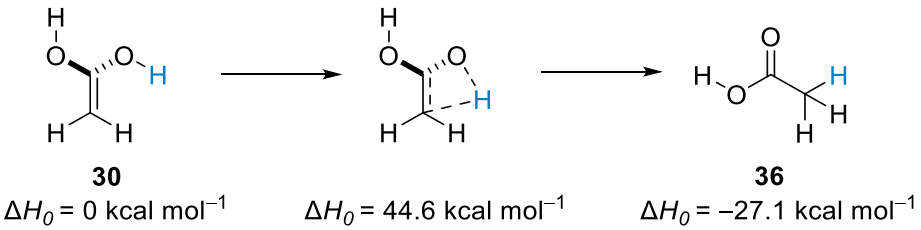

Figure 12: Formation of **36** from **30** through a [1,3]H-shift.[90]

Photolysis experiments resulted in the production of a carboxylic acid through a [1,3]H-shift (Figure 12). Both pathways were confirmed by computations at the AE-CCSD(T)/ccpVTZ level of theory. Quantum mechanical hydrogen tunneling from the enol to the carboxylic acid was not observed, since the enol remained unchanged over the course of several days. This was further corroborated by a computed barrier of 40-50 kcal mol^{-1}. Interestingly, in studies that investigated enols with additional hydroxy groups, the formation of a ketene + water complex was observed. For example, the decarboxylation of malonic acid forms not only **30** but also ketene **47** by water elimination. Ketene was identified by a strong band at 2138 cm^{-1}. This identification was further confirmed by a significant redshift in the deuterated isotopolog and comparison to the calculated IR spectra. These findings could indicate a potential pathway to the formation of the enol in interstellar space by surface-catalyzed hydration of ketene on ice grains.[91-92] Additionally, **47** has been observed in space in large quantities.[93]

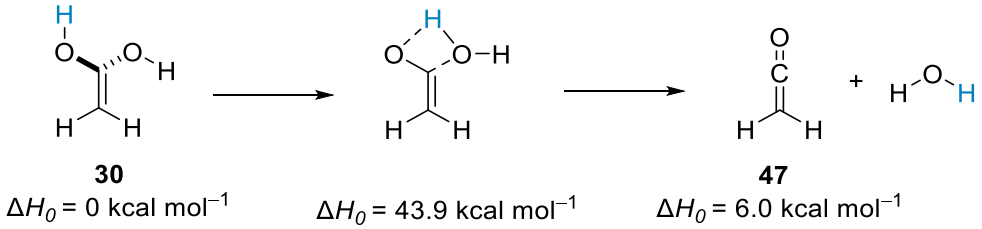

Figure 13: Formation of **47** from **30** through water elimination.[90]

In this thesis, we investigated the enol tautomer of propionic acid (**48**)[94] and isobutyric acid (**49**).[95] The goal of this study was providing spectroscopic data, which are needed for the detection of these molecules in space via radio astronomy, and for studying the reactivity of the enols. Similar to the approaches of Mardyukov *et al.*, we synthesized the enediol by pyrolysis of methylmalonic acid (**50**) at 500 °C or dimethylmalonic acid (**51**) at 750 °C and captured all generated products in an argon matrix at 3.5 K (Figure 14).

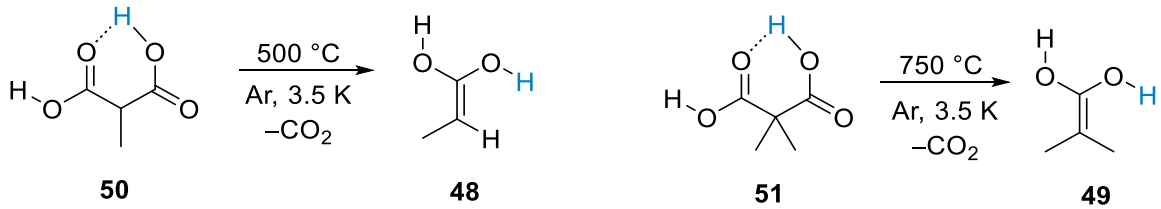

Figure 14: Generation of prop-1-ene-1,1-diol (**48**) from methylmalonic acid (**50**) and generation of 2-methyl-prop-1-ene-1,1-diol (**49**) from dimethylmalonic acid (**51**).

Spectroscopic studies revealed characteristic bands that can be attributed to the enols and were confirmed by computational studies at the B3LYP/def2-TZVP level of theory. Furthermore, isotope labeling validated the generation of the enols by displaying characteristic shifts. Both UV/Vis spectra showed absorption maxima at 190 nm, assigned to a $\pi \rightarrow \pi^*$ transition, similar to the other characterized enols.[57, 88-90]

Interestingly, methylketene (**52**) was also generated by pyrolysis of **50**. Compound **52** could also be a key intermediate for prebiotic chemistry as it has been identified in interstellar space[96] and can be converted back to its enol form (+35.5 kcal mol^{-1}). In contrast, dimethylketene (**53**) is only generated after irradiation with 254 nm. Moreover, irradiation experiments show the formation of the carboxylic acids through a [1,3]H-shift via a transition state of 41.9 kcal mol^{-1} for propionic acid (**54**) and 51.3 kcal mol^{-1} for isobutyric acid (**55**).

Furthermore, we reported the formation of propene (**56**), which is likely to occur via a photochemical mechanism of the **53**. This mechanism may involve either a concerted [1,2]H-shift (TS1) or the conversion of the **53** into a singlet carbene (**57**), which then releases CO upon photoexcitation. Subsequently, **57** undergoes a [1,2]H-shift (TS2), resulting in the formation of **56**. Given the small half-life of **57**, it is not possible to distinguish between the two pathways (Figure 15).

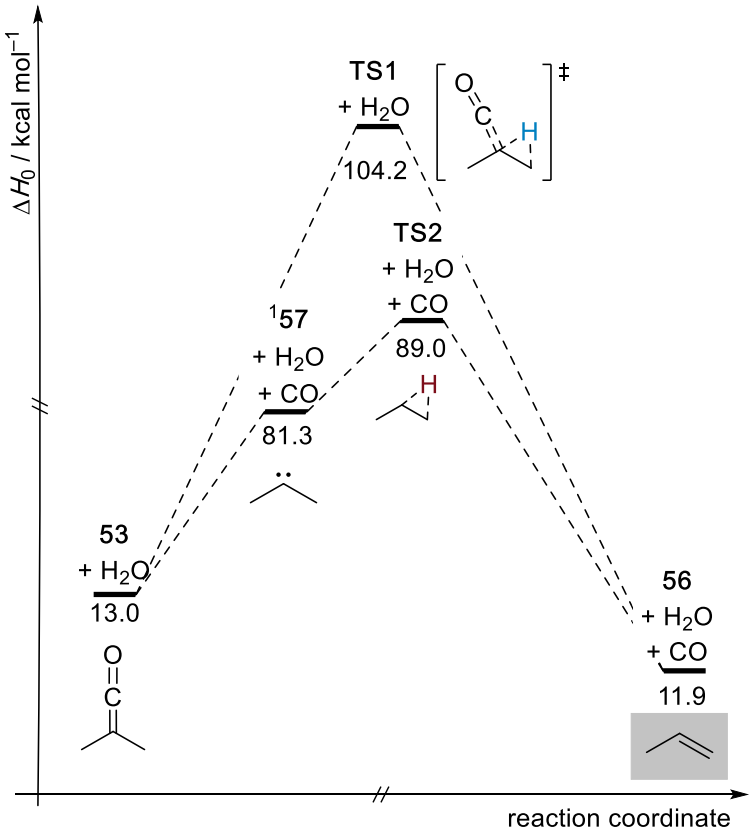

Figure 15: Potential energy profile (ΔH_0) in kcal mol^{-1} of the reactions of **53** at DLPNO-CCSD(T)/cc-pVQZ//B3LYP/def2-TZVP+ZPVE at 0 K.

The attempt to detect singlet alkyl carbene **57** was unsuccessful. Carbenes are highly reactive intermediates (see 1.3), and they may contribute to the formation of complex organic molecules in interstellar environments similar to enols. This includes molecules

crucial for the origins of life, such as amino acids,[97] nucleobases,[98] and sugars (*vide supra*).[97] The following part focuses on explaining the reactivity of these molecules, with particular emphasis on singlet alkyl carbenes and their unique tunneling reactivity.

1.3 Carbene Chemistry

Carbenes are defined by a carbon atom with a formal valence of two with six electrons. This deviation from the octet rule makes this reactive intermediate amphiphilic. The two unpaired valence electrons on the carbon can exist in four states. Either they exist in three spin-paired (singlet state, $S = 0$, $\sigma^1 p_\pi^1$, p_π^2, σ^2) or in one spin unpaired (triplet state, $S = 1$, $\sigma^1 p_\pi^1$) configurations. Depending on their electronic structure, the states show different behavior. Typically singlet carbenes have a bond angle of <120°, which is comparable to typical sp^2-hybridization and is caused by the significant orbital overlap, whereas triplet carbenes show bond angles greater than 120°. Triplet carbenes can be considered as diradicals.[99]

Carbenes can be stabilized by incorporating either electron-donating (EDG) or electron-withdrawing (EWG) groups at the electron-deficient carbene center (Figure 16). Three different types of stabilization are possible: (a) pull-pull stabilization with two EWG **58**,[100-101] (b) push-pull or captodative stabilization,[102] where one substituent donates and the other withdraws electrons, exemplified by **59a-c**[103-105] and (c) push-push stabilization with two EDG **60**.[100, 106-107] Stabilization can be enhanced by heteroatoms with a π-donating lone pair, such as nitrogen, attached to the carbon center **61**, **64**, and **65**. This can favor a singlet ground state by p-p_π interaction between the lone pair and the empty p_π orbital of the carbene.

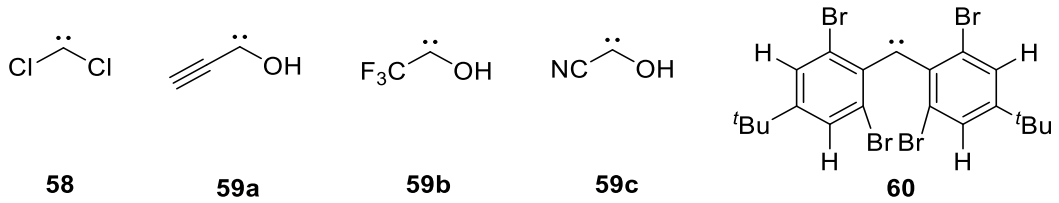

58 **59a** **59b** **59c** **60**

Figure 16: Some examples of stabilized carbenes.

Due to their fleeting character, it took nearly a century to isolate the first "stable" carbene.[72, 108-111] In 1988, Bertrand synthesized the first persistent carbene (**63**)[112] by implementing different substituents and enhancing stability through an electron donating effect. Surprisingly, carbene **63** demonstrated remarkable stability over weeks. The work by Wanzlick[113] and Öfele[114] on metal-carbene complexes and the equilibrium between monomeric **61** and dimeric imidazolidin-2-ylidenes (**62**), enabled Arduengo to successfully synthesize the first "bottle-able" carbene **64**.[100, 115] This carbene is stabilized by two π-electron donating nitrogen atoms and the aromaticity of the imidazole ring.[116] The dimerization proposed in the Wanzlick equilibrium was kinetically hindered by the bulky substituents. Eventually, Enders *et al*. achieved the synthesis of the first commercially available carbene **65** in 1995 (Figure 17).[117]

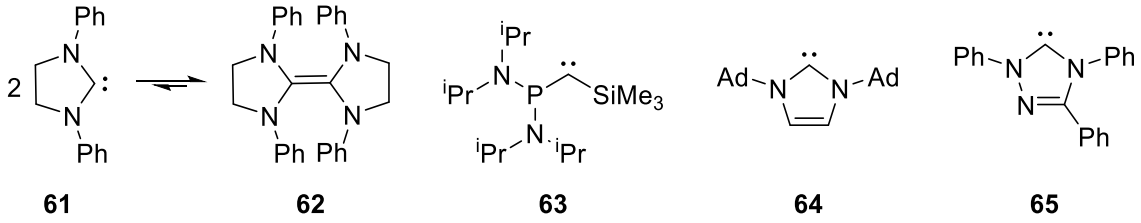

Figure 17: Historical developments in stable carbene chemistry.

To study transient carbenes, techniques such as ultrafast gas-phase spectroscopy or kinetic stabilization at cryogenic temperatures are required. The latter is often achieved through matrix isolation. Notable examples (Figure 18) include dichlorocarbene (**58a**),[101] difluorocarbene (**58b**),[118] di-*tert*-butylcarbene (**58c**),[119] diadamantylcarbene (**58d**),[120] dicyclopropylcarbene (**58e**),[121] ethynylhydroxycarbene (**59a**),[103] trifluoromethylhydroxycarbene (**59b**),[104] cyanohydroxycarbene (**59c**),[105] cyclopropylidene (**66**),[122] vinylidene carbene (propadienylidene, **67**),[123] propinylcarbene (propargylene, **68**),[124] and heterocyclic carbenes such as 2,3-dihydrothiazol-2-ylidene (**69a**)[125] 2,3-dihydroimidazol-2-ylidene (**69b**).[126]

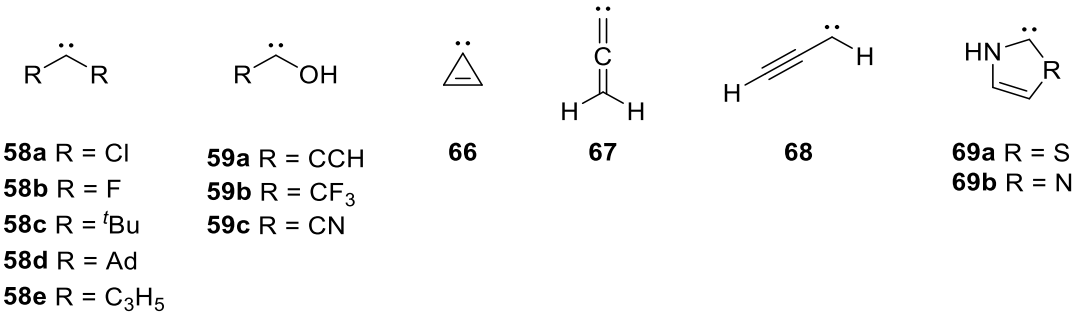

Figure 18: Several selected reactive carbenes that have been prepared experimentally.

Despite multiple attempts, ethylidene, the simplest alkyl carbene besides methylene, has not been spectroscopically characterized due to its tendency to undergo rapid [1,2]H-shift.[127-134] By replacing hydrogen atoms with fluorine, the stability was enhanced and observation of 2,2,2-trifluoroethylidene was possible.[135] Perhaps unsurprisingly, most research on singlet alkyl carbenes stems from computational work.[136] Cyclic alkyl carbenes,[137-138] due to their unique structure, are stabilized through through-space interactions, non-classic bonding schemes, and hyperconjugation.[139] Some examples are norbornen-7-ylidene (**70**),[140] cyclobutylidene (**71**),[141] and tricyclooct-8-ylidene (**72**)[142] (Figure 19), which have only been investigated theoretically. Adamantylidene (**73**)[143] and pentacyclo[5.4.0.0^{2,6}.0^{3,10}.0^{5,9}]undecanylidene (PCU-carbene) (**74**) are among the few singlet alkyl carbenes that have been spectroscopically characterized,[119-121] the latter of which was investigated in this work.

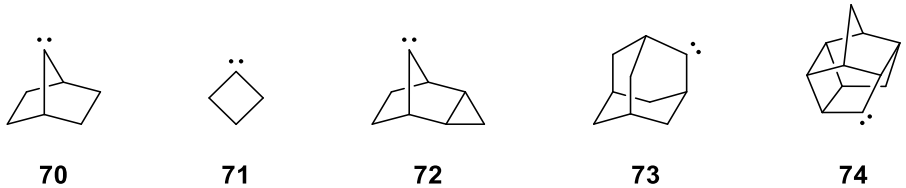

Figure 19: Examples of cyclic alkyl carbenes.

1.3.1 Tunneling Reactions of Alkyl Carbenes

Quantum mechanical tunneling allows particles to penetrate a potential energy barrier without sufficient kinetic energy.[144-146] The tunneling probability depends linearly on the barrier width,[147] the square root of the barrier height,[147] and the effective mass of the particles.[148] This process, even if seemingly insignificant in comparison to thermodynamic or kinetic reactivity, enhances reaction rates by allowing more particles to transition to the product side of a reaction. In very cold environments, such as outer space or matrix isolation setups, tunneling can play a significant role in determining reaction rates. This makes QMT particularly important for long-term processes, such as those occurring on astronomical timescales, and thus must be considered to gain accurate values of rate constants.[149-150] Electron or hydrogen tunneling can change the reaction rates or the reaction outcomes entirely; this also holds true for organic chemistry, where QMT is widely regarded as a minor influence on a reaction outcome.

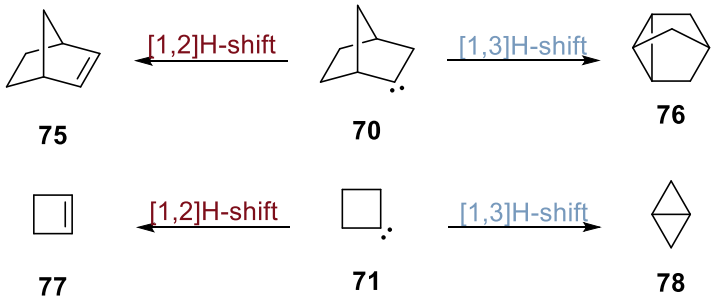

Figure 20: Theoretical examples of H-shifts in cyclic singlet alkyl carbenes.[141] Carbene **70** can either undergo a [1,2]H-shift to form norbornene (**75**) or a [1,3]H-shift to form nortricyclene (**76**). Carbene **71** can either undergo a [1,2]H-shift to form cyclobutene (**77**) or a [1,3]H-shift to form bicyclo[1.1.0]butane (**78**).

Cyclic singlet alkyl carbenes can undergo different tunneling reactions. Usually, H-shifts are most common (Figure 20); however, when the de Broglie wavelength of a particle approaches the same magnitude as the width of the energy barrier it is penetrating, heavy-atom tunneling can occur.[151] This suggests that even carbon tunneling should be considered for accurate reaction rates if the barriers are sufficiently narrow. Usually, ring expansion and insertion- reactions of C–C bonds through heavy atom tunneling can take place (Figure 21).[152-153]

This makes accurate predictions reliant on precise modeling of the potential energy surface (PES). Accurate computational predictions can be achieved[154] by techniques such as Canonical Variational Transition State Theory (CVT)[155] corrected for small-curvature tunneling (SCT),[156] and combined with density functional theory (DFT).[157-158]

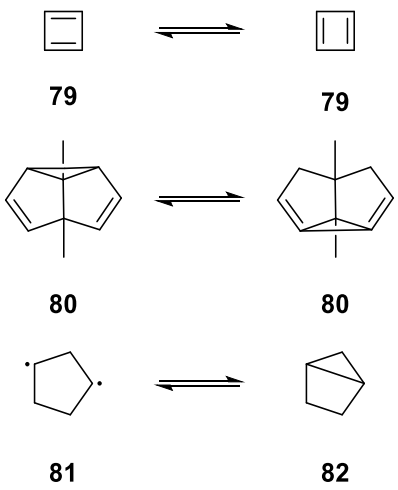

Figure 21: Examples of heavy-atom QMT in cyclic carbenes. Automerization in cyclobutadiene (**79**)[159] and 1,5-dimethylsemibullvalene (**80**)[160-161] as well as ring closure of cyclopentane-1,3-diyl (**81**)[162] to bicyclo[2.1.0]pentane (**82**).[160]

As part of this thesis, we aimed to investigate the tunneling behavior of cage alkyl carbenes under cryogenic conditions. We began with adamantylidene (**73**), a singlet alkyl carbene known to be stable under cryogenic conditions. Bally and Platz only observed the rearrangement of **73** to dehydroadamantane (**83**) after UV irradiation.[143] Although the authors did not report any QMT reactivity,[143] in 2014, Kozuch *et al.*, computed a tunneling half-life of 62.2 h for **73** at the CVT/SCT//B3LYP/6-31G(d,p) level of theory.[152] We replicated the experiment, but allowed the reaction to proceed overnight in the dark. Interestingly, we noticed diminished IR signals corresponding to **73**, and the concomitant formation of **83**, indicating a QMT process. We also extended our investigations to pentacyclo[5.4.0.0^{2,6}.0^{3,10}.0^{5,9}]undecanylidene (PCU-carbene) (**75**), marking only one of a few full spectroscopic characterization of a singlet alkyl carbene.[119-121] Unexpectedly, PCU-carbene did not exhibited QMT reactivity, as it proved to be stable under the cryogenic conditions. Only upon irradiation, a ring-opening reaction to homohypostrophene (**84**) occurred (Figure 22). We then shifted our focus to a third cage alkyl carbene, protoadamantylidene (**85**).

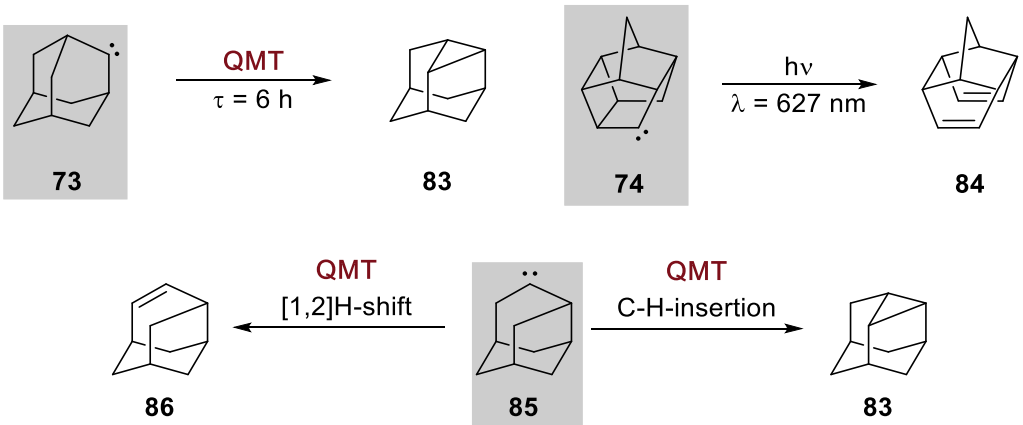

Figure 22: QMT reactivity of alkyl carbenes **73**, **74**, and **85**.

Despite having a half-life too short to capture **85**, we could determine two competing QMT reactions: either a [1,2]H-shift forming **86** or a C–H-insertion generating **83**. In the

next section, we will explore how to influence these competing QMT processes through an isotope-controlled selective approach to specifically favor one of these reactions.

1.3.2 Controlling Tunneling Reactivity

In 2011, a new paradigm, known as tunneling control, was established.[163] This makes it the third principle besides kinetic and thermodynamic control,[136, 164] the established cornerstones of mechanistic reasoning. In tunneling control, the consideration of width between species on the potential energy surface is as important as reaction free energies and barrier heights (*vide supra*).[147, 165] In the many examples of tunneling control,[144, 166-167] reactions defy transition state theory (TST), as thermodynamic products can form more rapidly than kinetic ones due to the presence of a higher but narrower energy barrier.[144] In the Schreiner group, tunneling control has been uncovered and extensively investigated. In 2017, Schreiner *et al.* demonstrated that matrix-isolated methylhydroxycarbene (**87**) does not react as expected to the kinetically favored vinyl alcohol (**38**) but to the thermodynamically more stable product (acetaldehyde, **88**) instead (Figure 23a).[144] Lacking external influence due to the cold environment of the matrix setup (11 K), tunneling control provides the only explanation for the observed phenomenon. This was corroborated by high-level computations, employing a focal-point analysis (FPA)[168-170] on top of coupled-cluster-optimized geometries.[171-172] In 2017, Schreiner *et al.* could show the exclusive formation of a tunneling product, deviating from classic expectations (Figure 23b).[173]

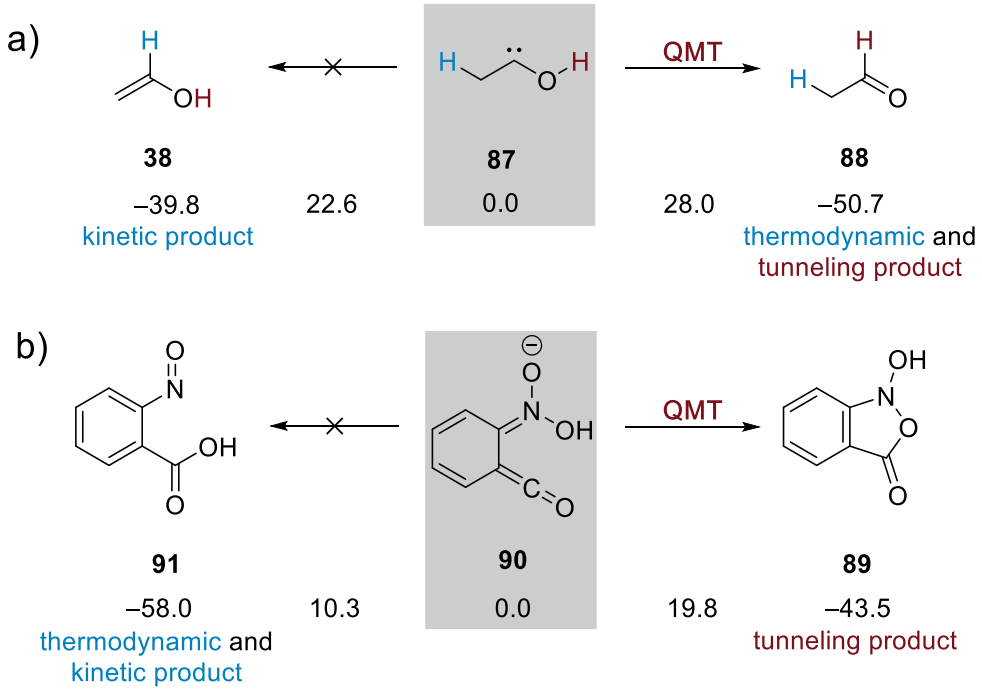

Figure 23: a) QMT control in methylhydroxycarbene (**87**). Relative energies in kcal mol^{-1} were computed at the FPA//AE-CCSD(T)/cc-pCVQZ level of theory.[144] b) The formation of the tunneling product **89** from ketene **90**, rather than the expected thermodynamic and kinetic product **91**, was observed. Relative energies in kcal mol^{-1} were computed at the CCSD(T)/cc-pVTZ//MP2/aug-cc-pVDZ level of theory.[173]

In a theoretical study about influencing competing tunneling reactions, Nandi *et al.* investigated the QMT reactivity of cyclopropylmethylcarbene (**92**).[174] They revealed that, in principle, three QMT reactions can occur: Ring expansion to 1-methylcyclobut-1-ene (**93**) and two [1,2]H-shifts to **94** and **95**, respectively (Figure 24).

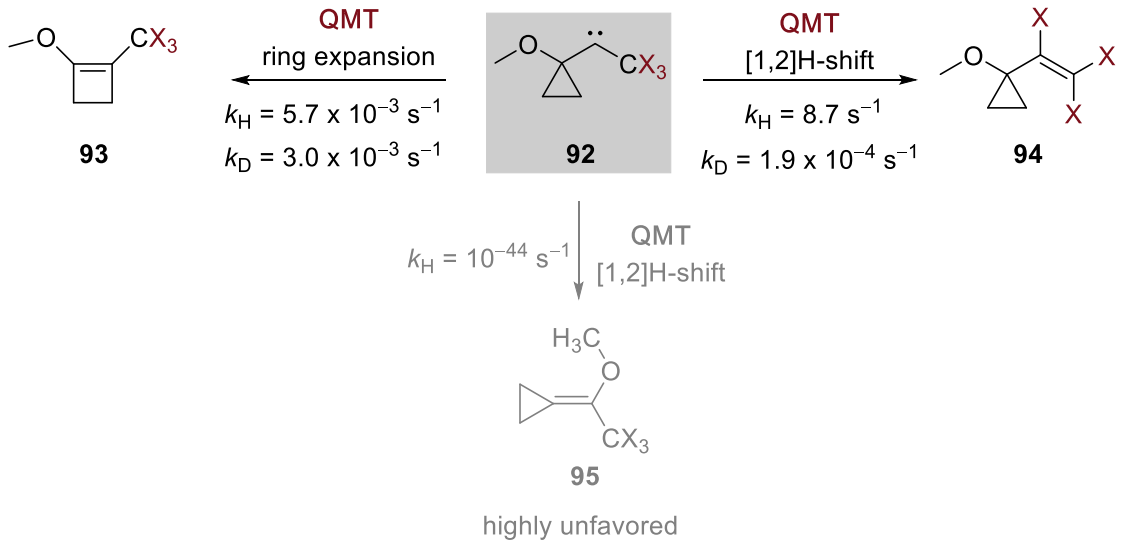

Figure 24: Isotope-controlled selectivity via QMT: The isotope significantly alters rate constants and determines whether **92** reacts to form **93** or **94**, as shown by B3LYP/6-31G(d,p) computations.[174]

At high temperatures, ring expansion is favored due to a lower energy barrier. However, at low temperatures, a hydrogen shift by tunneling is enabled. The hydrogen shift is favored despite the activation barrier being higher, making this reaction tunneling-controlled. Computations on the rate constants for both ring expansion and hydrogen shift were performed, which revealed that introducing methoxy groups with different hydrogen isotopes led to distinct outcomes for hydrogen and deuterium tunneling pathways.[174] This novel concept was coined isotope-controlled selectivity (ICS). The ICS refers to a reactive system in which the formation of a specific product in a QMT reaction is determined entirely by the isotopic composition of the substrate.[174] Although, theoretically investigated, to this date, there are no experimental studies to the concept of ICS.

In this thesis, we applied this approach to the newly generated singlet alkyl carbene **85**. As mentioned earlier, carbene **85** has two competing tunneling reactions. Computations at the UB3LYP/6-31G(d) level of theory reveal the half-life for the C–H insertion to be 4×10^{-9} h and 3×10^{-4} h for the competing [1,2]H-shift. This makes **83** more favorable and indeed experiments showed a ratio of 2:1 in favor of **83**. The short half-life of **85** prevents direct observation of the carbene under matrix isolation conditions, making product analysis necessary for its indirect detection. Replacing hydrogen with deuterium at the α-position changed the ratio to 20:1 in favor of d_2-**83**. This outcome also aligns with computational results, as there is a greater discrepancy in half-lifes for the deuterated isotopolog compared to the protium isotopolog. This substantial shift in product distribution upon deuteration highlights the significant influence of isotopic substitution, providing strong support for ICS and making it the first experimental evidence.

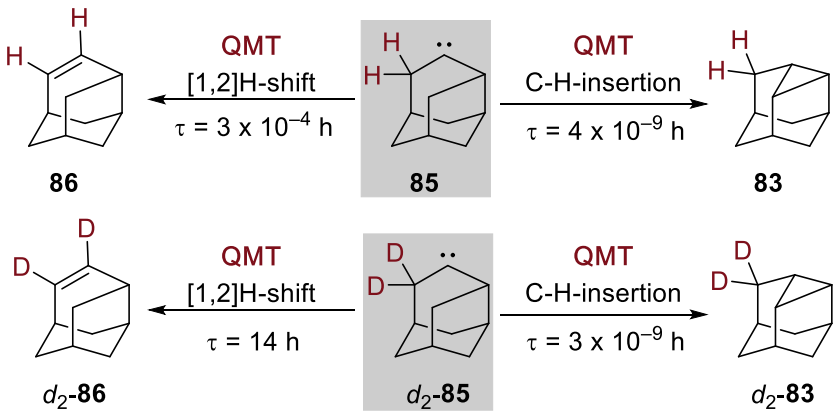

Figure 25: Reactivity of matrix isolated of **85** and d_2-**85** after pyrolysis at 800 °C and ratios of formed products.

1.4 Outlook

Despite extensive research on various sulfur-containing compounds, there is a surprising lack of information about the formation of thioacetamide (**96**). Thioamides, such as **96**, are prevalent in different reactions such as prebiotic building block for amino acid synthesis.[175] Additionally, thioamides serve as relevant compounds in the atmosphere by forming grain-like structures that facilitate water condensation like other sulfur containing compounds already investigated through matrix isolation (Figure 26).[176]

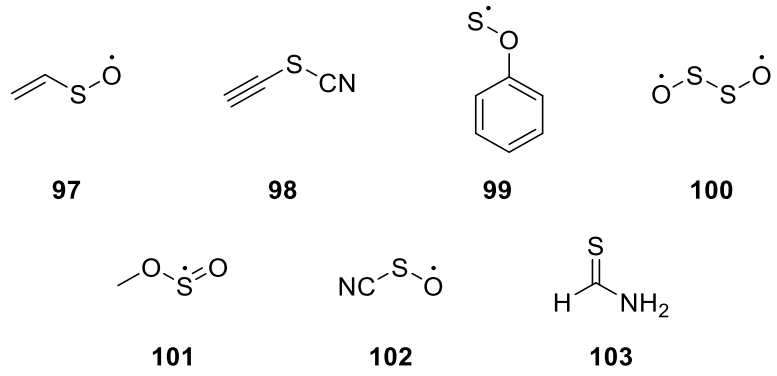

Figure 26: Examples of sulfur-containing compounds including the vinylsulfinyl radical (**97**) alkynyl thiocyanate (**98**)[177] and isomers,[178] the phenylsulfinyl radical (**99**),[179] disulfur dioxide (**100**),[180] methoxysulfinyl radical (**101**),[181] hypothiocyanide radical (**102**)[182] and methanethioamide (**103**).[183]

As previously discussed, enols could play a significant role in the formation of complex organic molecules in the interstellar medium. Hence, we suggest the formation of thioacetamide (**96**) through its higher energy enol tautomer **104**, which could form in space from hydrogen cyanide (HCN)[184] and methanthiole (CH_3SH),[185] both of which have been detected in interstellar environments. By generating the enol **104** similarly to the previously generated enols,[57, 88-90, 94-95] we suggest a pathway to generate **96** from **105**, without implying that the transformation of **105** to **104** occurs under interstellar conditions. (Figure 27).

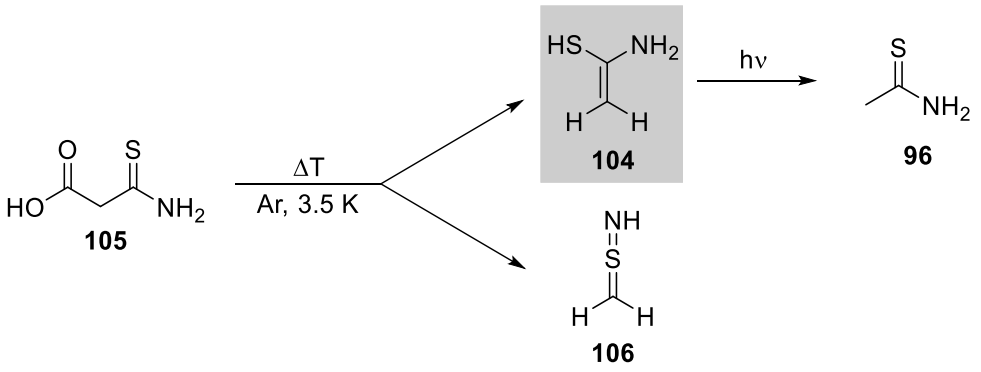

Figure 27: Generation of **104** and subsequent photorearrangement to **96**.

1.5 Conclusion

In our first two publications, we successfully isolated two novel enols, **48** and **49** (Figure 28). These reactive intermediates are predicted to be precursor molecules in the interstellar medium.[6, 53, 54] These enols were generated by pyrolysis of a suitable precursor and subsequently trapped all products using matrix isolation techniques. Their structures were confirmed through IR and UV/Vis spectroscopy. In addition, the corresponding ketenes, **52** and **53**, were also isolated and characterized. The ketenes are considered significant prebiotic molecules as well.[91-92] Upon UV irradiation, both enols underwent rearrangement, forming the corresponding carboxylic acids. Quantum mechanical calculations were used to validate both the IR and the UV/Vis – spectra and to further investigate their potential energy surface.

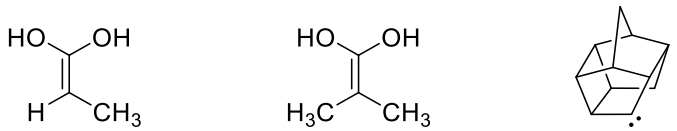

Figure 28: Overview of novel reactive intermediates generated in this work.

In the third publication, we investigated different cage alkyl carbenes. We successfully generated pentacyclo[5.4.0.0^{2,6}.0^{3,10}.0^{5,9}]undecanylidene (**74**) in the matrix and characterized it through IR and UV/Vis spectroscopy (Figure 28). Carbene **75** only underwent [1,2]H-migration to homohypostrophene (**84**) via irradiation with green light, making it otherwise stable under cryogenic conditions. Isolating protoadamantylidene **85** was unsuccessful due to fast tunneling. Two competing QMT reactions were observed, mainly [1,2]H-migration and C–H insertion. To exploit the tunneling reactions and control product outcomes, hydrogen isotopes were strategically employed as directing groups. This successfully changed the product ratio and demonstrated the ability to perform isotope-controlled selectivity in tunneling reactions.

Bibliography

1. McGuire, B. A., 2021 Census of Interstellar, Circumstellar, Extragalactic, Protoplanetary Disk, and Exoplanetary Molecules. *Astrophys. J. Suppl. Ser.* **2022**, *259*, 30.
2. Anders, E., Pre-biotic organic matter from comets and asteroids. *Nature* **1989**, *342*, 255-257.
3. Sephton, M. A., Organic compounds in carbonaceous meteorites. *Nat. Prod. Rep.* **2002**, *19*, 292-311.
4. Stoks, P. G.; Schwartz, A. W., Uracil in carbonaceous meteorites. *Nature* **1979**, *282*, 709-710.
5. Shimoyama, A.; Ogasawara, R., Dipeptides and Diketopiperazines in the Yamato-791198 and Murchison Carbonaceous Chondrites. *Orig. Life Evol. Biosph.* **2002**, *32*, 165-179.
6. Kvenvolden, K.; Lawless, J.; Pering, K.; Peterson, E.; Flores, J.; Ponnamperuma, C.; Kaplan, I. R.; Moore, C., Evidence for Extraterrestrial Amino-acids and Hydrocarbons in the Murchison Meteorite. *Nature* **1970**, *228*, 923-926.
7. Goesmann, F.; Rosenbauer, H.; Bredehöft, J. H.; Cabane, M.; Ehrenfreund, P.; Gautier, T.; Giri, C.; Krüger, H.; Le Roy, L.; MacDermott, A. J., Organic compounds on comet 67P/Churyumov-Gerasimenko revealed by COSAC mass spectrometry. *Science* **2015**, *349*, aab0689.
8. Chyba, C.; Sagan, C., Comets as a source of prebiotic organic molecules for the early Earth. In *Comets and the Origin and Evolution of Life*, Springer: 1997; pp 147-173.
9. Chyba, C. F.; Thomas, P. J.; Brookshaw, L.; Sagan, C., Cometary delivery of organic molecules to the early Earth. *Science* **1990**, *249*, 366-373.
10. Alexander, C. O. D.; Fogel, M.; Yabuta, H.; Cody, G., The origin and evolution of chondrites recorded in the elemental and isotopic compositions of their macromolecular organic matter. *Geochim. Cosmochim. Acta.* **2007**, *71*, 4380-4403.
11. Gibson Jr, E. K., Volatiles in interplanetary dust particles: a review. *J. Geophys. Res. Planets* **1992**, *97*, 3865-3875.
12. Clemett, S. J.; Maechling, C. R.; Zare, R. N.; Swan, P. D.; Walker, R. M., Identification of complex aromatic molecules in individual interplanetary dust particles. *Science* **1993**, *262*, 721-725.
13. Halliday, D.; Resnick, R., *Fundamentals of physics*. John Wiley & Sons: 2013.
14. Woon, D., Interstellar and circumstellar molecules. 2021.
15. Herbst, E., Chemistry in the Interstellar Medium. *Annu. Rev. Phys. Chem.* **1995**, *46*, 27-54.
16. Nicotera, P.; Orrenius, S., Role of thiols in protection against biological reactive intermediates. In *Biological Reactive Intermediates III: Mechanisms of Action in Animal Models and Human Disease*, Springer: 1986; pp 41-51.
17. Parke, D. V.; Ioannides, C., Role of mixed-function oxidases in the formation of biological reactive intermediates. *Biological Reactive Intermediates—II: Chemical Mechanisms and Biological Effects Part A* **1982**, 23-38.
18. Krest, C. M.; Onderko, E. L.; Yosca, T. H.; Calixto, J. C.; Karp, R. F.; Livada, J.; Rittle, J.; Green, M. T., Reactive intermediates in cytochrome P450 catalysis. *J. Biol. Chem.* **2013**, *288*, 17074-17081.
19. Hayes, C. J.; Merle, J. K.; Hadad, C. M., The chemistry of reactive radical intermediates in combustion and the atmosphere. *Adv. Phys. Org. Chem.* **2009**, *43*, 79-134.
20. Vereecken, L.; Harder, H.; Novelli, A., The reaction of Criegee intermediates with NO, RO_2, and SO_2, and their fate in the atmosphere. *Phys. Chem. Chem. Phys.* **2012**, *14*, 14682-14695.
21. Varey, J. E.; Hindmarsh, C. J.; Thomas, K. M., The detection of reactive intermediates in the combustion and pyrolysis of coals, chars and macerals. *Fuel* **1996**, *75*, 164-176.
22. Reymond, J.-L.; Awale, M., Exploring Chemical Space for Drug Discovery Using the Chemical Universe Database. *ACS Chem. Neurosci.* **2012**, *3*, 649-657.
23. Chuss, D. T. Cosmic Background Explorer. https://lambda.gsfc.nasa.gov/product/cobe/.
24. Whittle, E.; Dows, D. A.; Pimentel, G. C., Matrix isolation method for the experimental study of unstable species. *J. Chem. Phys.* **1954**, *22*, 1943-1943.
25. Ilyushin, V. V.; Margulès, L.; Tercero, B.; Motiyenko, R. A.; Dorovskaya, O.; Alekseev, E. A.; Alonso, E. R.; Kolesniková, L.; Cernicharo, J.; Guillemin, J. C., Submillimeter wave spectroscopy of propanoic acid (CH_3CH_2COOH) and its ISM search. *J. Mol. Spectrosc.* **2021**, *379*, 111454.
26. Meyer, K. H., Über das Gleichgewicht desmotroper Verbindungen in verschiedenen Lösungsmitteln (Über Keto-Enol-Tautomerie. IX). *Ber. Dtsch. Chem. Ges.* **1914**, *47*, 826-832.
27. Biali, S. E.; Nugiel, D. A.; Rappoport, Z., Stable simple enols. Part 19. Steric effects and threshold rotational mechanisms in 1-substituted 2, 2-dimesitylethenols. *J. Am. Chem. Soc.* **1989**, *111*, 846-852.
28. Jiménez-Cruz, F.; Ríos-Olivares, H.; García-Gutiérrez, J. L.; Mar, L. F., Electronic effects on keto–enol tautomerism of p-substituted aryl-1, 3-diketone malonates. *J. Mol. Struct.* **2015**, *1101*, 162-169.
29. Mukhopadhyaya, J. K.; Sklenak, S.; Rappoport, Z., Enols of carboxylic acid amides with β-electron-withdrawing substituents. *J. Am. Chem. Soc.* **2000**, *122*, 1325-1336.
30. Rablen, P. R.; Bentrup, K. H., Are the enolates of amides and esters stabilized by electrostatics? *J. Am. Chem. Soc.* **2003**, *125*, 2142-2147.
31. O'Neill, P.; Hegarty, A. F., The first acid and ester enols: 2, 2-bis (pentamethylphenyl) ethene-1, 1-diol and 1-t-butoxy-2, 2-bis (pentamethylphenyl) ethenol, and their oxidation to stable free radicals. *J. Chem. Soc., Chem. Commun.* **1987**, 744-745.
32. Allen, B. M.; Hegarty, A. F.; O'Neill, P., Sterically hindered enols of carboxylic acids and esters. The ketonisation reactions of 2, 2-bis (2, 4, 6-trimethylphenyl) ethene-1, 1-diol and 2, 2-bis (pentamethylphenyl) ethene-1, 1-diol. *J. Chem. Soc., Perkin Trans. 2* **1997**, 2733-2736.

33. Frey, J.; Rappoport, Z., Reactions of the Relatively Persistent Carboxylic Acid Enol 2, 2-Ditipylethene-1, 1-diol. The Reversibility of Ketene Hydration. *J. Am. Chem. Soc.* **1996**, *118*, 5182-5191.
34. Frey, J.; Rappoport, Z., Generation and Detection of a Relatively Persistent Carboxylic Acid Enol 2, 2-Bis (2‘, 4‘, 6‘-triisopropylphenyl) ethene-1, 1-diol. *J. Am. Chem. Soc.* **1996**, *118*, 5169-5181.
35. Andraos, J.; Chiang, Y.; Kresge, A.; Popik, V., Flash Photolysis of 10-Diazo-9 (10 H)-phenanthrenone in Aqueous Solution. Hydration of Fluorenylideneketene and the Fluorene-9-carboxylic Acid Keto− Enol System. *J. Am. Chem. Soc.* **1997**, *119*, 8417-8424.
36. Andraos, J.; Chiang, Y.; Huang, C.; Kresge, A.; Scaiano, J., Flash photolytic generation and study of ketene and carboxylic acid enol intermediates formed by the photolysis of diazonaphthoquinones in aqueous solution. *J. Am. Chem. Soc.* **1993**, *115*, 10605-10610.
37. Tureček, F.; Vivekananda, S.; Sadílek, M.; Polášek, M., Lactone enols are stable in the gas phase but highly unstable in solution. *J. Am. Chem. Soc.* **2002**, *124*, 13282-13289.
38. Schwarz, H.; Williams, D. H.; Wesdemiotis, C., Potential energy profile for gas-phase, unimolecular reactions of ionized acetic acid and its enol. The barrier to a 1, 3-hydrogen migration. *J. Am. Chem. Soc.* **1978**, *100*, 7052-7055.
39. Paul, M.; Peckelsen, K.; Thomulka, T.; Neudörfl, J.; Martens, J.; Berden, G.; Oomens, J.; Berkessel, A.; Meijer, A. J.; Schäfer, M., Hydrogen tunneling avoided: enol-formation from a charge-tagged phenyl pyruvic acid derivative evidenced by tandem-MS, IR ion spectroscopy and theory. *Phys. Chem. Chem. Phys.* **2019**, *21*, 16591-16600.
40. Saito, S., Microwave spectroscopic detection of vinyl alcohol, CH_2=CHOH. *Chem. Phys. Lett.* **1976**, *42*, 399-402.
41. Levandowski, B. J.; Raines, R. T.; Houk, K., Hyperconjugative $\pi \rightarrow \sigma^*$ CF Interactions Stabilize the Enol Form of Perfluorinated Cyclic Keto–Enol Systems. *J. Org. Chem.* **2019**, *84*, 6432-6436.
42. Shayan, K.; Nowroozi, A., DFT and TD-DFT study of the enol and thiol tautomers of 3-thioxopropanal in the ground and first singlet excited states. *Comput. Theor. Chem.* **2017**, *16*, 1750034.
43. Monge-Palacios, M.; Grajales-González, E.; Sarathy, S. M., Ab initio, transition state theory, and kinetic modeling study of the HO_2-Assisted keto–enol tautomerism propen-2-ol + HO_2 ⇔ acetone +HO_2 under combustion, atmospheric, and interstellar conditions. *J. Phys. Chem. A* **2018**, *122*, 9792-9805.
44. Sung, K.; Tidwell, T. T., Amination of ketene: A theoretical study. *J. Am. Chem. Soc.* **1998**, *120*, 3043-3048.
45. Almstead, J. I. K.; Urwyler, B.; Wirz, J., Flash Photolysis of. alpha.-Diazonaphthoquinones in Aqueous Solution: Determination of Rates and Equilibria for Keto-Enol Tautomerization of 1-Indene-3-carboxylic Acid. *J. Am. Chem. Soc.* **1994**, *116*, 954-960.
46. Urwyler, B.; Wirz, J., The Tautomeric Equilibrium between Cyclopentadienyl-1-carboxylic Acid and Fulvene-6,6-diol in Aqueous Solution. *Angew. Chem. Int. Ed.* **1990**, *29*, 790-792.
47. Chiang, Y.; Kresge, A. J.; Pruszynski, P.; Schepp, N.; Wirz, J., The Enol of Mandelic Acid, Detection, Acidity in Aqueous Solution, and Estimation of the Keto-Enol Equilibrium Constant and Carbon Acidity of Mandelic Acid. *Angew. Chem. Int. Ed.* **1990**, *29*, 792-794.
48. Attia, S.; Schmidt, M. C.; Schröder, C.; Pessier, P.; Schauermann, S., Surface-Driven Keto–Enol Tautomerization: Atomistic Insights into Enol Formation and Stabilization Mechanisms. *Angew. Chem. Int. Ed.* **2018**, *130*, 16901-16906.
49. Taatjes, C. A.; Hansen, N.; McIlroy, A.; Miller, J. A.; Senosiain, J. P.; Klippenstein, S. J.; Qi, F.; Sheng, L.; Zhang, Y.; Cool, T. A.; Wang, J.; Westmoreland, P. R.; Law, M. E.; Kasper, T.; Kohse-Höinghaus, K., Enols Are Common Intermediates in Hydrocarbon Oxidation. *Science* **2005**, *308*, 1887-1889.
50. Kleimeier, N. F.; Kaiser, R. I., Interstellar Enolization-Acetaldehyde (CH_3CHO) and Vinyl Alcohol ($H_2CCH(OH)$) as a Case Study. *ChemPhysChem* **2021**, *22*, 1229-1236.
51. Turner, B. E.; Apponi, A. J., Microwave detection of interstellar vinyl alcohol, CH_2= CHOH. *Astrophys. J.* **2001**, *561*, L207.
52. Wang, J.; Li, Y.; Zhang, T.; Tian, Z.; Yang, B.; Zhang, K.; Qi, F.; Zhu, A.; Cui, Z.; Ng, C.-Y., Interstellar enols are formed in plasma discharges of alcohols. *Astrophys. J.* **2008**, *676*, 416-419.
53. Furukawa, Y.; Chikaraishi, Y.; Ohkouchi, N.; Ogawa, N. O.; Glavin, D. P.; Dworkin, J. P.; Abe, C.; Nakamura, T., Extraterrestrial ribose and other sugars in primitive meteorites. *Proc. Natl. Acad. Sci. U.S.A.* **2019**, *116*, 24440-24445.
54. Ando, A.; Shioiri, T., Enantioselective synthesis of β-hydroxy-α-methyl carbonyl compounds by aldol reaction. *Tetrahedron* **1989**, *45*, 4969-4988.
55. Ménez, B.; Pisapia, C.; Andreani, M.; Jamme, F.; Vanbellingen, Q. P.; Brunelle, A.; Richard, L.; Dumas, P.; Réfrégiers, M., Abiotic synthesis of amino acids in the recesses of the oceanic lithosphere. *Nature* **2018**, *564*, 59-63.
56. Ehrenfreund, P.; Charnley, S. B., Organic Molecules in the Interstellar Medium, Comets, and Meteorites: A Voyage from Dark Clouds to the Early Earth. *Annu. Rev. Astron. Astrophys.* **2000**, *38*, 427-483.
57. Mardyukov, A.; Keul, F.; Schreiner, P. R., Preparation and characterization of the enol of acetamide: 1-aminoethenol, a high-energy prebiotic molecule. *Chem. Sci.* **2020**, *11*, 12358-12363.
58. Foo, L.; Surányi, A.; Guljas, A.; Szőri, M.; Villar, J. J.; Viskolcz, B.; Csizmadia, I. G.; Rágyanszki, A.; Fiser, B., Formation of acetamide in interstellar medium. *Mol. Astrophys.* **2018**, *13*, 1-5.
59. Hollis, J. M.; Lovas, F. J.; Remijan, A. J.; Jewell, P. R.; Ilyushin, V. V.; Kleiner, I., Detection of Acetamide (CH_3CONH_2): The Largest Interstellar Molecule with a Peptide Bond. *Astrophys. J.* **2006**, *643*, L25.
60. Halfen, D. T.; Ilyushin, V.; Ziurys, L. M., Formation of peptide bonds in space: a comprehensive study of formamide and acetamide in Sgr B2 (N). *Astrophys. J.* **2011**, *743*, 60.

61. Altwegg, K.; Balsiger, H.; Berthelier, J. J.; Bieler, A.; Calmonte, U.; Fuselier, S. A.; Goesmann, F.; Gasc, S.; Gombosi, T. I.; Le Roy, L.; de Keyser, J.; Morse, A.; Rubin, M.; Schuhmann, M.; Taylor, M. G. G. T.; Tzou, C.-Y.; Wright, I., Organics in comet 67P – a first comparative analysis of mass spectra from ROSINA–DFMS, COSAC and Ptolemy. *Mem. R. Astron. Soc.* **2017**, *469*, S130-S141.
62. Richard, J. P.; Williams, G.; O'Donoghu, A. C.; Amyes, T. L., Formation and Stability of Enolates of Acetamide and Acetate Anion: An Eigen Plot for Proton Transfer at α-Carbonyl Carbon. *J. Am. Chem. Soc.* **2002**, *124*, 2957-2968.
63. Acton, A. W.; Allen, A. D.; Antunes, L. M.; Fedorov, A. V.; Najafian, K.; Tidwell, T. T.; Wagner, B. D., Amination of Pyridylketenes: Experimental and Computational Studies of Strong Amide Enol Stabilization by the 2-Pyridyl Group. *J. Am. Chem. Soc.* **2002**, *124*, 13790-13794.
64. Badal, M. M. R.; Zhang, M.; Kobayashi, S.; Mishima, M., Amination of phenylketenes. Substituent effect on amine-catalyzed tautomerization of amide enol. *J. Phys. Org. Chem.* **2013**, *26*, 1071-1076.
65. Allen, A. D.; Tidwell, T. T., Amination of Ketenes: Kinetic and Mechanistic Studies. *J. Org. Chem.* **1999**, *64*, 266-271.
66. Raspoet, G.; Nguyen, M. T.; Kelly, S.; Hegarty, A. F., Amination of Ketenes: Evidence for a Mechanism Involving Enols of Amides as Intermediates. *J. Org. Chem.* **1998**, *63*, 9669-9677.
67. F. Hegarty, A.; G. Kelly, J.; M. Relihan, C., Formation of hemiaminals by N-protonation of ketenimines (etheneimines) sterically hindered at carbon. *J. Chem. Soc., Perkin Trans. 2* **1997**, 1175-1182.
68. Woodall, J.; Agúndez, M.; Markwick-Kemper, A. J.; Millar, T. J., The UMIST database for astrochemistry 2006. *Astron. Astrophys.* **2007**, *466*, 1197-1204.
69. Ricardo, A.; Carrigan, M.; Olcott, A.; Benner, S., Borate minerals stabilize ribose. *Science* **2004**, *303*, 196-196.
70. Hollis, J. M.; Lovas, F. J.; Jewell, P. R., Interstellar Glycolaldehyde: The First Sugar. *Astrophys. J.* **2000**, *540*, L107-L110.
71. Breslow, R., On the mechanism of the formose reaction. *Tetrahedron Lett.* **1959**, *1*, 22-26.
72. Butlerow, A., Bildung einer zuckerartigen Substanz durch Synthese. *Liebigs Ann.* **1861**, *120*, 295-298.
73. Eckhardt, A. K.; Linden, M. M.; Wende, R. C.; Bernhardt, B.; Schreiner, P. R., Gas-phase sugar formation using hydroxymethylene as the reactive formaldehyde isomer. *Nat. Chem.* **2018**, *10*, 1141-1147.
74. Schreiner, P. R.; Reisenauer, H. P.; Pickard Iv, F. C.; Simmonett, A. C.; Allen, W. D.; Mátyus, E.; Császár, A. G., Capture of hydroxymethylene and its fast disappearance through tunnelling. *Nature* **2008**, *453*, 906-909.
75. Rivilla, V. M.; Colzi, L.; Jiménez-Serra, I.; Martín-Pintado, J.; Megías, A.; Melosso, M.; Bizzocchi, L.; López-Gallifa, Á.; Martínez-Henares, A.; Massalkhi, S., Precursors of the RNA world in space: detection of (Z)-1, 2-ethenediol in the interstellar medium, a key intermediate in sugar formation. *Astrophys. J. Lett.* **2022**, *929*, L11.
76. Kim, H.-J.; Ricardo, A.; Illangkoon, H. I.; Kim, M. J.; Carrigan, M. A.; Frye, F.; Benner, S. A., Synthesis of Carbohydrates in Mineral-Guided Prebiotic Cycles. *J. Am. Chem. Soc.* **2011**, *133*, 9457-9468.
77. Kleimeier, N. F.; Eckhardt, A. K.; Kaiser, R. I., Identification of Glycolaldehyde Enol (HOHC═CHOH) in Interstellar Analogue Ices. *J. Am. Chem. Soc.* **2021**, *143*, 14009-14018.
78. Muchowska, K. B.; Varma, S. J.; Moran, J., Synthesis and breakdown of universal metabolic precursors promoted by iron. *Nature* **2019**, *569*, 104-107.
79. Cooper, G.; Kimmich, N.; Belisle, W.; Sarinana, J.; Brabham, K.; Garrel, L., Carbonaceous meteorites as a source of sugar-related organic compounds for the early Earth. *Nature* **2001**, *414*, 879-883.
80. Kebukawa, Y.; Kilcoyne, A. D.; Cody, G. D., Exploring the potential formation of organic solids in chondrites and comets through polymerization of interstellar formaldehyde. *Astrophys. J.* **2013**, *771*, 19.
81. Monroe, A. A.; Pizzarello, S., The soluble organic compounds of the Bells meteorite: Not a unique or unusual composition. *Geochim. Cosmochim. Acta*. **2011**, *75*, 7585-7595.
82. Yeghikyan, A. G., Irradiation of dust in molecular clouds. II. Doses produced by cosmic rays. *Astrophysics* **2011**, *54*, 87-99.
83. Bennett, C. J.; Kaiser, R. I., The Formation of Acetic Acid (CH_3COOH) in Interstellar Ice Analogs. *Astrophys. J.* **2007**, *660*, 1289.
84. Bergantini, A.; Zhu, C.; Kaiser, R. I., A Photoionization Reflectron Time-of-flight Mass Spectrometric Study on the Formation of Acetic Acid (CH_3COOH) in Interstellar Analog Ices. *Astrophys. J.* **2018**, *862*, 140.
85. Wang, J.; Nikolayev, A. A.; Zhang, C.; Marks, J. H.; Azyazov, V. N.; Eckhardt, A. K.; Mebel, A. M.; Kaiser, R. I., Synthesis of interstellar propen-2-ol ($CH_3C(OH)CH_2$) – the simplest enol tautomer of a ketone. *Phys. Chem. Chem. Phys.* **2023**, *25*, 17460-17469.
86. Kleimeier, N. F.; Kaiser, R. I., Bottom-Up Synthesis of 1,1-Ethenediol ($H_2CC(OH)_2$)─The Simplest Unsaturated Geminal Diol─In Interstellar Analogue Ices. *J. Phys. Chem. Lett.* **2022**, *13*, 229-235.
87. Kleimeier, N. F.; Eckhardt, A. K.; Kaiser, R. I., A Mechanistic Study on the Formation of Acetic Acid (CH_3COOH) in Polar Interstellar Analog Ices Exploiting Photoionization Reflectron Time-of-flight Mass Spectrometry. *Astrophys. J.* **2020**, *901*, 84.
88. Mardyukov, A.; Keul, F.; Schreiner, P. R., 1,1,2-Ethenetriol: The Enol of Glycolic Acid, a High-Energy Prebiotic Molecule. *Angew. Chem. Int. Ed.* **2021**, *60*, 15313-15316.
89. Mardyukov, A.; Wende, R. C.; Schreiner, P. R., Matrix isolation and photorearrangement of *cis*- and *trans*-1,2-ethenediol to glycolaldehyde. *Chem. Commun.* **2023**, *59*, 2596-2599.
90. Mardyukov, A.; Eckhardt, A. K.; Schreiner, P. R., 1,1-Ethenediol: The Long Elusive Enol of Acetic Acid. *Angew. Chem. Int. Ed.* **2020**, *59*, 5577-5580.
91. Ghoshal, S.; Hazra, M. K., New mechanism for autocatalytic decomposition of H_2CO_3 in the vapor phase. *J. Phys. Chem. A* **2014**, *118*, 2385-2392.

92. Kumar, M.; Busch, D. H.; Subramaniam, B.; Thompson, W. H., Organic acids tunably catalyze carbonic acid decomposition. *J. Phys. Chem. A* **2014**, *118*, 5020-5028.
93. Turner, B., Microwave detection of interstellar ketene. *Astrophys. J.* **1977**, *213*, L75-L79.
94. Danho, A.; Mardyukov, A.; Schreiner, P. R., The enol of propionic acid. *Chem. Commun.* **2023**, *59*, 11524-11527.
95. Danho, A.; Mardyukov, A.; Schreiner, P. R., The enol of isobutyric acid. *Chem. Commun.* **2024**, *60*, 5161-5164.
96. Fuentetaja, R.; Bermúdez, C.; Cabezas, C.; Agúndez, M.; Tercero, B.; Marcelino, N.; Pardo, J. R.; Margulès, L.; Motiyenko, R. A.; Guillemin, J.-C.; de Vicente, P.; Cernicharo, J., Discovery of CH_3CHCO in TMC-1 with the QUIJOTE line survey⋆. *A&A* **2023**, *671*, L6-L11.
97. Das, T.; Ghule, S.; Vanka, K., Insights into the origin of life: Did it begin from HCN and H_2O? *ACS Cent. Sci.* **2019**, *5*, 1532-1540.
98. Green, N. J.; Xu, J.; Sutherland, J. D., Illuminating life's origins: UV photochemistry in abiotic synthesis of biomolecules. *J. Am. Chem. Soc.* **2021**, *143*, 7219-7236.
99. Kirmse, W., *Carbene chemistry*. Elsevier: New York 2013; Vol. 1.
100. Bourissou, D.; Guerret, O.; Gabbaï, F. P.; Bertrand, G., Stable Carbenes. *Chem. Rev.* **2000**, *100*, 39-92.
101. Tevault, D. E.; Andrews, L., Laser-induced fluorescence spectrum of argon matrix-isolated dichlorocarbene. *J. Mol. Spectrosc.* **1975**, *54*, 110-120.
102. Viehe, H. G.; Janousek, Z.; Merenyi, R.; Stella, L., The captodative effect. *Acc. Chem. Res.* **1985**, *18*, 148-154.
103. Bernhardt, B.; Ruth, M.; Eckhardt, A. K.; Schreiner, P. R., Ethynylhydroxycarbene (H–C≡ C–C̈–OH). *J. Am. Chem. Soc.* **2021**, *143*, 3741-3746.
104. Mardyukov, A.; Quanz, H.; Schreiner, P. R., Conformer-specific hydrogen atom tunnelling in trifluoromethylhydroxycarbene. *Nat. Chem.* **2017**, *9*, 71-76.
105. Eckhardt, A. K.; Erb, F. R.; Schreiner, P. R., Conformer-specific [1,2]H-tunnelling in captodatively-stabilized cyanohydroxycarbene (NC–C̈–OH). *Chem. Sci.* **2019**, *10*, 802-808.
106. Tomioka, H.; Watanabe, T.; Hirai, K.; Furukawa, K.; Takui, T.; Itoh, K., 2,2',4,4',6,6'-Hexabromodiphenylcarbene. The First Stable Triplet Carbene in Fluid Solution at Low Temperature and in the Crystal State at Room Temperature. *J. Am. Chem. Soc.* **1995**, *117*, 6376-6377.
107. Tomioka, H.; Hattori, M.; Hirai, K.; Murata, S., Anomalous Effects of Para Substituents on the Stability of Sterically Congested Triplet Diarylcarbenes. The First Triplet Carbene Surviving over Minutes under Normal Conditions. *J. Am. Chem. Soc.* **1996**, *118*, 8723-8724.
108. Nef, J. U., Ueber das zweiwerthige Kohlenstoffatom. *Liebigs Ann.* **1892**, *270*, 267-335.
109. Nef, J. U., Ueber das zweiwerthige Kohlenstoffatom. *Liebigs Ann.* **1894**, *280*, 291-342.
110. Nef, J., Ueber das zweiwerthige Kohlenstoffatom. Die Chemie des Cyans und des Isocyans. *Liebigs Ann.* **1895**, *287*, 265-359.
111. Butlerow, A., Ueber das Jodmethylen. *Liebigs Ann.* **1861**, *120*, 356-356.
112. Igau, A.; Grutzmacher, H.; Baceiredo, A.; Bertrand, G., Analogous , α,α'-Bis-Carbenoid Triply Bonded Species: Synthesis of a Stable λ^3-Phosphinocarbene-λ^5-Phosphaacetylene. *J. Am. Chem. Soc.* **1988**, *110*, 6463-6466.
113. Wanzlick, H. W., Aspects of Nucleophilic Carbene Chemistry. *Angew. Chem. Int. Ed.* **1962**, *74*, 129-134.
114. Öfele, K., 1, 3-Dimethyl-4-imidazolinyliden-(2)-pentacarbonylchrom ein neuer Übergangsmetall-carben-komplex. *J. Organomet. Chem.* **1968**, *12*, P42-P43.
115. Arduengo III, A. J.; Harlow, R. L.; Kline, M., A stable crystalline carbene. *J. Am. Chem. Soc.* **1991**, *113*, 361-363.
116. Hopkinson, M. N.; Richter, C.; Schedler, M.; Glorius, F., An overview of N-heterocyclic carbenes. *Nature* **2014**, *510*, 485-496.
117. Enders, D.; Breuer, K.; Raabe, G.; Runsink, J.; Teles, J. H.; Melder, J. P.; Ebel, K.; Brode, S., Preparation, Structure, and Reactivity of 1, 3, 4-Triphenyl-4, 5-dihydro-1H-1, 2, 4-triazol-5-ylidene, a New Stable Carbene. *Angew. Chem. Int. Ed.* **1995**, *107*, 1119-1122.
118. Brahms, D. L. S.; Dailey, W. P., Fluorinated carbenes. *Chem. Rev.* **1996**, *96*, 1585-1632.
119. Gano, J. E.; Wettach, R. H.; Platz, M. S.; Senthilnathan, V., Di-*tert*-butylcarbene: the low temperature photochemistry of Di-*tert*-butyldiazomethane. *J. Am. Chem. Soc.* **1982**, *104*, 2326-2327.
120. Myers, D. R.; Senthilnathan, V.; Platz, M. S.; Jones, M., Diadamantylcarbene in solution. *J. Am. Chem. Soc.* **1986**, *108*, 4232-4233.
121. Ammann, J. R.; Subramanian, R.; Sheridan, R. S., Dicyclopropylcarbene: direct characterization of a singlet dialkylcarbene. *J. Am. Chem. Soc.* **1992**, *114*, 7592-7594.
122. Reisenauer, H. P.; Maier, G.; Riemann, A.; Hoffmann, R. W., Cyclopropenylidene. *Angew. Chem. Int. Ed.* **1984**, *23*, 641-641.
123. Maier, G.; Reisenauer, H. P.; Schwab, W.; Carsky, P.; Hess Jr, B. A.; Schaad, L. J., Vinylidene carbene: a new C_3H_2 species. *J. Am. Chem. Soc.* **1987**, *109*, 5183-5188.
124. Maier, G.; Reisenauer, H. P.; Schwab, W.; Čársky, P.; Špirko, V.; Hess Jr, B. A.; Schaad, L. J., Propargylene: A C_3H_2 isomer with unusual bonding. *J. Chem. Phys.* **1989**, *91*, 4763-4773.
125. Maier, G.; Endres, J.; Reisenauer, H. P., 2, 3-Dihydrothiazol-2-ylidene. *Angew. Chem. Int. Ed.* **1997**, *36*, 1709-1712.
126. Maier, G.; Endres, J., 2, 3-Dihydroimidazol-2-ylidene. *Eur. J. Org. Chem.* **1998**, *1998*, 1517-1520.
127. Rice, F.; Glasebrook, A., The thermal decomposition of organic compounds from the standpoint of free radicals. VII. The ethylidene radical. *J. Am. Chem. Soc.* **1934**, *56*, 741-743.

128. Bawn, C.; Milsted, J., The stability of hydrocarbon biradicals and their reactions. *J. Trans. Faraday Soc.* **1939**, *35*, 889-896.
129. Volman, D.; Leighton, P.; Blacet, F.; Brinton, R., Free Radical Formation in the Photolysis of Some Aliphatic Aldehydes, Acetone, Azomethane, and Diazoethane. *J. Chem. Phys.* **1950**, *18*, 203-206.
130. Brinton, R.; Volman, D., The Ultraviolet Absorption Spectra of Gaseous Diazomethane and Diazoethane. Evidence for the Existence of Ethylidine Radicals in Diazoethane Photolysis. *J. Chem. Phys.* **1951**, *19*, 1394-1395.
131. Kramer, K.; Wright, A., Ethylidene insertion in phenylsilane. *Tetrahedron Lett.* **1962**, *3*, 1095-1096.
132. Tschuikow-Roux, E.; McNesby, J. R.; Jackson, W. M.; Faris, J. L., Reactions of ethylidene in the vacuum ultraviolet photolysis of ethylene. *J. Phys. Chem.* **1967**, *71*, 1531-1533.
133. Seburg, R. A.; McMahon, R. J., Photochemistry of matrix-isolated diazoethane and methyldiazirine: ethylidene trapping? *J. Am. Chem. Soc.* **1992**, *114*, 7183-7189.
134. Modarelli, D. A.; Platz, M. S., Experimental evidence for ethylidene-d_4. *J. Am. Chem. Soc.* **1993**, *115*, 470-475.
135. O'Gara, J. E.; Dailey, W. P., Matrix-Isolation and ab Initio Molecular Orbital Study of 2,2,2-Trifluoroethylidene. *J. Am. Chem. Soc.* **1994**, *116*, 12016-12021.
136. Rosenberg, M. G.; Brinker, U. H., Constrained Carbenes. *Eur. J. Org. Chem.* **2006**, *2006*, 5423-5440.
137. Gleiter, R.; Hoffmann, R., Stabilizing a singlet methylene. *J. Am. Chem. Soc.* **1968**, *90*, 5457-5460.
138. Hoffmann, R., Trimethylene and the addition of methylene to ethylene. *J. Am. Chem. Soc.* **1968**, *90*, 1475-1485.
139. Gopinath, J. S.; Parameswaran, P., Pentacycloundecanylidene and pentacycloundecanone – hyperconjugatively stabilized carbene and ketone. *Phys. Chem. Chem. Phys.* **2024**, *26*, 13452-13462.
140. Brinker, U. H.; Bespokoev, A. A.; Reisenauer, H. P.; Schreiner, P. R., Conformations and Reactions of Bicyclo[3.2.1]oct-6-en-8-ylidene. *J. Org. Chem.* **2012**, *77*, 3800-3807.
141. Sulzbach, H. M.; Platz, M. S.; Schaefer, H. F.; Hadad, C. M., Hydrogen Migration vs Carbon Migration in Dialkylcarbenes. A Study of the Preferred Product in the Carbene Rearrangements of Ethylmethylcarbene, Cyclobutylidene, 2-Norbornylidene, and 2-Bicyclo[2.1.1]hexylidene. *J. Am. Chem. Soc.* **1997**, *119*, 5682-5689.
142. Apeland, I. M.; Rosenberg, M. G.; Arion, V. B.; Kählig, H.; Brinker, U. H., Intermolecular Reactions of a Foiled Carbene with Carbonyl Compounds: The Effects of Trishomocyclopropyl Stabilization. *J. Org. Chem.* **2015**, *80*, 11877-11887.
143. Bally, T.; Matzinger, S.; Truttmann, L.; Platz, M. S.; Morgan, S., Matrix Spectroscopy of 2-Adamantylidene, a Dialkylcarbene with Singlet Ground State. *Angew. Chem. Int. Ed.* **1994**, *33*, 1964-1966.
144. Schreiner, P. R., Tunneling control of chemical reactions: the third reactivity paradigm. *J. Am. Chem. Soc.* **2017**, *139*, 15276-15283.
145. Borden, W. T., Reactions that involve tunneling by carbon and the role that calculations have played in their study. *WIRES Comput. Mol. Sci.* **2016**, *6*, 20-46.
146. Meisner, J.; Kästner, J., Atom tunneling in chemistry. *Angew. Chem. Int. Ed.* **2016**, *55*, 5400-5413.
147. Qiu, G.; Schreiner, P. R., The Intrinsic Barrier Width and Its Role in Chemical Reactivity. *ACS Cent. Sci.* **2023**, *9*, 2129-2137.
148. Castro, C.; Karney, W. L., Heavy-Atom Tunneling in Organic Reactions. *Angew. Chem. Int. Ed.* **2020**, *59*, 8355-8366.
149. Greer, E. M.; Kwon, K.; Greer, A.; Doubleday, C., Thermally activated tunneling in organic reactions. *Tetrahedron* **2016**, *72*, 7357-7373.
150. Schäfer, M.; Peckelsen, K.; Paul, M.; Martens, J.; Oomens, J.; Berden, G.; Berkessel, A.; Meijer, A. J., Hydrogen tunneling above room temperature evidenced by infrared ion spectroscopy. *J. Am. Chem. Soc.* **2017**, *139*, 5779-5786.
151. De Broglie, L., Waves and quanta. *Nature* **1923**, *112*, 540-540.
152. Kozuch, S., The reactivity game: theoretical predictions for heavy atom tunneling in adamantyl and related carbenes. *Phys. Chem. Chem. Phys.* **2014**, *16*, 7718-7727.
153. Moss, R. A.; Sauers, R. R.; Sheridan, R. S.; Tian, J.; Zuev, P. S., Carbon tunneling in the ring expansion of noradamantylchlorocarbene. *J. Am. Chem. Soc.* **2004**, *126*, 10196-10197.
154. Karmakar, S.; Datta, A., Tunneling Control: Competition between 6π-Electrocyclization and [1,5]H-Sigmatropic Shift Reactions in Tetrahydro-1*H*-cyclobuta[*e*]indene Derivatives. *J. Org. Chem.* **2017**, *82*, 1558-1566.
155. Truhlar, D. G.; Garrett, B. C., Variational Transition State Theory. *Annu. Rev. Phys. Chem* **1984**, *35*, 159-189.
156. Hu, W.-P.; Liu, Y.-P.; Truhlar, D. G., Variational transition-state theory and semiclassical tunnelling calculations with interpolated corrections: a new approach to interfacing electronic structure theory and dynamics for organic reactions. *J. Chem. Soc., Faraday Trans.* **1994**, *90*, 1715-1725.
157. Lee, C.; Yang, W.; Parr, R. G., Development of the Colle-Salvetti correlation-energy formula into a functional of the electron density. *Phys. Rev. B* **1988**, *37*, 785-789.
158. Becke, A. D., Density-functional thermochemistry. III. The role of exact exchange. *J. Chem. Phys.* **1993**, *98*, 5648-5652.
159. Carpenter, B. K., Heavy-atom tunneling as the dominant pathway in a solution-phase reaction? Bond shift in antiaromatic annulenes. *J. Am. Chem. Soc.* **1983**, *105*, 1700-1701.
160. Schleif, T.; Tatchen, J.; Rowen, J. F.; Beyer, F.; Sanchez-Garcia, E.; Sander, W., Heavy-Atom Tunneling in Semibullvalenes: How Driving Force, Substituents, and Environment Influence the Tunneling Rates. *Chem. Eur. J.* **2020**, *26*, 10452-10458.

161. Schleif, T.; Mieres-Perez, J.; Henkel, S.; Ertelt, M.; Borden, W. T.; Sander, W., The Cope rearrangement of 1, 5-dimethylsemibullvalene-2 (4)-d_1: Experimental evidence for heavy-atom tunneling. *Angew. Chem. Int. Ed.* **2017**, *56*, 10746-10749.
162. Liu, Q.; Wang, Z.; Abe, M., Impacts of Solvent and Alkyl Chain Length on the Lifetime of Singlet Cyclopentane-1,3-diyl Diradicaloids with π-Single Bonding. *J. Org. Chem.* **2022**, *87*, 1858-1866.
163. Schreiner, P. R.; Reisenauer, H. P.; Ley, D.; Gerbig, D.; Wu, C.-H.; Allen, W. D., Methylhydroxycarbene: Tunneling control of a chemical reaction. *Science* **2011**, *332*, 1300-1303.
164. Woodward, R.; Baer, H., Studies on Diene-addition reactions. II. 1 The reaction of 6, 6-pentamethylenefulvene with maleic anhydride. *J. Am. Chem. Soc.* **1944**, *66*, 645-649.
165. Kästner, J., Path length determines the tunneling decay of substituted carbenes. *Chem. Eur. J.* **2013**, *19*, 8207-8212.
166. Burd, T. A.; Shan, X.; Clary, D. C., Hydrogen tunnelling in the rearrangements of carbenes: the role of dynamical calculations. *Phys. Chem. Chem. Phys.* **2020**, *22*, 962-965.
167. Cheng, L.; Doubleday, C.; Breslow, R., Evidence for tunneling in base-catalyzed isomerization of glyceraldehyde to dihydroxyacetone by hydride shift under formose conditions. *Proc. Natl. Acad. Sci. U.S.A.* **2015**, *112*, 4218-4220.
168. East, A. L.; Allen, W. D., The heat of formation of NCO. *J. Chem. Phys.* **1993**, *99*, 4638-4650.
169. Schuurman, M. S.; Muir, S. R.; Allen, W. D.; Schaefer III, H. F., Toward subchemical accuracy in computational thermochemistry: Focal point analysis of the heat of formation of NCO and [H, N, C, O] isomers. *J. Chem. Phys.* **2004**, *120*, 11586-11599.
170. Bartlett, M. A.; Liang, T.; Pu, L.; Schaefer, H. F.; Allen, W. D., The multichannel *n*-propyl+ O_2 reaction surface: Definitive theory on a model hydrocarbon oxidation mechanism. *J. Chem. Phys.* **2018**, *148*.
171. Stanton, J. F., Why CCSD (T) works: a different perspective. *Chem. Phys. Lett.* **1997**, *281*, 130-134.
172. Čížek, J., On the correlation problem in atomic and molecular systems. Calculation of wavefunction components in Ursell-type expansion using quantum-field theoretical methods. *J. Chem. Phys.* **1966**, *45*, 4256-4266.
173. Gerbig, D.; Schreiner, P. R., Formation of a Tunneling Product in the Photorearrangement of *o*-Nitrobenzaldehyde. *Angew. Chem. Int. Ed.* **2017**, *56*, 9445-9448.
174. Nandi, A.; Gerbig, D.; Schreiner, P. R.; Borden, W. T.; Kozuch, S., Isotope-controlled selectivity by quantum tunneling: Hydrogen migration versus ring expansion in cyclopropylmethylcarbenes. *J. Am. Chem. Soc.* **2017**, *139*, 9097-9099.
175. Patel, B. H.; Percivalle, C.; Ritson, D. J.; Duffy, C. D.; Sutherland, J. D., Common origins of RNA, protein and lipid precursors in a cyanosulfidic protometabolism. *Nat. Chem.* **2015**, *7*, 301-307.
176. Wang, S.; Maltrud, M.; Elliott, S.; Cameron-Smith, P.; Jonko, A., Influence of dimethyl sulfide on the carbon cycle and biological production. *Biogeochemistry* **2018**, *138*, 49-68.
177. Wu, Z.; Wang, L.; Lu, B.; Eckhardt, A. K.; Schreiner, P. R.; Zeng, X., Spectroscopic characterization and photochemistry of the vinylsulfinyl radical. *Phys. Chem. Chem. Phys.* **2021**, *23*, 16307-16315.
178. Lu, B.; Wu, Z.; Wang, L.; Zhu, B.; Rauhut, G.; Zeng, X., The simplest alkynyl thiocyanate HCCSCN and its isomers. *Chem. Commun.* **2021**, *57*, 3343-3346.
179. Xu, J.; Wu, Z.; Wan, H.; Deng, G.; Lu, B.; Eckhardt, A. K.; Schreiner, P. R.; Trabelsi, T.; Francisco, J. S.; Zeng, X., Phenylsulfinyl radical: Gas-phase generation, photoisomerization, and oxidation. *J. Am. Chem. Soc.* **2018**, *140*, 9972-9978.
180. Wu, Z.; Wan, H.; Xu, J.; Lu, B.; Lu, Y.; Eckhardt, A. K.; Schreiner, P. R.; Xie, C.; Guo, H.; Zeng, X., The near-UV absorber OSSO and its isomers. *Chem. Commun.* **2018**, *54*, 4517-4520.
181. Liu, Q.; Wu, Z.; Xu, J.; Lu, Y.; Li, H.; Zeng, X., Methoxysulfinyl radical CH_3OSO: Gas-phase generation, photochemistry, and oxidation. *J. Phys. Chem. A* **2017**, *121*, 3818-3825.
182. Wu, Z.; Liu, Q.; Xu, J.; Sun, H.; Li, D.; Song, C.; Andrada, D. M.; Frenking, G.; Trabelsi, T.; Francisco, J. S., Heterocumulene sulfinyl radical OCNSO. *Angew. Chem. Int. Ed.* **2017**, *129*, 2172-2176.
183. Bernhardt, B.; Dressler, F.; Eckhardt, A. K.; Becker, J.; Schreiner, P. R., Characterization of the simplest thiolimine: the higher energy tautomer of thioformamide. *Chem. Eur. J.* **2021**, *27*, 6732-6739.
184. Snyder, L. E.; Buhl, D., Observations of radio emission from interstellar hydrogen cyanide. *Astrophys. J.* **1971**, *163*, L47.
185. Linke, R. A.; Frerking, M. A.; Thaddeus, P., Interstellar methyl mercaptan. *Astrophys. J.* **1979**, *234*, L139-L142.

2. Publications

2.1 The enol of propionic acid

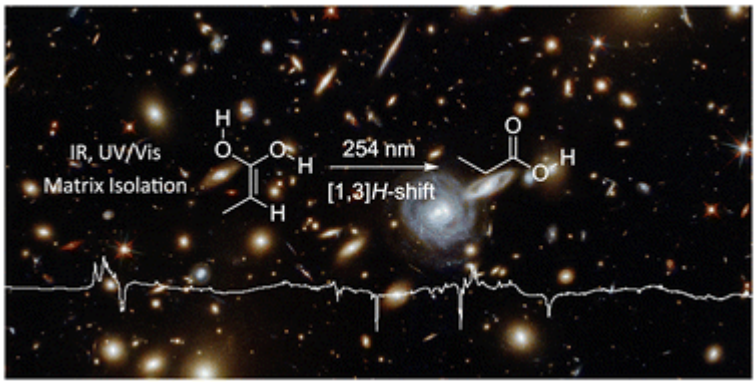

Abstract:

We demonstrate the gas-phase synthesis of prop-1-ene-1,1-diol, the hitherto unreported higher energy tautomer of propionic acid. The enol was trapped in an argon matrix and characterized by IR and UV/Vis spectroscopy in combination with density functional theory computations. Upon photolysis, the enol rearranges to propionic acid and methylketene.

Reference:

Akkad Danho, Artur Mardyukov and Peter R. Schreiner *Chem Commun.* **2023**, *59*, 11524-11527. (DOI: 10.1039/d3cc03711h)

Reproduced with permission from:

ChemComm

COMMUNICATION

View Article Online
View Journal | View Issue

Cite this: *Chem. Commun.*, 2023, **59**, 11524

Received 31st July 2023,
Accepted 25th August 2023

DOI: 10.1039/d3cc03711h

rsc.li/chemcomm

The enol of propionic acid†

Akkad Danho, Artur Mardyukov and Peter R. Schreiner *

We demonstrate the gas-phase synthesis of prop-1-ene-1,1-diol, the hitherto unreported higher energy tautomer of propionic acid. The enol was trapped in an argon matrix and characterized by IR and UV/Vis spectroscopy in combination with density functional theory computations. Upon photolysis, the enol rearranges to propionic acid and methylketene.

Complex molecules like proteins, DNA, and carbohydrates, may have arisen through "chemical evolution", a gradual transformation of simple compounds into more complex ones, powered by natural phenomena like radiation, lightning, volcanic activity, and chemical reactions.[1] The formation of organic molecules, like amino acids, sugars, and nucleotides, from simple compounds like water, carbon dioxide, and nitrogen is a critical phase in chemical evolution.[2,3] These organic molecules may react with each other to form more complex molecules, culminating in the synthesis of biomolecules in the absence of biochemical machinery.[4] While the mechanisms behind the formation of (organic) molecules remain under study, researchers have made significant progress in simulating key steps in the laboratory. These simulations have provided valuable insights into possible scenarios for the origins of life on Earth.[5,6] Interstellar cold gas clouds are thought to be a potential source of complex organic molecules, which arise from random energy fluctuations and reactions with stable molecular building blocks.[7–11] For instance, the discovery of glycolaldehyde in space in 2000 has stimulated interest in understanding its gas phase formation mechanism.[12] It has been proposed that glycolaldehyde forms from the reaction of the high-energy tautomer of formaldehyde, hydroxymethylene,[13] with H_2CO, even in the low-temperature environment of space.[14]

In solution, enols are highly reactive species and readily isomerize to the thermodynamically more stable keto tautomers.[15] Enols exhibit much greater stability in the gas phase[16] due to the significantly high energy barriers (40–45 kcal mol^{-1})[17,18] for [1,3]H-shifts and the low probability of bimolecular reactions. As a result, enols, including vinyl alcohol, can persist as long-lived species in the gas phase or in matrices.[16] This is exemplified by the discovery of ethenol in space.[19] Enols can undergo a variety of chemical reactions, including aldol and Michael addition reactions, which can lead to the formation of more complex molecules.[20] Enol chemistry is suggested to have played an important role in the chemical evolution that led to the origin of life on Earth.[21] A fascinating possibility is that a variety of enols might have made their way to Earth through meteorites and comets, and may have given rise to prebiotically relevant compounds.[21–24] These compounds serve as crucial intermediates in the biosynthesis of various essential natural products, such as amino acids,[25] sugars,[26] and carboxylic acids.[27,28]

Propionic acid (**3**, also propanoic acid) is an organic molecule that holds a key role in human metabolism and in other organisms.[29,30] Only in 2021 acid **3** has been proposed as a potentially detectable molecule in the interstellar medium.[31] A variety of spectroscopic investigations has been undertaken in the context of **3**.[32–34] Compound **3** has been detected in the Murchison meteorite with high likelihood, raising the question of its origin.[35] Methylketene (**4**, prop-1-en-1-one), which can also be considered as a precursor for the generation of **3** through the addition of water, has recently been detected in

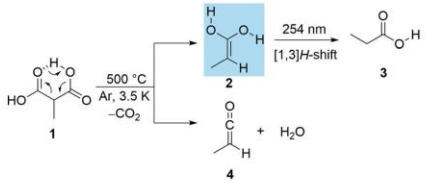

Scheme 1 Prop-1-ene-1,1-diol (**2**) generated from methylmalonic acid (**1**) through pyrolysis and trapping in an argon matrix. Subsequent photorearrangement to propionic acid (**3**) and methylketene (**4**).

Institute of Organic Chemistry, Justus Liebig University, Heinrich-Buff-Ring 17, Giessen 35392, Germany. E-mail: prs@uni-giessen.de

† Electronic supplementary information (ESI) available. See DOI: https://doi.org/10.1039/d3cc03711h

space.[36] Prop-1-ene-1,1-diol (**2**) is the high energy tautomer of **3** but its preparation or spectroscopic data have not been reported. Enediol **2** is expected to form *via* a similar mechanism as demonstrated for the preparation of the enediol of acetic acid, which had been prepared only in 2020.[5] It was demonstrated that the pyrolysis of malonic acid produces 1,1-ethenediol, which was trapped in an argon matrix at 10 K. Here we present the synthesis and spectroscopic characterization of enediol **2**, which we prepare in the gas phase by thermolysis of methylmalonic acid (**1**, Scheme 1).

Enediol **2** was generated through the thermal decarboxylation of **1**. In this allowed thermochemical process, **1** was evaporated from a container at 70 °C and pyrolyzed in a quartz tube at 500 °C. The pyrolysis products were then condensed onto a cold matrix window at 3.5 K using a large excess of argon. Under these conditions, several bands were readily identified, such as the prominent asymmetric CO_2 stretching vibration at 2343 cm^{-1}, the vibration patterns associated with water and **3**, and additional newly observed infrared bands attributed to **2** (Fig. 1). The identity of **3** was corroborated by comparison with a matrix-isolated IR spectrum of an authentic sample. Upon irradiation with wavelengths ranging from 180 to 200 nm, matrix-isolated **2** undergoes a series of reactions, resulting in the formation of **3**, leading to the disappearance of all IR absorptions assigned to **2**. In parallel, new IR bands of **3** emerged (Fig. S2, ESI†). The experimentally observed IR spectrum of **2** matches the computed IR spectrum of **2** at B3LYP/def2-TZVP level very well. For example, the strong stretching vibration of the C=C bond in **2** at 1744 cm^{-1} is in the range of the IR band of 1,1-ethenediol at 1712 cm^{-1}.[5] For a more accurate assessment of the stability and expected reactivity of **2**, we computed molecular electrostatic potential (ESP) maps of **2** and compared these with other enols (*vide infra*) (Table S1, ESI†). The incorporation of a methyl group results in an increased electron density of the C=C bond, leading to a higher C=C stretching vibration in **2** (1744 cm^{-1}) in comparison to C=C stretching vibration for 1,2 ethenediol (1711 cm^{-1})[37] and 1,1-ethenediol[5] (1712 cm^{-1}). This suggests that **2** should exhibit the highest nucleophilicity within this series.

When repeating the experiment with deuterated d_3-**1**, the bands of d_3-**2** also match well with the computed spectrum and characteristic isotopic shifts were observed. The stretching vibration of the C=C bond is red-shifted by 23 cm^{-1} (calculated: 28 cm^{-1}) in d_3-**2**. Similarly, the stretching vibrations of the OH groups in d_3-**2** at 2986 cm^{-1} and 2946 cm^{-1} are red-shifted by 662 cm^{-1} and 684 cm^{-1} (calculated: 697 cm^{-1} and 750 cm^{-1}). Overall, the experimentally measured and computed shifts match very well, providing strong evidence that enol **2** was successfully synthesized. In the pyrolysis IR spectrum we also found IR bands that can be assigned to methylketene (**4**). The strong IR band at 2122 cm^{-1} (computed: 2201 cm^{-1}) corresponds to the CCO stretching vibration of **4**. For deuterated ketene (d_1-**4**) an identical peak with a red-shift of 6 cm^{-1} was observed (calculated: 6 cm^{-1}, Fig. 1).

The formation of **2** was also followed by UV/Vis spectroscopy. The FVP spectrum of **1** shows a broad transition at 190 nm, which agrees well with the computed TD-DFT spectrum of **2**. The absorption band at 190 nm arises from a HOMO–LUMO+3 excitation, which corresponds to a $\pi \rightarrow \pi^*$ transition. In line with IR experiments, the broad band at 190 nm vanishes upon irradiation at 254 nm (Fig. 2).

For a better understanding of the thermochemistry, we computed the potential energy hyperface around **2** at B3LYP/def2-TZVP. According to these computations, **2** can adopt four distinct conformations determined by the s-*cis* and s-*trans* orientations of the OH groups relative to the opposing C–O bond: s-*cis*, s-*trans* **2ct**, s-*trans*, s-*trans* **2tt**, s-*cis*, s-*cis* **2cc**, and s-*trans*, s-*cis* **2tc**. Among these conformers, **2ct** is most stable: **2tc**, **2cc**, and **2tt** are higher in energy by 0.7, 2.0, and 2.3 kcal mol^{-1} (Fig. 2), respectively. Conformational isomerization from **2ct** to **2tt** requires an activation energy (**TS1**) of 4.1 kcal mol^{-1}. The activation energies

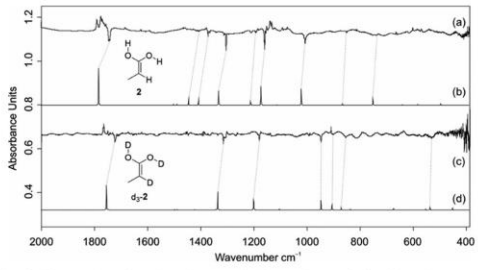

Fig. 1 IR spectra showing the pyrolysis product of **1** with subsequent trapping in an argon matrix at 3.5 K. (a) IR difference spectra showing the photochemistry of **2** after irradiation with λ = 254 nm in argon at 3.5 K. Downward bands assigned to **2** disappear while upward bands assigned to **3** appear after 20 min irradiation time. (b) IR spectrum of **2** computed at B3LYP/def2TZVP. (c) IR difference spectra showing the photochemistry of d_4-**2** after irradiation with λ = 254 nm in argon at 3.5 K. Downward bands assigned to d_3-**2** disappear while upward bands assigned to d_3-**3** appear after 20 min irradiation time. (d) IR spectrum of d_3-**2** computed at B3LYP/def2TZVP.

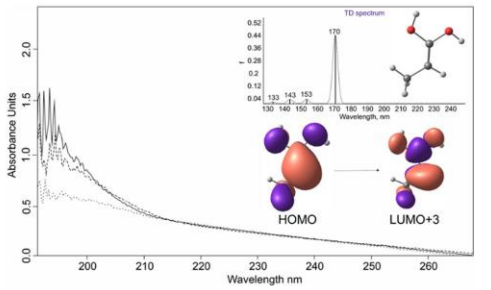

Fig. 2 Solid line: UV/Vis spectrum showing the pyrolysis product of **1** with subsequent trapping in an argon matrix at 3.5 K. Dashed line: after irradiation at λ = 254 for 6 min in argon matrix at 3.5 K. Dotted line: after irradiation at λ = 254 for 20 min in argon matrix at 3.5 K. Inset: Computed B3LYP/def2-TZVP electronic transitions for **2**.

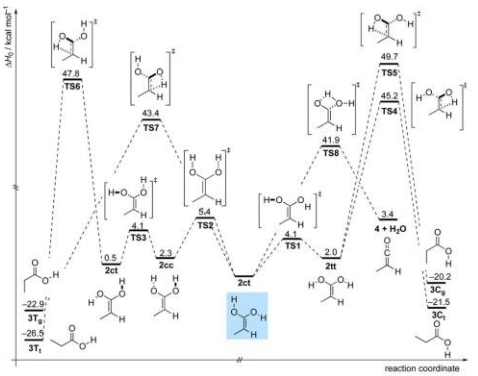

Fig. 3 Potential energy profile (ΔH_0) in kcal mol^{-1} of the reactions of dienol **2** at B3LYP/def2TZVP at 0 K.

for the **2ct** to **2cc**, and **2cc** to **2ct** conformational isomerizations are 5.4 and 4.1 kcal mol^{-1} (**TS2** and **TS3**), respectively. The only conformer present in the matrix after FVP experiments was the favored **2ct** conformer, owing to the likely rapid quantum-mechanical tunneling (QMT) rotamerization typical for OH groups.[5,6,37] The propionic acid conformers[38] display a staggered arrangement around the C_β–C_α bond and *trans* arrangements around the C_α–C and C–O bonds (*gauche* and *anti* C–C–C–O and C–C–O–H dihedral angles). From the **2tt** conformer, two conformers of **3** can be generated *via* [1,3]H-shifts. The activation barriers are 45.2 and 49.7 kcal mol^{-1} (**TS4** and **TS5**), respectively, and QMT is unlikely owing to large barrier widths.[39,40] The **2ct** → **3** (*trans–gauche*, $\mathbf{3T_g}$) tautomerization is associated with a somewhat lower but still substantial activation barrier of 43.4 kcal mol^{-1} (**TS7**). In fact, $\mathbf{3T_g}$ only forms after high-energy photoexcitation of **2ct** at 254 nm.

Apart from keto–enol tautomerization into $\mathbf{3T_g}$, **2ct** can also interconvert to ketene **4** + H_2O *via* transition state **TS8**, which exhibits an energy barrier of 41.9 kcal mol^{-1}. Unsurprisingly, **4** can readily be observed under our pyrolysis reaction conditions. The formation of the most thermodynamically stable conformer **3** (*trans–trans*, $\mathbf{3T_t}$) can occur from **2ct** through **TS6**, requiring an activation energy of 47.8 kcal mol^{-1} (Fig. 3).

Our findings indicate that acid tautomers can be readily prepared in the gas phase and that they are likely to play a significant role in chemical reactions. The spectroscopic identification of **2** makes it a candidate for a relevant prebiotic molecule.[21–24] Furthermore, **4** has also been identified in space,[31] and either **1** or **2** may serve as precursors. The formation of **3** starting from **2** under interstellar conditions is unlikely due to the high energy barrier of 43.4 kcal mol^{-1}. However, **2** could also form through the facile hydration of **4**; the hydration of ketenes to the corresponding carboxylic acids is well known and requires only little activation.[41,42] Alternatively, **3** may form through surface catalysis on ice particles or dust surfaces.[43,44] These results bear implications for comprehending the formation of larger organic molecules and the fascinating processes involved in their synthesis.

This project has received funding from the European Research Council (ERC) under the European Union's Horizon 2020 research and innovation programme (Advanced Grant No. 101054751 COLDOC to P. R. S). Views and opinions expressed are those of the authors only and do not necessarily reflect those of the European Union or the European Research Council. Neither the European Union nor the granting authority can be held responsible for them.

Conflicts of interest

There are no conflicts to declare.

Notes and references

1 W. M. Garrison, D. C. Morriso, J. G. Hamilton, A. A. Benson and M. Calvin, Reduction of carbon dioxide in aqueous solutions by ionizing radiation, *Science*, 1951, **114**, 416–418.
2 G. R. Tilton and R. H. Steiger, Lead Isotopes and the Age of the Earth, *Science*, 1965, **150**, 1805–1808.
3 H. N. Russell, On the Composition of the Sun's Atmosphere, *Astrophys. J.*, 1929, **70**, 11.
4 J. Oró, Chemical evolution and the origin of life, *Adv. Space Res.*, 1983, **3**, 77–94.
5 A. Mardyukov, A. K. Eckhardt and P. R. Schreiner, 1,1-Ethenediol: The Long Elusive Enol of Acetic Acid, *Angew. Chem., Int. Ed.*, 2020, **59**, 5577–5580.
6 A. Mardyukov, F. Keul and P. R. Schreiner, 1,1,2-Ethenetriol: The Enol of Glycolic Acid, a High-Energy Prebiotic Molecule, *Angew. Chem., Int. Ed.*, 2021, **60**, 15313–15316.
7 S. L. Miller and H. C. Urey, Organic Compound Synthesis on the Primitive Earth, *Science*, 1959, **130**, 245–251.
8 A. Nummelin, P. Bergman, Å. Hjalmarson, P. Friberg, W. M. Irvine, T. J. Millar, M. Ohishi and S. Saito, A Three-Position Spectral Line Survey of Sagittarius B2 between 218 and 263 GHz. II. Data Analysis, *Astrophys. J.*, 2000, **128**, 213.
9 R. T. Garrod, S. L. W. Weaver and E. Herbst, Complex Chemistry in Star-forming Regions: An Expanded Gas-Grain Warm-up Chemical Model, *Astrophys. J.*, 2008, **682**, 283.
10 J. L. Bada, New insights into prebiotic chemistry from Stanley Miller's spark discharge experiments, *Chem. Soc. Rev.*, 2013, **42**, 2186–2196.
11 K. Ruiz-Mirazo, C. Briones and A. de La Escosura, Prebiotic Systems Chemistry: New Perspectives for the Origins of Life, *Chem. Rev.*, 2014, **114**, 285–366.
12 J. M. Hollis, F. J. Lovas and P. R. Jewell, Interstellar Glycolaldehyde: The First Sugar, *Astrophys. J.*, 2000, **540**, L107.
13 P. R. Schreiner, H. P. Reisenauer, F. C. Pickard IV, A. C. Simmonett, W. D. Allen, E. Mátyus and A. G. Császár, Capture of hydroxymethylene and its fast disappearance through tunnelling, *Nature*, 2008, **453**, 906–909.
14 A. K. Eckhardt, M. M. Linden, R. C. Wende, B. Bernhardt and P. R. Schreiner, Gas-phase sugar formation using hydroxymethylene as the reactive formaldehyde isomer, *Nat. Chem.*, 2018, **10**, 1141–1147.
15 K. H. Meyer, Über das Gleichgewicht desmotroper Verbindungen in verschiedenen Lösungsmitteln (Über Keto-Enol-Tautomerie. IX), *Ber. Dtsch. Chem. Ges.*, 1914, **47**, 826–832.
16 C. A. Taatjes, N. Hansen, A. McIlroy, J. A. Miller, J. P. Senosiain, S. J. Klippenstein, F. Qi, L. Sheng, Y. Zhang, T. A. Cool, J. Wang, P. R. Westmoreland, M. E. Law, T. Kasper and K. Kohse-Höinghaus, Enols Are Common Intermediates in Hydrocarbon Oxidation, *Science*, 2005, **308**, 1887–1889.
17 G. da Silva, Carboxylic Acid Catalyzed Keto-Enol Tautomerizations in the Gas Phase, *Angew. Chem., Int. Ed.*, 2010, **49**, 7523–7525.
18 N. F. Kleimeier and R. I. Kaiser, Interstellar Enolization-Acetaldehyde (CH_3CHO) and Vinyl Alcohol ($H_2CCH(OH)$) as a Case Study, *Chem. Phys. Chem.*, 2021, **22**, 1229–1236.

19 B. E. Turner and A. J. Apponi, Microwave Detection of Interstellar Vinyl Alcohol, CH_2=CHOH, *Astrophys. J.*, 2001, **561**, L207.
20 C. Palomo, M. Oiarbide and J. M. García, Current progress in the asymmetric aldol addition reaction, *Chem. Soc. Rev.*, 2004, **33**, 65–75.
21 B. Ménez, C. Pisapia, M. Andreani, F. Jamme, Q. P. Vanbellingen, A. Brunelle, L. Richard, P. Dumas and M. Réfrégiers, Abiotic synthesis of amino acids in the recesses of the oceanic lithosphere, *Nature*, 2018, **564**, 59–63.
22 C. F. Chyba, P. J. Thomas, L. Brookshaw and C. Sagan, Cometary Delivery of Organic Molecules to the Early Earth, *Science*, 1990, **249**, 366–373.
23 P. Ehrenfreund and S. B. Charnley, Organic Molecules in the Interstellar Medium, Comets, and Meteorites: A Voyage from Dark Clouds to the Early Earth, *Annu. Rev. Astron. Astrophys.*, 2000, **38**, 427–483.
24 V. K. Pearson, M. A. Sephton, A. T. Kearsley, P. A. Bland, I. A. Franchi and I. Gilmour, Clay mineral-organic matter relationships in the early solar system, *Meteorit. Planet. Sci.*, 2002, **37**, 1829–1833.
25 K. Kvenvolden, J. Lawless, K. Pering, E. Peterson, J. Flores, C. Ponnamperuma, I. R. Kaplan and C. Moore, Evidence for extraterrestrial amino-acids and hydrocarbons in the Murchison meteorite, *Nature*, 1970, **228**, 923–926.
26 Y. Furukawa, Y. Chikaraishi, N. Ohkouchi, N. O. Ogawa, D. P. Glavin, J. P. Dworkin, C. Abe and T. Nakamura, Extraterrestrial ribose and other sugars in primitive meteorites, *Proc. Natl. Acad. Sci. U. S. A.*, 2019, **116**, 24440–24445.
27 A. Ando and T. Shioiri, Enantioselective synthesis of β-hydroxy-α-methyl carbonyl compounds by aldol reaction, *Tetrahedron*, 1989, **45**, 4969–4988.
28 V. M. Rivilla, L. Colzi, I. Jiménez-Serra, J. Martín-Pintado, A. Megías, M. Melosso, L. Bizzocchi, Á. López-Gallifa, A. Martínez-Henares, S. Massalkhi, B. Tercero, P. de Vicente, J.-C. Guillemin, J. García de la Concepción, F. Rico-Villas, S. Zeng, S. Martín, M. A. Requena-Torres, F. Tonolo, S. Alessandrini, L. Dore, V. Barone and C. Puzzarini, Precursors of the RNA World in Space: Detection of (Z)-1,2-ethenediol in the Interstellar Medium, a Key Intermediate in Sugar Formation, *Astrophys. J.*, 2022, **929**, L11.
29 H. Sa'ad, M. P. Peppelenbosch, H. Roelofsen, R. J. Vonk and K. Venema, Biological effects of propionic acid in humans; metabolism, potential applications and underlying mechanisms, *Biochim. Biophys. Acta*, 2010, **1801**, 1175–1183.
30 S. C. Grünert, S. Müllerleile, L. de Silva, M. Barth, M. Walter, K. Walter, T. Meissner, M. Lindner, R. Ensenauer and R. Santer, Propionic acidemia: clinical course and outcome in 55 pediatric and adolescent patients, *Orphanet J. Rare Dis.*, 2013, **8**, 1–9.
31 V. V. Ilyushin, L. Margulès, B. Tercero, R. A. Motiyenko, O. Dorovskaya, E. A. Alekseev, E. R. Alonso, L. Kolesniková, J. Cernicharo and J. C. Guillemin, Submillimeter wave spectroscopy of propanoic acid (CH_3CH_2COOH) and its ISM search, *J. Mol. Spectrosc.*, 2021, **379**, 111454.
32 V. Blagojevic, S. Petrie and D. K. Bohme, Gas-phase syntheses for interstellar carboxylic and amino acids, *Mon. Not. R. Astron. Soc.*, 2003, **339**, L7–L11.
33 E. M. S. Maçôas, L. Khriachtchev, M. Pettersson, R. Fausto and M. Räsänen, Internal Rotation in Propionic Acid: Near-Infrared-Induced Isomerization in Solid Argon, *J. Phys. Chem. A*, 2005, **109**, 3617–3625.
34 W. Sander and M. Gantenberg, Aggregation of acetic and propionic acid in argon matrices—A matrix isolation and computational study, *Spectrochim. Acta, Part A*, 2005, **62**, 902–909.
35 G. Yuen, N. Blair, D. J. Des Marais and S. Chang, Carbon isotope composition of low molecular weight hydrocarbons and monocarboxylic acids from Murchison meteorite, *Nature*, 1984, **307**, 252–254.
36 R. Fuentetaja, C. Bermúdez, C. Cabezas, M. Agúndez, B. Tercero, N. Marcelino, J. R. Pardo, L. Margules, R. A. Motiyenko and J.-C. Guillemin, Discovery of CH_3CHCO in TMC-1 with the QUIJOTE line survey, *Astron. Astrophys.*, 2023, **671**, L6.
37 A. Mardyukov, R. C. Wende and P. R. Schreiner, Matrix isolation and photorearrangement of *cis*-and *trans*-1, 2-ethenediol to glycolaldehyde, *Chem. Commun.*, 2023, **59**, 2596–2599.
38 E. M. S. Macoâs, L. Khriachtchev, M. Pettersson, R. Fausto and M. Räsänen, Internal rotation in propionic acid: Near-infrared-induced isomerization in solid Argon, *J. Phys. Chem. A*, 2005, **109**, 3617–3625.
39 P. R. Schreiner, H. P. Reisenauer, D. Ley, D. Gerbig, C.-H. Wu and W. D. Allen, Methylhydroxycarbene: Tunneling Control of a Chemical Reaction, *Science*, 2011, **332**, 1300–1303.
40 P. R. Schreiner, Tunneling Control of Chemical Reactions: The Third Reactivity Paradigm, *J. Am. Chem. Soc.*, 2017, **139**, 15276–15283.
41 E. Bothe, H. Meier, D. Schulte-Frohlinde and C. von Sonntag, Rate of Acid Formation from Phenylketenes in Aqueous Solution, *Angew. Chem., Int. Ed. Engl.*, 1976, **15**, 380–381.
42 S. H. Kabir, H. R. Seikaly and T. T. Tidwell, Acid-catalyzed hydration of di-tert-butylketene, *J. Am. Chem. Soc.*, 1979, **101**, 1059–1060.
43 M. Kumar, D. H. Busch, B. Subramaniam and W. H. Thompson, Organic acids tunably catalyze carbonic acid decomposition, *J. Phys. Chem. A*, 2014, **118**, 5020–5028.
44 S. Ghoshal and M. K. Hazra, New mechanism for autocatalytic decomposition of H_2CO_3 in the vapor phase, *J. Phys. Chem. A*, 2014, **118**, 2385–2392.

2.2 The enol of isobutyric acid

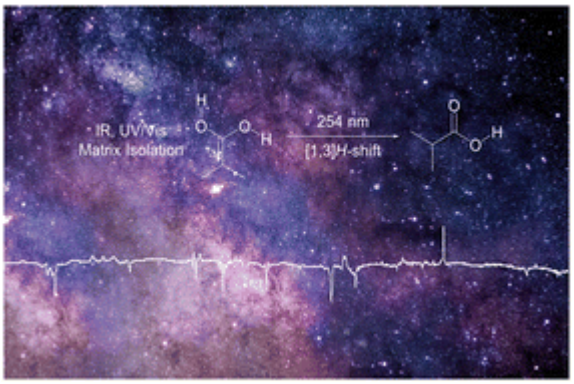

Abstract:

We present the gas-phase synthesis of 2-methyl-prop-1-ene-1,1-diol, an unreported higher energy tautomer of isobutyric acid. The enol was captured in an argon matrix at 3.5 K, characterized spectroscopically and by DFT computations. The enol rearranges likely photochemically to isobutyric acid and dimethylketene. We also identified propene, likely photochemically formed from dimethylketene.

Reference:

Akkad Danho, Artur Mardyukov and Peter R. Schreiner *Chem Commun.* **2024**, *60*, 5161-5164. (DOI: 10.1039/d4cc01140f)

Reproduced with permission from:

ChemComm

ROYAL SOCIETY OF CHEMISTRY

COMMUNICATION

View Article Online
View Journal | View Issue

Cite this: *Chem. Commun.*, 2024, **60**, 5161

Received 11th March 2024,
Accepted 15th April 2024

DOI: 10.1039/d4cc01140f

rsc.li/chemcomm

The enol of isobutyric acid†

Akkad Danho, Artur Mardyukov and Peter R. Schreiner *

We present the gas-phase synthesis of 2-methyl-prop-1-ene-1,1-diol, an unreported higher energy tautomer of isobutyric acid. The enol was captured in an argon matrix at 3.5 K, characterized spectroscopically and by DFT computations. The enol rearranges likely photochemically to isobutyric acid and dimethylketene. We also identified propene, likely photochemically formed from dimethylketene.

The exploration of interstellar media (ISM) and meteorites has unveiled a rich array of complex organic molecules, encompassing amino acids,[1] sugars,[2] purine bases,[3,4] and short peptides.[5] The identification of over 300 distinct compounds has spurred investigations into the origins of life and the fundamental chemical processes involved.[6] Under the challenging conditions of the interstellar medium (ISM), characterized by low temperatures and high dilution, the formation of highly reactive species becomes essential for prebiotic organic reactions.[7–10] While the formation mechanisms of such molecules are essentially "in the dark", they must involve activating thermodynamically stable small molecules, such as CO, CO_2, H_2O, CH_4, HCN, formaldehyde, simple alcohols, and various carboxylic acids.[11–13] While our understanding of organic chemistry thrives in controlled (wet) laboratory environments, it faces limitations when extending into the much less well-understood conditions of the ISM. One challenging aspect is that the energy for initiating chemical reactions often is concentrated in terms of time and space, and is primarily provided by stellar energy beams.[14] Hence, high-energy isomers of thermodynamically very stable molecules play a crucial role in the formation of biologically relevant compounds.[8,9,15] The remarkable discovery of glycolaldehyde only in the year 2000 represents such a molecule.[16] Its proposed formation mechanism, suggested only in 2018,[17] involves the higher energy tautomer of formaldehyde, hydroxymethylene (H–C̈–OH), engaging in a highly facile, low-barrier process ($\Delta H^{\neq} \approx 1$ kcal mol^{-1}) with H_2CO, even at the extremely low average temperature of space (~2.7 K).[18]

Enols are considered crucial intermediates in the organic chemistry in space[19–22] and several enol tautomers have been identified in the ISM. For instance, the simplest enol, vinyl alcohol (CH_2=CHOH), was discovered in the analysis of microwave emissions from Sagittarius B2.35 in 2001.[23] The gas phase stability of enols has also been validated through laboratory experiments, including those involving the enols of acetamide,[24] acetic acid,[25] glycolic acid,[26] glycolaldehyde,[27] and propionic acid.[28] In solution, enols display high reactivity and isomerize rapidly into the more thermodynamically more stable keto tautomers through bimolecular acid–base reactions.[29] In the gas phase, however, enols are considerably more stable[30] due to significant energy barriers (ranging from 40 to 45 kcal mol^{-1})[30,31] for [1,3]H-shifts. Consequently, enols can endure as long-lasting entities in the gas phase or in cold matrices, both of which model some aspects of the ISM (Scheme 1).[30]

While the existence of dimethylketene **4** in ISM has not been proven to date, the presence of related molecules including parent ketene[32] and methylketene,[33] and their role as potential intermediates in the generation of prebiotic molecules has been suggested.[25,28] That is, demonstrating the feasibility of **2**

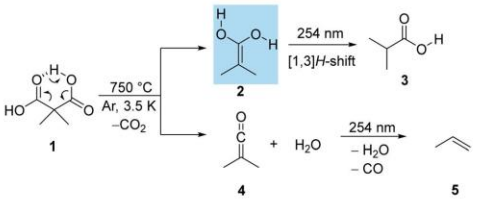

Scheme 1 2-Methyl-prop-1-ene-1,1-diol (**2**) generated from dimethylmalonic acid (**1**) through pyrolysis and trapping in an argon matrix. Subsequent photorearrangement to isobutyric acid (**3**) and dimethylketene (**4**) as well as the photorearrangement of **4** to propene (**5**).

Institute of Organic Chemistry, Justus Liebig University, Heinrich-Buff-Ring 17, Giessen 35392, Germany. E-mail: prs@uni-giessen.de

† Electronic supplementary information (ESI) available. See DOI: https://doi.org/10.1039/d4cc01140f

and **4** under conditions akin to the ISM ($T \sim 3$ K and high dilution) would encourage their identification *via* radioastronomy; our methods of preparation can readily be transferred to complementary experimental setups including microwave emission experiments. Following the approach adopted in prior studies,[25] we report here the generation of **2** alongside **4** *via* pyrolysis of dimethylmalonic acid (**1**) as the precursor. The resulting molecules are subsequently captured in an argon matrix at a temperature of 3.5 K and characterized by IR and UV/vis spectroscopy and quantum chemical computations.

Enediol **2** was synthesized through the thermal decarboxylation of **1**. This thermochemical process involved evaporating **1** at a temperature of 80 °C and subjecting it to pyrolysis in a quartz tube. We determined that the ideal pyrolysis temperature for enol generation is 750 °C; concurrently a significant amount of **4** forms as well. The pyrolysis products were subsequently condensed onto a cold matrix window at a temperature of 3.5 K, utilizing an abundant excess of argon as the condensing medium. Under these conditions, several characteristic bands were easily discernible in the spectroscopic analysis. Notably, the asymmetric CO_2 stretching vibration at 2343 cm^{-1}, the vibrational signatures corresponding to water and compound **3**, and additional infrared bands attributed to **2** were readily identifiable (Fig. 1). The identification of **3** was verified through a comparison with a matrix-isolated IR spectrum of an authenticated sample. When subjected to irradiation at 254 nm, matrix-isolated **2** underwent [1,3]H-shift leading to **3**. This transformation resulted in the disappearance of all IR absorption signals associated with **2**. Simultaneously, new IR bands emerged, corresponding to isobutyric acid (**3**) (Fig. S2, ESI†).

The experimental IR spectrum of **2** exhibits a remarkable concordance with the computed IR spectrum of **2** obtained with B3LYP/def2-TZVP computations. After repeating the experiment using deuterated d_2-**1**, the bands observed in d_2-**2** are also in good agreement with the computed spectrum; the isotopic shifts agree well. Specifically, the stretching vibration of the C=C bond at 1753 cm^{-1} exhibited a red-shift of 5 cm^{-1} (calculated: 14 cm^{-1}) in d_2-**2**. Analogously, the stretching vibrations of the OH groups in d_2-**2**, at 2986 cm^{-1} and 2949 cm^{-1}, were red-shifted by 662 cm^{-1} and 681 cm^{-1}, respectively (calculated: 684 cm^{-1} and 730 cm^{-1}). The good agreement between experimentally measured and computed shifts provides compelling evidence for the successful synthesis of **2**. In the pyrolysis IR spectrum, we also identified bands corresponding to **4**. The characteristic IR band at 2129 cm^{-1} (computed: 2183 cm^{-1}) corresponds to the CCO stretching vibration of **4** (Fig. S1, ESI†).

The UV/Vis absorption spectrum of **2** displays a broad transition at 190 nm, in agreement with the computed TD-DFT spectrum that gives λ_{max} = 192 nm. This absorption band originates from a HOMO–LUMO+3 excitation, which correlates with a $\pi \rightarrow \pi^*$ transition. In congruence with the IR experiments, the 190 nm band diminishes upon exposure to irradiation at 254 nm (Fig. 2).

As previously mentioned, pyrolysis led to the formation of **4** through the elimination of water from the enol in the gas phase. Unlike the enol tautomer of propionic acid,[28] the generation of the enol from the precursor requires high activation energy (E_a = 31.1 kcal mol^{-1} computed at B3LYP/def2-TZVP), contributing to the formation of **4**. Subsequent irradiation (λ = 254 nm) revealed the formation of propene (**5**). The distinct band at 1027 cm^{-1} can be assigned to the C=C wagging mode of **5**; likewise, additional vibrations can be attributed to **5** (Fig. S4, ESI†). One question revolves around the mechanism of formation for **5**, whether it occurs through a concerted mechanism from **4** or *via* a facile [1,2]H-shift from elusive dimethyl carbene (**6**), which may form through photochemical decarbonylation of **4**. To date, only one free alkyl carbene has been characterized, namely 2-adamantyl carbene.[34] In a previous examination of the rearrangement of **6** to propene, Evanseck and Houk theoretically estimated the activation

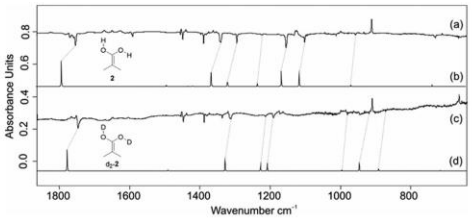

Fig. 1 IR spectra after the pyrolysis of **1**, followed by subsequent isolation in an argon matrix at 3.5 K. (a) Infrared difference spectra after irradiating **2** subsequent with a wavelength of 254 nm in an argon matrix at 3.5 K. Downward bands are attributed to **2** diminish, while bands assigned to **3** emerge after 20 min irradiation. (b) Computed infrared spectrum of **2** at B3LYP/def2-TZVP (unscaled). (c) Infrared difference spectra highlight the photoreactivity of deuterated d_2-**2** following irradiation with a wavelength of 254 nm in an argon matrix at 3.5 K. Downward bands corresponding to d_2-**2** decrease, while upward bands associated with d_2-**3** appear after 20 min of irradiation. (d) Computed infrared spectrum of deuterated d_2-**2** at B3LYP/def2-TZVP (unscaled).

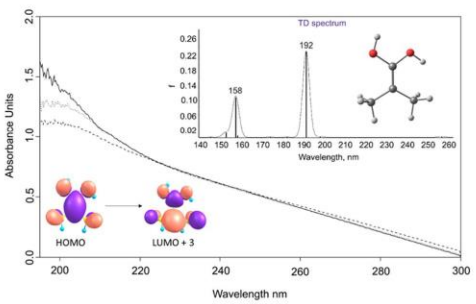

Fig. 2 Solid line: UV/vis spectrum after pyrolysis of **1**, followed by its isolation in an argon matrix at T = 3.5 K. Dotted line: The spectrum after irradiation with a wavelength of 254 nm for 6 min in an argon matrix at 3.5 K. Dashed line: The spectrum after irradiation with a wavelength of 254 nm for 20 min in an argon matrix at 3.5 K. Inset: Computed electronic transitions for **2** at TD-B3LYP/def2-TZVP.

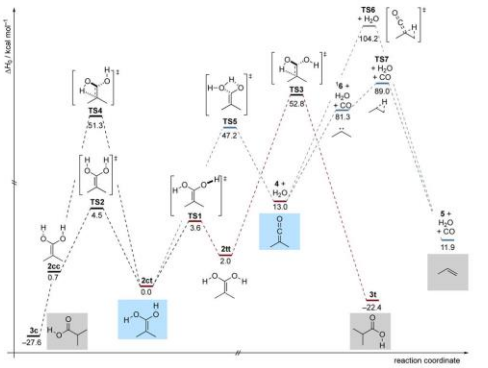

Fig. 3 Potential energy profile (ΔH_0) in kcal mol^{-1} of the reactions of dienol **2** at DLPNO-CCSD(T)/cc-pVQZ//B3LYP/def2-TZVP+ZPVE at 0 K.

energy for the [1,2]H-shift reaction to be 4.7 kcal mol^{-1}.[35] This low-energy process is probably also accompanied by some quantum mechanical tunneling (QMT) as suggested for the 1,2-hydrogen shift in methylchlorocarbene (in solution),[36] a conclusion that would probably also hold for pure alkyl carbenes, thereby making their isolation even more challenging. As deuteration should slow QMT quite significantly, we also used d_6-**1** in an attempt to isolate d_6-**6**, which, however, remained elusive, despite a somewhat higher computed barrier of 7.7 kcal mol^{-1}.

To gain deeper insight into the thermochemistry of **2**, we performed computations on the potential energy profile around **2** at DLPNO-CCSD(T)/cc-pVQZ//B3LYP/def2-TZVP+ZPVE at 0 K (ΔH_0). Our computations reveal that **2** can exist in three distinct conformations, characterized by the orientations of the OH groups relative to the opposing C–O bond. These conformations are referred to as: s-*cis*, s-*trans* **2ct**, s-*trans*, s-*trans* **2tt** and s-*cis*, s-*cis* **2cc**. Among these conformers, **2ct** is the most stable, with **2cc** and **2tt** being higher in energy by 0.7 and 2.0 kcal mol^{-1} (Fig. 3), respectively. The conformational isomerization from **2ct** to **2tt** involves an activation energy (**TS1**) of 3.6 kcal mol^{-1}, while the activation energy for the **2ct** to **2cc** rotamerization is 4.5 kcal mol^{-1} (**TS2**). In our FVP experiments, **2ct** is the predominant conformer in the matrix. Even with d_2-**1**, no other conformer of **2** besides **2ct** was observed. This is likely due to rapid (on the time scale of our experiments) QMT rotamerization, which is typical for OH groups.[25–27] From the **2tt** conformer, propionic acid conformer **3t** can be generated through a [1,3]H-shift, which is associated with an activation barrier of 50.8 kcal mol^{-1} (**TS3**). The tautomerization from **2ct** to **3c** (the most thermodynamically stable conformer) involves an activation barrier of 51.3 kcal mol^{-1} (**TS4**). Apart from keto–enol tautomerization to **3c**, **2ct** can also dehydrate into **4** (**4** + H_2O) through transition state **TS5**, with an energy barrier of 47.2 kcal mol^{-1}. Besides rapid rotation around the C–O bond, **2** exhibits limited reactivity due to the high and broad energy barriers surrounding it on its potential energy profile.[37] This is demonstrated by the unchanged infrared bands of **2ct** and d_2-**2ct** when stored in the dark at 3.5 K for five days. As expected, under our pyrolysis reaction conditions, **4** readily formed. Fig. S1 (ESI†) reveals the emergence of **5** most likely originating from a concerted mechanism involving both a [1,2]H-shift and CO release from the ketene through **TS6**, featuring an activation barrier of 91.2 kcal mol^{-1}. Given that this formation exclusively depends on irradiation and is associated with an excessively high activation barrier, it is apparent that **5** is exclusively accessible photochemically. It is also possible for the ketene to undergo a conversion to singlet carbene ^{1}**6**, releasing CO upon photoexcitation. Carbene ^{1}**6** reacts to form propene through a [1,2]H-shift (**TS7**), facilitated by its low activation barrier 7.7 kcal mol^{-1} (which is also prone to QMT, *vide supra*). We can therefore not differentiate between the two photochemical paths and **6** remains elusive.

Our results underscore the facile synthesis of acid tautomers in the gas phase, in particular, in the first preparation of **2** and its characterization by IR and UV/Vis spectroscopies as well as quantum chemical computations. Enol **2** therefore also constitutes a detectable interstellar gas-phase molecule. In the ISM, **2** may be accessible through the exothermic addition (by 13.0 kcal mol^{-1}, Fig. 3) of water (*e.g.*, on ice grains) to **4**. While **4** has not been identified in the ISM yet, the presence of parent ketene[32] and very closely related methyl ketene[33] has been confirmed. Finally, we also reveal the formation of propene, most likely through a photochemical mechanism from **4**.

This project has received funding from the European Research Council (ERC) under the European Union's Horizon 2020 research and innovation programme (Advanced Grant No. 101054751 "COLDOC" to PRS). Views and opinions expressed are those of the authors only and do not necessarily reflect those of the European Union or the European Research Council. Neither the European Union nor the granting authority can be held responsible for them.

Conflicts of interest

There are no conflicts to declare.

Notes and references

1 K. Kvenvolden, J. Lawless, K. Pering, E. Peterson, J. Flores, C. Ponnamperuma, I. R. Kaplan and C. Moore, Evidence for Extraterrestrial Amino-acids and Hydrocarbons in the Murchison Meteorite, *Nature*, 1970, **228**(5275), 923–926.
2 Y. Furukawa, Y. Chikaraishi, N. Ohkouchi, N. O. Ogawa, D. P. Glavin, J. P. Dworkin, C. Abe and T. Nakamura, Extraterrestrial ribose and other sugars in primitive meteorites, *Proc. Natl. Acad. Sci. U. S. A.*, 2019, **116**(49), 24440–24445.
3 M. P. Callahan, K. E. Smith, H. J. Cleaves, J. Ruzicka, J. C. Stern, D. P. Glavin, C. H. House and J. P. Dworkin, Carbonaceous meteorites contain a wide range of extraterrestrial nucleobases, *Proc. Natl. Acad. Sci. U. S. A.*, 2011, **108**(34), 13995–13998.
4 P. G. Stoks and A. W. Schwartz, Uracil in carbonaceous meteorites, *Nature*, 1979, **282**(5740), 709–710.
5 A. Shimoyama and R. Ogasawara, Dipeptides and Diketopiperazines in the Yamato-791198 and Murchison Carbonaceous Chondrites, *Origins Life Evol. Biospheres*, 2002, **32**(2), 165–179.
6 **https://cdms.astro.uni-koeln.de/classic/molecules**. (accessed March 05, 2024).

7 S. L. Miller and H. C. Urey, Organic Compound Synthesis on the Primitive Earth, *Science*, 1959, **130**(3370), 245–251.
8 J. L. Bada, New insights into prebiotic chemistry from Stanley Miller's spark discharge experiments, *Chem. Soc. Rev.*, 2013, **42**(5), 2186–2196.
9 G. M. Muñoz Caro, U. J. Meierhenrich, W. A. Schutte, B. Barbier, A. Arcones Segovia, H. Rosenbauer, W. H. P. Thiemann, A. Brack and J. M. Greenberg, Amino acids from ultraviolet irradiation of interstellar ice analogues, *Nature*, 2002, **416**(6879), 403–406.
10 K. Ruiz-Mirazo, C. Briones and A. de la Escosura, Prebiotic systems chemistry: new perspectives for the origins of life, *Chem. Rev.*, 2014, **114**(1), 285–366.
11 C. R. Arumainayagam, R. T. Garrod, M. C. Boyer, A. K. Hay, S. T. Bao, J. S. Campbell, J. Wang, C. M. Nowak, M. R. Arumainayagam and P. J. Hodge, Extraterrestrial prebiotic molecules: photochemistry *vs.* radiation chemistry of interstellar ices, *Chem. Soc. Rev.*, 2019, **48**(8), 2293–2314.
12 W. M. Irvine, Extraterrestrial Organic Matter: A review, *Origins Life Evol. Biospheres*, 1998, **28**(4), 365–383.
13 J. M. Hollis, F. J. Lovas, A. J. Remijan, P. R. Jewell, V. V. Ilyushin and I. Kleiner, Detection of Acetamide (CH_3CONH_2): The Largest Interstellar Molecule with a Peptide Bond, *Astrophys. J.*, 2006, **643**(1), L25.
14 C. R. Arumainayagam, R. T. Garrod, M. C. Boyer, A. K. Hay, S. T. Bao, J. S. Campbell, J. Wang, C. M. Nowak, M. R. Arumainayagam and P. J. Hodge, Extraterrestrial prebiotic molecules: photochemistry vs. radiation chemistry of interstellar ices, *Chem. Soc. Rev.*, 2019, **48**(8), 2293–2314.
15 S. L. Miller and H. C. Urey, Organic compound synthesis on the primitive Earth: Several questions about the origin of life have been answered, but much remains to be studied, *Science*, 1959, **130**(3370), 245–251.
16 J. M. Hollis, F. J. Lovas and P. R. Jewell, Interstellar Glycolaldehyde: The First Sugar, *Astrophys. J.*, 2000, **540**(2), L107.
17 A. K. Eckhardt, M. M. Linden, R. C. Wende, B. Bernhardt and P. R. Schreiner, Gas-phase sugar formation using hydroxymethylene as the reactive formaldehyde isomer, *Nat. Chem.*, 2018, **10**(11), 1141–1147.
18 P. R. Schreiner, H. P. Reisenauer, F. C. T. Pickard, A. C. Simmonett, W. D. Allen, E. Mátyus and A. G. Császár, Capture of hydroxymethylene and its fast disappearance through tunnelling, *Nature*, 2008, **453**(7197), 906–909.
19 B. Ménez, C. Pisapia, M. Andreani, F. Jamme, Q. P. Vanbellingen, A. Brunelle, L. Richard, P. Dumas and M. Réfrégiers, Abiotic synthesis of amino acids in the recesses of the oceanic lithosphere, *Nature*, 2018, **564**(7734), 59–63.
20 C. F. Chyba, P. J. Thomas, L. Brookshaw and C. Sagan, Cometary delivery of organic molecules to the early Earth, *Science*, 1990, **249**, 366–373.
21 P. Ehrenfreund and S. B. Charnley, Organic Molecules in the Interstellar Medium, Comets, and Meteorites: A Voyage from Dark Clouds to the Early Earth, *Annu. Rev. Astron. Astrophys.*, 2000, **38**(1), 427–483.
22 V. K. Pearson, M. A. Sephton, A. T. Kearsley, P. A. Bland, I. A. Franchi and I. Gilmour, Clay mineral-organic matter relationships in the early solar system, *Meteorit. Planet. Sci.*, 2002, **37**(12), 1829–1833.
23 B. E. Turner and A. J. Apponi, Microwave detection of interstellar vinyl alcohol, CH_2=CHOH, *Astrophys. J.*, 2001, **561**(2), L207.
24 A. Mardyukov, F. Keul and P. R. Schreiner, Preparation and characterization of the enol of acetamide: 1-aminoethenol, a high-energy prebiotic molecule, *Chem. Sci.*, 2020, **11**(45), 12358–12363.
25 A. Mardyukov, A. K. Eckhardt and P. R. Schreiner, 1,1-Ethenediol: The Long Elusive Enol of Acetic Acid, *Angew. Chem., Int. Ed.*, 2020, **59**(14), 5577–5580.
26 A. Mardyukov, F. Keul and P. R. Schreiner, 1,1,2-Ethenetriol: The Enol of Glycolic Acid, a High-Energy Prebiotic Molecule, *Angew. Chem., Int. Ed.*, 2021, **60**(28), 15313–15316.
27 A. Mardyukov, R. C. Wende and P. R. Schreiner, Matrix isolation and photorearrangement of *cis*- and *trans*-1,2-ethenediol to glycolaldehyde, *Chem. Commun.*, 2023, **59**(18), 2596–2599.
28 A. Danho, A. Mardyukov and P. R. Schreiner, The enol of propionic acid, *Chem. Commun.*, 2023, **59**, 11524–11527.
29 K. H. Meyer, Über das Gleichgewicht desmotroper Verbindungen in verschiedenen Lösungsmitteln (Über Keto-Enol-Tautomerie. IX), *Ber. Dtsch. Chem. Ges.*, 1914, **47**(1), 826–832.
30 C. A. Taatjes, N. Hansen, A. McIlroy, J. A. Miller, J. P. Senosiain, S. J. Klippenstein, F. Qi, L. Sheng, Y. Zhang and T. A. Cool, Enols are common intermediates in hydrocarbon oxidation, *Science*, 2005, **308**(5730), 1887–1889.
31 N. F. Kleimeier and R. I. Kaiser, Interstellar Enolization-Acetaldehyde (CH_3CHO) and Vinyl Alcohol ($H_2CCH(OH)$) as a Case Study, *ChemPhysChem*, 2021, **22**(12), 1229–1236.
32 B. Turner, Microwave detection of interstellar ketene, *Astrophys. J.*, 1977, **213**, L75–L79.
33 C. Bermúdez, B. Tercero, R. Motiyenko, L. Margulès, J. Cernicharo, Y. Ellinger and J.-C. Guillemin, The millimeter-wave spectrum of methyl ketene and the astronomical search for it, *Astron. Astrophys.*, 2018, **619**, A92.
34 T. Bally, S. Matzinger, L. Truttmann, M. S. Platz and S. Morgan, Matrix Spectroscopy of 2-Adamantylidene, a Dialkylcarbene with Singlet Ground State, *Angew. Chem., Int. Ed. Engl.*, 1994, **33**(19), 1964–1966.
35 K. Raghavachari, R. A. Whiteside, J. A. Pople and P. V. R. Schleyer, Molecular orbital theory of the electronic structure of organic molecules. 40. Structures and energies of C_1–C_3 carbocations including effects of electron correlation, *J. Am. Chem. Soc.*, 1981, **103**(19), 5649–5657.
36 E. J. Dix, M. S. Herman and J. L. Goodman, The 1,2-hydrogen rearrangement of methylchlorocarbene: contribution of quantum mechanical tunneling, *J. Am. Chem. Soc.*, 1993, **115**(22), 10424–10425.
37 D. Ley, D. Gerbig and P. R. Schreiner, Tunnelling control of chemical reactions – the organic chemist's perspective, *Org. Biomol. Chem.*, 2012, **10**(19), 3781–3790.

3. Unpublished Results

3.1 Cage Alkyl Carbenes Provide Experimental Evidence for Isotope Controlled Selectivity

Akkad Danho, Bastian Bernhardt, Dennis Gerbig, Marija Alešković, and Peter R. Schreiner *J. Am. Chem. Soc.* **2025**, Revision submitted on 10 February 2025. Published in ChemRxiv on 17 December 2024. DOI: 10.26434/chemrxiv-2024-qb4mt.

3.1.1 Abstract

We report the gas-phase synthesis and reactivity of adamantylidene (**1**) and pentacyclo[5.4.0.0^{2,6}.0^{3,10}.0^{5,9}]undecanylidene (**2**). The latter previously unreported carbene, is persistent under cryogenic conditions and has been characterized spectroscopically. The singlet carbenes were generated through irradiation of their corresponding diazirine precursors followed by trapping the products in argon or nitrogen matrices at 3.5 K. Analyses using IR and UV/Vis spectroscopy, together with density functional theory computations provide strong evidence for the successful preparation of these reactive species. Carbene **1** (ΔE_{ST} = –3.0 kcal mol^{-1}) undergoes a slow hitherto unreported but theoretically predicted quantum mechanical tunneling (QMT) C–H-bond insertion and ring-closure to 2,4-dehydroadamantane (**4**). In contrast, **2** (ΔE_{ST} = –5.2 kcal mol^{-1}) remains unchanged under cryogenic conditions but rearranges to homohypostrophene (**9**) upon λ = 627 nm irradiation. Attempts to prepare protoadamantylidene (**3**) (ΔE_{ST} = –5.1 kcal mol^{-1}) in a similar fashion did not allow the direct observation of the free carbene, but enabled follow-up QMT reactions, whose selectivities are determined by the ^{1}H and ^{2}H isotopologs, thereby demonstrating isotope-controlled selectivity (ICS).

3.1.2 Introduction

Isotope-controlled selectivity (ICS) is defined as a molecular system where one of two conceivable products both resulting from a quantum mechanical tunneling (QMT) reaction from the same starting material forms predominantly, only depending on isotopic

composition.[1] This novel concept of controlling reactivity has been theoretically predicted[1] but not been demonstrated experimentally. Here we investigate the effect of isotopic substitution (hydrogen vs. deuterium) in the reactivity of singlet protoadamantylidene and provide spectroscopic evidence for the formation of different products as a result of ICS. This work is organized to highlight important revelations and unexpected challenges associated with our quest of finding a cage carbene system that would demonstrate ICS, and to underscore that even structurally very similar systems can have quite varying reactivity when QMT operates.

Singlet alkyl carbenes are highly unstable, with only a few spectroscopic reports available, including di-*tert*-butylcarbene,[2] diadamantylcarbene,[3] dicyclopropylcarbene,[4] and adamantylidene[5] (**1**, Figure 1). The majority of research into these carbenes stems from computational and theoretical studies.[6] Beyond methylene (which has a triplet ground state), singlet ethylidene represents the simplest alkyl carbene, which, however, undergoes a very facile [1,2]H-shift; despite multiple attempts, the direct spectroscopic characterization of ethylidene has remained elusive.[7-14] Analogs such as 2,2,2-trifluoroethylidene[15] have been generated and characterized in noble gas matrices at low temperatures. Carbenes including norbornen-7-ylidene,[16-17] cyclobutylidene,[17] and tricyclooct-8-ylidene[18] have all been investigated theoretically. Such so-called foiled carbenes[19-20] display a combination of through-space interactions, non-classical bonding, and hyperconjugative interaction.[21] Apart from fast 1,2-shifts, cyclic singlet carbenes may also undergo ring expansion by heavy-atom QMT through C–C or C–H bond insertion reactions.[22-23] Heavy-atom QMT is less common,[24] owing to the mass dependence of the tunneling rate, which typically results in significantly extended tunneling half-lives unless the reaction barrier is narrow.[25] Examples of reactions involving carbon tunneling include automerizations of cyclobutadiene,[26] 1,5-dimethylsemibullvalene,[27] and the ring closure of cyclopentane-1,3-diyl.[28] As QMT half-lives depend profoundly on particle mass but even more so on barrier height and width,[25] computational predictions require a suitable potential energy hypersurface (PES). Canonical Variational Transition State Theory (CVT)[29] corrected for small-curvature tunneling (SCT)[30] in conjunction with density functional theory (DFT)[31-32] provides results in reasonably good agreement with experiment.[33]

Alkyl carbene **1** was first isolated and spectroscopically characterized using the matrix isolation technique by Bally and Platz *et al.*.[5] In 2014, Kozuch *et al.* studied the tunneling reactivity of **1** and calculated a tunneling half-life of 62.2 h at the CVT/SCT//B3LYP/6-31G(d,p) level of theory.[22] While Bally and Platz *et al*.[5] observed the rearrangement of **1** to dehydroadamantane (**4**) upon UV irradiation, they (unintentionally) did not wait long enough to also observe its reactivity in the dark. As such, we sought to experimentally examine the predicted QMT ring closure reaction of **1** to **4** in the dark, and to take this QMT reactivity as a model for possibly observing ICS with a carbene. As we will outline, **1** proved not to be suitable for this purpose, even though it does show the predicted QMT reactivity, because alternative rearrangements pathways are not competitive. We then investigated pentacyclo[5.4.0.0^{2,6}.0^{3,10}.0^{5,9}]-undecanylidene (PCU-carbene) (**2**), also a cage structure, with the hope that it would undergo competing QMT reactivity.[34] Surprisingly, **2** does *not* display observable QMT reactivity because it is unexpectedly stable under our conditions, most likely due to stabilization through a carbene-carbon-nitrogen complex, which hinders QMT.[35-36] We finally arrived at protoadamantylidene

(**3**), an isomer of **1** that has rather short QMT half-lives, but does demonstrate H/D-ICS in competing QMT reactions.

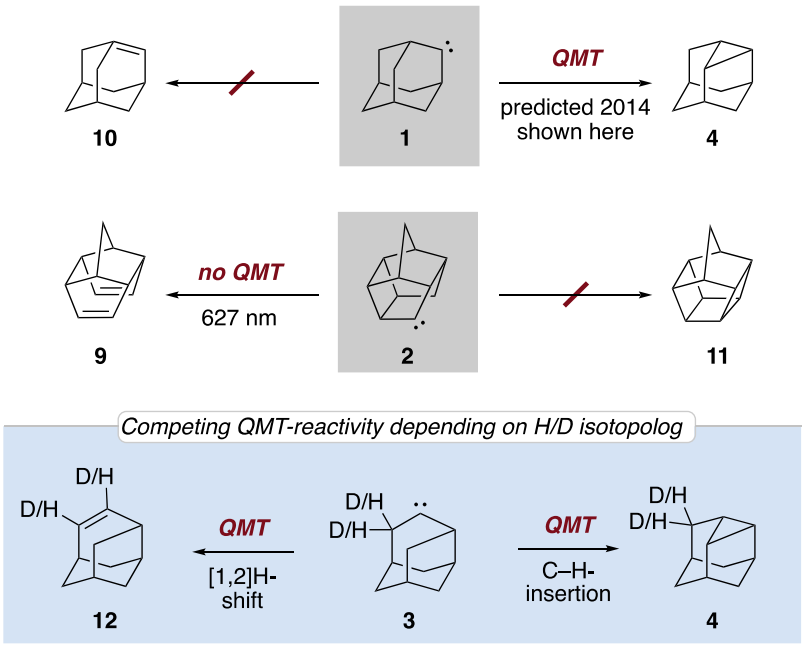

Figure 1. Outlining the hitherto unreported reactivities of known carbene **1** and the reactivities of novel carbenes **2** and **3**.

3.1.3 Results and Discussion

Adamantane diazirine (**5**) and pentacyclo[5.4.0.0^{2,6}.0^{3,10}.0^{5,9}]undecan-8-diazirine (PCU-diazirine **6**, Figure 2) were synthesized according to literature procedures from the corresponding ketones **7** and **8**.[5, 37] Due to their high volatility **5** and **6** could easily be evaporated onto the cold matrix window using an excess of argon as the host gas.

Our matrix-IR spectrum of **5** is in excellent agreement with reported data[5] (see Supporting Information, SI, for matrix IR spectra and signal assignments). Upon irradiation with 365 nm, matrix-isolated **5** and **6** undergo a series of reactions, resulting in the formation of **1** and **2**, and leading to the concomitant disappearance of all IR absorptions assigned to **5** and **6**. In parallel, new IR bands corresponding to **1** and **2** emerged (Fig. S23 and S24). The experimentally observed IR spectra of **1** and **2** match well the computed IR spectra at B3LYP/6-311++G(3df,2pd). Due to the overlapping of most bands above 1500 cm^{-1}, the assignments are difficult. In the range of 1500-600 cm^{-1}, cage vibrations dominate, with very weak intensities as compared to the stretching vibrations.

In extension to the previous study by Bally and Platz *et al.*, **1**,[5] we found that over the course of several hours the bands of **1** gradually disappeared (in the dark) while those of **4** slowly emerged (Fig. S24). The observed reactivity of **1** under these experimental conditions with a half-life of 6 h can only be explained by QMT, in line with the prediction by Kozuch[22] and our computational data (*vide infra*). Carbene **1**, generated from irradiation of **5** at 365 nm, exhibits a UV/Vis spectrum with an absorption maximum at around 610 nm (Fig. 2a). After 18 h in the dark, this UV/Vis signal disappears

completely, confirming the QMT reactivity observed also in the IR spectra. Only **4** was obtained, rendering **1** unsuitable for the investigation of ICS. Consequently, our attention shifted to **2**, because the precursor materials can as easily be synthesized as for **1**.

To our surprise, **2**, generated from **6** by 365 nm irradiation, did *not* display QMT reactivity even after several days in the dark; this strongly indicates that **2** is persistent under cryogenic conditions. Only after irradiating **2** with 627 nm light, we observed the disappearance of the bands of **2** and the simultaneous appearance of bands corresponding to homohypostrophene (**9**). This excludes **2** from experiments related to ICS. In moving forward, however, we had to first understand the QMT behavior of **1** and **2** to identify a suitable cage carbene.

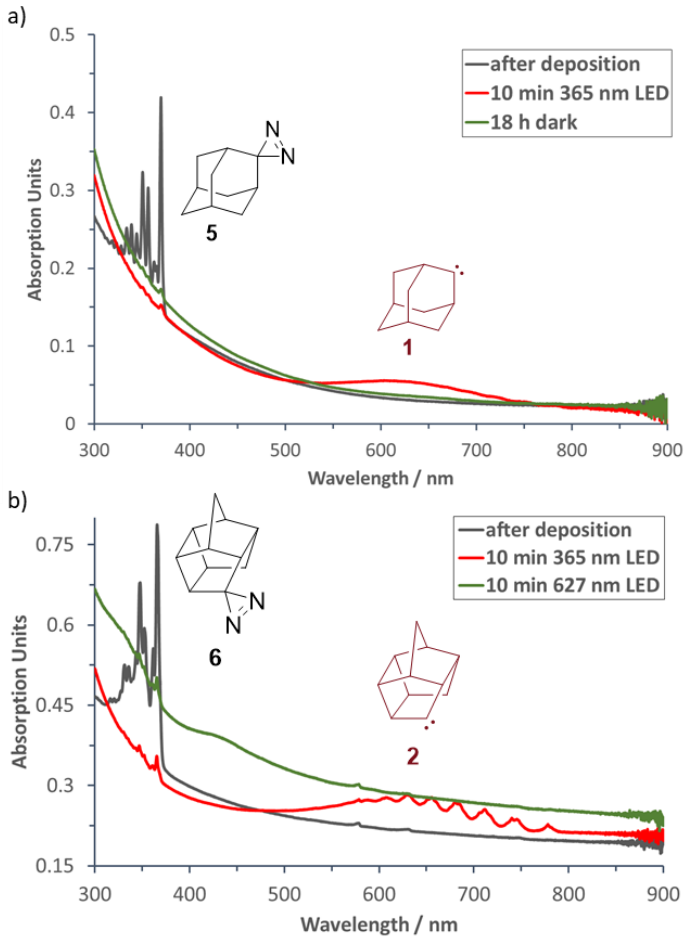

Figure 2. Experimental UV/Vis spectra. A): The spectra of **5** (black) and **1** (red) are in good agreement with literature data.[5] Carbene **1** vanishes when keeping the matrix in the dark for 18 h (green). B): Analogous spectra were recorded before (black) and after (red) irradiation of **6**. However, **2** is persistent and its fine-structured UV/Vis absorption (red) only vanishes (green) when the matrix is irradiated at 627 nm.

To understand the different QMT reactivities of **1** and **2**, we conducted a detailed analysis of their intrinsic reaction coordinates (IRC) for the QMT pathways using the UB3LYP/6-31G(d) level of theory (Figure 3), according to Kozuch *et al.*[22] Concurrently, we employed CVT/SCT[29-30] to compute the half-lives (τ) for these reactions at the same level of theory, which enabled us to quantitatively assess the likelihood of QMT occurring under our experimental conditions. For the **1** → **4** C–H bond insertion reaction, the

computed half-life of 20 h agrees well with the experimental value. At UB3LYP/6-31G(d) the reaction leading towards *anti*-Bredt adamantene[38] (**10**) gives a computed half-life of $> 9 \times 10^{22}$ h, indicating that this reaction is not competitive (Figure 3A); indeed, **10** was not detectable in our experiments. This also implies that ICS cannot be studied with **1**.

In comparing the IRCs for the **2** → **9** and **2** → **11** rearrangements (Figure 3a), it is evident that the former reaction involves a much lower energy barrier of 14.8 kcal mol^{-1}, favoring the reaction to **9**; this barrier can readily be surpassed by irradiation at 627 nm (45.6 kcal mol^{-1}), leading to **9**. Still, QMT reactivity was not experimentally observed for **2**, even though the computations indicate a very short QMT half-life for the reaction to **9** (7.1×10^{-9} h) and no QMT for the reaction to **11** ($> 8 \times 10^{11}$ h). As noted above, we reasoned that **2** is stabilized through a complex with N_2 that is trapped (from precursor **6**) in the same matrix site; the effects on the spectroscopy for such complexes, which have been reported before, are small.[35-36] Hence, we needed a system that has a *lower* and *thinner* barrier and would show QMT behavior in the right time interval. We turned our attention to hitherto also unreported carbene **3**, which is an isomer of **1** that may show the right reactivity.

According to our UB3LYP/6-31G(d) computations, the half-life for the C–H insertion reaction of **3** to **4** is 4×10^{-9} h while the half-life for the competing [1,2]H shift to **12** is 3×10^{-4} h (Figure 3b). These values suggest that the C–H insertion occurs much more readily than the [1,2]H shift, thus favoring the formation of **4** as the dominant product in the protio-case. The extremely short half-lives of **3** in either reaction means, however, that the free carbene cannot be observed directly under our matrix isolation conditions, and that we must rely on product analysis.

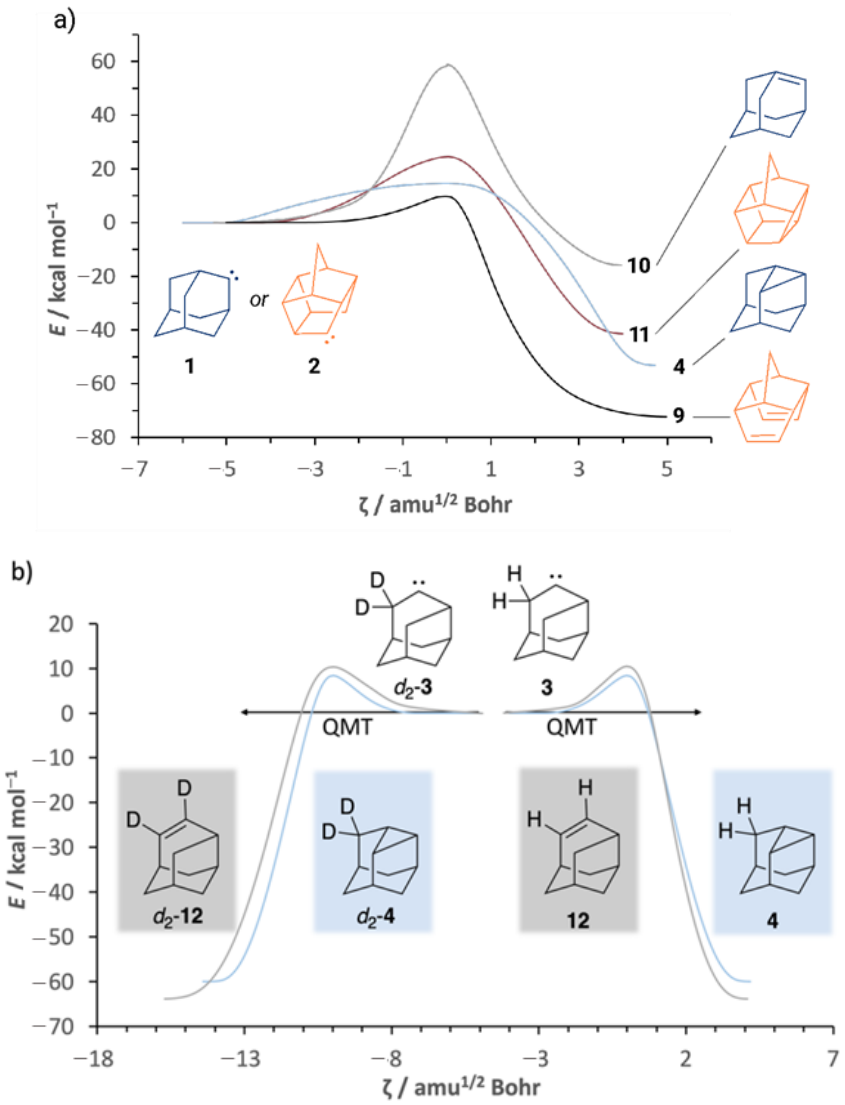

Figure 3. Intrinsic reaction coordinates for the cage alkyl carbenes of the present study computed at the UB3LYP/def2-TZVPP level of theory.

To generate **3**, we initially irradiated the precursor diazirine (**13**) at 365 nm, leading to its expected and well-known rearrangement into the diazo form,[39-40] as observed in similar molecules.[34] As this intermediate absorbs at the same wavelength (254 nm) as the carbene (as judged from the computed UV spectrum), this route had to be abandoned. Instead, we generated **3** via high vacuum flash pyrolysis (HVFP) which also alleviates the potential complexation with matrix-trapped N_2 and recorded the typical carbene follow-up reactions leading to products **4** and **12**, whose ratio depending on isotopic substitution should then reveal whether ICS does occur.

The determination of the product ratios of the reactions of **3** to investigate ICS is based on identifying the characteristic IR bands (Figure 4) and the corresponding, red-shifted bands of the isotopolog. Specifically, the strongest vibrational signal for each product was identified and integrated. To accurately compare the isotopolog ratios, a correction factor was applied. This factor was derived from the computed intensity ratios of the vibrational signals in the deuterated and parent molecules, allowing for direct comparison between the undeuterated and deuterated peaks. The experimental intensities were then

normalized using the correction factor (Tables S3-S6), ensuring that the observed data accurately reflect the underlying reaction dynamics. The intensities obtained for the H- and D-isotopologs were subsequently used to calculate the selectivity between the competing reactions (Tables S3-S6).

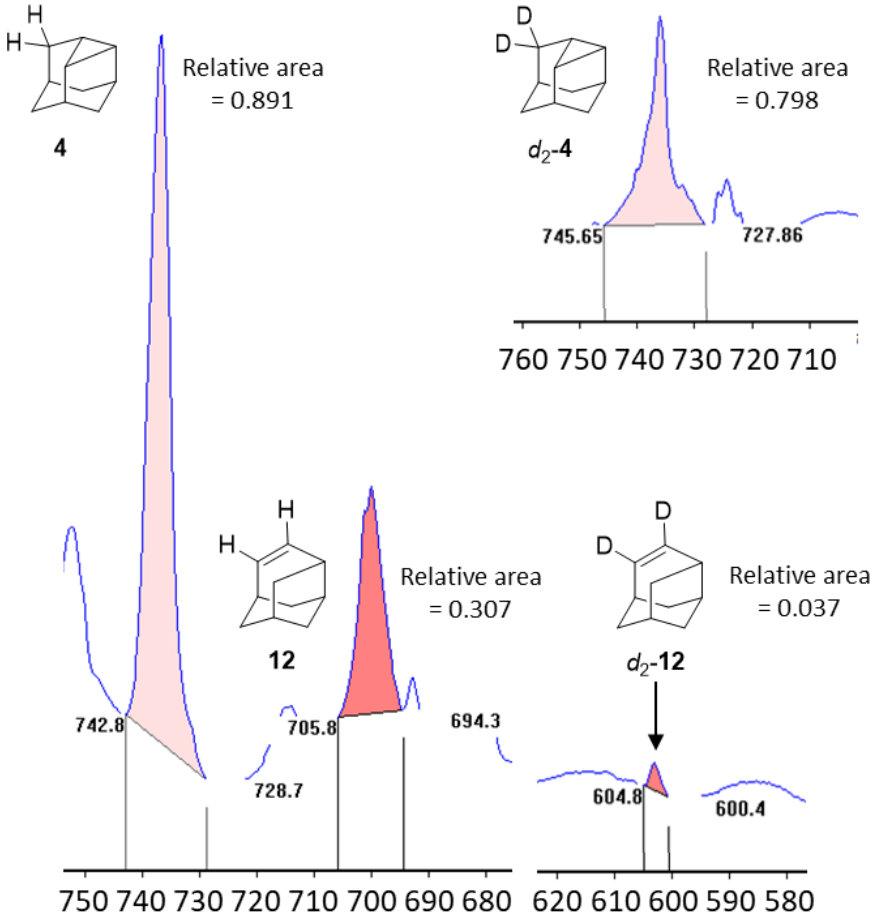

Figure 4. Representative IR spectra showing the pyrolysis products of protoadamantane diazirine (**13**) and d_2-protoadamantane diazirine (d_2-**13**), each trapped in an argon matrix at 3.5 K. The spectra were analyzed by integrating the peaks to determine the product distribution.

As evident from the IR spectrum after HVFP, conducted three times for both H-/D-isotopologs (Figures S35 and S37), the product distribution shows a ratio of 2:1 favoring **4** (Figure 5). Substituting hydrogen with deuterium at the α-position of **13**, leading to intermediate carbene d_2-**3**, changed the product ratio to 20:1, favoring d_2-**4**, which was also qualitatively predicted computationally (Table S27 and S28). The markedly different product ratios highlight the significant impact of deuterium substitution, providing strong evidence for ICS.

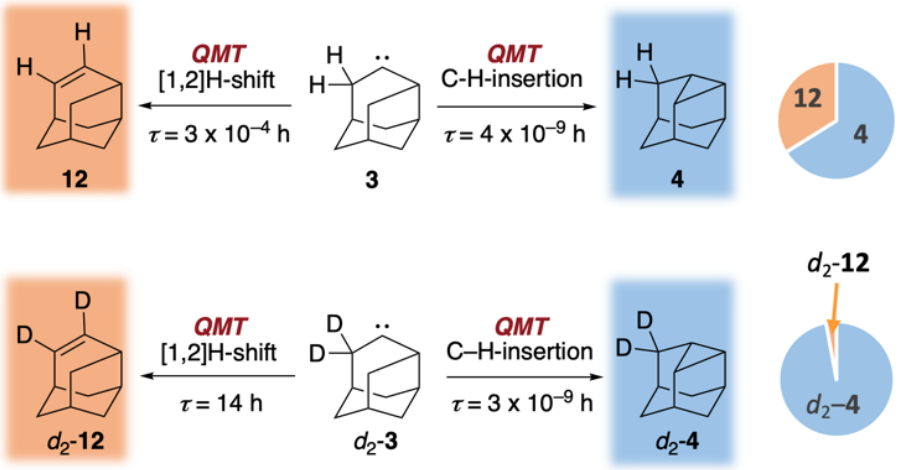

Figure 5. Reactivity of matrix isolated of **3** and d_2-**3** after pyrolysis at 800 °C, with calculated half-lives at the UB3LYP/6-31G(d) level of theory at 10 K.

3.1.4 Conclusion

In conclusion, we generated three cage alkyl carbenes to test their suitability to provide evidence for ICS. Known carbene **1** underwent a QMT reaction as computationally predicted, with a half-life of 6 h, while **2** unexpectedly remained stable under cryogenic conditions but rapidly rearranged to **9** upon 627 nm irradiation. Much more reactive and closely related carbene **3** was generated *in situ* and *α*-deuterium substitution of the diazirene precursor significantly altered the ratio of the [1,2]H-shift vs. C–H-insertion products, thereby providing the first experimental evidence of isotope-controlled selectivity.

3.1.5 Experimental Section

General Information

All chemicals were purchased from Sigma Aldrich, Carl Roth, Acros Organics, or TCI in the highest purity grade possible and used without further purification. All solvents were distilled prior to use. If necessary, reactions were carried out under argon atmosphere using standard Schlenk techniques. Dry solvents were ordered from Acros Organics (H_2O <50 ppm). Analytical thin-layer chromatography was performed on plastic-backed silica gel 60 plates coated with a fluorescence indicator by Macherey Nagel. Visualization was performed by UV light (254 nm) and/or ceric ammonium molybdate (CAM) stain (180 mL H_2O, 5 g ammonium molybdate tetrahydrate, 2 g cerium ammonium sulfate dihydrate, 20 mL conc. H_2SO_4). Reaction control was performed via TLC-MS by an Advion expression® CMS or GC-MS analysis (Agilent 7820 GC with 5977B MSD). High resolution masses were obtained on a Bruker MicrOTof or Bruker Impact II. Nuclear Magnetic Resonance Spectra were recorded on a Bruker AV 400, AV 400 HD, or AV 600 spectrometer at 298 K. Chemical shifts in ppm are reported relative to the residual $CDCl_3$ signal (7.26 ppm / 77.16 ppm). Signal multiplicities are reported as

follows: s – singlet, br s – broad singlet, d – doublet, t – triplet, q – quartet, hept – septet, m – multiplet or combinations thereof. All spectral data are reported based on appearance.

Matrix Apparatus Design. A Sumitomo cryostat system consisting of an RDK 408D2 closed-cycle refrigerator cold head and an F-70 compressor unit was used for matrix isolation experiments. A polished CsI window was mounted in the cold head sample holder. The sample holder, connected with silicon diodes for temperature measurements, was covered by a vacuum shroud, which was equipped with KBr windows to allow for IR measurements. In some experiments BaF_2 windows were used due to their higher transparency when measuring UV/vis spectra. The sample and the host gas (Ar, purity of 99.999%) were co-deposited at 3.5 K. All spectral data were collected at 3.5 K. The pyrolysis zone was equipped with a heatable 90 mm long quartz tube (inner diameter 7 mm), controlled by a Ni/CrNi thermocouple. The travel distance of the sample from the pyrolysis zone to the matrix was ∼45 mm. Ar was stored in a 2 L gas balloon, which was evacuated and filled three times before every experiment. The samples were evaporated from a Schlenk tube at –20 °C (EtOH and dry ice) and reduced pressure (∼3×10^{-6} mbar) and co-deposited with a high excess of argon for **5**, **6**, and **11** and nitrogen for **13** und d_2-**13** on both sides of the matrix window in the dark (preventing unwanted photochemistry) at a rate of ∼1 mbar min^{-1}, based on the pressure inside the Ar/N_2 balloon. Pyrolyses were carried out at 800 °C. IR spectra were recorded between 7000 and 350 cm^{-1} with a resolution of 0.7 cm^{-1} on Bruker Vertex 70 FTIR spectrometer. A spectrum of the cold matrix window before deposition was used as background spectrum for the subsequent IR measurements. Kinetic IR measurements were taken every half h for 48 h. UV/Vis spectra were recorded between 190 and 800 nm with a resolution of 1 nm with a Jasco V-760 spectrophotometer. A high-pressure-mercury lamp equipped with a monochromator (LOT Quantum Design) or a low-pressure-mercury lamp (Gräntzel) fitted with a Vycor filter were used for irradiation of the matrix during photochemical experiments.

Computations. All DFT computations were performed with the Gaussian16, Revision C.01 (full citations for electronic structure codes are given at the end of this document) at the B3LYP/6-311++G(3df,2pd) and B3LYP/def2-TZVPP[41-42] level of theory. The keywords Opt and Freq=NoRaman were used for the characterization of minima on the PES. For transition structures the keyword Opt=(ts,tight,calcfc,noeigen) was used. UV/Vis absorptions were computed by using the keyword td(50-50,nstates=10). The reaction rates were computed using the multidimensional, small-curvature tunneling (SCT) method,[43] implemented in the program *Polyrate*.

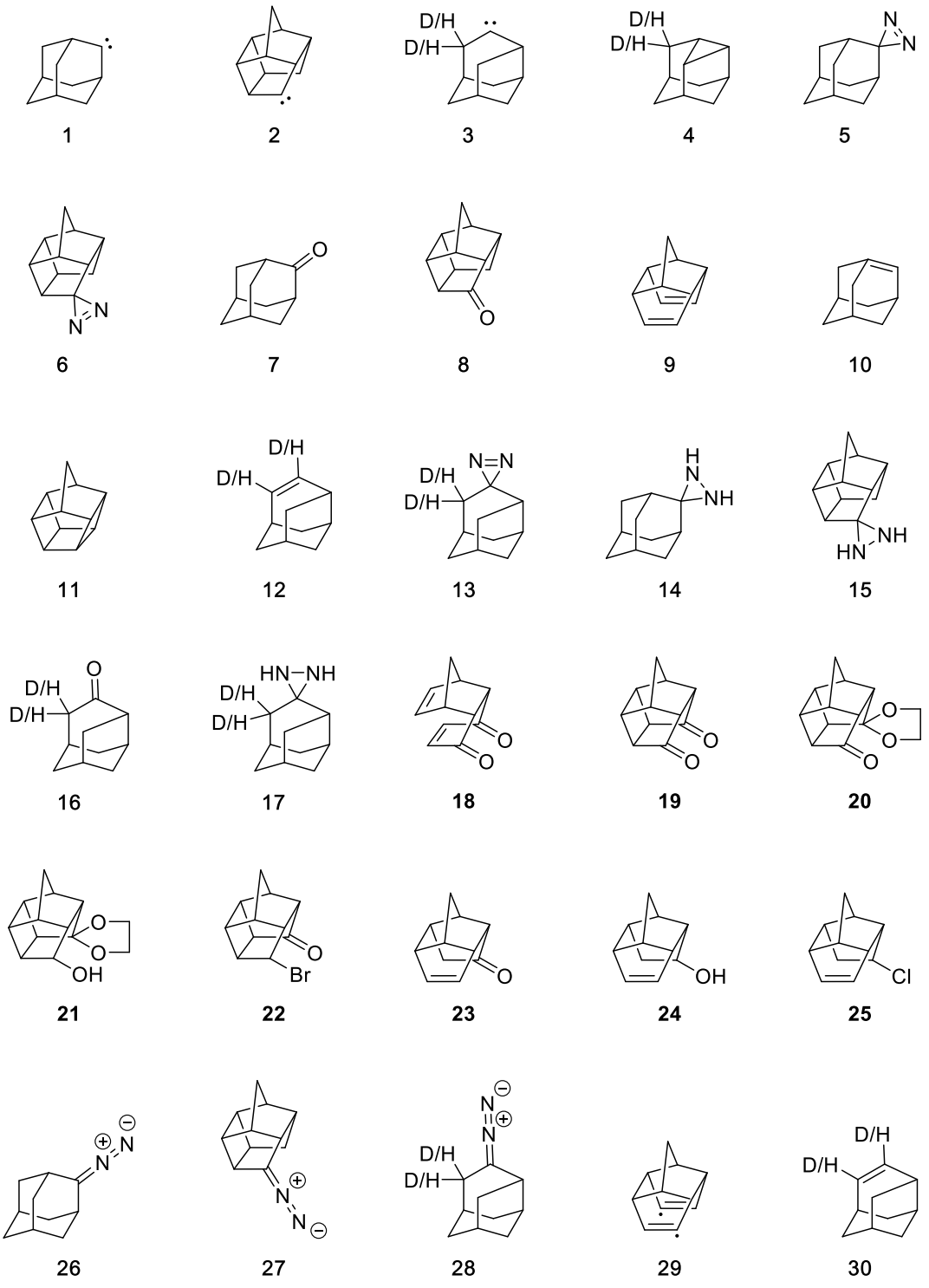

Figure S1: Structures under consideration in this study.

Synthesis

Adamantane diaziridine[34] (14)

To a solution of 0.300 g (1.99 mmol, 1.00 equiv) of adamantanone in 5 mL of MeOH at –78 °C, 20 mL of NH_3 was added via a cold finger cooled to –40 °C (using ethanol and dry ice). The reaction was stirred for 1 h at –78 °C, and then a solution of 0.500 g (4.42 mmol, 2.22 equiv) of hydroxylamine-*O*-sulfonic acid in 5 mL of MeOH was added in two portions. The reaction mixture was stirred at 0 °C for 16 h. Subsequently, 10 mL of H_2O was added, the resulting mixture was extracted three times with 10 mL of CH_2Cl_2. The combined organic layers were dried with $MgSO_4$, filtered, and the solvent was removed under reduced pressure, yielding a colorless solid. Due to product lability, it was immediately utilized for the subsequent step.

Adamantane diazirine (5)

To a solution of 0.328 g of crude **14** in 10 mL of MeOH at room temperature, 0.671 g (3.95 mmol) of $AgNO_3$ dissolved in 2 mL of water and 0.160 g (4.00 mmol) of NaOH dissolved in 2 mL of H_2O were added. The reaction mixture was stirred for 30 min, the inorganic precipitate was filtered off, and then washed with MeOH and H_2O. The filtrate was then extracted two times with 10 mL of CH_2Cl_2. The combined organic layers were dried with $MgSO_4$, filtered, and the solvent was removed under reduced pressure. Purification by flash column chromatography (using *n*-hexane) yielded 0.098 g (0.604 mmol) of adamantane diazirine as a colorless solid in 30% yield in two steps.

The obtained spectra are consistent with the literature.[34]

^{1}H NMR (300 MHz, $CDCl_3$): δ/ppm = 1.99-2.14 (m, 6H), 1.73-1.86 (m, 6H), 0.65 (s, 2H)

^{13}C NMR (75 MHz, $CDCl_3$): δ/ppm = 37.06, 35.39, 34.73, 27.81

Pentacycloundecane diaziridine[34] (15)

To a solution of 0.320 g (1.99 mmol, 1.00 equiv) of pentacycloundecanone in 5 mL of MeOH at –78 °C, 20 mL of NH_3 was added via a cold finger cooled to –40 °C (using ethanol and dry ice). The reaction was stirred for 1 h at –78 °C, and then a solution of 0.500 g (4.42 mmol, 2.22 equiv) of hydroxylamine-*O*-sulfonic acid in 5 mL of MeOH was added in two portions. The reaction mixture was stirred at 0 °C for 16 h. Subsequently, 10 mL of H_2O was added, and the resulting mixture was extracted three times with 10 mL of CH_2Cl_2. The combined organic layers were dried over $MgSO_4$, filtered, and the solvent was removed under reduced pressure, yielding a colorless solid. Due to product lability, it was immediately utilized for the subsequent step.

Pentacycloundecane diazirine (6)

To a solution of 0.328 g of crude **15** in 10 mL of MeOH at room temperature, 0.671 g (3.95 mmol) of $AgNO_3$ dissolved in 2 mL of water and 0.160 g (4.00 mmol) of NaOH

dissolved in 2 mL of H_2O were added. The reaction mixture was stirred for 30 min, the inorganic precipitate was filtered off, and then washed with MeOH and H_2O. The filtrate was then extracted two times with 10 mL of CH_2Cl_2. The combined organic layers were dried with $MgSO_4$, filtered, and the solvent was removed under reduced pressure. Purification by flash column chromatography (using *n*-hexane) yielded 0.158 g (0.919 mmol) of pentacycloundecane diazirine as a colorless solid in 46% yield in two steps.

The obtained spectra are consistent with the literature.[34]

^{1}H NMR (600 MHz, $CDCl_3$): δ/ppm = 2.78-2.86 (m, 2H), 2.62-2.64 (m, 2H), 2.49-2.53 (m, 1H), 2.38-2.43 (m, 2H), 1.68 (d, 1H, *J* = 10.6 Hz), 1.47-1.51 (m, 1H), 1.38 (dt, 1H, *J* = 4.1 Hz, *J* = 12.3 Hz), 1.33 (d, 1H, *J* = 10.6 Hz), 1.16-1.20 (m, 1H)

^{13}C NMR (150 MHz, $CDCl_3$): δ/ppm = 47.75, 46.17, 44.20, 43.89, 43.12, 41.40, 39.28, 38.27, 37.44, 35.39, 30.13

Protoadamantanone (16)

Under Schlenk conditions, 58.3 g (0.132 mol, 2.03 equiv) of lead tetraacetate, 37.4 g (0.147 mol, 2.26 equiv) of iodine, and 10.0 g (0.065 mol, 1.00 equiv) 1-adamantanol were dissolved in 600 mL of dry benzene. The flask was heated for 20 min at 80 °C and then for 2 h at 72 °C. The mixture was allowed to cool to room temperature for 1 h. The inorganic salts were filtered off and washed with five 50 mL portions of diethyl ether. The combined organic layers were shaken with 500 mL of saturated aqueous sodium bisulfite until the dark red color disappeared. The organic phase was then washed with 500 mL of H_2O and 250 mL of saturated aqueous sodium hydrogen carbonate. Afterwards, the organic phase was dried over $MgSO_4$, filtered, and the solvent was removed under reduced pressure to approximately 20 mL, as *endo*-7-iodomethylbicyclo[3.3.1]nonan-3-one is unstable and was immediately used in the next step.

7-Iodomethylbicyclo[3.3.1]nonan-3-one was dissolved in 150 mL of MeOH, to which 7 g (0.1 mol) of KOH were added, and the reaction mixture was refluxed for 3 h. Afterwards, the reaction mixture was quenched with 300 mL of ice-cold H_2O. The resulting mixture was then extracted five times with 100 mL of diethyl ether. The combined organic layers were dried over $MgSO_4$, filtered, and the solvent was removed under reduced pressure. Purification by flash column chromatography (using *n*-pentane and activity III neutral alumina) yielded 7.0 g of protoadamantanone as a colorless solid in 71% yield.

The obtained spectra are consistent with the literature.[44]

^{1}H NMR (400 MHz, $CDCl_3$): δ/ppm = 2.73 (m, 1H), 2.61 (m, 1H), 2.54 (m, 1H), 2.41 (m, 1H), 2.25 (m, 1H), 1.95 (m, 2H), 1.81 (m, 1H), 1.76-1.50 (m, 6H)

^{13}C NMR (100 MHz, $CDCl_3$): δ/ppm = 216.75, 51.19, 45.09, 41.44, 38.20, 37.44, 37.31, 37.21, 34.89, 29.59

HRMS (ESI): m/z = 153.0940 $[M+Na]^+$, 153.0937 (calcd)

Protoadamantane diaziridine (17)

To a solution of 300 mg (1.99 mmol, 1.00 equiv) of **16** in 5 mL of NH_3 in MeOH (7M) at 0 °C, 300 mg (2.65 mmol, 1.33 equiv) of hydroxylamine-*O*-sulfonic acid in 3 mL of MeOH was added. The reaction mixture was stirred for 4 days at 0 °C. The solid was separated, and the liquid was removed under reduced pressure. To both solids, 20 mL of CH_2Cl_2 was added, and the resulting suspension was filtered. The extract was washed three times with 10 mL of 1M H_2SO_4 cooled to 0 °C. To the aqueous layer, 10 mL of cold (0 °C) 2M NaOH was added. The aqueous layer was then extracted three times with 30 mL of CH_2Cl_2. The combined organic layers were dried over $MgSO_4$, filtered, and the solvent was removed under reduced pressure, yielding a colorless solid. Due to product lability, it was immediately utilized for the subsequent step.

Protoadamantane diazirine (13)

To a solution of 0.244 g of crude **17** in 10 mL of MeOH at room temperature, 0.671 g (3.95 mmol) of $AgNO_3$ dissolved in 2 mL of water and 0.160 g (4.00 mmol) of NaOH dissolved in 2 mL of H_2O were added. The reaction mixture was stirred for 30 min, the inorganic precipitate was filtered off, and then washed with MeOH and H_2O. The filtrate was then extracted two times with 10 mL of CH_2Cl_2. The combined organic layers were dried over $MgSO_4$, filtered, and the solvent was removed under reduced pressure. Purification by flash column chromatography (using *n*-pentane) yielded 0.016 g (0.099 mmol) of protoadamantane diazirine as a colorless solid in 5% yield over two steps.

^{1}H NMR (400 MHz, $CDCl_3$): δ/ppm = 2.46 (q, *J* = 4.0 Hz, 1H), 2.24 (m, 1H), 2.05 (m, 3H), 1.91-1.76 (m, 3H), 1.61 (m, 1H), 1.54 (m, 3H), 1.00 (t, *J* = 6.1 Hz, 1H), 0.72 (qt, *J* = 2.1Hz, 4Hz, 1H)

^{13}C NMR (100 MHz, $CDCl_3$): δ/ppm = 41.26, 41.16, 38.90, 38.19, 36.22, 35.35, 34.43, 34.41, 28.63

HRMS (ESI): m/z = 135.1171 $[M–N_2+H]^+$, 135.1168 (calcd)

Deuteration of protoadamantane (*d_2*-16)

A solution of 1.000 g (6.442 mmol, 1 equiv) of protoadamantanone, 3 mL NaOD (in D_2O 40% w/w), and 5 mL of dry dioxane was refluxed for 24 h. After cooling the reaction mixture to rt, dioxane was evaporated and the obtained crude oil reaction mixture was divided between water and CH_2Cl_2. The water layer was extracted 3 times with CH_2Cl_2. The combined organic layers were dried over $MgSO_4$, filtered, and the solvent was removed under reduced pressure. This process was repeated three times and yielded 0.721 g (4.737 mmol, 74%) of *d_2*-protoadamantanone.

^{1}H NMR (400 MHz, $CDCl_3$): δ/ppm = 2.73 (m, 1H), 2.61 (m, 1H), 2.41 (m, 1H), 2.22 (m, 1H), 2.00-1.91 (m, 2H), 1.83-1.49 (m, 6H)

^{13}C NMR (100 MHz, $CDCl_3$): δ/ppm = 216.89, 51.18, 41.43, 38.14, 37.40, 37.35, 37.21, 34.82, 29.41

HRMS (ESI): m/z = 175.1063 $[M+Na]^+$, 175.1062 (calcd)

d$_2$-Protoadamantane diaziridine (*d*$_2$-17)

To a solution of 300 mg (1.99 mmol, 1.00 equiv) of *d*$_2$-protoadamantanone in 5 mL of NH_3 in MeOH (7M) at 0 °C, 300 mg (2.65 mmol, 1.33 equiv) of hydroxylamine-*O*-sulfonic acid in 3 mL of MeOH was added. The reaction mixture was stirred for 4 days at 0 °C. The solid was separated, and the liquid was removed under reduced pressure. To both solids, 20 mL of CH_2Cl_2 was added, and the resulting suspension was filtered. The extract was washed three times with 10 mL of 1M H_2SO_4 cooled to 0 °C. To the aqueous layer, 10 mL of cold (0 °C) 2M NaOH was added. The aqueous layer was then extracted three times with 30 mL of CH_2Cl_2. The combined organic layers were dried over $MgSO_4$, filtered, and the solvent was removed under reduced pressure, yielding a colorless solid. Due to product lability, it was immediately utilized for the subsequent step.

d$_2$-Protoadamantane diazirine (*d*$_2$-13)

To a solution of 0.244 g of crude *d*$_2$-**15** in 10 mL of MeOH at room temperature, 0.671 g (3.95 mmol) of $AgNO_3$ dissolved in 2 mL of water and 0.160 g (4.00 mmol) of NaOH dissolved in 2 mL of water were added. The reaction mixture was stirred for 30 min, the inorganic precipitate was filtered off, and then washed with MeOH and H_2O. The filtrate was then extracted two times with 10 mL of CH_2Cl_2. The combined organic layers were dried over $MgSO_4$, filtered, and the solvent was removed under reduced pressure. Purification by flash column chromatography (using *n*-pentane) yielded 0.018 g (0.099 mmol) of ***d*$_2$-11** as a colorless solid in 5% yield in two steps.

^{1}H NMR (400 MHz, $CDCl_3$): δ/ppm = 2.46 (q, J = 4.0 Hz, 1H), 2.24 (m, 1H), 2.08-2.00 (m, 3 H), 1.90 (m, 1H), 1.82 (m, 1H), 1.61 (m, 1H), 1.55-1.50 (m, 3H), 1.00 (m, 1H)

^{13}C NMR (100 MHz, $CDCl_3$): δ/ppm = 41.43, 41.28, 39.00, 36.41, 35.52, 34.57, 34.55, 28.58

HRMS (ESI): m/z = 137.1296 $[M–N_2+H]^+$, 137.1294 (calcd)

1,4,4a,8a-Tetrahydro-1,4-methanonaphthalene-5,8-dione (18)

28.75 g (267.7 mmol, 1.1 equiv) of freshly cracked cyclopentadiene was added to 17.77 g (248.3 mmol, 1.0 equiv) of purified benzoquinone in 125 mL of ethyl acetate and stirred in an ice bath for 30 min. After adding another 120 mL of ethyl acetate, the reaction mixture was stirred for 30 min at room temperature. Removing the solvent under reduced pressure yielded 38.91 g (223.4 mmol, 90%) of a brown solid.

The obtained spectra are consistent with the literature.[45]

Pentacyclo[5.4.0.0^{2,6}.0^{3,10}.0^{5,6}]undecane-8,11-dione (19)

38.91 g (223.4 mmol, 1.0 equiv) of **18** was dissolved in 100 mL of ethyl acetate and irradiated in the photo reactor for 20 h. The solvent was removed under reduced pressure. The crude product was recrystallized in ethyl acetate and yielded 10.596 g (57.42 mmol, 25%) of a yellow solid.

The obtained spectra are consistent with the literature.[46]

Pentacyclo[5.4.0.0^{2,6}.0^{3,10}.0^{5,9}]undecane-8,11-dione monoethylene ketal (20)

23.52 g (135.0 mmol, 1.00 equiv) of **19**, 8.42 g (135.7 mmol, 1.01 equiv), and 0.301 g (1.74 mmol, 0.01 equiv) of *p*-toluenesulfonic acid were dissolved in 110 mL of benzene. The mixture was stirred under reflux at 85 °C for 5 h. The mixture was then poured onto 50 mL of ice-cold 10% aqueous Na_2CO_3. The organic phase was extracted with CH_2Cl_2. The combined organic layers were dried over $MgSO_4$, filtered, and the solvent was removed under reduced pressure. Purification by flash column chromatography (using CH_2Cl_2) yielded 17.211 g (77.89 mmol, 58%) of a yellow solid.

The obtained spectra are consistent with the literature.[47]

Octahydrospiro[2,4,1-(epiethane[1,1,2]triyl)cyclobuta[*cd*]pentalene-5,2'-[1,3]dioxolan]-7-ol (21)

2.205 g (10.10 mmol, 1.0 equiv) of **20** was dissolved in 25 mL of ethanol, and 0.772 g (20.41 mmol, 2.0 equiv) of $NaBH_4$ was added portion wise, while the solution was stirred at 0 °C. After 2 h, the ice bath was removed, and the solution was stirred for 2 h at room temperature. Then, 17 mL of H_2O, 10 mL of 1N HCl, and 20 mL of CH_2Cl_2 were added. The organic phase was separated, and the aqueous phase was extracted twice with 20 mL of CH_2Cl_2. The combined organic layers were dried over $MgSO_4$, filtered, and the solvent was removed under reduced pressure, yielding 2.144 g (9.73 mmol, 96%) of a yellow liquid.

The obtained spectra are consistent with the literature.[48]

***exo*-11-Bromopentacyclo [5.4.0.0^{2,6}.0^{3,10}.0^{5,9}]undecane-8-one (22)**

2.284 g (10.37 mmol) of **21** was dissolved in 30 mL of 47% HBr. The solution was stirred for 3 h at 80 °C. After cooling to room temperature, the solution was quenched with 100 mL of ice-cold H_2O. The precipitate was washed with water. The organic layer was dried over $MgSO_4$, filtered, and the solvent was removed under reduced pressure, yielding 1.747 g (7.31 mmol, 71%) of a grey solid.

The obtained spectra are consistent with the literature.[48]

Tetracyclo[6.3.0.0^{4,11}.0^{5,9}]undec-2-en-6-one (23)

14.15 g (59.17 mmol, 1.0 equiv) of **22** and 22.50 g (344.1 mmol, 5.8 equiv) of zinc powder were added to 200 mL of glacial acetic acid. The suspension was stirred at 125 °C for 8 h, and after cooling to room temperature, the mixture was filtered, and the solid was washed with diethyl ether. The organic phase was washed with water and twice with aqueous $NaHCO_3$. The organic layer was dried over $MgSO_4$, filtered, and the solvent was removed under reduced pressure, yielding 6.507 g (40.62 mmol, 69%) of a colorless solid.

The obtained spectra are consistent with the literature.[48]

Tetracyclo[6.3.0.0^{4,11}.0^{5,9}]undec-2-en-6-ol (24)

To a solution of 1.744 g (45.96 mmol, 1.1 equiv) of $LiAlH_4$ in 46 mL of diethyl ether in an ice bath, 6.507 g (40.62 mmol, 1.0 equiv) of **23** in 46 mL of diethyl ether was added. The mixture was stirred for 3 h at 0 °C. Then, the mixture was stirred for 17 h at room temperature. The reaction mixture was quenched with $NaOH_{(aq)}$. After filtering the mixture, the solid was washed with diethyl ether and H_2O. The organic phase was washed twice with H_2O. The organic layer was dried over $MgSO_4$, filtered, and the solvent was removed under reduced pressure, yielding 5.986 g (36.90 mmol, 91%) of a colorless solid.

^{1}H NMR (400 MHz, $CDCl_3$): δ/ppm = 6.39 (q, *J* = 2.1 Hz, 1H), 6.03 (q, *J* = 2.0 Hz, 1H), 4.45 (m, 1H), 2.91 (s, 1H), 2.58-2.51 (m, 1H), 2.50-2.42 (m, 2H), 2.32-2.19 (m, 2H), 1.79-1.72 (m, 1H), 1.60-1.52 (m, 2 H) 1.48 (dd, *J* = 4.1 Hz , *J* = 4.1 Hz, 1H)

^{13}C NMR (100 MHz, $CDCl_3$): δ/ppm = 140.09, 139.56, 59.59, 52.57, 51.78, 47.93, 46.89, 42.55, 39.20, 32.51

Tetracyclo[6.3.0.0^{4,11}.0^{5,9}]undec-2-en-6-chloride (25)

To a solution at 0°C of 5.986 g (36.90 mmol, 1.0 equiv) of **24** and 50 mL of pyridine, 17 mL (27.97 g, 182.4 mmol, 4.9 equiv) of PCl_3 were added. After stirring at 100 °C for 5 h, the mixture was poured into 200 mL of iced water. The organic phase was separated, and the aqueous phase was extracted four times with *n*-pentane. The combined organic phase was washed with 100 mL of 10% $HCl_{(aq)}$ and 10% $NaHCO_{3(aq)}$, followed by H_2O and $NaCl_{(aq)}$. The organic layer was dried over $MgSO_4$, filtered, and the solvent was removed under reduced pressure, yielding 4.504 g (24.93 mmol, 68%) of a yellow oil.

^{1}H NMR (400 MHz, $CDCl_3$): δ/ppm = 5.90 (m, 4H), 3.17 (m, 2H), 2.33 (m, 4H), 1.64 (m, 2H)

^{13}C NMR (100 MHz, $CDCl_3$): δ/ppm = 137.27, 65.07, 49.13, 31.85

Homohypostrophene (9)

To a solution of 4.504 g (24.93 mmol, 1.0 equiv) of **25** in 20 mL of DMSO was added 5.105 g (45.50 mmol) of KO^{t}Bu in 80 mL of DMSO. The solution was stirred for 10 h at

100 °C. H_2O was added, and the mixture was extracted four times with *n*-pentane. The *n*-pentane extract was filtered through a neutral alumina column. The organic layer was dried over $MgSO_4$, filtered, and the solvent was removed under reduced pressure, yielding 1.99 g (13.80 mmol, 55%) of a colorless solid.

The obtained spectra are consistent with the literature.[48]

Homopentaprismane (11)

A solution of 1.013 g (7.02 mmol) **9** in 15 mL benzene were irradiated for 22 h in a photoreactor. Removing the solvent under reduced pressure, yields 0.7861 g (5.45 mmol, 78%) of a colorless solid.

The obtained spectra are consistent with the literature.[48]

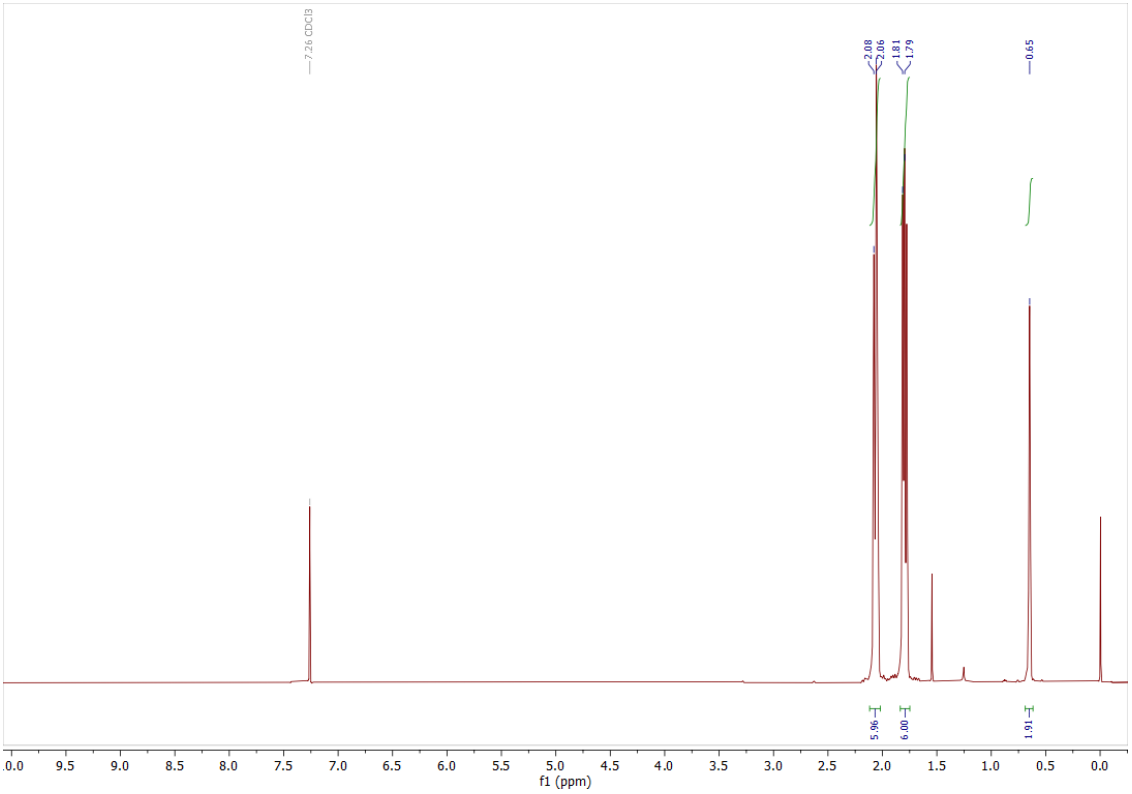

Figure S2: ^{1}H NMR of adamantane diazirine (**5**)

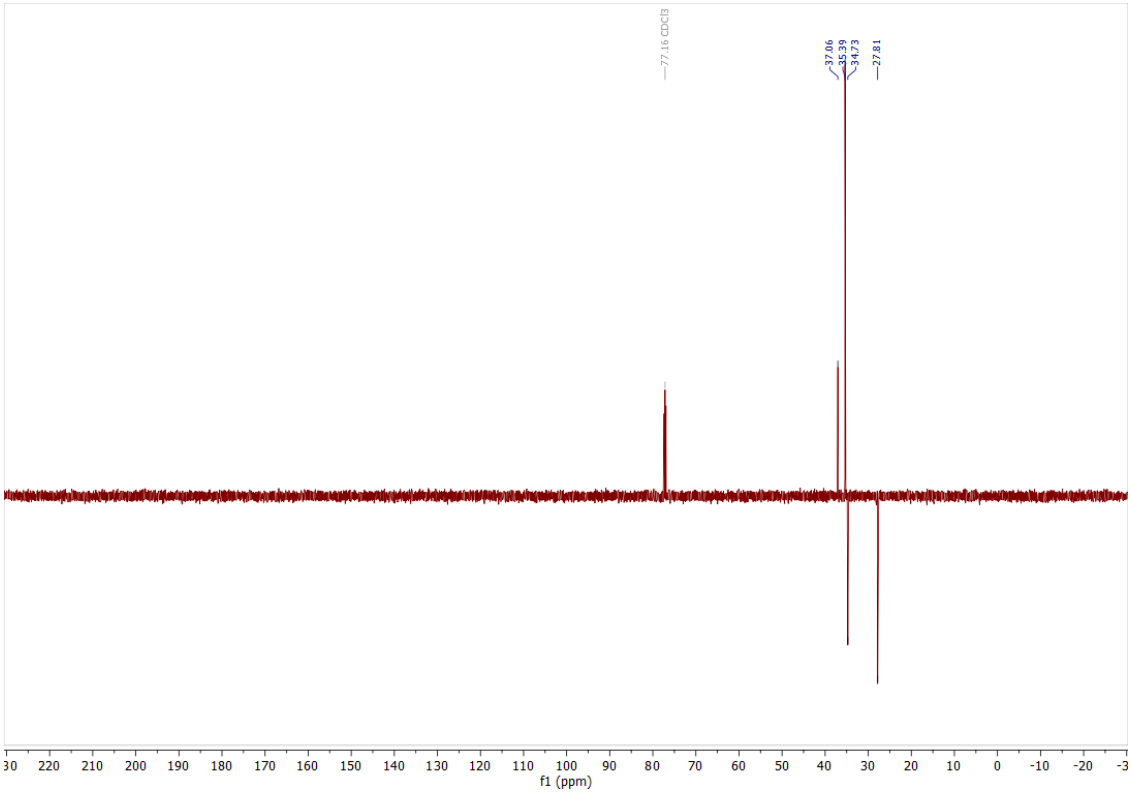

Figure S3: ^{13}C NMR (DEPT-135) of adamantane diazirine **(5)**

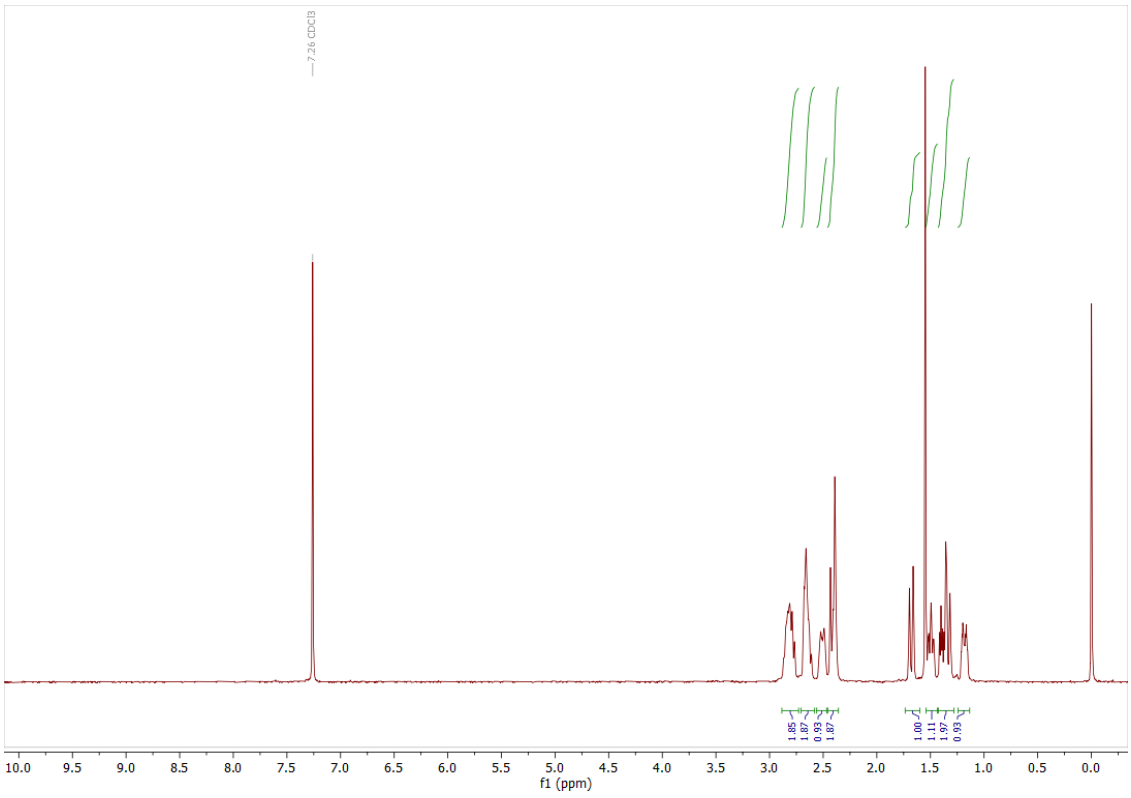

Figure S4: ^{1}H NMR of pentacycloundecane diazirine **(6)**

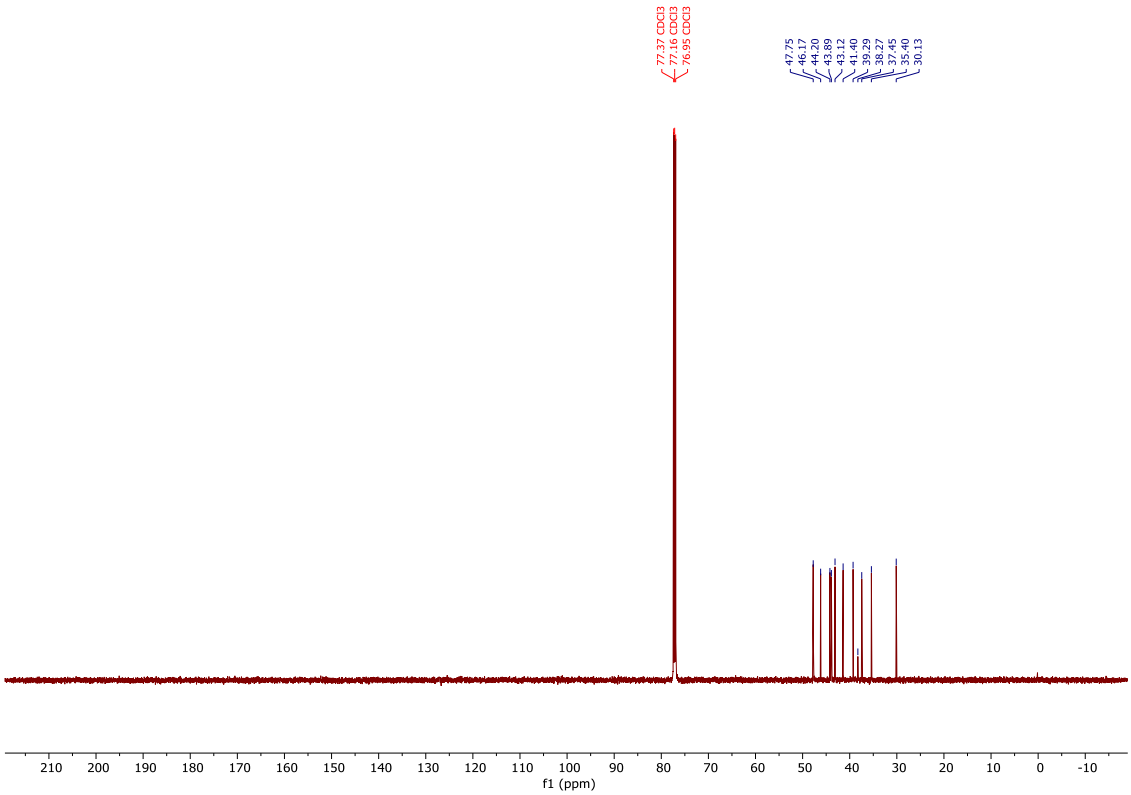

Figure S5: ^{13}C NMR of pentacycloundecane diazirine **(6)**

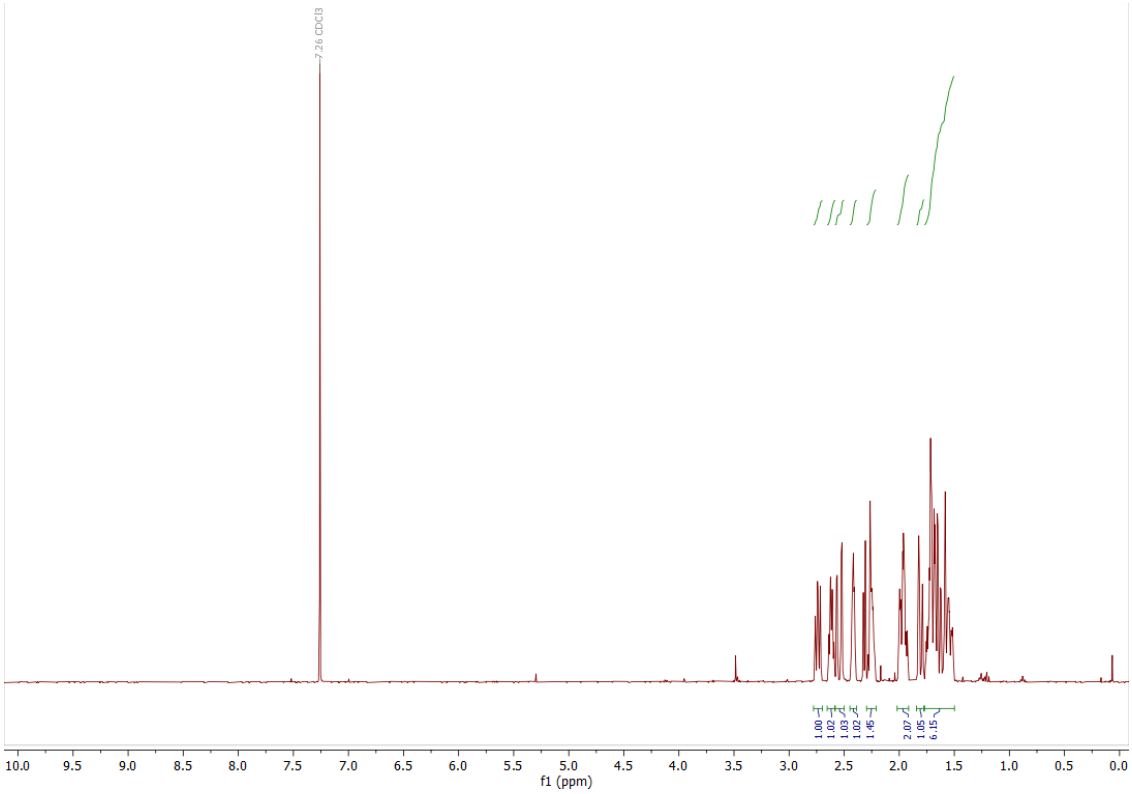

Figure S6: ^{1}H NMR of protoadamantanone **(16)**

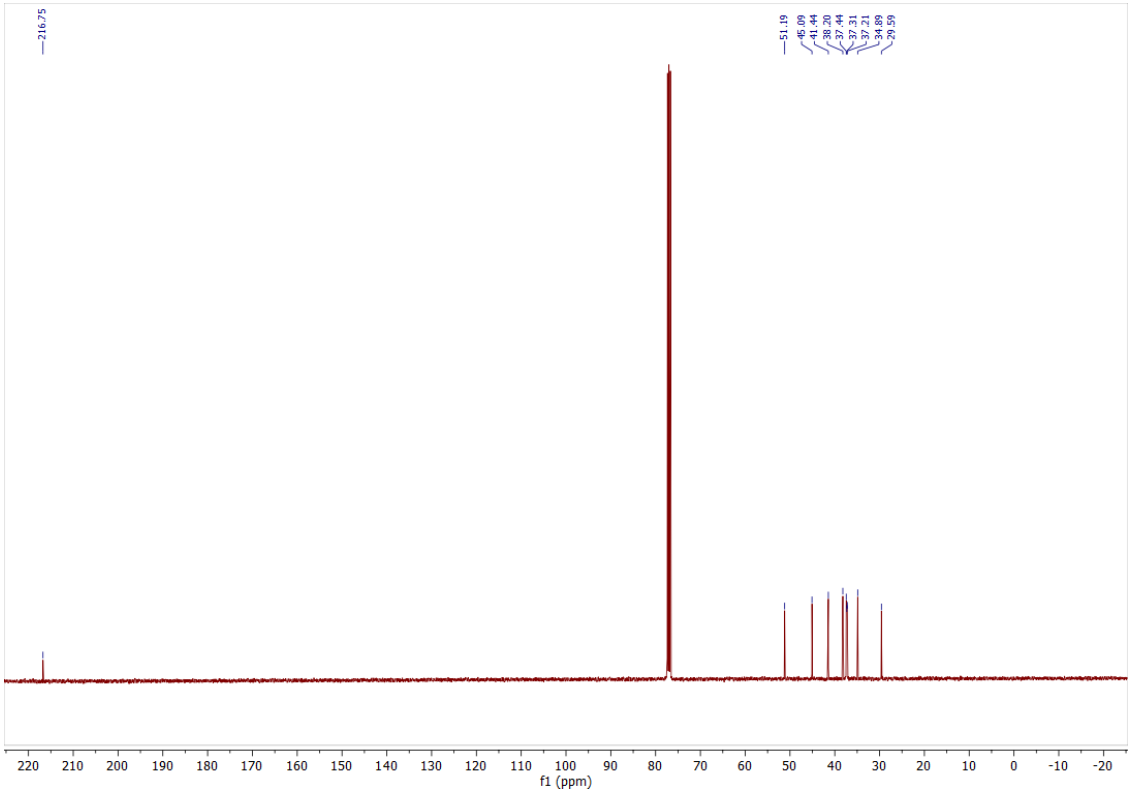

Figure S7: ^{13}C NMR of protoadamantanone **(16)**

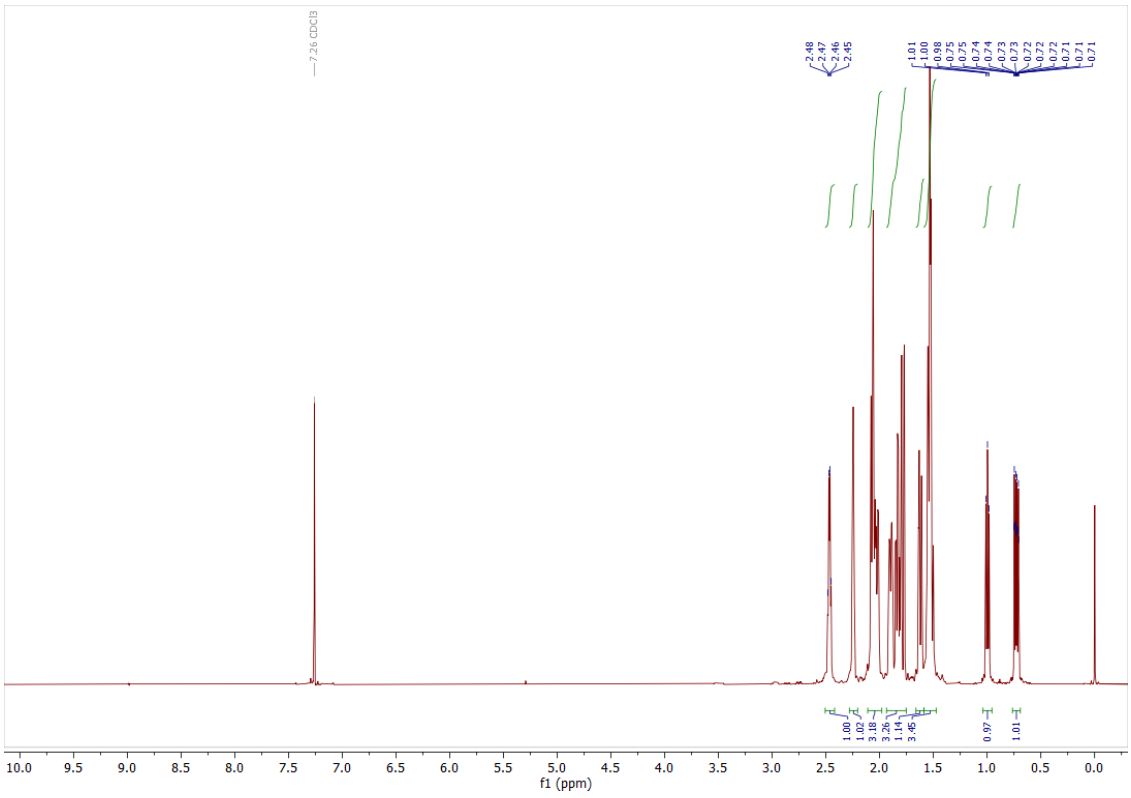

Figure S8: ^{1}H NMR of protoadamantane diazirine **(13)**

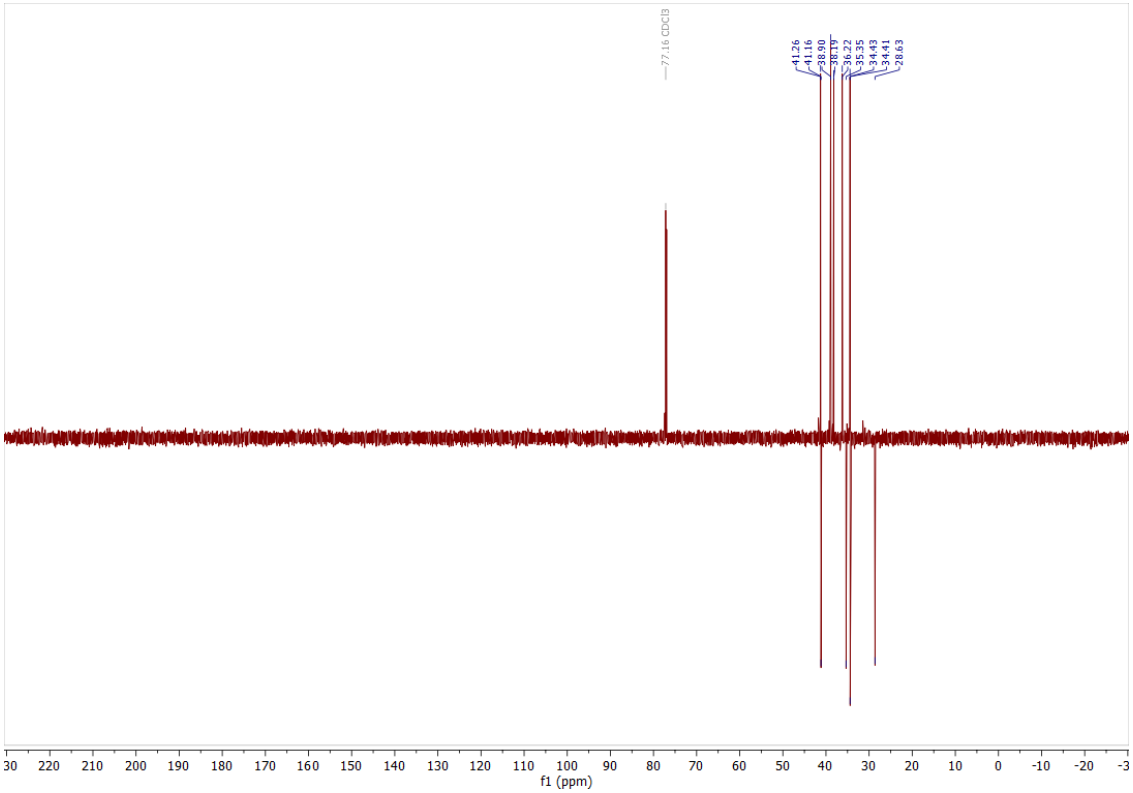

Figure S9: ^{13}C NMR (DEPT-135) of protoadamantane diazirine **(13)**

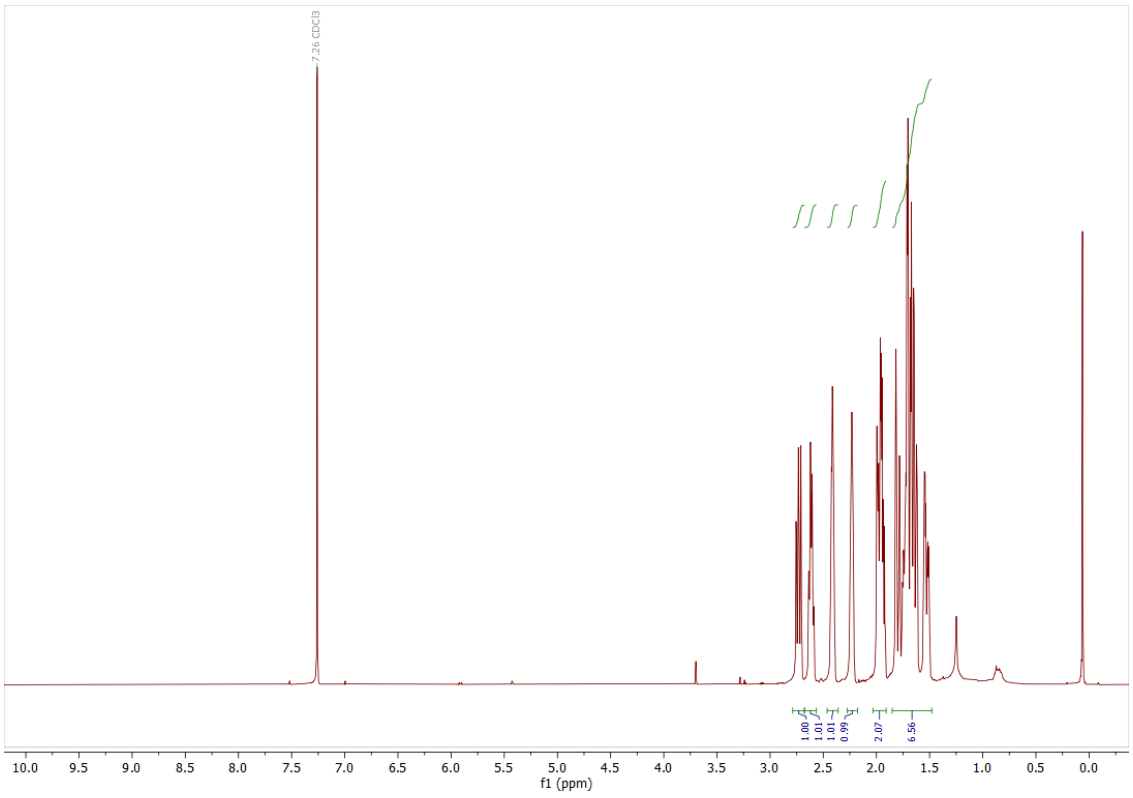

Figure S10: ^{1}H NMR of d_2-protoadamantanone **(d_2-16)**

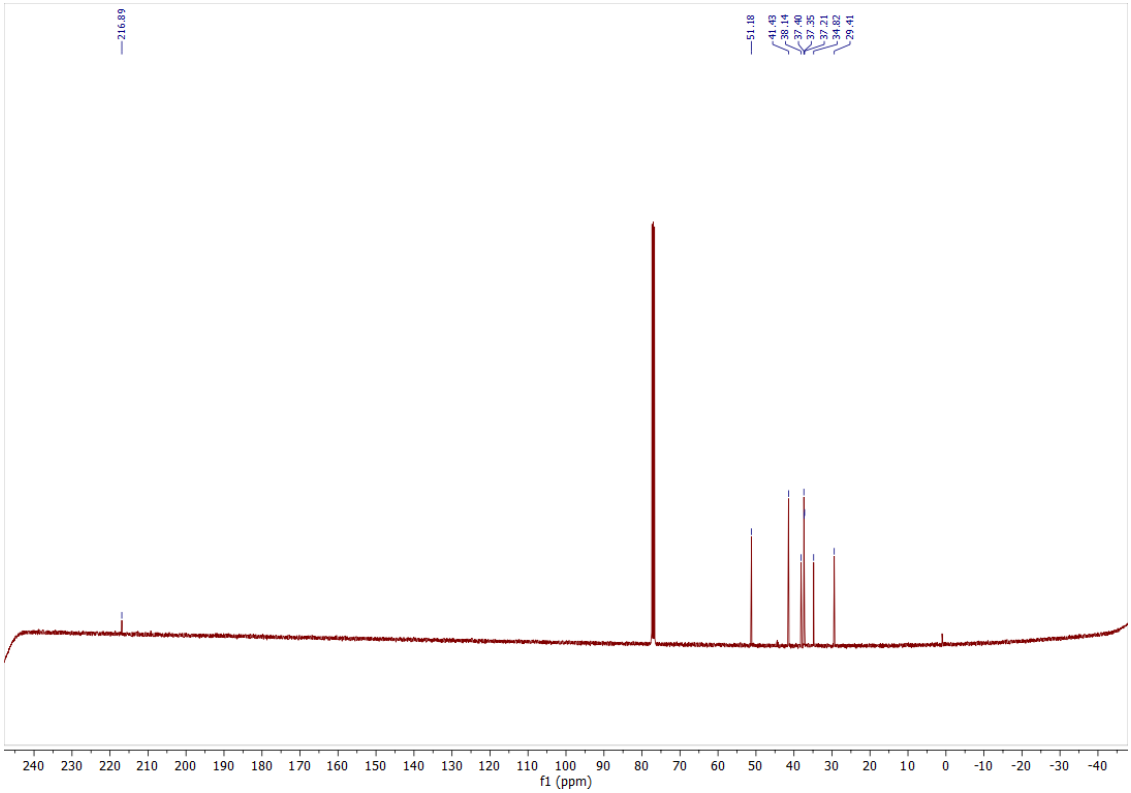

Figure S11: ^{13}C NMR of d_2-protoadamantanone **(d_2-16)**

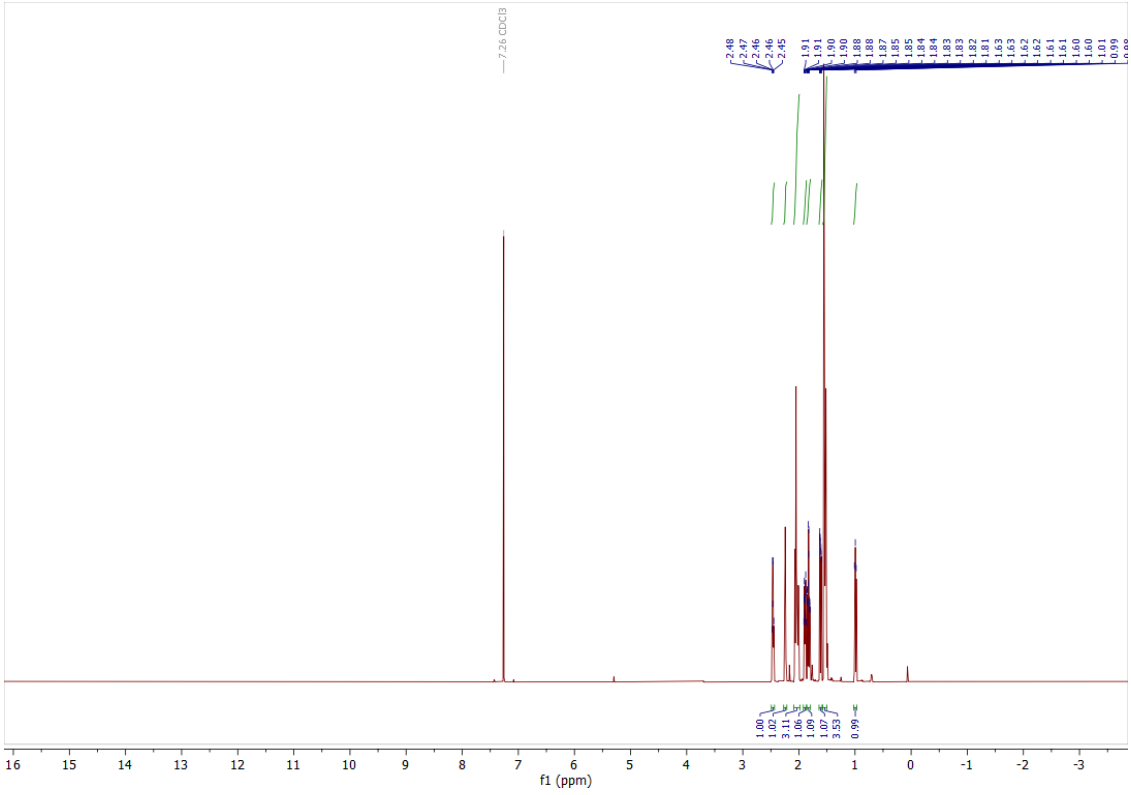

Figure S12: ^{1}H NMR of d_2-protoadamantane diazirine **(d_2-13)**

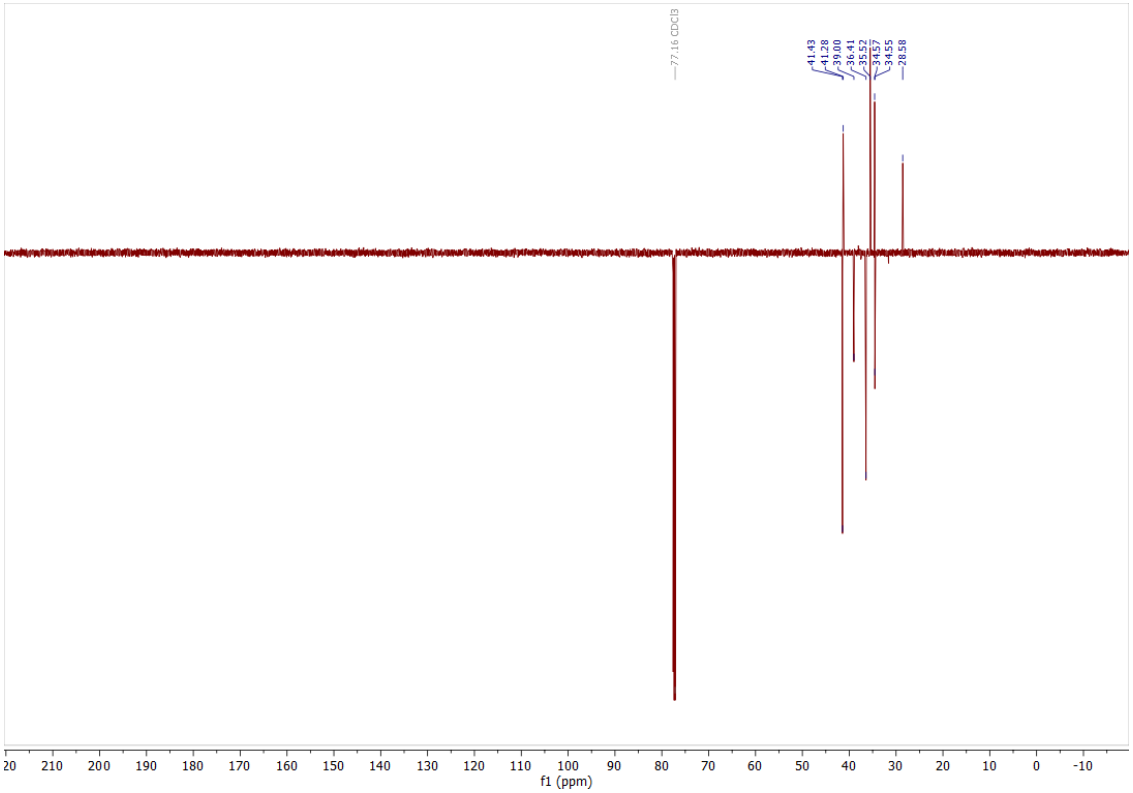

Figure S13: ^{13}C NMR (DEPT-135) of d_2-protoadamantane diazirine **(d_2-13)**

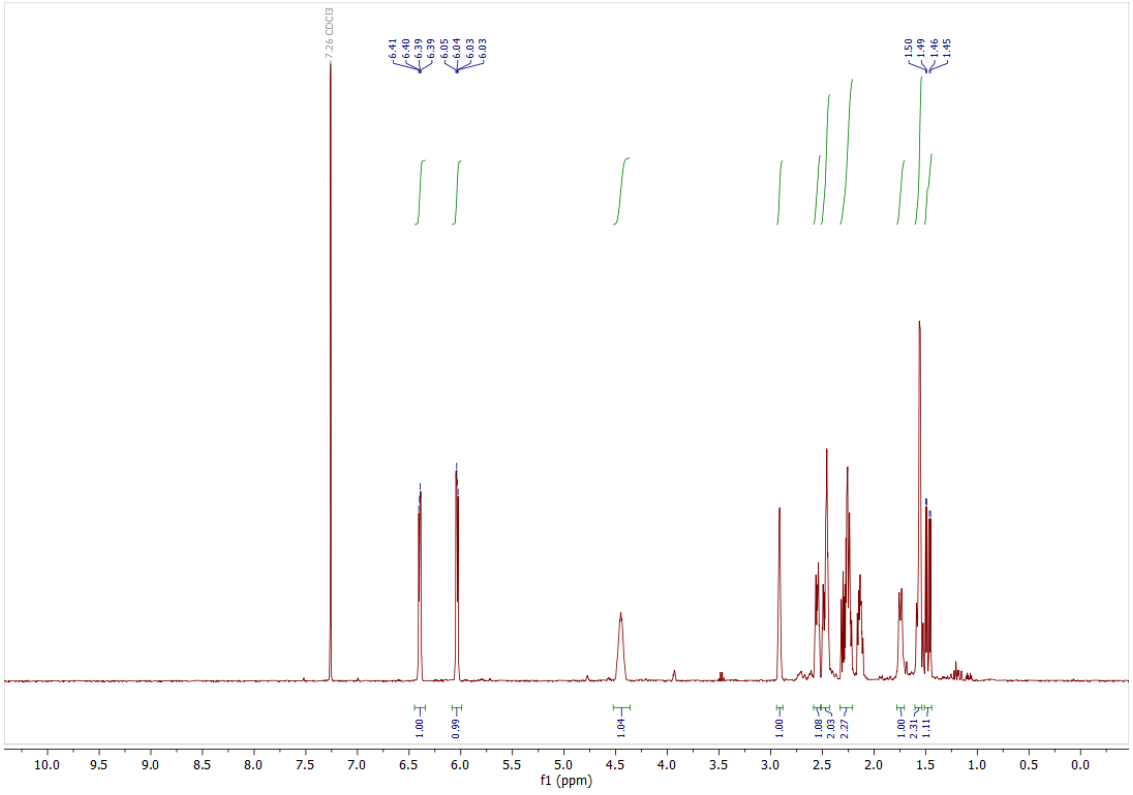

Figure S14: ^{1}H NMR of tetracyclo[6.3.0.0^{4,11}.0^{5,9}]undec-2-en-6-ol **(24)**

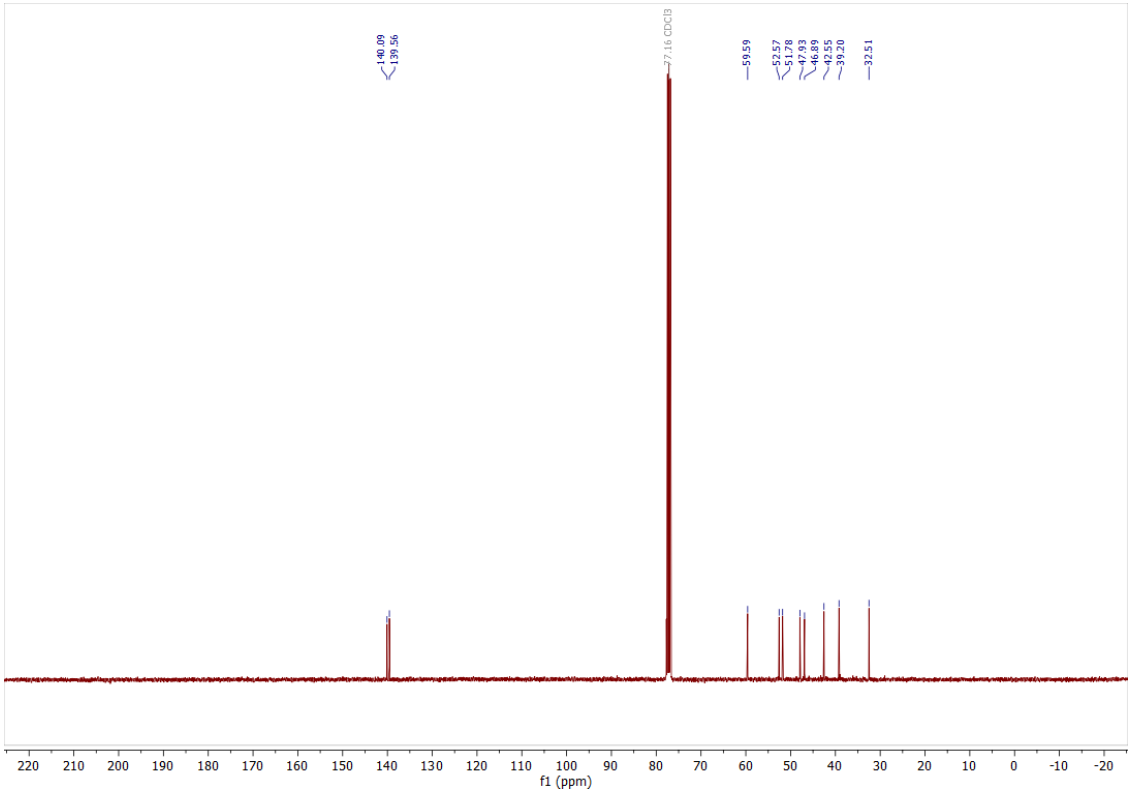

Figure S15: ^{13}C NMR of tetracyclo[6.3.0.0^{4,11}.0^{5,9}]undec-2-en-6-ol **(24)**

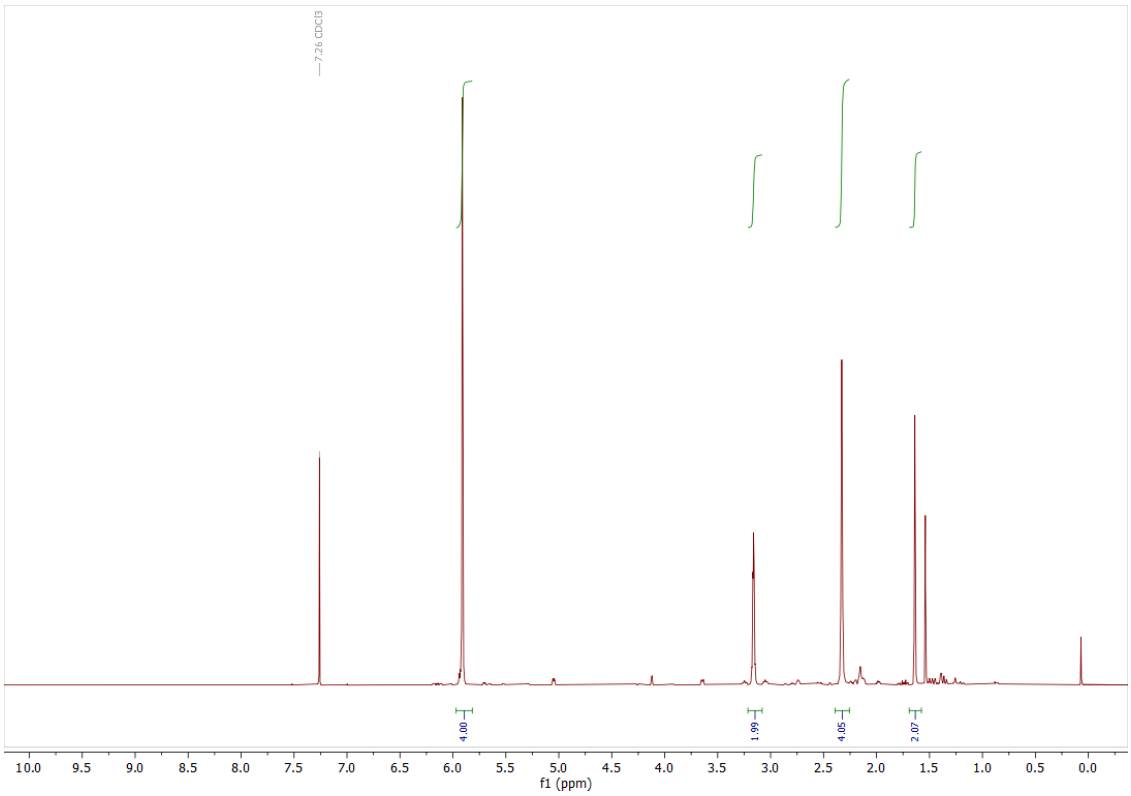

Figure S16: ^{1}H NMR of tetracyclo[6.3.0.0^{4,11}.0^{5,9}]undec-2-en-6-chloride **(25)**

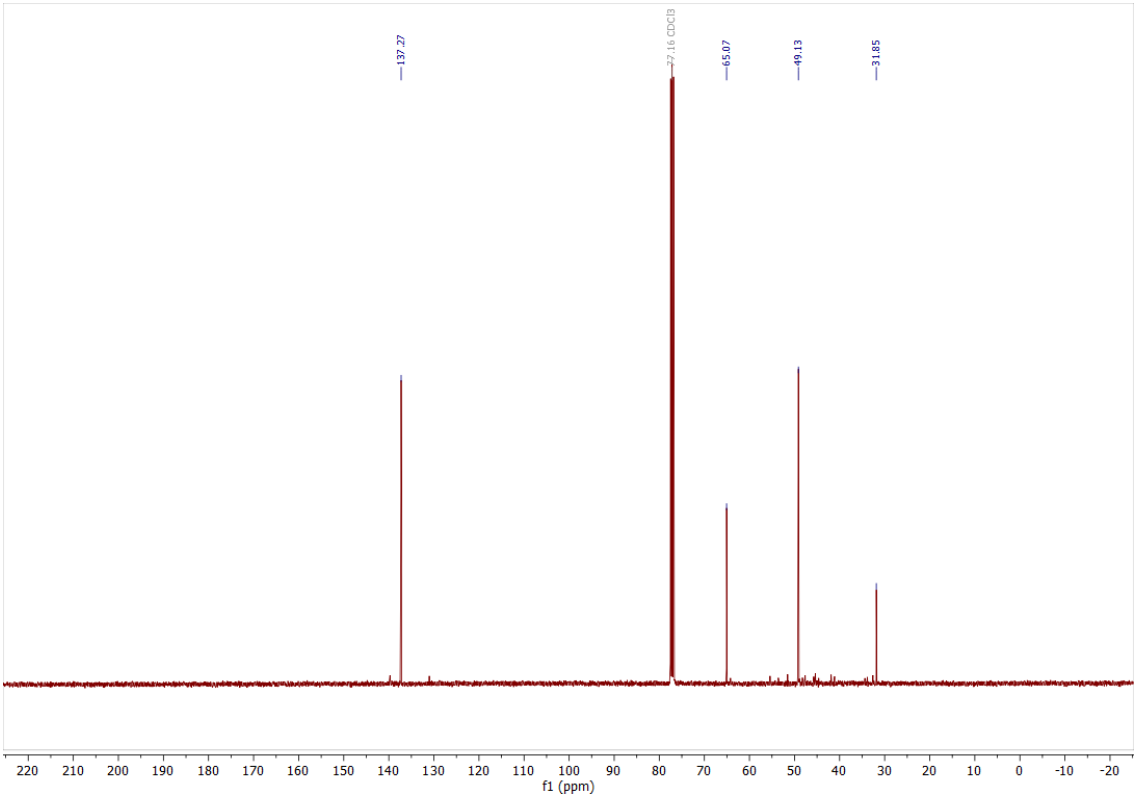

Figure S17: ^{13}C NMR of tetracyclo[6.3.0.0^{4,11}.0^{5,9}]undec-2-en-6-chloride **(25)**

IR Spectral Data

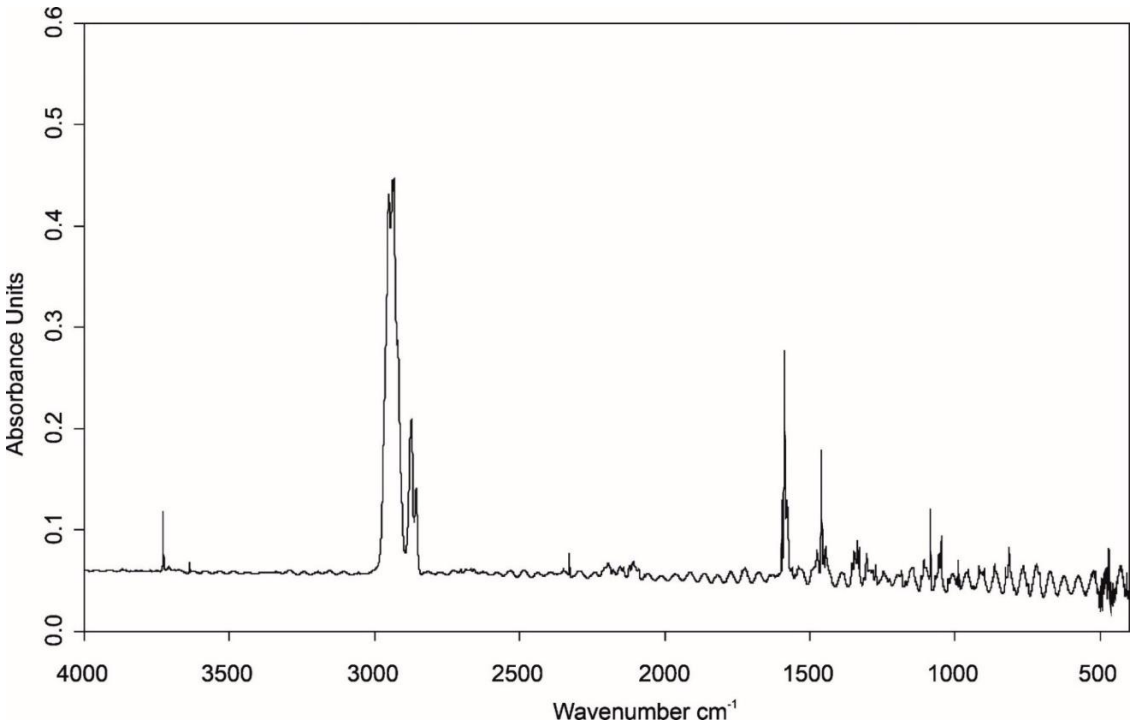

Figure S18: IR spectra showing the deposition of **5** with subsequent trapping in a nitrogen matrix at 3.5 K.

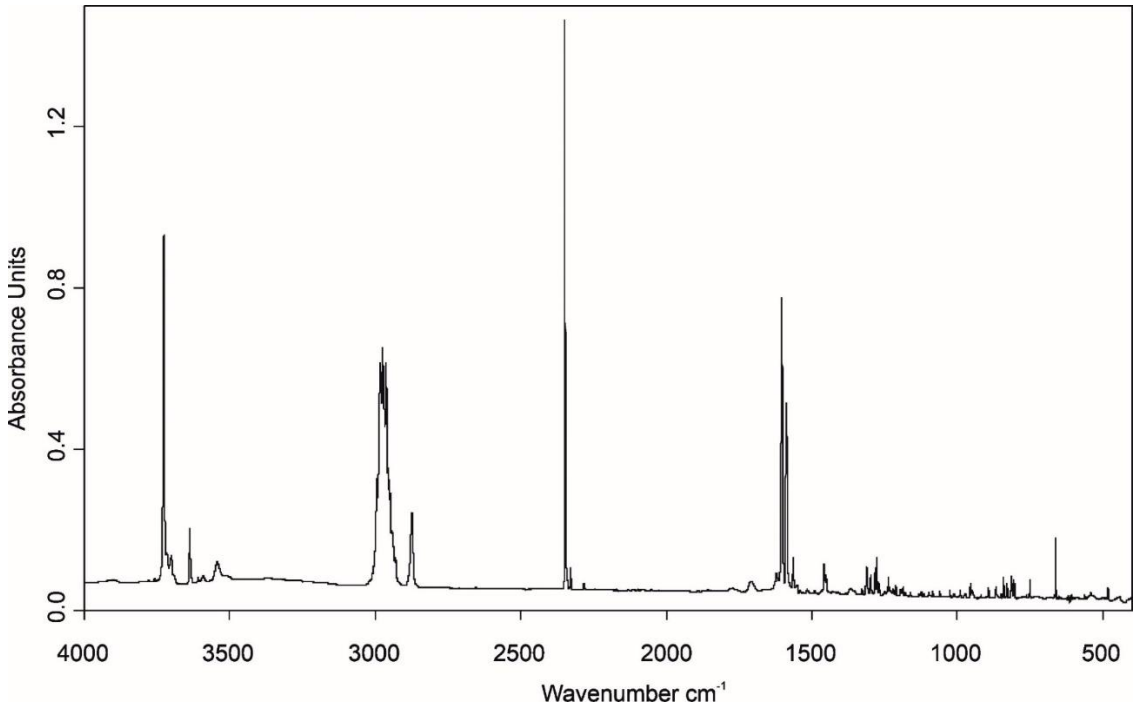

Figure S19: IR spectra showing the deposition of **6** with subsequent trapping in a nitrogen matrix at 3.5 K.

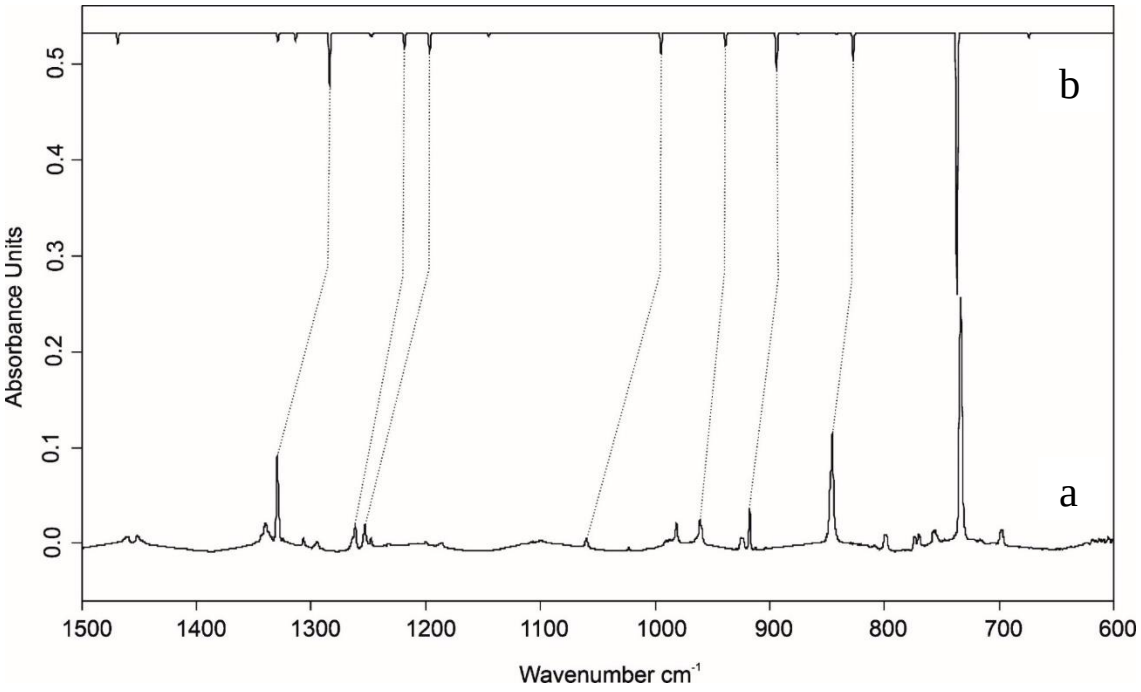

Figure S20: a) IR spectra showing the deposition of **9** with subsequent trapping in a nitrogen matrix at 3.5 K. b) IR spectrum of **9** computed at UB3LYP/6-311++G(3df,2pd) (anharmonic).

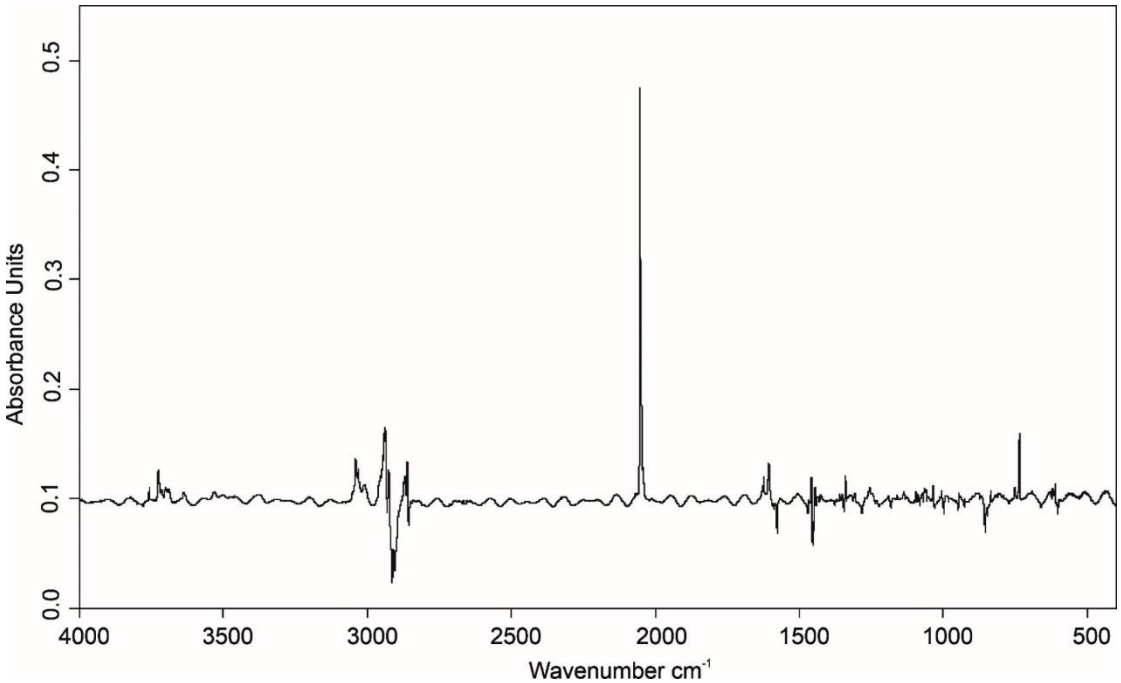

Figure S21: IR difference spectra showing the photochemistry of **5** after irradiation with λ = 365 nm in argon at 3.5 K. Downward bands assigned to **5** disappear after 20 min irradiation. Upward bands assigned to adamantane diazo (**26**) and **1** appear after 20 min irradiation.

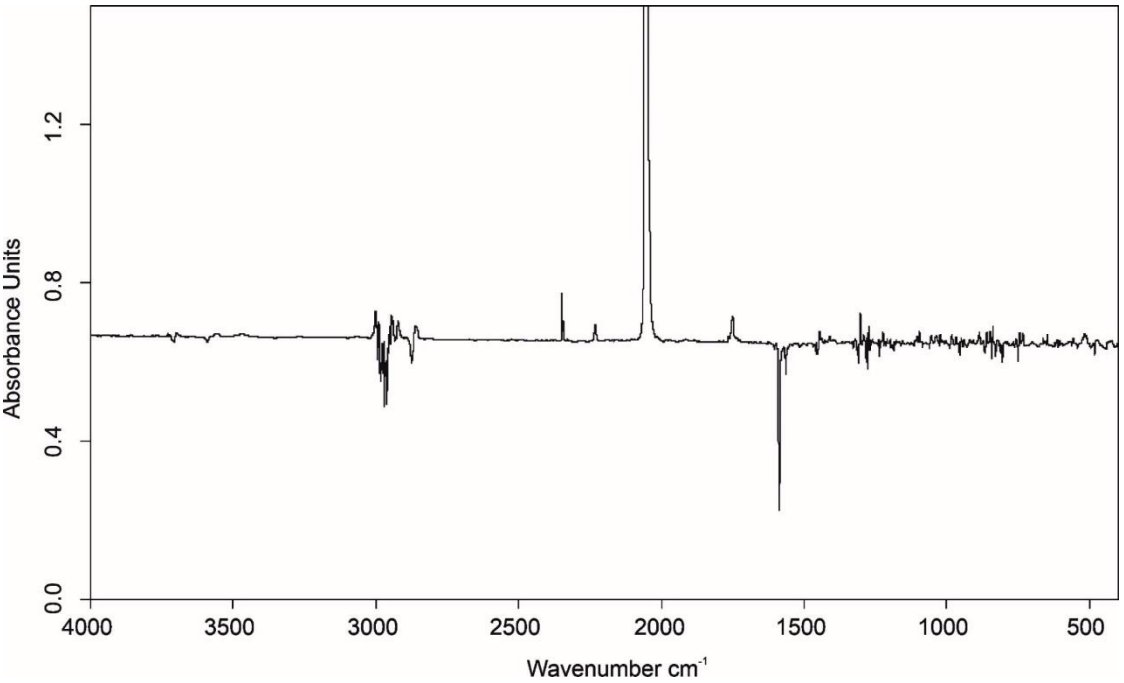

Figure S22: IR difference spectra showing the photochemistry of **6** after irradiation with λ = 365 nm in argon at 3.5 K. Downward bands assigned to **6** disappear after 20 min irradiation. Upward bands assigned to pentacycloundecane diazo (**27**) and **2** appear after 20 min irradiation.

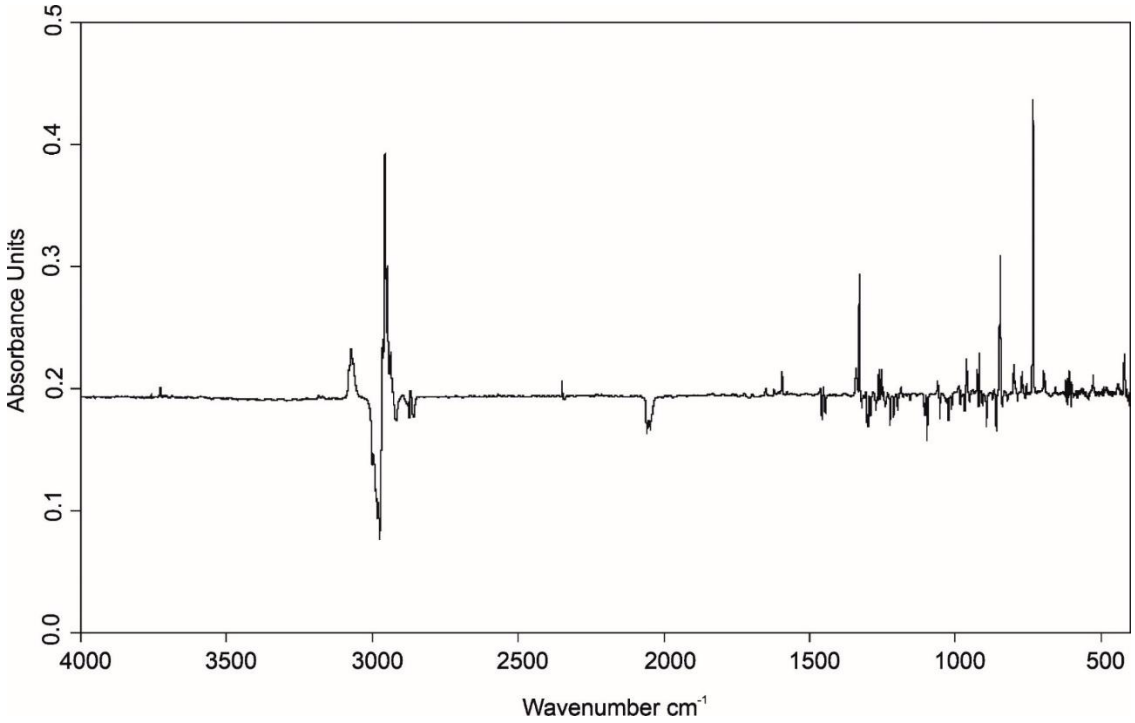

Figure S23: IR difference spectra showing the photochemistry of **2** after irradiating for 10 min at λ = 627 nm in argon at 3.5 K. Downward bands assigned to **2** disappear after irradiation. Upward bands assigned to **9** appear after irradiation.

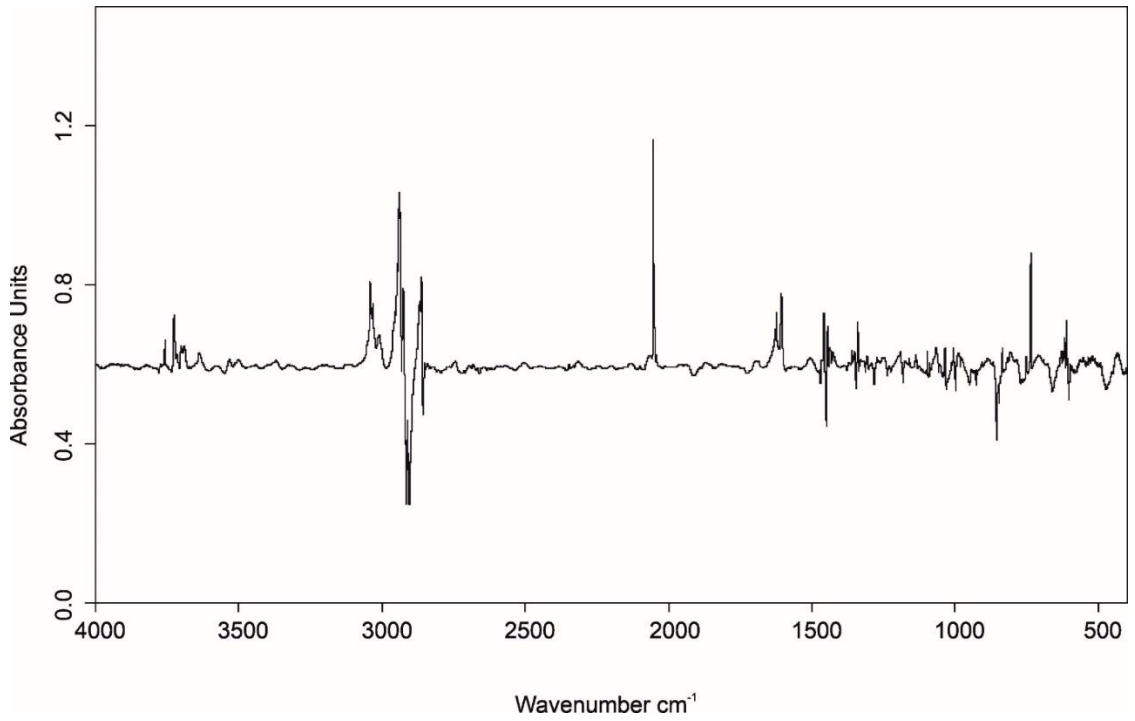

Figure S24: IR difference spectra showing the tunneling of **1** after waiting 16 h in argon at 3.5 K. Downward bands assigned to **1** disappear after 16 h waiting. Upward bands assigned to **4** appear after 16 h waiting.

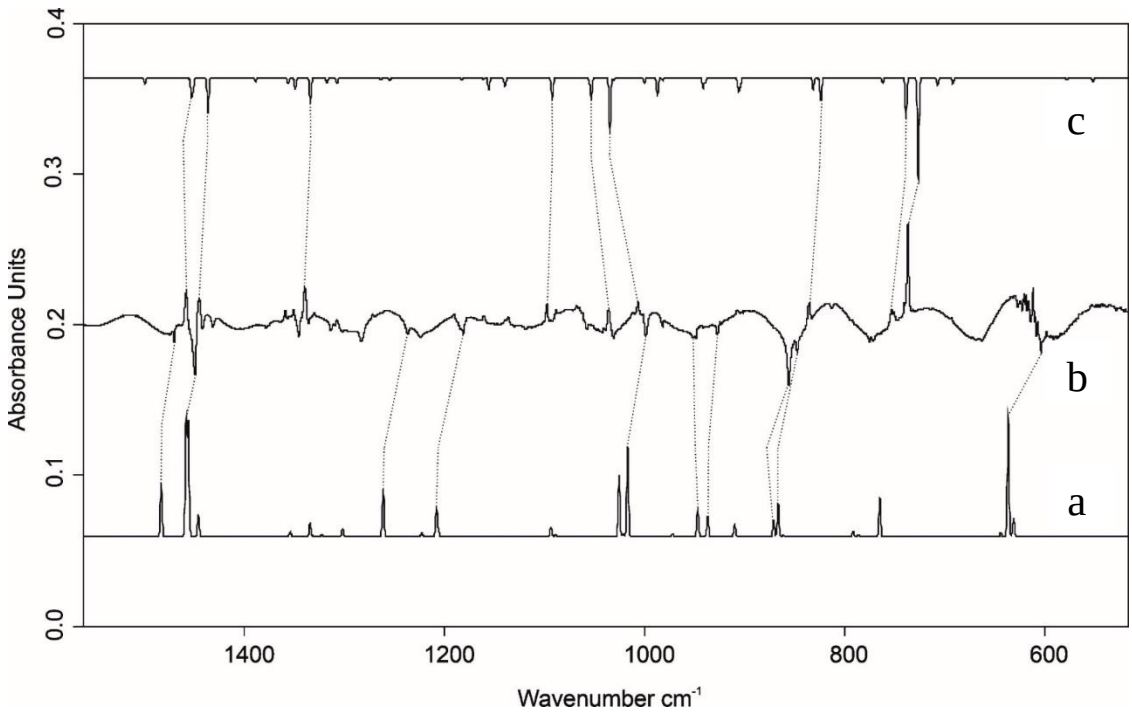

Figure S25: (a) IR spectrum of **1** computed at UB3LYP/6-311++G(3df,2pd) (anharmonic). (b) IR difference spectra showing the tunneling of **1** after 16 h in argon at 3.5 K. Downward bands assigned to **1** disappear after 16 h. Upward bands assigned **4** appear after 16 h waiting. (c) IR spectrum of **4** computed at B3LYP/6-311++G(3df,2pd) (anharmonic).

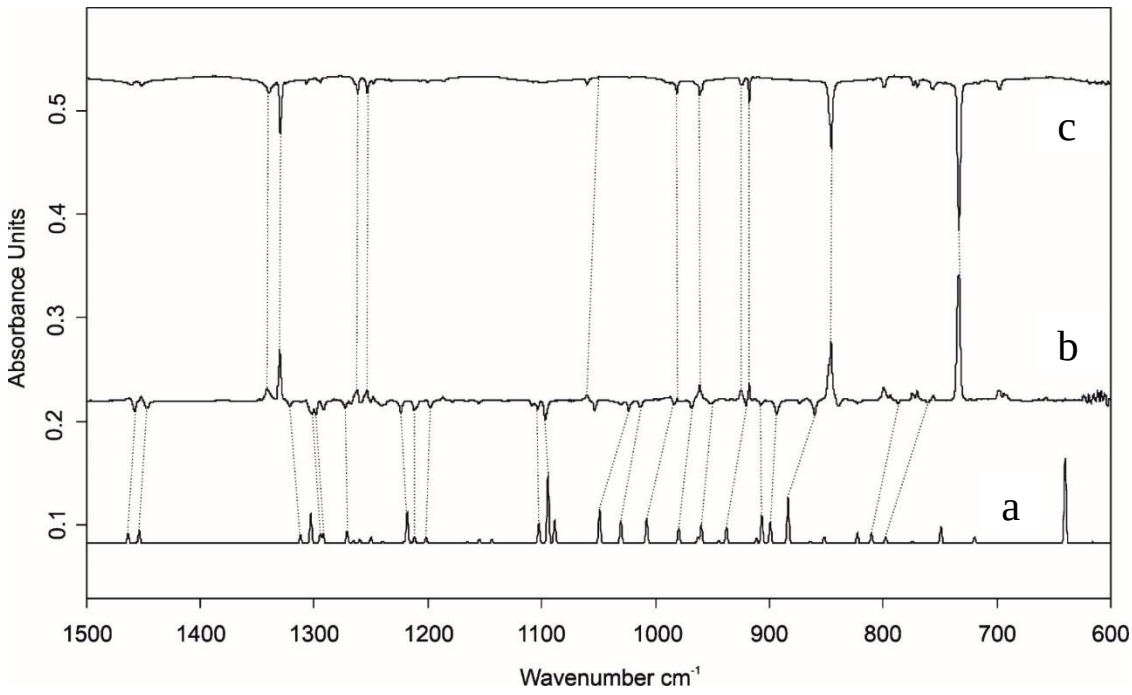

Figure S26: (a) IR spectrum of **2** computed at B3LYP/6-311++G(3df,2pd) (anharmonic). (b) IR difference spectra showing the photochemistry of **2** after irradiating for 10 min at λ = 627 nm in argon at 3.5 K. Downward bands assigned to **2** disappear after irradiation. Upward bands assigned **9** appear after irradiation. (c) IR spectra showing the deposition of **9** with subsequent trapping in a nitrogen matrix at 3.5 K.

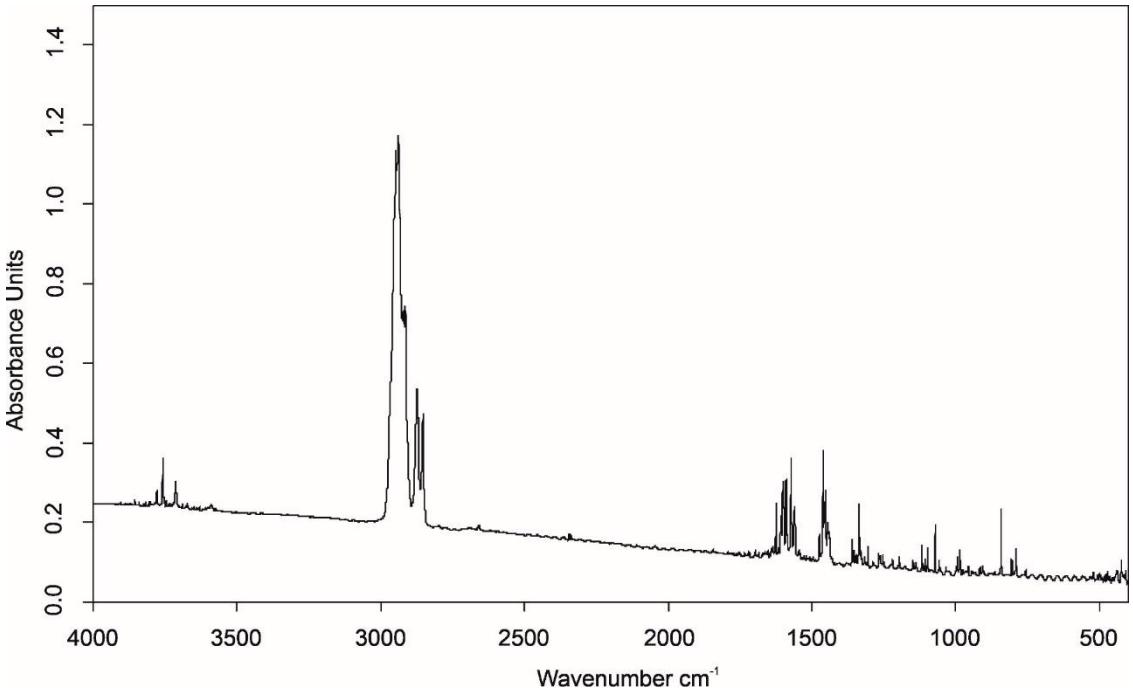

Figure S27: IR spectra showing the deposition of **13** with subsequent trapping in a nitrogen matrix at 3.5 K.

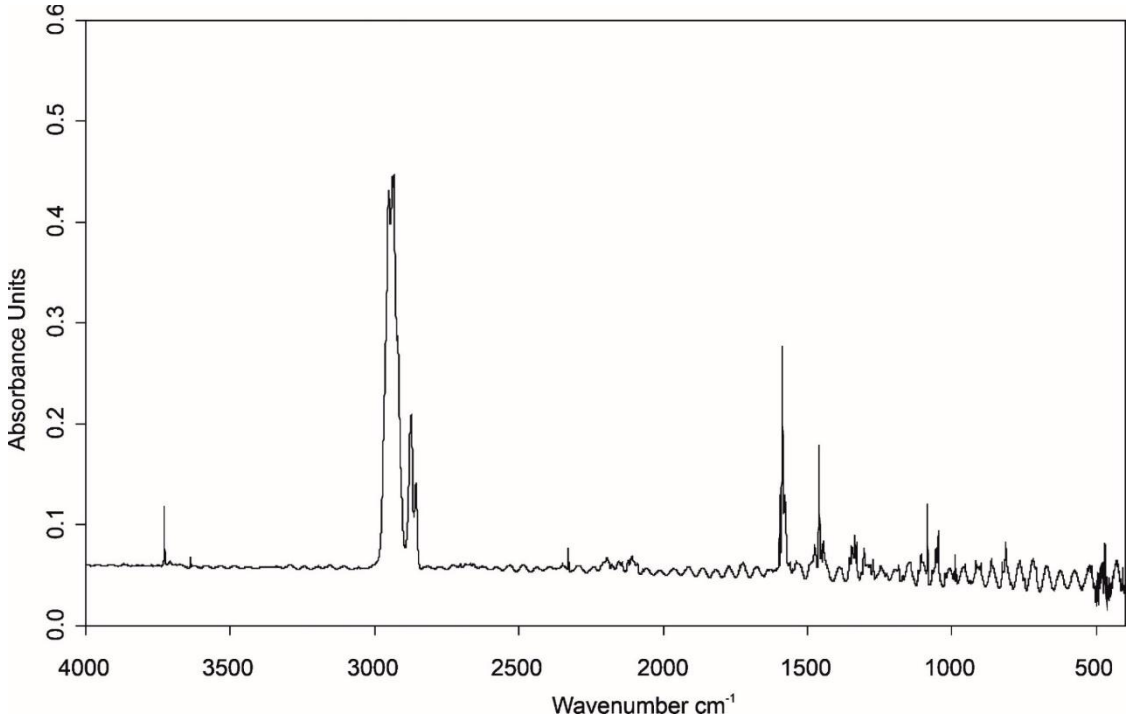

Figure S28: IR spectra showing the deposition of (d_2-**13** with subsequent trapping in a nitrogen matrix at 3.5 K.

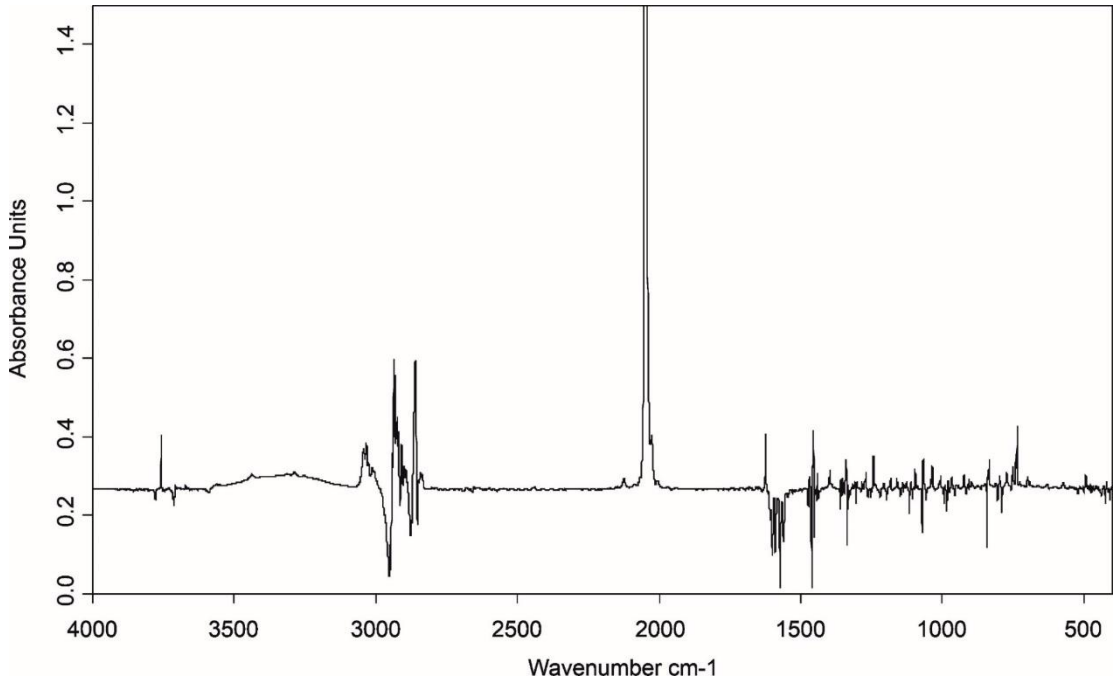

Figure S29: IR difference spectra showing the photochemistry of **13** after irradiation with λ = 365 nm in argon at 3.5 K. Downward bands assigned to **13** disappear after 20 min irradiation. Upward bands assigned to protoadamantane diazo (**28**) appear after 20 min irradiation.

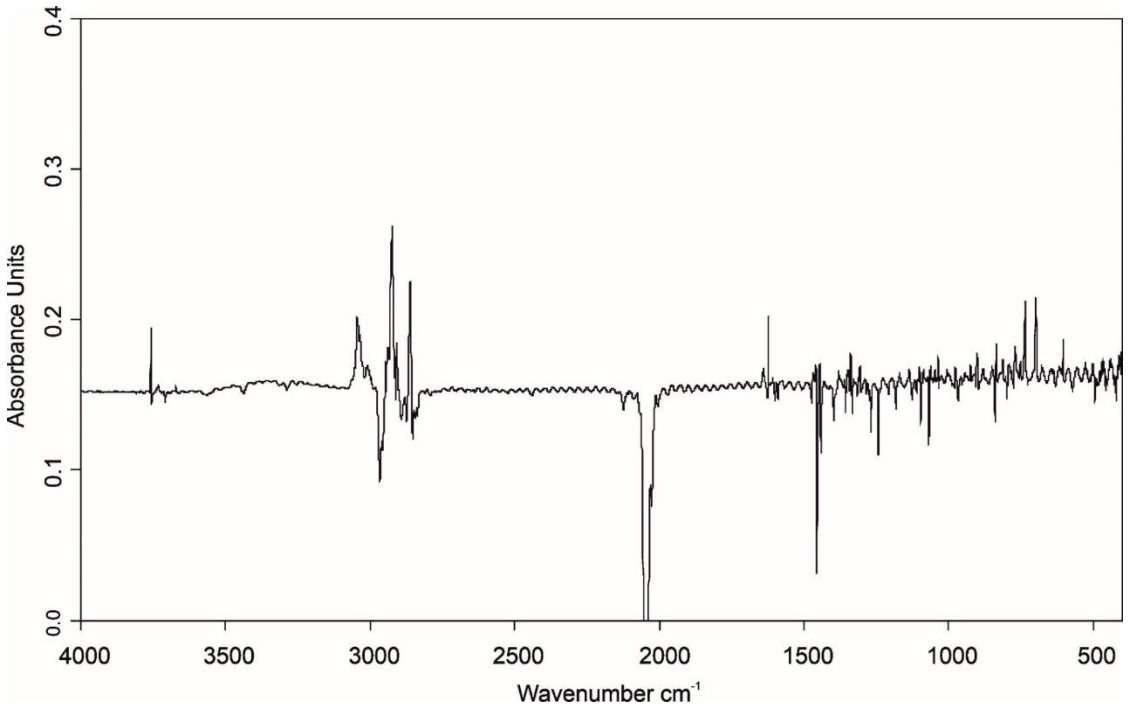

Figure S30: IR difference spectra showing the photochemistry of **28** after irradiation with λ = 254 nm in argon at 3.5 K. Downward bands assigned to **28** disappear after 20 min irradiation. Upward bands assigned to **4** and **12** appear after 20 min irradiation.

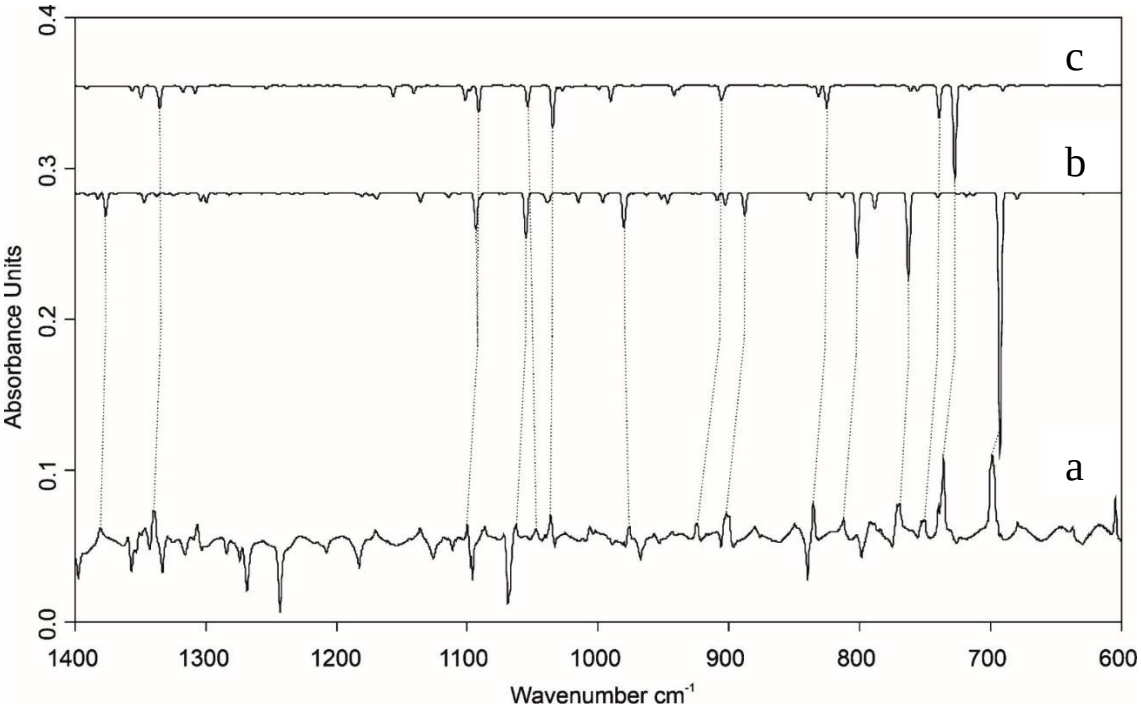

Figure S31: **Figure S29**: (a) IR difference spectra showing the photochemistry of **28** after irradiation with λ = 254 nm in argon at 3.5 K. Downward bands assigned to **28** disappear after 20 min irradiation. Upward bands assigned to **12** and **4** appear after 20 min irradiation. (b) IR spectrum of **12** computed at B3LYP/6-311++G(3df,2pd) (anharmonic). (c) IR spectrum of **4** computed at B3LYP/6-311++G(3df,2pd) (anharmonic).

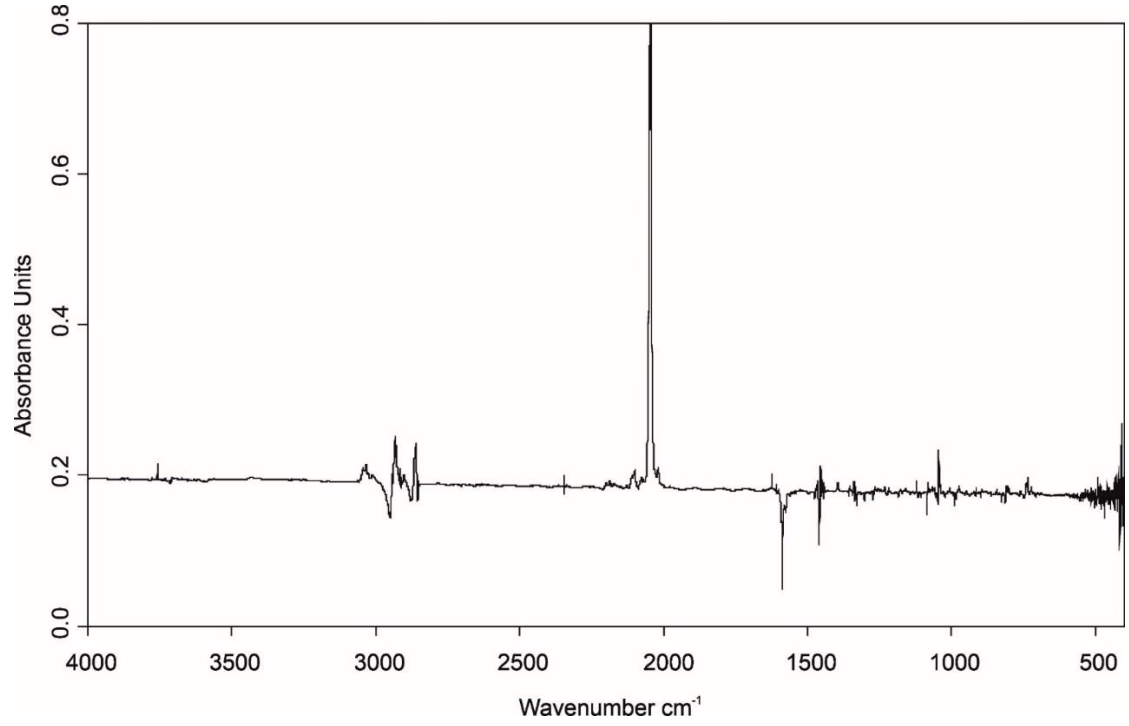

Figure S32: IR difference spectra showing the photochemistry of d_2-**28** after irradiation with λ = 365 nm in argon at 3.5 K. Downward bands assigned to d_2-**28** disappear after 20 min irradiation. Upward bands assigned to d_2-**28** appear after 20 min irradiation.

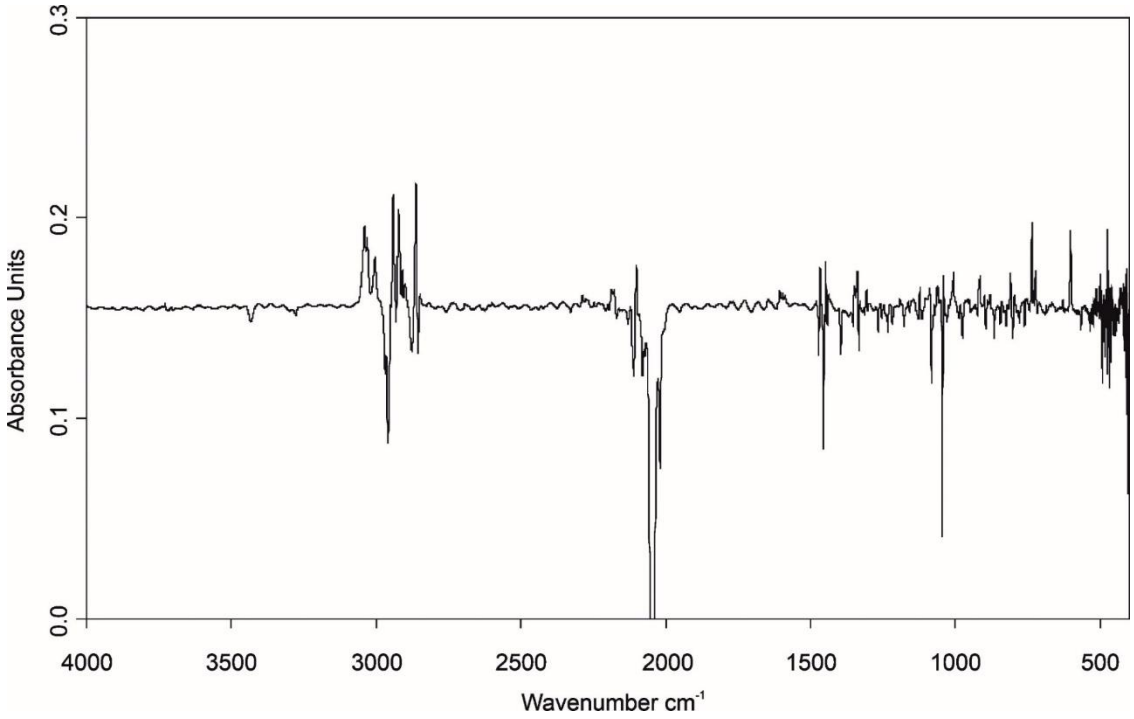

Figure S33: IR difference spectra showing the photochemistry of d_2-**28** after irradiation with λ = 254 nm in argon at 3.5 K. Downward bands assigned to d_2-**28** disappear after 20 min irradiation. Upward bands assigned to d_2-**12** and d_2-**4** appear after 20 min irradiation.

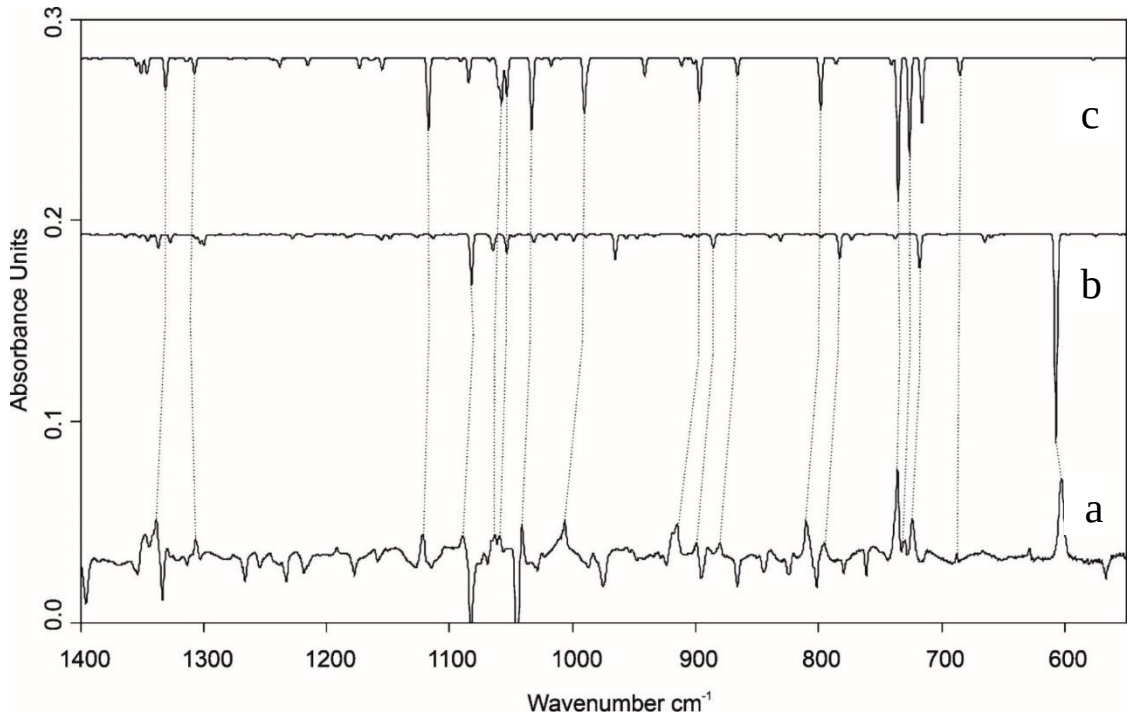

Figure S34: (a) IR difference spectra showing the photochemistry of d_2-**28** after irradiation with λ = 254 nm in argon at 3.5 K. Downward bands assigned to d_2-**28** disappear after 20 min irradiation. Upward bands assigned to d_2-**12** and d_2-**4** appear after 20 min irradiation. (b) IR spectrum of d_2-**12** computed at B3LYP/6-311++G(3df,2pd) (anharmonic). (c) IR spectrum of d_2-**4** computed at B3LYP/6-311++G(3df,2pd) (anharmonic).

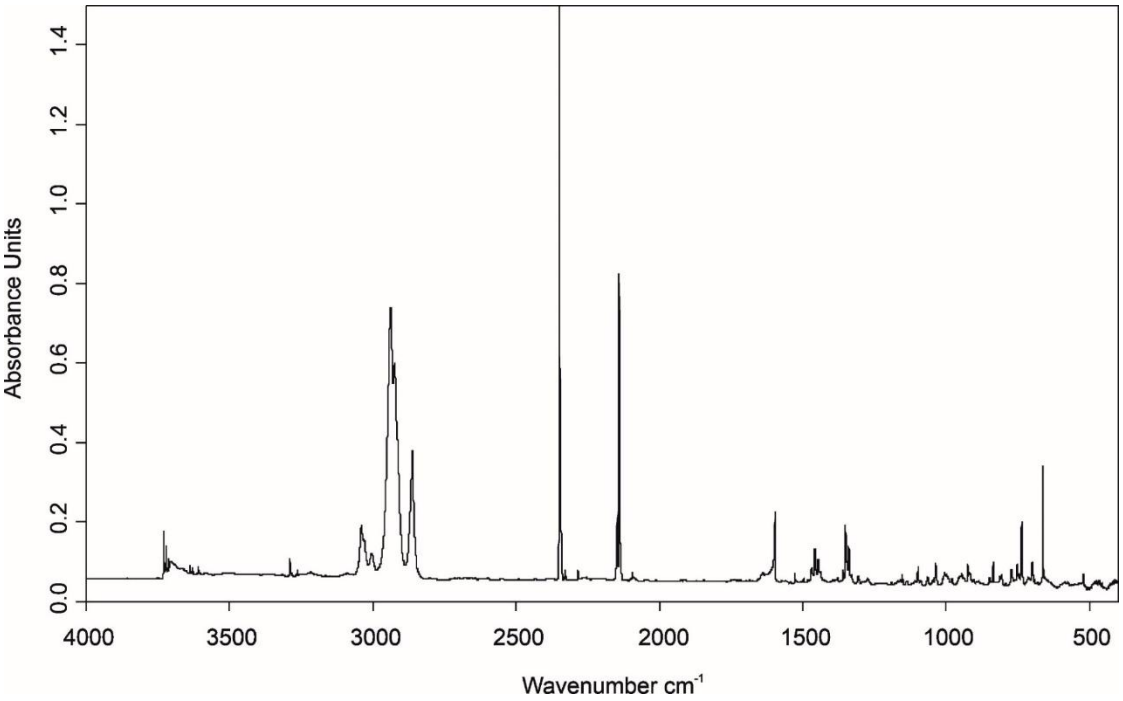

Figure S35: IR spectra showing the pyrolysis product of **13** with subsequent trapping in an argon matrix at 3.5 K.

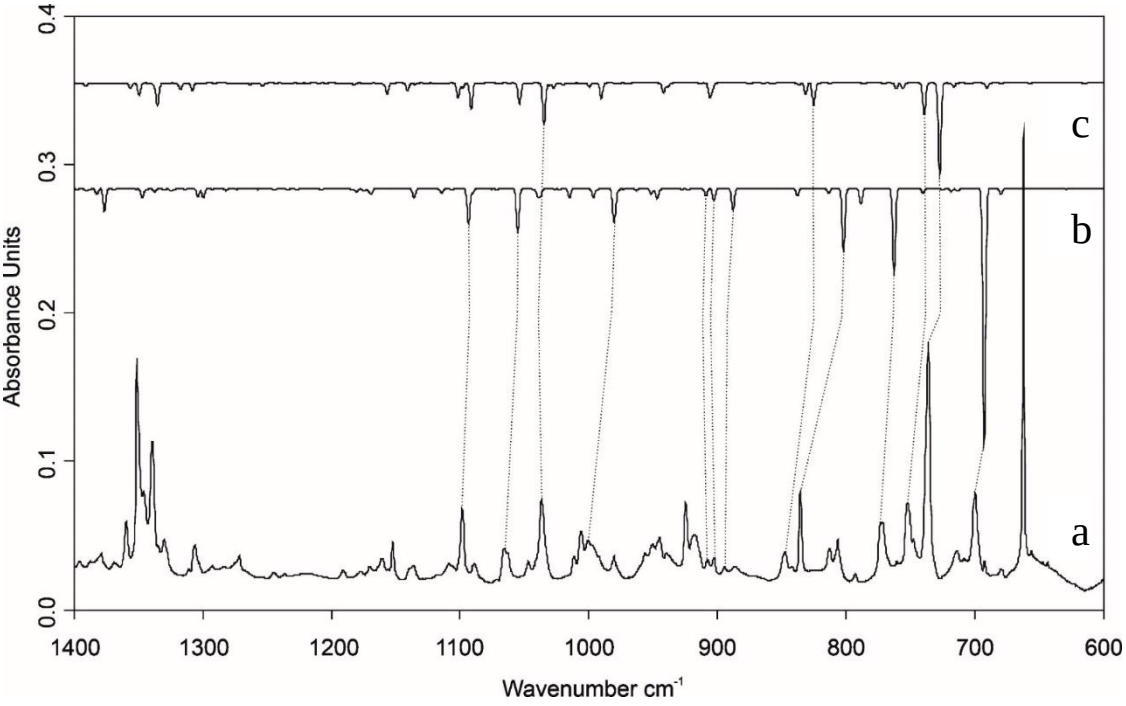

Figure S36: (a) IR spectra showing the pyrolysis product of **13** with subsequent trapping in an argon matrix at 3.5 K. (b) IR spectrum of **12** computed at B3LYP/6-311++G(3df,2pd) (anharmonic). (c) IR spectrum of **4** computed at B3LYP/6-311++G(3df,2pd) (anharmonic).

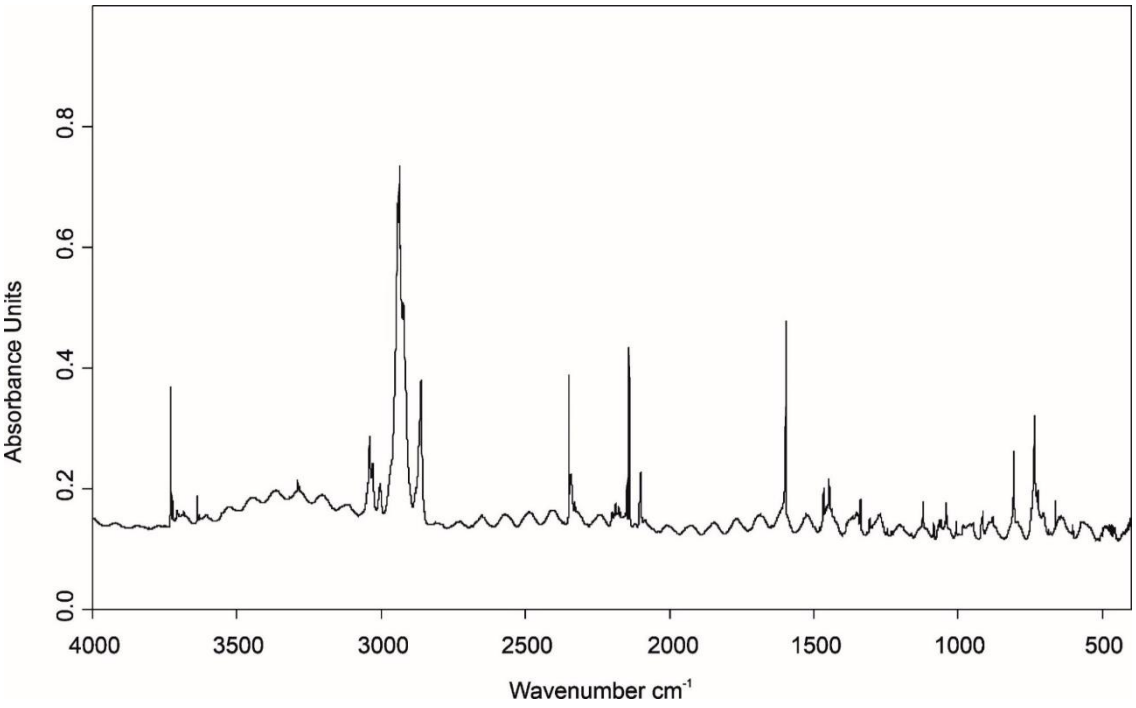

Figure S37: IR spectra showing the pyrolysis product of d_2-**13** with subsequent trapping in an argon matrix at 3.5 K.

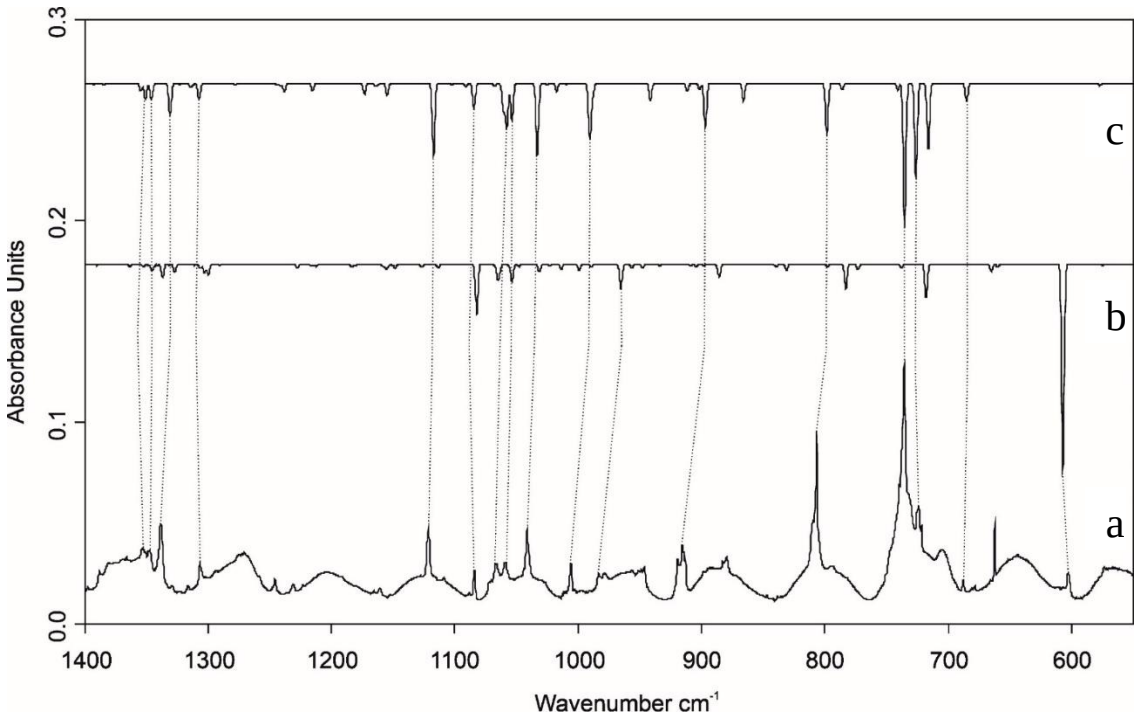

Figure S38: (a) IR spectra showing the pyrolysis product of d_2-**13** with subsequent trapping in an argon matrix at 3.5 K. (b) IR spectrum of d_2-**12** computed at B3LYP/6-311++G(3df,2pd) (anharmonic). (c) IR spectrum of d_2-**4** computed at B3LYP/6-311++G(3df,2pd) (anharmonic).

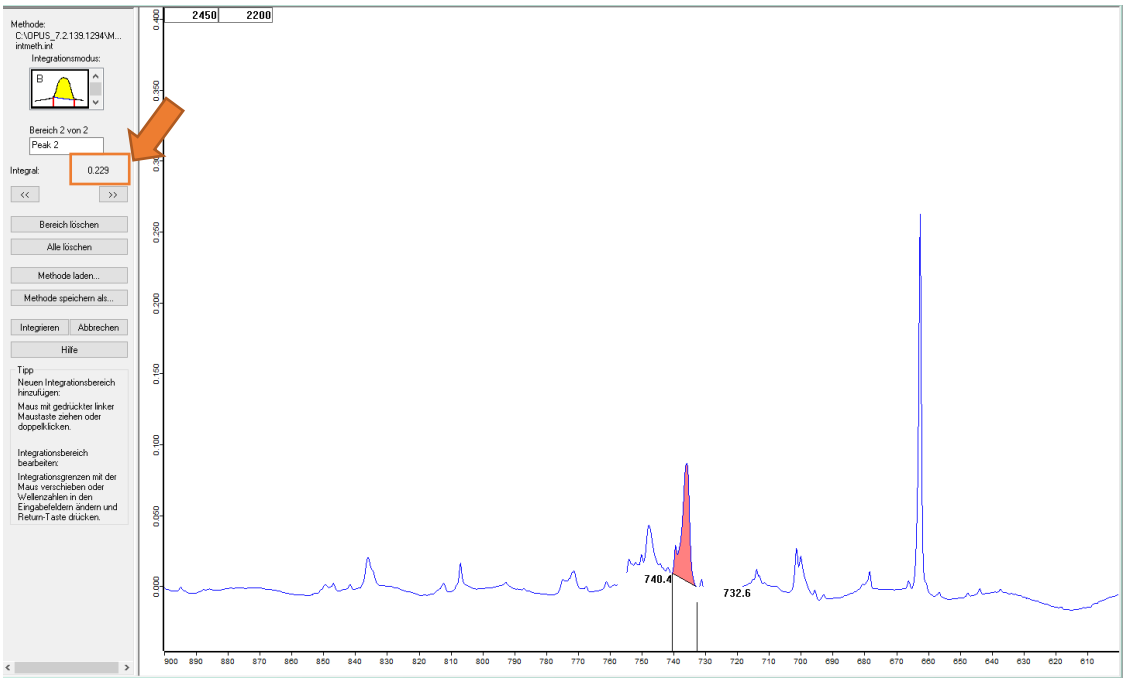

Figure S39: Screenshot of the IR spectrum showing the pyrolysis product of **13**, subsequently trapped in an argon matrix at 3.5 K. Integration of a peak from molecule **4**.

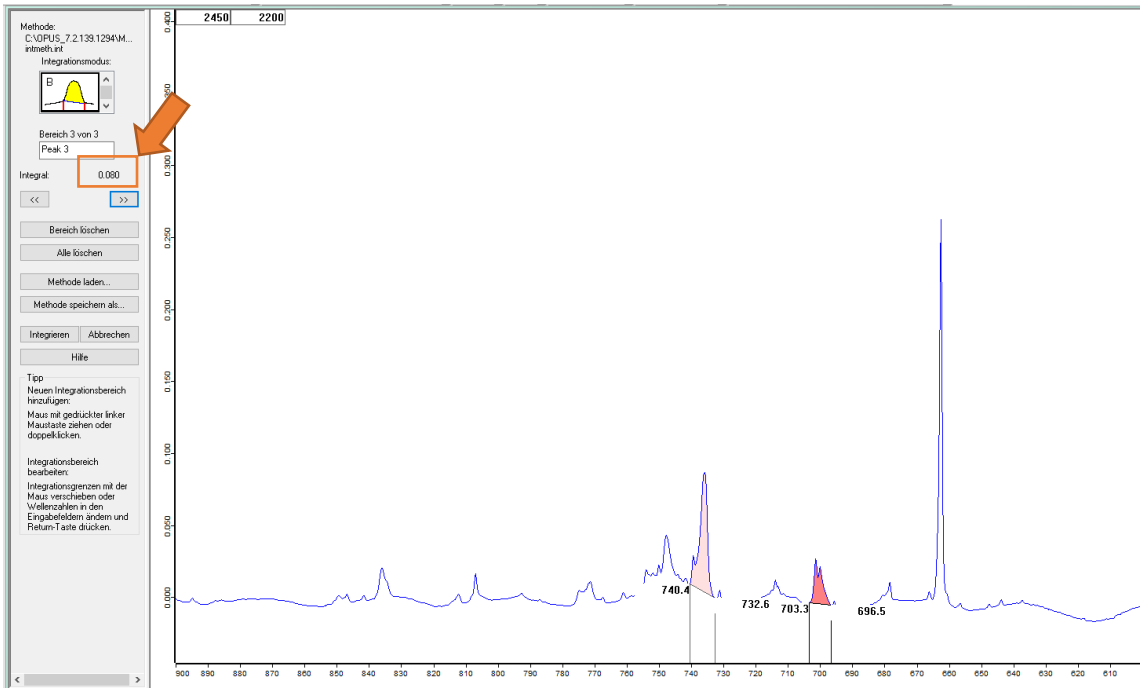

Figure S40: Screenshot of the IR spectrum showing the pyrolysis product of **13**, subsequently trapped in an argon matrix at 3.5 K. Integration of a peak from molecule **12**.

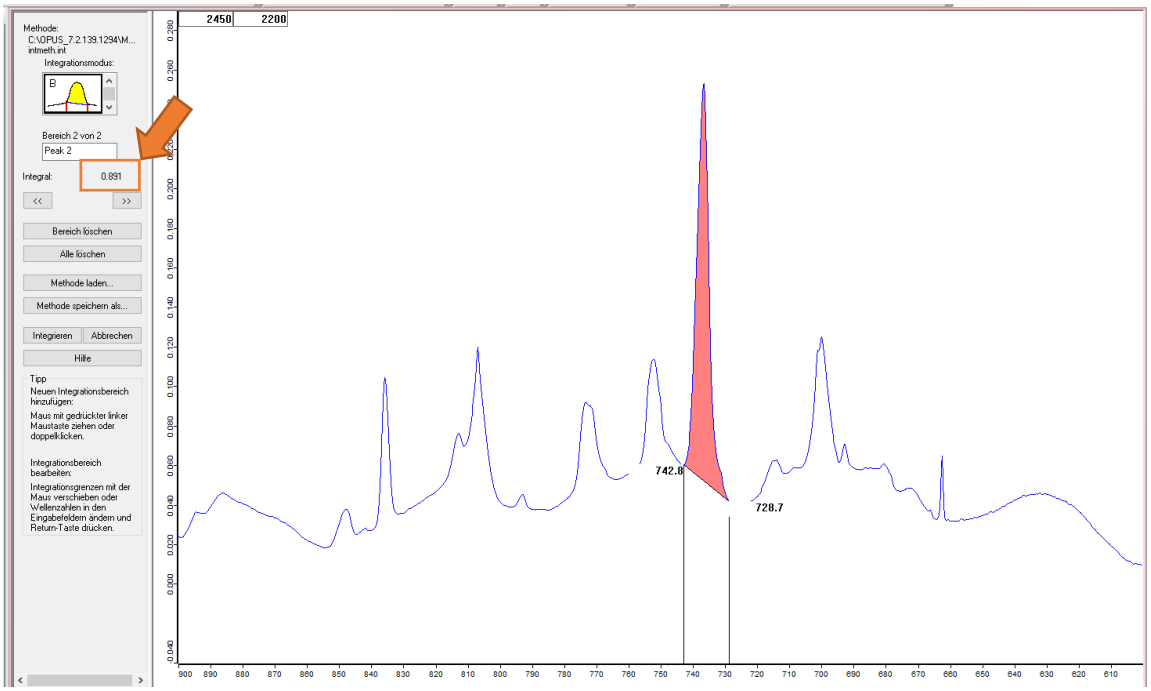

Figure S41: Screenshot of the IR spectrum showing the pyrolysis product of **13**, subsequently trapped in an argon matrix at 3.5 K. Integration of a peak from molecule **4**.

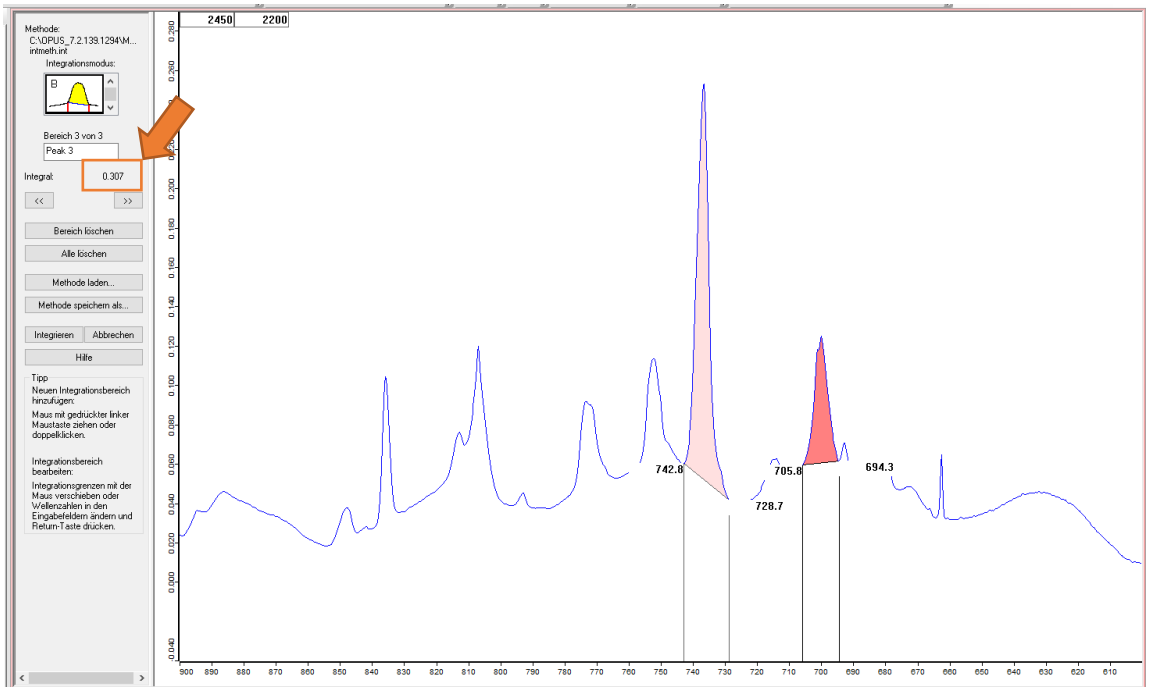

Figure S42: Screenshot of the IR spectrum showing the pyrolysis product of **13**, subsequently trapped in an argon matrix at 3.5 K. Integration of a peak from molecule **12**.

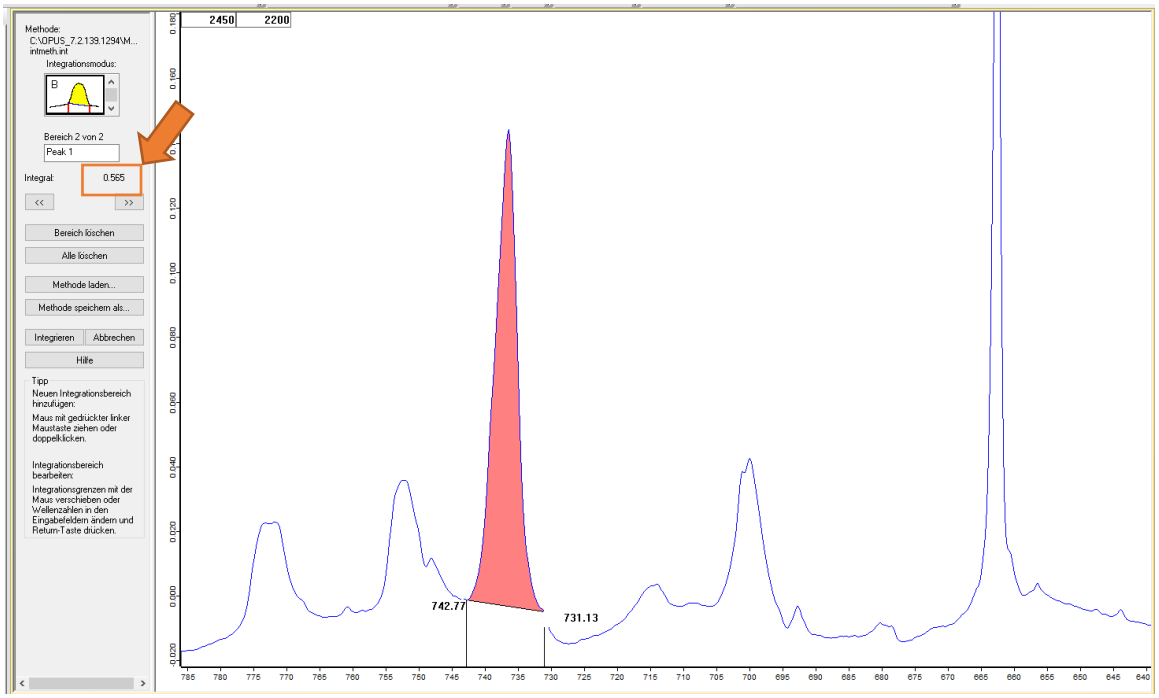

Figure S43: Screenshot of the IR spectrum showing the pyrolysis product of **13**, subsequently trapped in an argon matrix at 3.5 K. Integration of a peak from molecule **4**.

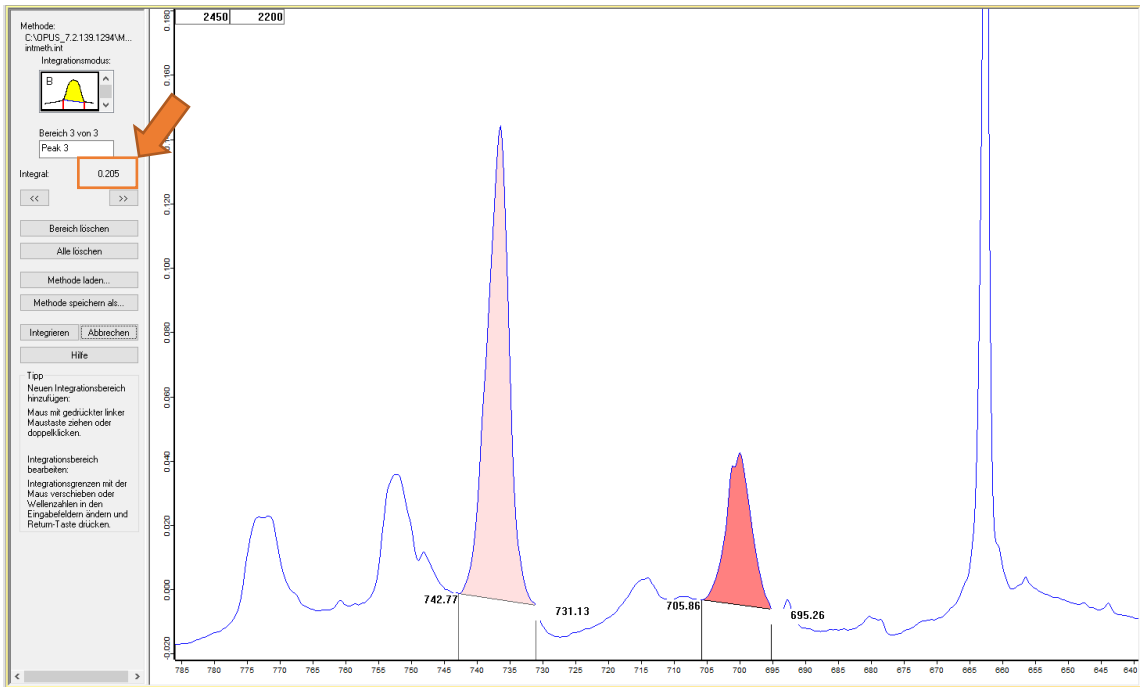

Figure S44: Screenshot of the IR spectrum showing the pyrolysis product of **13**, subsequently trapped in an argon matrix at 3.5 K. Integration of a peak from molecule **12**.

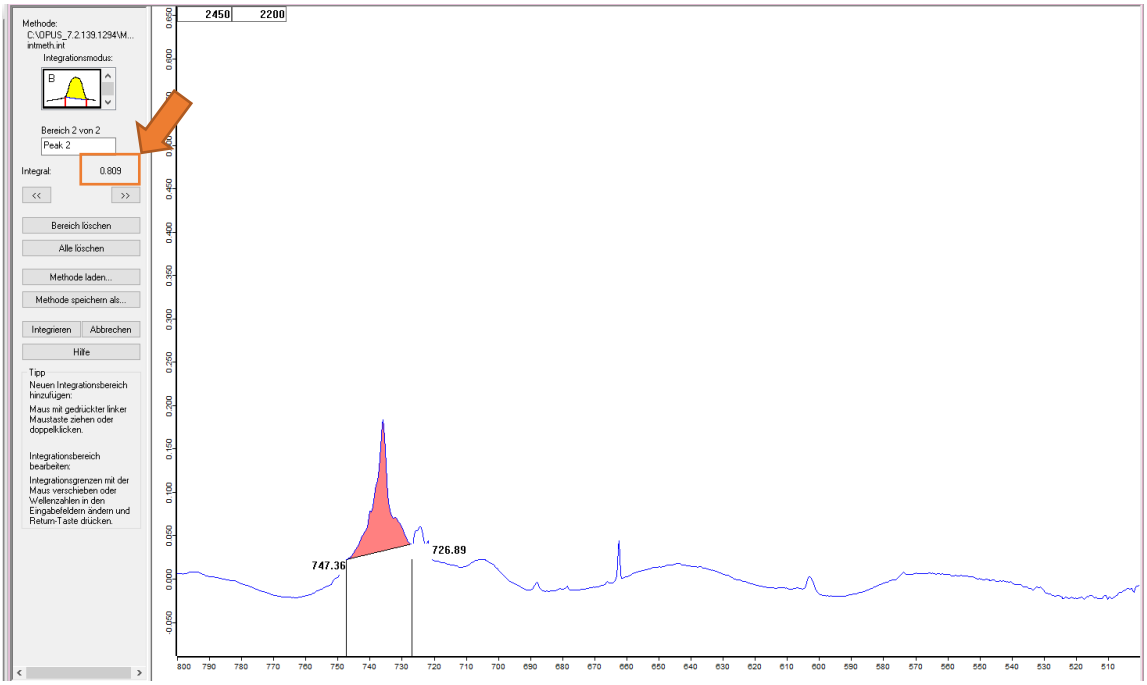

Figure S45: Screenshot of the IR spectrum showing the pyrolysis product of d_2-**13**, subsequently trapped in an argon matrix at 3.5 K. Integration of a peak from molecule d_2-**4**.

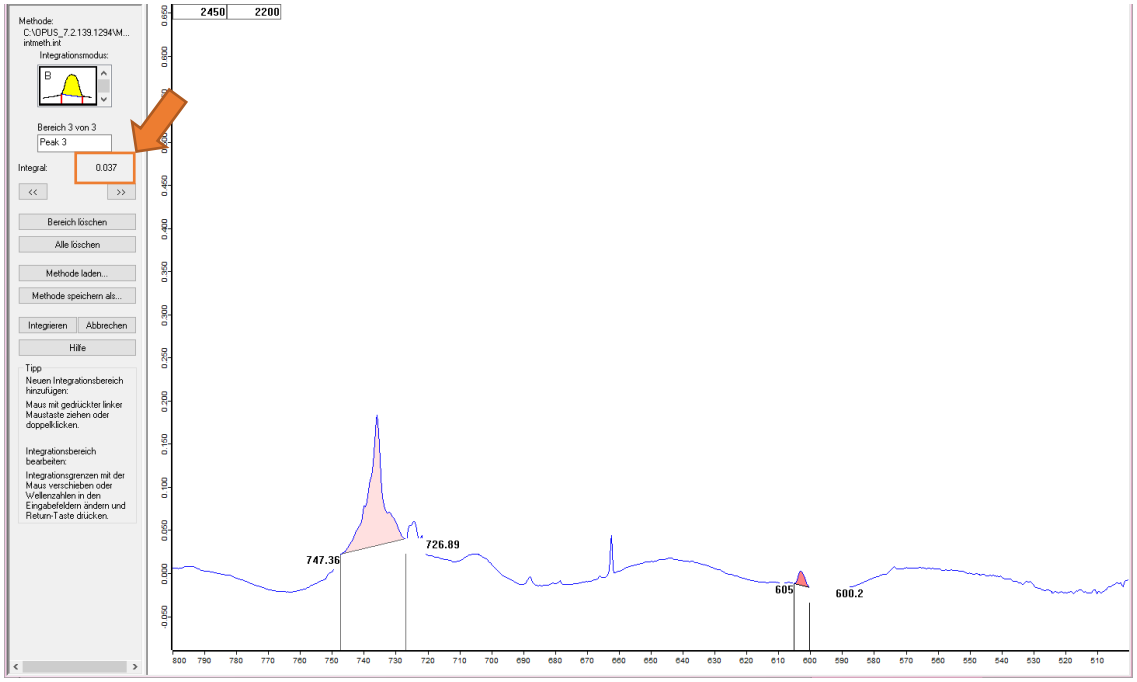

Figure S46: Screenshot of the IR spectrum showing the pyrolysis product of d_2-**13**, subsequently trapped in an argon matrix at 3.5 K. Integration of a peak from molecule d_2-**12**.

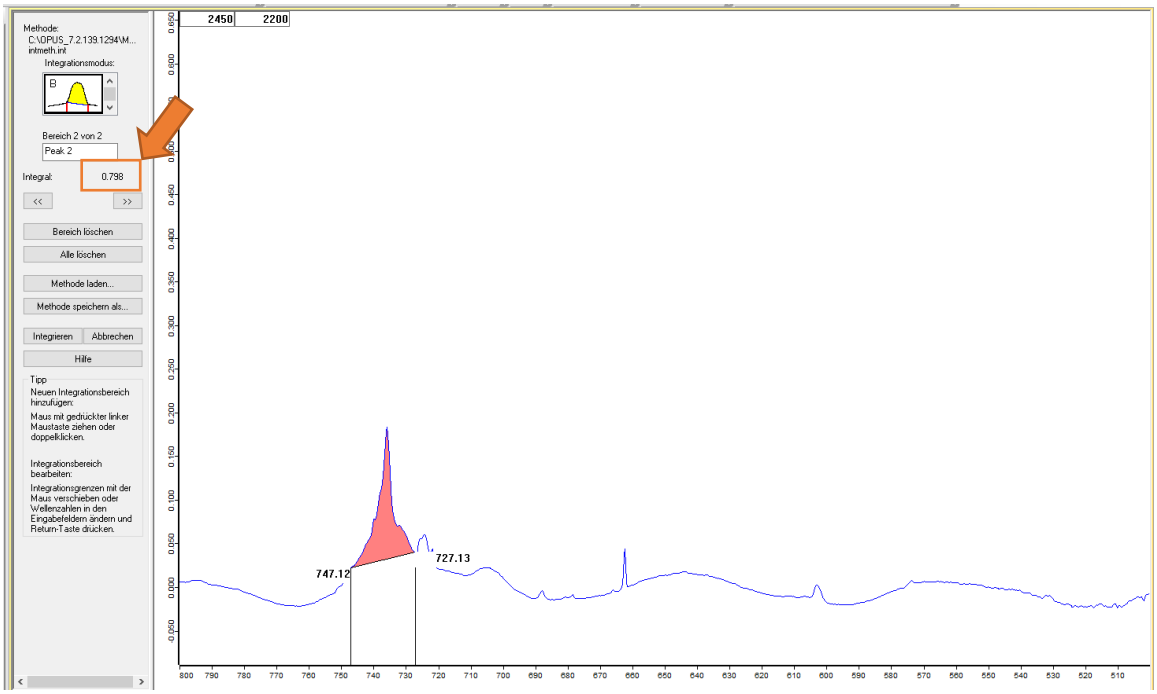

Figure S47: Screenshot of the IR spectrum showing the pyrolysis product of d_2-**13**, subsequently trapped in an argon matrix at 3.5 K. Integration of a peak from molecule d_2-**4**.

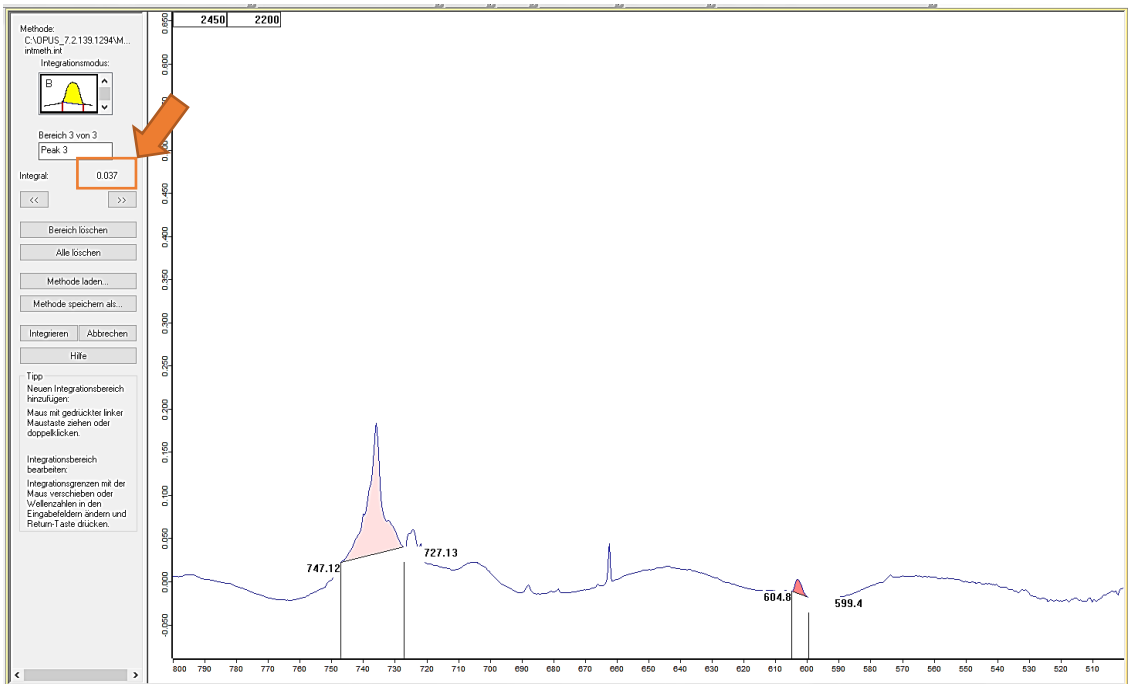

Figure S48: Screenshot of the IR spectrum showing the pyrolysis product of d_2-**13**, subsequently trapped in an argon matrix at 3.5 K. Integration of a peak from molecule d_2-**12**.

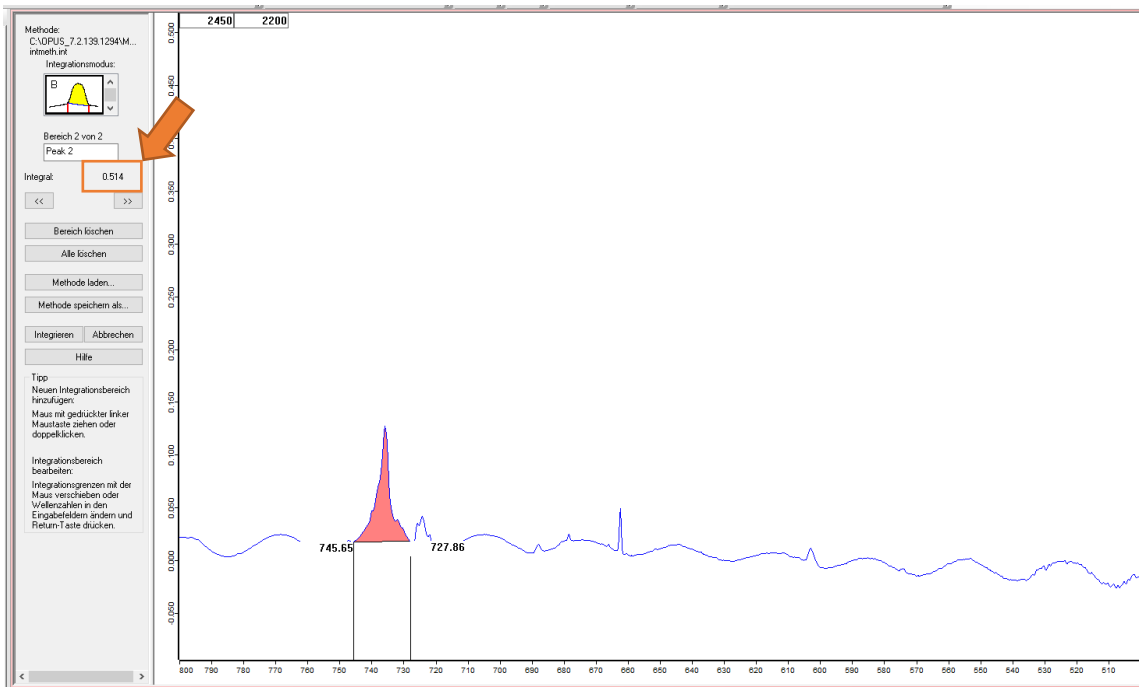

Figure S49: Screenshot of the IR spectrum showing the pyrolysis product of d_2-**13**, subsequently trapped in an argon matrix at 3.5 K. Integration of a peak from molecule d_2-**4**.

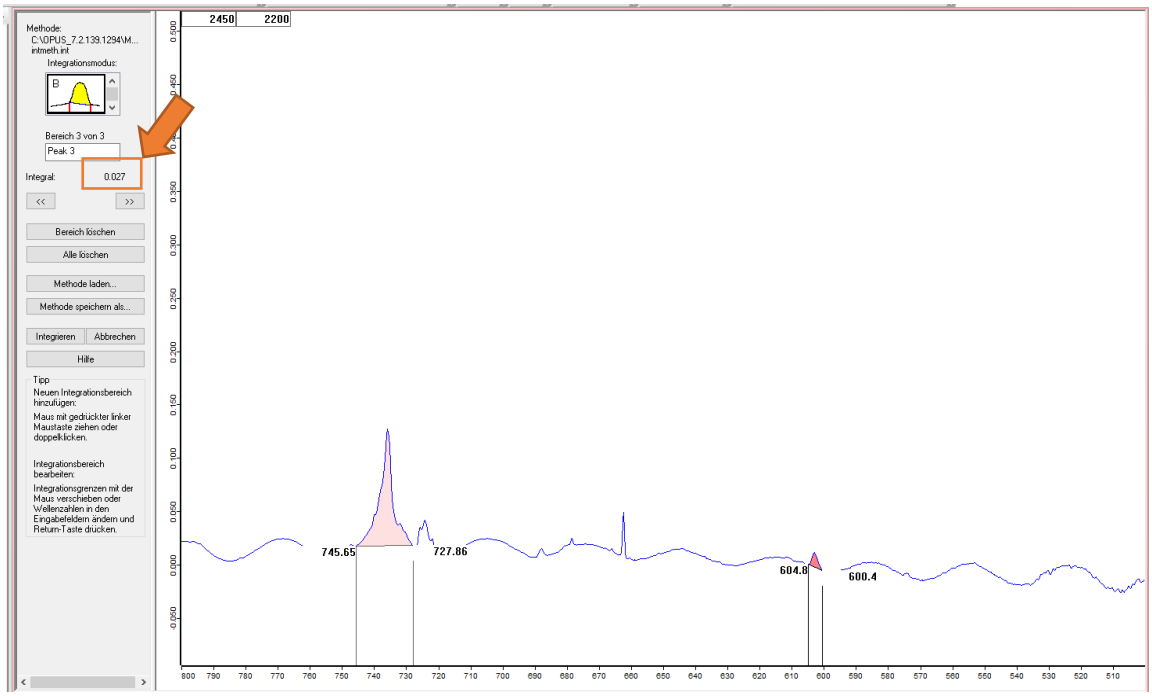

Figure S50: Screenshot of the IR spectrum showing the pyrolysis product of d_2-**13**, subsequently trapped in an argon matrix at 3.5 K. Integration of a peak from molecule d_2-**12**.

Table S1: Experimental (Ar matrix, 3.5 K) and computed IR frequencies of **1** band origins in cm^{-1}, computed intensities (km mol^{-1}) in parantheses.

Mode	**1** Computed[a]	**1** N_2 3.5 K[b]	Assignment
1	3056 (38.8)	not definitively identifiable	Antisymmetric stretching C–H (CH_2)
2	3056 (71.4)	not definitively identifiable	Antisymmetric stretching C–H (CH_2)
3	3054 (32.6)	not definitively identifiable	Antisymmetric stretching C–H (CH_2)
5	3043 (41.0)	not definitively identifiable	Antisymmetric stretching C–H (CH_2)
6	3035 (32.6)	not definitively identifiable	Symmetric stretching C–H (CH_2)
7	3026 (94.4)	not definitively identifiable	Symmetric stretching C–H (CH_2)
8	3026 (169.3)	not definitively identifiable	Symmetric stretching C–H (CH_2)
9	3024 (57.3)	not definitively identifiable	Symmetric stretching C–H (CH)
11	3010 (22.8)	not definitively identifiable	Symmetric stretching C–H (CH_2)
12	3010 (4.5)	not definitively identifiable	Symmetric stretching C–H (CH_2)
14	3006 (13.6)	not definitively identifiable	Symmetric stretching C–H (CH_2)
15	1516 (2.7)	not definitively identifiable	Scissoring C–H (CH_2)
16	1499 (9.6)	1470 (m)	Scissoring C–H (CH_2)
17	1495 (10.2)	1470 (m)	Scissoring C–H (CH_2)
18	1490 (3.5)	/	Scissoring C–H (CH_2)
24	1368 (1.0)	1357 (w)	Wagging C–H
27	1339 (0.7)	1313 (w)	Wagging C–H (CH)

Mode	**1** Computed[a]	**1** N_2 3.5 K[b]	Assignment
33	1238 (3.2)	1235 (m)	Twisting C–H (CH)
37	1113 (0.9)	1111 (w)	Wagging C–H
40	1046 (7.1)	1043 (m)	Scissoring C–C
41	1042 (4.5)	1038 (w)	Rocking C–C
43	978 (1.4)	982 (w)	Scissoring C–C
44	957 (1.5)	951 (m)	Scissoring C–C
45	932 (1.3)	927 (m)	Wagging C–C
49	886 (3.5)	870 (w)	Wagging C–C
51	784 (2.2)	775 (w)	Twisting C–C
54	643 (7.8)	602 (s)	Twisting C–C

[a]B3LYP/6-311++G(3df,2pd), anharmonic, unscaled frequencies, intensities (in parentheses) in km mol^{-1}. [b]Experiment: argon matrix, 3.5 K; approximate relative intensities (w: weak, m: medium, s: strong).

Table S2: Experimental (Ar matrix, 3.5 K) and computed IR frequencies of **2** band origins in cm^{-1}, computed intensities (km mol^{-1}) in parantheses.

Mode	**2** Computed[a]	**2** N_2 3.5 K[b]	Assignment
1	3006 (11.4)	not definitively identifiable	Symmetric stretching C–H (CH)
2	2982 (45.3)	not definitively identifiable	Symmetric stretching C–H
3	2974 (72.6)	not definitively identifiable	Symmetric stretching C–H (CH)
4	2964 (10.3)	not definitively identifiable	Symmetric stretching C–H (CH)
5	2951 (64.9)	not definitively identifiable	Symmetric stretching C–H (CH)
6	2942 (66.9)	not definitively identifiable	Antisymmetric stretching C–H (CH2)
7	2935 (84.7)	not definitively identifiable	Antisymmetric stretching C–H (CH2)

Mode	**2** Computed[a]	**2** N_2 3.5 K[b]	Assignment
8	2925 (8.4)	not definitively identifiable	Antisymmetric stretching C–H (CH2)
9	2911 (18.1)	not definitively identifiable	Antisymmetric stretching C–H (CH2)
10	2865 (28.9)	not definitively identifiable	Antisymmetric stretching C–H (CH)
11	2847 (26.5)	not definitively identifiable	Antisymmetric stretching C–H (CH2)
12	1463 (1.0)	1458 (m)	Scissoring C–H (CH2)
13	1454 (1.3)	1446 (m)	Scissoring C–H (CH2)
14	1311 (0.8)	1303 (m)	Scissoring C–H (CH2)
15	1303 (3.1)	1298 (m)	Scissoring C–H (CH2)
16	1292 (1.0)	1291 (w)	Rocking C–H (CH2)
17	1271 (1.2)	1272 (w)	Wagging C–H (CH2)
18	1217 (3.3)	1223 (m)	Wagging C–H (CH)
19	1212 (0.7)	1211 (m)	Twisting C–H
20	1201 (0.6)	1198 (w)	Wagging C–H (CH2)
21	1102 (2.1)	1104 (w)	Twisting C–H (CH)
22	1094 (7.1)	1096 (s)	Twisting C–H (CH2)
23	1088 (2.4)	/	Twisting C–H (CH2)
24	1049 (3.6)	1054 (m)	Twisting C–H (CH2)
25	1030 (2.4)	1023 (m)	Wagging C–H
26	1008 (2.6)	1013 (w)	Rocking C–C
27	980 (1.6)	984 (w)	Rocking C–C
28	962 (0.6)	969 (w)	Scissoring C–C
29	938 (1.7)	951 (w)	Rocking C–C
30	906 (2.9)	909 (w)	Scissoring C–C

Mode	**2** Computed[a]	**2** N_2 3.5 K[b]	Assignment
31	899 (2.2)	893 (s)	Scissoring C–C
32	883 (1.1)	860 (s)	Twisting C–C
33	823 (1.1)	/	Wagging C–C
34	810 (1.1)	/	Twisting C–C
35	749 (1.7)	/	Wagging C–C
36	640 (8.9)	/	Twisting C–C

[a]B3LYP/6-311++G(3df,2pd), anharmonic, unscaled frequencies, intensities (in parentheses) in km mol^{-1}. [b]Experiment: argon matrix, 3.5 K; approximate relative intensities (w: weak, m: medium, s: strong).

Table S3: Integrals, ratio, and mean of the undeuterated compounds.

	Figure S39-S40	Figure S41-S42	Figure S43-S44
4	0.229	0.891	0.565
12	0.080	0.307	0.205
Ratio	0.651	0.655	0.637
Mean	0.648		

Table S4: Integrals, ratio, and mean of the deuterated compounds.

	Figure S45-S46	Figure S47-S48	Figure S49-S50
d_2-**4**	0.809	0.798	0.514
d_2-**12**	0.037	0.037	0.027
Ratio	0.954	0.954	0.947
Mean	0.952		

Table S5: Determination of the vibrational frequency scaling factors for the deuterated and undeuterated compounds.

	Wavenumber	Intensitiy
4	727.395	8.8313
d_2-**4**	726.107	4.2802
Factor (**4**)	2.063	
12	692.806	22.987
d_2-**12**	615.781	18.357
Factor (**12**)	1.252	

Table S6: Normalizaed experimental intensities using scaling factor.

	Figure S45-S46	Figure S47-S48	Figure S49-S50
4 (with correction)	1.669	1.647	1.061
12 (with correction)	0.046	0.046	0.033
Ratio (with correction)	0.972	0.972	0.968
Mean (with correction)	0.971		

UV/Vis Spectral Data

Table S7: TD-B3LYP/6-311++G(3df,2pd) computed vertical excitation energies of adamantane diazirine (**5**).

Excitation Energy λ / nm	Oscillator Strength (*f*)
369.88	0.0007
234.59	0.0029
200.57	0.0019

Table S8: TD-B3LYP/6-311++G(3df,2pd) computed vertical excitation energies of diazoadamantane (**26**).

Excitation Energy λ / nm	Oscillator Strength (*f*)
295.64	0.0014
256.37	0.0217
233.00	0.0023
227.41	0.0098
225.25	0.0053
221.88	0.0065
212.50	0.1004
204.25	0.0059

Table S9: TD-B3LYP/6-311++G(3df,2pd) computed vertical excitation energies of adamantylidene (**1**).

Excitation Energy λ / nm	Oscillator Strength (*f*)
1083.82	0.0030
674.31	0.0011
296.77	0.0038
291.06	0.0058
258.88	0.0117
254.50	0.0063
251.39	0.0038
251.03	0.0013
246.71	0.0070

Table S10: TD-B3LYP/6-311++G(3df,2pd) computed vertical excitation energies of 2,4-dehydroadamantane (**4**).

Excitation Energy λ / nm	Oscillator Strength (*f*)
210.51	0.0076

Table S11: TD-B3LYP/6-311++G(3df,2pd) computed vertical excitation energies of adamantane alkene (**10**).

Excitation Energy λ / nm	Oscillator Strength (*f*)
339.62	0.0442
293.39	0.0148
261.6	0.0199
259.25	0.0206
250.98	0.0022
236.1	0.0035
233.77	0.0107
228.32	0.0054
224.94	0.0055
220.84	0.0119
209.63	0.0035
204.01	0.0156

Table S12: TD-B3LYP/6-311++G(3df,2pd) computed vertical excitation energies of pentacycloundecane diazirine (**6**).

Excitation Energy λ / nm	Oscillator Strength (*f*)
366.57	0.0009
240.64	0.0019
212.18	0.0014

Table S13: TD-B3LYP/6-311++G(3df,2pd) computed vertical excitation energies of pentacycloundecane diazo (**27**).

Excitation Energy λ / nm	Oscillator Strength (*f*)
258.31	0.0174
254.53	0.0173
252.75	0.0027
231.48	0.0379
226.98	0.0076
225.82	0.0095
223.26	0.0051
220.11	0.0128
214.9	0.0196

Table S14: TD-B3LYP/6-311++G(3df,2pd) computed vertical excitation energies of pentacycloundecane-carbene (**2**).

Excitation Energy λ / nm	Oscillator Strength (*f*)
974.94	0.0043
727.79	0.0010
274.78	0.0018
273.51	0.0010
251.71	0.0012
250.38	0.0046
248.18	0.0037
247.41	0.0038
244.18	0.0017

Table S15: TD-B3LYP/6-311++G(3df,2pd) computed vertical excitation energies of churchane (**11**).

Excitation Energy λ / nm	Oscillator Strength (*f*)
192.38	0.0094

Table S16: TD-B3LYP/6-311++G(3df,2pd) computed vertical excitation energies of homohypostrophene (**9**).

Excitation Energy λ / nm	Oscillator Strength (*f*)
233.45	0.0279
221.66	0.0211
215.15	0.0092
210.17	0.0098
209.38	0.0097

Table S17: TD-B3LYP/6-311++G(3df,2pd) computed vertical excitation energies of protoadamantane diazirine (**13**).

Excitation Energy λ / nm	Oscillator Strength (*f*)
225.54	0.0036
215.34	0.0021
210.58	0.0016

Table S18: TD-B3LYP/6-311++G(3df,2pd) computed vertical excitation energies of protoadamantane diazo (**28**).

Excitation Energy λ / nm	Oscillator Strength (*f*)
295.5	0.0007
260.55	0.0077
256	0.0070
253.15	0.0028
235.05	0.0305
231.06	0.0378
228.98	0.0039
226.11	0.0112
221.5	0.0063
210.33	0.0878

Table S19: TD-B3LYP/6-311++G(3df,2pd) computed vertical excitation energies of protoadamantylidene (**3**).

Excitation Energy λ / nm	Oscillator Strength (*f*)
531.88	0.0033
308.42	0.0018
271.5	0.0045
267.77	0.0037
259.35	0.0374
238.76	0.0019
233.55	0.0030
223.82	0.0038
207.31	0.0065

Table S20: TD-B3LYP/6-311++G(3df,2pd) computed vertical excitation energies of protoadamantane dehydro (**4**).

Excitation Energy λ / nm	Oscillator Strength (*f*)
210.48	0.0076

Table S21: TD-B3LYP/6-311++G(3df,2pd) computed vertical excitation energies of protoadamantane alkene (**12**).

Excitation Energy λ / nm	Oscillator Strength (*f*)
228.43	0.0135
208.54	0.0269
206.9	0.0151
202.41	0.0609
201.45	0.0082

Table S22: TD-B3LYP/6-311++G(3df,2pd) computed vertical excitation energies of d_2-protoadamantane diazirine (d_2-**13**).

Excitation Energy λ / nm	Oscillator Strength (*f*)
225.54	0.0036
215.34	0.0021
210.58	0.0016

Table S23: TD-B3LYP/6-311++G(3df,2pd) computed vertical excitation energies of d_2-protoadamantane diazo (d_2-**28**).

Excitation Energy λ / nm	Oscillator Strength (*f*)
260.55	0.0077
256	0.0070
253.15	0.0028
235.05	0.0305
231.06	0.0378
228.98	0.0039
226.11	0.0112
221.5	0.0063
210.33	0.0878

Table S24: TD-B3LYP/6-311++G(3df,2pd) computed vertical excitation energies of d_2-protoadamantylidene (d_2-**3**).

Excitation Energy λ / nm	Oscillator Strength (*f*)
531.88	0.0033
308.42	0.0018
271.5	0.0045
267.77	0.0037
259.35	0.0374
238.76	0.0019
233.55	0.0030
223.82	0.0038
207.31	0.0065

Table S25: TD-B3LYP/6-311++G(3df,2pd) computed vertical excitation energies of d_2-protoadamantane dehydro (d_2-**4**).

Excitation Energy λ / nm	Oscillator Strength (*f*)
210.48	0.0076

Table S26: TD-B3LYP/6-311++G(3df,2pd) computed vertical excitation energies of d_2-protoadamantane alkene (d_2-**12**).

Excitation Energy λ / nm	Oscillator Strength (*f*)
228.43	0.0135
208.54	0.0269
206.9	0.0151
202.41	0.0609
201.45	0.0082

Computed Potential Energy Surfaces

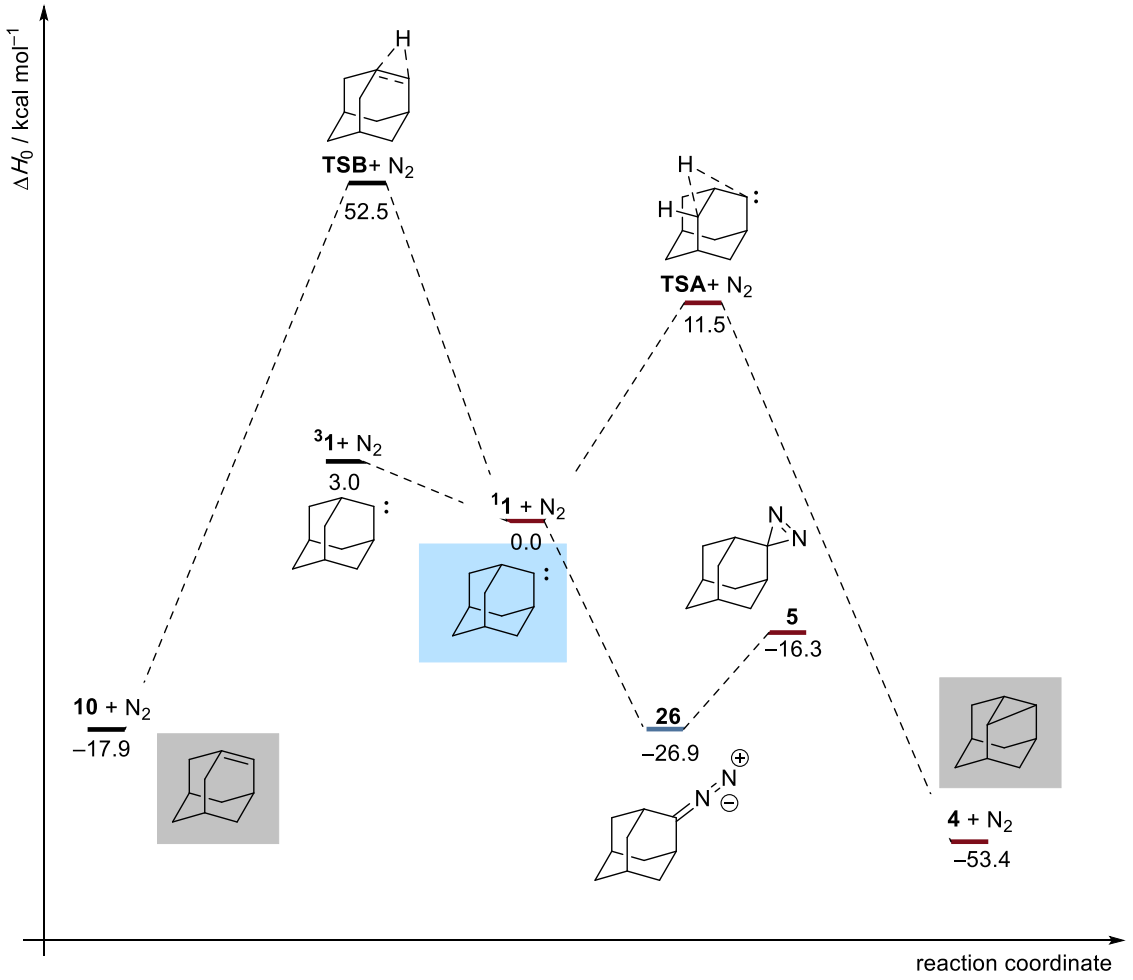

Figure S51: Potential energy profile (ΔH_0) in kcal mol^{-1} of the reactions of **1** at UB3LYP/def2TZVPP+ZPVE at 0 K.

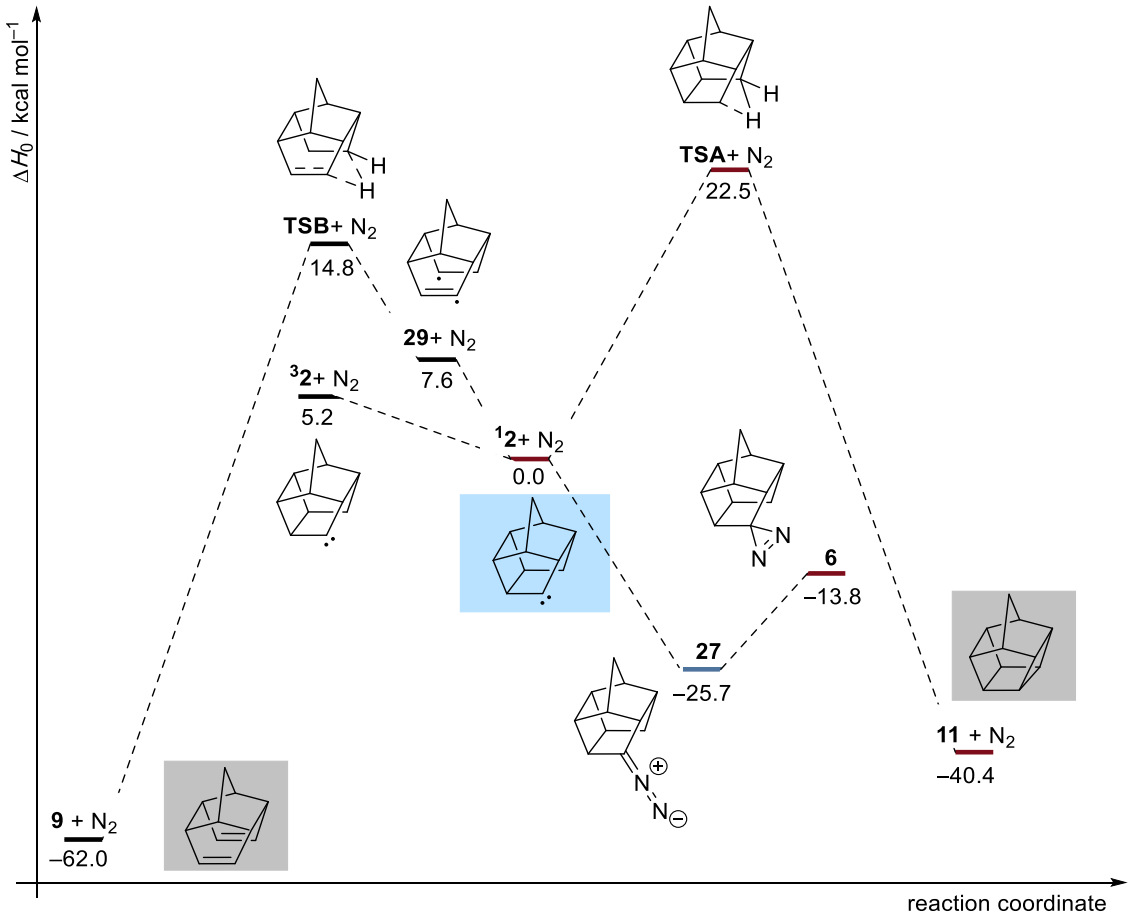

Figure S52: Potential energy profile ($\Delta \boldsymbol{H}_0$) in kcal mol^{-1} of the reactions of **3** at UB3LYP/def2TZVPP+ZPVE at 0 K.

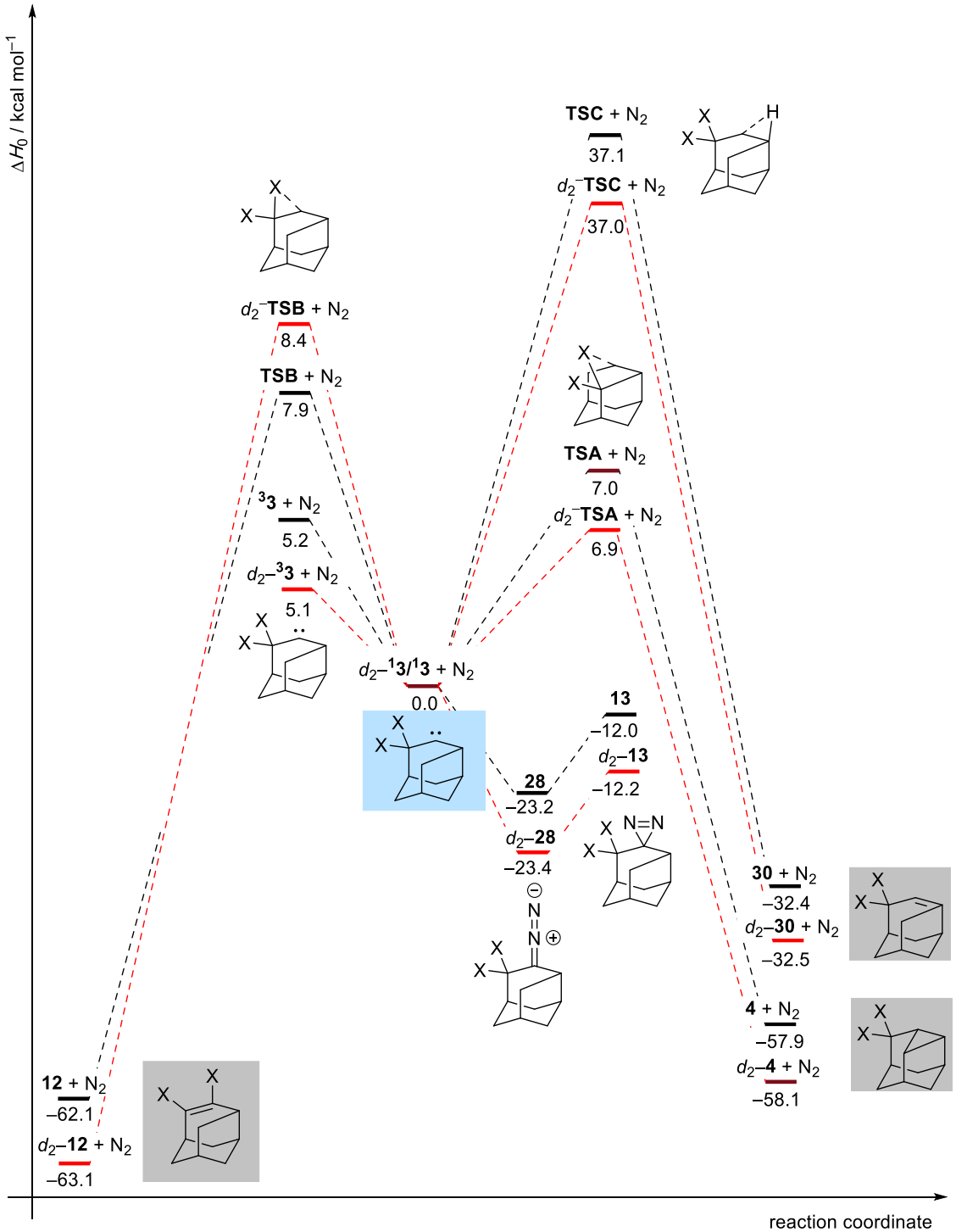

Figure S53: Potential energy profile (ΔH_0) in kcal mol^{-1} of the reactions of **13** and d_2–**13** at UB3LYP/def2TZVPP+ZPVE at 0 K. (X = H/D)

Tunneling Computations

Table S27: Overview of computed QMT half-lives and rate constants at the CVT/SCT//B3LYP/def2-TZVPP level of theory.

Reaction	QMT Half-Life (s^{-1}) at 10 K	Rate constants CVT/SCT 10 K
adamantane TSA (**1** to **4**)	5457851815	1.27×10^{-10}
adamantane TSB (**1** to **10**)	$> 3.28 \times 0^{30}$	$< 2.11 \times 10^{-31}$
PCU TSA (**2** to **9**)	$> 2.27 \times 10^{18}$	$< 3.05 \times 10^{-19}$
PCU TSB (**2** to **11**)	4.20×10^{-6}	1.65×10^{5}
protoadamantane TSA (**3** to **4**)	3.30×10^{-5}	2.10×10^{4}
protoadamantane TSB (**3** to **12**)	4.01×10^{-3}	1.73×10^{2}
d_2-protoadamantane TSA (d_2-**3** to d_2-**4**)	2.75×10^{-5}	2.52×10^{4}
d_2-protoadamantane TSB (d_2-**3** to d_2-**12**)	245.80	2.82×10^{-3}

Table S28: Overview of computed QMT half-lives and rate constants at the CVT/SCT//B3LYP/6-31G(d) level of theory.

Reaction	QMT Half-Life (s^{-1}) at 10 K	Rate constants CVT/SCT 10 K
adamantane TSA (**1** to **4**)	70873.95	9.78×10^{-6}
adamantane TSB (**1** to **10**)	$> 3.08 \times 10^{26}$	$< 2.25 \times 10^{-27}$
PCU TSA (**2** to **9**)	$> 2.91 \times 10^{15}$	$< 2.38 \times 10^{-16}$
PCU TSB (**2** to **11**)	2.55×10^{-13}	2.72×10^{12}
protoadamantane TSA (**3** to **4**)	1.35×10^{-5}	5.14×10^{4}
protoadamantane TSB (**3** to **12**)	1.18	5.88×10^{-1}
d_2-protoadamantane TSA (d_2-**3** to d_2-**4**)	1.13×10^{-5}	6.13×10^{4}
d_2-protoadamantane TSB (d_2-**3** to d_2-**12**)	50228.06	1.38×10^{-5}

Cartesian Coordinates of Computed Geometries

In the following, the cartesian coordinates of all computationally optimized geometries are given in Ångstrom. Electronic energies (in hartree mol^{-1}) and zero-point vibrational energies (ZPVE, in hartree) are provided.

B3LYP/6-311++G(3df,2pd)

Adamantane diazirine (C_{2v})

6	0.000000000	0.000000000	-2.269240941
6	1.259223000	0.000000000	-1.383939941
6	-1.259223000	0.000000000	-1.383939941
1	0.000000000	-0.878020000	-2.920655941
1	0.000000000	0.878020000	-2.920655941
6	1.261032000	-1.257869000	-0.495210941
6	-1.261032000	-1.257869000	-0.495210941
6	0.000000000	-1.264289000	0.394488059
1	-1.278536000	-2.157610000	-1.115276941
1	-2.158096000	-1.279732000	0.127724059
1	1.278536000	-2.157610000	-1.115276941
1	2.158096000	-1.279732000	0.127724059
6	-1.261032000	1.257869000	-0.495210941
1	-2.151432000	0.000000000	-2.014071941
6	1.261032000	1.257869000	-0.495210941
1	2.151432000	0.000000000	-2.014071941
6	0.000000000	0.000000000	1.226864059
1	0.000000000	-2.137851000	1.048525059
6	0.000000000	1.264289000	0.394488059
1	1.278536000	2.157610000	-1.115276941
1	2.158096000	1.279732000	0.127724059
1	-2.158096000	1.279732000	0.127724059
1	-1.278536000	2.157610000	-1.115276941
1	0.000000000	2.137851000	1.048525059
7	0.613341000	0.000000000	2.565146059
7	-0.613341000	0.000000000	2.565146059

E = −498.870751
ZPVE = 0.228429

2-Diazoadamantane (C_{2v})

6	0.000000000	0.000000000	2.352855992
6	-1.258517000	0.000000000	1.466089992
6	1.258517000	0.000000000	1.466089992
1	0.000000000	-0.878155000	3.004093992
1	0.000000000	0.878155000	3.004093992
6	-1.259571000	-1.263753000	0.583800992
6	1.259571000	-1.263753000	0.583800992
6	0.000000000	-1.273422000	-0.311123008
1	1.271583000	-2.157018000	1.214465992
1	2.156697000	-1.293411000	-0.038085008
1	-1.271583000	-2.157018000	1.214465992
1	-2.156697000	-1.293411000	-0.038085008
6	1.259571000	1.263753000	0.583800992
1	2.151057000	0.000000000	2.095906992
6	-1.259571000	1.263753000	0.583800992
1	-2.151057000	0.000000000	2.095906992
6	0.000000000	0.000000000	-1.129328008
1	0.000000000	-2.146777000	-0.963660008
6	0.000000000	1.273422000	-0.311123008
1	-1.271583000	2.157018000	1.214465992
1	-2.156697000	1.293411000	-0.038085008
1	2.156697000	1.293411000	-0.038085008
1	1.271583000	2.157018000	1.214465992
1	0.000000000	2.146777000	-0.963660008
7	0.000000000	0.000000000	-2.409272008
7	0.000000000	0.000000000	-3.553974008

E = −498.887387
ZPVE = 0.228512

Singlet adamantylidene (C_s)

6	-1.393498000	0.998124000	0.000000000
6	-1.407777000	-0.540077000	0.000000000
6	0.058278000	1.506596000	0.000000000
1	-1.922915000	1.377336000	0.878194000
1	-1.922915000	1.377336000	-0.878194000
6	-0.682991000	-1.067713000	1.244417000
6	0.791386000	0.990311000	1.244268000
6	0.791386000	-0.566863000	1.236963000
1	0.308747000	1.336459000	2.162335000
1	1.817675000	1.362553000	1.262772000
1	-1.165990000	-0.721701000	2.162325000
1	-0.705201000	-2.159195000	1.263396000
6	0.791386000	0.990311000	-1.244268000
1	0.064374000	2.599650000	0.000000000
6	-0.682991000	-1.067713000	-1.244417000
1	-2.440652000	-0.897784000	0.000000000
6	1.461269000	-1.047298000	0.000000000
1	1.302319000	-0.932829000	2.130089000
6	0.791386000	-0.566863000	-1.236963000
1	-1.165990000	-0.721701000	-2.162325000
1	-0.705201000	-2.159195000	-1.263396000
1	1.817675000	1.362553000	-1.262772000
1	0.308747000	1.336459000	-2.162335000
1	1.302319000	-0.932829000	-2.130089000

E = –389.290947
ZPVE = 0.216203

Triplet adamantylidene (C_1)

6	1.379712000	0.985715000	0.000000000
6	-0.072813000	1.496961000	0.000000000
6	1.392511000	-0.553913000	0.000000000
1	1.909549000	1.364312000	0.878349000
1	1.909549000	1.364312000	-0.878349000
6	-0.792339000	0.990667000	1.265085000
6	0.680030000	-1.070474000	1.265420000
6	-0.792339000	-0.566182000	1.269550000
1	1.196528000	-0.711803000	2.160946000
1	0.695046000	-2.161402000	1.294355000
1	-0.285466000	1.362453000	2.160622000
1	-1.819693000	1.357742000	1.293920000
6	0.680030000	-1.070474000	-1.265420000
1	2.425650000	-0.910258000	0.000000000

6	-0.792339000	0.990667000	-1.265085000
1	-0.074415000	2.589897000	0.000000000
6	-1.407285000	-1.006388000	0.000000000
1	-1.320071000	-0.942310000	2.147919000
6	-0.792339000	-0.566182000	-1.269550000
1	-0.285466000	1.362453000	-2.160622000
1	-1.819693000	1.357742000	-1.293920000
1	0.695046000	-2.161402000	-1.294355000
1	1.196528000	-0.711803000	-2.160946000
1	-1.320071000	-0.942310000	-2.147919000

E = –389.282811
ZPVE = 0.216850

2,4-Dehydroadamantane (C_s)

6	-0.207780028	-1.142344494	1.271884000
6	-1.079812471	-1.107049711	0.000000000
6	0.902536535	-0.078368265	1.185929000
1	0.248008171	-2.127928978	1.396585000
1	-0.838767848	-0.970810261	2.147738000
6	-0.207780028	-1.142344494	-1.271884000
6	1.824189046	-0.433306336	0.000000000
6	0.902536535	-0.078368265	-1.185929000
1	-0.838767848	-0.970810261	-2.147738000
1	0.248008171	-2.127928978	-1.396585000
1	2.155210812	-1.475002170	0.000000000
1	2.709716652	0.205187965	0.000000000
6	-1.887753076	0.196243804	0.000000000
1	-1.763864607	-1.958211030	0.000000000
6	0.361327169	1.302176527	0.759739000
1	1.438323755	-0.013364316	2.133047000
6	0.361327169	1.302176527	-0.759739000
1	1.438323755	-0.013364316	-2.133047000
6	-0.941496991	1.373159073	0.000000000
1	-2.537355652	0.237789693	0.879026000
1	-2.537355652	0.237789693	-0.879026000
1	-1.418035383	2.346955939	0.000000000
1	0.685786171	2.171945526	1.314605000
1	0.685786171	2.171945526	-1.314605000

E = −389.374314
ZPVE = 0.218794

Adamantane Alkene (C_1)

6	-0.232226000	-0.960438000	1.391463000
6	1.027194000	-0.139720000	1.048315000
6	-1.282839000	-0.818836000	0.272097000
1	-0.644425000	-0.618927000	2.344223000
1	0.026351000	-2.015050000	1.520180000
6	0.591987000	1.338525000	0.884997000
6	-1.685605000	0.653023000	0.053837000
6	-0.455658000	1.495986000	-0.301844000
1	1.454943000	1.980747000	0.704094000
1	0.129057000	1.677880000	1.815778000
1	-2.147460000	1.058524000	0.957696000
1	-2.433071000	0.717181000	-0.739452000
6	1.713629000	-0.718643000	-0.281878000
1	1.754759000	-0.214709000	1.860441000
6	-0.628733000	-1.294918000	-1.034917000
1	-2.167135000	-1.414019000	0.514314000
6	0.593028000	-0.426199000	-1.239491000
1	1.969163000	-1.773222000	-0.148378000
1	2.620286000	-0.150572000	-0.491514000
1	-1.316643000	-1.194604000	-1.873773000
1	-0.344563000	-2.347428000	-0.968967000
6	0.436647000	0.914932000	-1.387787000
1	-0.724760000	2.545697000	-0.432162000
1	1.358952000	1.486229000	-1.491234000

E = −389.315485
ZPVE = 0.217172

PCU diazirine (C_1)

6	1.440544000	0.643028000	0.914295000
6	0.199074000	1.568958000	0.702010000
6	0.124202000	1.779118000	-0.811959000
6	0.626665000	0.420270000	-1.322832000
1	0.806628000	2.572998000	-1.123452000
1	-0.872725000	2.040344000	-1.165481000
6	1.911275000	0.166612000	-0.485498000
6	0.502592000	-0.515797000	1.380534000
6	-0.749209000	0.402805000	1.176447000
6	-1.443528000	-0.223492000	0.001268000
6	-0.326339000	-0.762927000	-0.855939000
6	0.556024000	-1.512170000	0.186562000
1	0.665343000	-0.956423000	2.360366000
1	2.228296000	0.971849000	1.587303000
1	0.796141000	0.390946000	-2.397665000
6	1.983636000	-1.356941000	-0.344221000
1	0.215938000	-2.519869000	0.414755000
1	2.150154000	-1.871684000	-1.291933000
1	2.741887000	-1.687314000	0.367739000
1	2.798278000	0.666763000	-0.870018000
1	-1.385122000	0.613118000	2.032233000
1	0.141341000	2.476836000	1.297318000
1	-0.664577000	-1.379867000	-1.685603000
7	-2.748905000	-0.888836000	0.105475000
7	-2.761267000	0.178196000	-0.501127000

E = −535.739023
ZPVE = 0.210977

PCU diazo (C_1)

6	1.549567000	0.752257000	0.777641000
6	0.276083000	1.624642000	0.540238000
6	0.099130000	1.658650000	-0.978321000
6	0.616610000	0.267939000	-1.370536000
1	0.720981000	2.436718000	-1.426350000
1	-0.932862000	1.838923000	-1.283316000
6	1.952189000	0.135575000	-0.588226000
6	0.673298000	-0.370011000	1.420352000
6	-0.617465000	0.494688000	1.197088000
6	-1.351314000	-0.272527000	0.141273000
6	-0.280115000	-0.882340000	-0.720716000
6	0.686688000	-1.488873000	0.343948000
1	0.899755000	-0.695575000	2.432282000
1	2.365446000	1.168149000	1.363398000
1	0.723793000	0.124582000	-2.444700000
6	2.075160000	-1.362104000	-0.288591000
1	0.386285000	-2.472058000	0.698923000
1	2.198949000	-1.973750000	-1.183987000
1	2.883972000	-1.596535000	0.405479000
1	2.802422000	0.609482000	-1.075620000
1	-1.202314000	0.788590000	2.064101000
1	0.225710000	2.592591000	1.033897000

1	-0.642488000	-1.593836000	-1.458655000
7	-2.613340000	-0.302085000	-0.060279000
7	-3.745036000	-0.351438000	-0.221201000

E = –535.757551
ZPVE = 0.210894

PCU singlet carbene (C_1)

6	0.013489000	0.349912000	-1.367941000
6	1.451312000	0.261463000	-0.767626000
6	1.450275000	1.250793000	0.396441000
6	0.013440000	1.080437000	0.904385000
1	1.591296000	2.268062000	0.021483000
1	2.215876000	1.055104000	1.145845000
6	-0.843281000	1.192157000	-0.382469000
6	-0.281714000	-1.114923000	-0.925994000
6	1.149283000	-1.239290000	-0.293004000
6	0.975390000	-1.222840000	1.174693000
6	-0.273826000	-0.437024000	1.366304000
6	-1.263827000	-0.934365000	0.259152000
1	-0.574883000	-1.836618000	-1.684185000
1	-0.094211000	0.605946000	-2.418982000
1	-0.270181000	1.773798000	1.693249000
6	-2.067575000	0.313446000	-0.117325000
1	-1.831041000	-1.822502000	0.529846000
1	-2.696148000	0.687006000	0.692687000
1	-2.693160000	0.164536000	-0.999856000
1	-1.033739000	2.218206000	-0.693836000
1	1.836349000	-1.981744000	-0.690210000
1	2.293393000	0.334037000	-1.450407000
1	-0.681343000	-0.464435000	2.374670000

E = –426.161270
ZPVE = 0.198940

PCU triplet carbene (C_1)

6	0.054221000	0.319774000	-1.371245000
6	1.482000000	0.257621000	-0.744364000
6	1.442476000	1.241925000	0.423748000
6	-0.013979000	1.105636000	0.886800000
1	1.638498000	2.261271000	0.081140000
1	2.165737000	1.001312000	1.204058000
6	-0.830183000	1.185018000	-0.431260000
6	-0.250258000	-1.135116000	-0.898543000
6	1.193284000	-1.234005000	-0.255381000
6	0.881749000	-1.226860000	1.178085000
6	-0.319441000	-0.391541000	1.390426000
6	-1.270008000	-0.923505000	0.259032000
1	-0.532475000	-1.879824000	-1.638579000
1	-0.034486000	0.540303000	-2.432303000
1	-0.311933000	1.839879000	1.633761000
6	-2.062253000	0.309196000	-0.182135000
1	-1.834566000	-1.808269000	0.543031000
1	-2.719621000	0.699476000	0.596978000
1	-2.655396000	0.137680000	-1.082388000
1	-1.015614000	2.200211000	-0.779155000
1	1.873338000	-1.992683000	-0.631449000
1	2.333746000	0.360019000	-1.413019000
1	-0.752879000	-0.408230000	2.386941000

E = −426.150287
ZPVE = 0.199445

PCU homopentaprismane (C_{2v})

6	-1.205610000	0.787212000	0.173871000
6	-0.777021000	0.782659000	-1.321239000
6	0.000000000	1.143320000	1.073497000
6	1.205610000	0.787212000	0.173871000
6	0.777021000	0.782659000	-1.321239000
6	-1.205610000	-0.787212000	0.173871000
1	-2.139026000	1.282978000	0.431935000
6	1.205610000	-0.787212000	0.173871000
1	2.139026000	1.282978000	0.431935000
6	0.000000000	-1.143320000	1.073497000
6	-0.777021000	-0.782659000	-1.321239000
1	-1.315366000	1.390502000	-2.043697000
1	-2.139026000	-1.282978000	0.431935000
6	0.777021000	-0.782659000	-1.321239000
1	1.315366000	1.390502000	-2.043697000
1	2.139026000	-1.282978000	0.431935000
1	-1.315366000	-1.390502000	-2.043697000
1	1.315366000	-1.390502000	-2.043697000
6	0.000000000	0.000000000	2.110176000
1	0.000000000	2.156947000	1.471609000
1	-0.885174000	0.000000000	2.748812000
1	0.885174000	0.000000000	2.748812000
1	0.000000000	-2.156947000	1.471609000

E = −426.226649
ZPVE = 0.200716

PCU dialkene_1 (C_{2v})

6	1.173949000	0.806088000	0.078802000
6	1.173949000	-0.806088000	0.078802000
6	0.000000000	1.117958000	1.056171000
6	0.000000000	-1.117958000	1.056171000
6	-1.173949000	-0.806088000	0.078802000
6	-1.173949000	0.806088000	0.078802000
6	0.000000000	0.000000000	2.082222000
1	0.000000000	2.141169000	1.427959000
1	-0.885862000	0.000000000	2.720429000
1	0.885862000	0.000000000	2.720429000
1	0.000000000	-2.141169000	1.427959000
6	0.665684000	1.423961000	-1.204697000
1	2.141000000	1.185302000	0.406603000
6	-0.665684000	1.423961000	-1.204697000
1	-2.141000000	1.185302000	0.406603000
1	1.300996000	1.747444000	-2.017270000
1	-1.300996000	1.747444000	-2.017270000
6	-0.665684000	-1.423961000	-1.204697000
1	-2.141000000	-1.185302000	0.406603000
6	0.665684000	-1.423961000	-1.204697000
1	2.141000000	-1.185302000	0.406603000
1	-1.300996000	-1.747444000	-2.017270000
1	1.300996000	-1.747444000	-2.017270000

E = −426.260526
ZPVE = 0.199790

PCU dialkene_2 (C_{2v})

6	1.320392000	0.788454000	0.211280000
6	1.320392000	-0.788454000	0.211280000
6	0.000000000	1.147674000	0.939879000
6	0.000000000	-1.147674000	0.939879000

6	-1.320392000	-0.788454000	0.211280000
6	-1.320392000	0.788454000	0.211280000
6	0.000000000	0.000000000	1.995676000
1	0.000000000	2.156383000	1.350653000
1	-0.885851000	0.000000000	2.633257000
1	0.885851000	0.000000000	2.633257000
1	0.000000000	-2.156383000	1.350653000
6	1.525141000	-0.666606000	-1.289788000
1	2.159552000	-1.247942000	0.738913000
6	1.525141000	0.666606000	-1.289788000
1	2.159552000	1.247942000	0.738913000
6	-1.525141000	-0.666606000	-1.289788000
1	-2.159552000	-1.247942000	0.738913000
6	-1.525141000	0.666606000	-1.289788000
1	-2.159552000	1.247942000	0.738913000
1	-1.632840000	-1.405528000	-2.072967000
1	-1.632840000	1.405528000	-2.072967000
1	1.632840000	-1.405528000	-2.072967000
1	1.632840000	1.405528000	-2.072967000

E = −426.179384
ZPVE = 0.197019

Protoadamantane diazirine (C_1)

6	0.437832000	1.576145000	-0.139995000
1	0.568643000	2.658833000	-0.184227000
6	1.550441000	0.940792000	-1.012795000
6	1.773598000	-0.567460000	-0.774444000
1	2.591280000	-0.916125000	-1.407435000
6	0.492064000	-1.384573000	-0.987366000
6	-0.372360000	-1.058880000	0.271683000
6	-1.458215000	-0.078504000	-0.085804000
7	-2.769417000	-0.589234000	-0.519318000
7	-2.754532000	-0.139993000	0.619776000
6	-0.997563000	1.260930000	-0.619489000
6	2.020162000	-0.824690000	0.719009000
6	0.648590000	-0.446616000	1.305835000
1	0.489850000	-0.848202000	2.305832000
6	0.548972000	1.090619000	1.315943000
1	2.489641000	1.459822000	-0.801789000
1	1.329364000	1.121826000	-2.068049000
1	0.733023000	-2.447966000	-1.012128000
1	-0.025789000	-1.151366000	-1.917866000
1	-0.826913000	-1.963250000	0.673168000
1	-1.678209000	2.034656000	-0.256652000
1	-1.060528000	1.281496000	-1.711844000
1	2.832484000	-0.230488000	1.140141000
1	2.253760000	-1.877872000	0.890124000
1	1.429950000	1.508548000	1.807129000
1	-0.320048000	1.428093000	1.884931000

E = –498.857697
ZPVE = 0.227837

Protoadamantane diazo (C_1)

7	-3.744270000	-0.419073000	0.067033000
7	-2.621794000	-0.220544000	-0.024694000
6	-1.364437000	0.014403000	-0.130298000
6	-0.864967000	1.376584000	-0.552593000
6	0.574876000	1.574837000	-0.017906000
1	0.756104000	2.650372000	0.025635000
6	1.674718000	0.958561000	-0.921621000
6	1.845053000	-0.570257000	-0.790715000
1	2.666343000	-0.896861000	-1.430756000
6	0.545991000	-1.330178000	-1.086922000
6	-0.343469000	-1.051553000	0.168961000
6	2.050598000	-0.943587000	0.684608000
6	0.680090000	-0.561369000	1.269588000
1	0.479859000	-1.032492000	2.231350000
6	0.633488000	0.972735000	1.396428000
1	-1.511183000	2.153203000	-0.137452000
1	-0.884912000	1.500732000	-1.641255000
1	2.628917000	1.426733000	-0.663902000
1	1.474842000	1.222540000	-1.963527000
1	0.755590000	-2.398111000	-1.169214000
1	0.057689000	-1.022875000	-2.011118000
1	-0.848673000	-1.959161000	0.493627000
1	2.872830000	-0.409486000	1.163178000
1	2.246220000	-2.013659000	0.782542000
1	1.515626000	1.320070000	1.937899000
1	-0.238452000	1.295262000	1.969446000

E = –498.875073
ZPVE = 0.227894

Singlet protoadamantylidene (C_1)

6	1.087201000	-1.043019000	-0.241525000
1	1.762591000	-1.881484000	-0.429856000
6	-0.047614000	-1.089634000	-1.290410000
6	-1.223537000	-0.143768000	-0.962369000
1	-1.981314000	-0.216480000	-1.745344000
6	-0.756824000	1.306436000	-0.789109000
6	-0.104387000	1.307954000	0.683157000
6	1.240260000	1.525548000	0.155622000
6	1.890954000	0.269497000	-0.312810000
6	-1.771173000	-0.461768000	0.433118000
6	-0.575074000	-0.051667000	1.310854000
1	-0.851726000	0.097230000	2.354370000
6	0.510289000	-1.128652000	1.179368000
1	-0.437326000	-2.109410000	-1.352819000
1	0.357670000	-0.851002000	-2.277702000
1	-1.582026000	2.016027000	-0.780150000
1	-0.072345000	1.641656000	-1.572023000
1	-0.487218000	2.157249000	1.246257000
1	2.765685000	0.212649000	0.355217000
1	2.342083000	0.433921000	-1.296702000
1	-2.054065000	-1.508476000	0.564650000
1	-2.650370000	0.150350000	0.647250000
1	0.079857000	-2.112476000	1.380765000
1	1.307935000	-0.975312000	1.910707000

E = –389.281186
ZPVE = 0.215491

Triplet protoadamantylidene (C_1)

6	1.176520000	-0.952570000	-0.185699000
1	1.870783000	-1.787537000	-0.303729000
6	0.005436000	-1.170286000	-1.179622000
6	-1.279023000	-0.359252000	-0.886279000
1	-2.051710000	-0.648438000	-1.601087000
6	-1.041639000	1.154640000	-0.881695000
6	-0.224894000	1.389618000	0.442712000
6	1.206272000	1.475382000	0.129026000
6	1.981020000	0.361105000	-0.442885000

6	-1.705682000	-0.572644000	0.573081000
6	-0.531517000	0.086282000	1.315478000
1	-0.768528000	0.353996000	2.344249000
6	0.659920000	-0.887189000	1.262235000
1	-0.261317000	-2.230923000	-1.159046000
1	0.350757000	-0.962122000	-2.195843000
1	-1.998176000	1.679350000	-0.835515000
1	-0.506496000	1.521956000	-1.756466000
1	-0.575753000	2.282328000	0.960165000
1	2.962657000	0.274474000	0.035554000
1	2.177061000	0.482530000	-1.517475000
1	-1.833123000	-1.621859000	0.845424000
1	-2.648965000	-0.059331000	0.771453000
1	0.337969000	-1.871192000	1.610642000
1	1.466364000	-0.563758000	1.923562000

E = –389.272711
ZPVE = 0.215979

2,4-Dehydroprotoadamantane (C_1)

6	1.069611000	-1.099318000	0.000000000
1	1.747280000	-1.955579000	0.000000000
6	0.197587000	-1.128212000	-1.271886000
6	-0.905284000	-0.056598000	-1.186028000
1	-1.440672000	0.012375000	-2.133026000
6	-0.354025000	1.320144000	-0.759563000
1	-0.672292000	2.192550000	-1.313845000
6	-0.354024000	1.320144000	0.759563000
6	0.949129000	1.381760000	-0.000001000
1	1.433246000	2.351812000	-0.000001000
6	1.887017000	0.197786000	-0.000001000
6	-1.829032000	-0.405314000	0.000001000
6	-0.905283000	-0.056597000	1.186029000
1	-1.440671000	0.012377000	2.133028000
6	0.197588000	-1.128211000	1.271888000
1	-0.265027000	-2.110598000	-1.396902000
1	0.829642000	-0.961025000	-2.147791000
1	-0.672291000	2.192551000	1.313844000
1	2.536963000	0.234603000	0.878941000
1	2.536962000	0.234602000	-0.878943000
1	-2.167290000	-1.444714000	0.000002000
1	-2.710169000	0.239163000	0.000001000
1	-0.265026000	-2.110597000	1.396904000
1	0.829644000	-0.961024000	2.147792000

E = –389.374298
ZPVE = 0.218812

Protoadamantane alkene (C_1)

6	-0.195200000	-1.121905000	-1.250053000
6	1.024627000	-1.124609000	-0.282965000
6	-1.335593000	-0.145118000	-0.865436000
1	-0.616474000	-2.131938000	-1.269035000
1	0.148573000	-0.909224000	-2.264997000
6	0.537069000	-1.102769000	1.182693000
6	-1.745417000	-0.369357000	0.595980000
6	-0.455057000	0.061969000	1.317239000
1	1.394764000	-0.988328000	1.846083000
1	0.038735000	-2.037052000	1.452368000
1	-2.026441000	-1.398468000	0.825504000
1	-2.591363000	0.272264000	0.853331000
6	1.915471000	0.091597000	-0.417580000
1	1.607361000	-2.026629000	-0.477938000
6	-0.882095000	1.318293000	-0.778648000
1	-2.165135000	-0.275273000	-1.563784000
6	1.460890000	1.251211000	0.045398000
6	0.025015000	1.335818000	0.495456000
1	-0.617604000	0.315304000	2.364440000
1	-1.757862000	1.956613000	-0.640640000
1	-0.350443000	1.671745000	-1.660990000
1	-0.141375000	2.242792000	1.075544000
1	2.916099000	-0.014648000	-0.818954000
1	2.062894000	2.152059000	0.026574000

E = –389.379737
ZPVE = 0.218349

d_2-Protoadamantane diazirine (C_1)

6	0.437832000	1.576145000	-0.139995000
1	0.568643000	2.658833000	-0.184227000
6	1.550441000	0.940792000	-1.012795000
6	1.773598000	-0.567460000	-0.774444000
1	2.591280000	-0.916125000	-1.407435000
6	0.492064000	-1.384573000	-0.987366000
6	-0.372360000	-1.058880000	0.271683000
6	-1.458215000	-0.078504000	-0.085804000
7	-2.769417000	-0.589234000	-0.519318000
7	-2.754532000	-0.139993000	0.619776000
6	-0.997563000	1.260930000	-0.619489000
6	2.020162000	-0.824690000	0.719009000
6	0.648590000	-0.446616000	1.305835000
1	0.489850000	-0.848202000	2.305832000
6	0.548972000	1.090619000	1.315943000
1	2.489641000	1.459822000	-0.801789000
1	1.329364000	1.121826000	-2.068049000
1	0.733023000	-2.447966000	-1.012128000
1	-0.025789000	-1.151366000	-1.917866000
1	-0.826913000	-1.963250000	0.673168000
1(Iso=2)	-1.678209000	2.034656000	-0.256652000
1(Iso=2)	-1.060528000	1.281496000	-1.711844000
1	2.832484000	-0.230488000	1.140141000
1	2.253760000	-1.877872000	0.890124000
1	1.429950000	1.508548000	1.807129000
1	-0.320048000	1.428093000	1.884931000

E = –498.864337
ZPVE = 0.221196

d_2-Protoadamantane diazo (C_1)

7	-3.744270000	-0.419073000	0.067033000
7	-2.621794000	-0.220544000	-0.024694000
6	-1.364437000	0.014403000	-0.130298000
6	-0.864967000	1.376584000	-0.552593000
6	0.574876000	1.574837000	-0.017906000
1	0.756104000	2.650372000	0.025635000
6	1.674718000	0.958561000	-0.921621000
6	1.845053000	-0.570257000	-0.790715000
1	2.666343000	-0.896861000	-1.430756000
6	0.545991000	-1.330178000	-1.086922000
6	-0.343469000	-1.051553000	0.168961000
6	2.050598000	-0.943587000	0.684608000
6	0.680090000	-0.561369000	1.269588000
1	0.479859000	-1.032492000	2.231350000
6	0.633488000	0.972735000	1.396428000
1(Iso=2)	-1.511183000	2.153203000	-0.137452000

1(Iso=2) -0.884912000 1.500732000 -1.641255000
1 2.628917000 1.426733000 -0.663902000
1 1.474842000 1.222540000 -1.963527000
1 0.755590000 -2.398111000 -1.169214000
1 0.057689000 -1.022875000 -2.011118000
1 -0.848673000 -1.959161000 0.493627000
1 2.872830000 -0.409486000 1.163178000
1 2.246220000 -2.013659000 0.782542000
1 1.515626000 1.320070000 1.937899000
1 -0.238452000 1.295262000 1.969446000

E = –498.881703
ZPVE = 0.221264

d_2-Singlet protoadamantylidene (C_1)

6 1.087201000 -1.043019000 -0.241525000
1 1.762591000 -1.881484000 -0.429856000
6 -0.047614000 -1.089634000 -1.290410000
6 -1.223537000 -0.143768000 -0.962369000
1 -1.981314000 -0.216480000 -1.745344000
6 -0.756824000 1.306436000 -0.789109000
6 -0.104387000 1.307954000 0.683157000
6 1.240260000 1.525548000 0.155622000
6 1.890954000 0.269497000 -0.312810000
6 -1.771173000 -0.461768000 0.433118000
6 -0.575074000 -0.051667000 1.310854000
1 -0.851726000 0.097230000 2.354370000
6 0.510289000 -1.128652000 1.179368000
1 -0.437326000 -2.109410000 -1.352819000
1 0.357670000 -0.851002000 -2.277702000
1 -1.582026000 2.016027000 -0.780150000
1 -0.072345000 1.641656000 -1.572023000
1 -0.487218000 2.157249000 1.246257000
1(Iso=2) 2.765685000 0.212649000 0.355217000
1(Iso=2) 2.342083000 0.433921000 -1.296702000
1 -2.054065000 -1.508476000 0.564650000
1 -2.650370000 0.150350000 0.647250000
1 0.079857000 -2.112476000 1.380765000
1 1.307935000 -0.975312000 1.910707000

E = –389.287561
ZPVE = 0.209115

d_2-Triplet protoadamantylidene (C_1)

6 1.176540000 -0.952558000 -0.185677000
1 1.870802000 -1.787530000 -0.303688000
6 0.005450000 -1.170318000 -1.179592000
6 -1.279027000 -0.359297000 -0.886264000
1 -2.051710000 -0.648518000 -1.601059000
6 -1.041683000 1.154594000 -0.881721000
6 -0.224916000 1.389627000 0.442671000
6 1.206253000 1.475388000 0.128984000
6 1.981016000 0.361113000 -0.442914000
6 -1.705669000 -0.572649000 0.573108000
6 -0.531510000 0.086320000 1.315481000
1 -0.768520000 0.354050000 2.344250000
6 0.659951000 -0.887129000 1.262259000
1 -0.261286000 -2.230959000 -1.158981000
1 0.350768000 -0.962171000 -2.195813000
1 -1.998234000 1.679272000 -0.835536000
1 -0.506572000 1.521909000 -1.756515000
1 -0.575761000 2.282354000 0.960098000
1 2.962660000 0.274510000 0.035516000
1 2.177033000 0.482519000 -1.517507000
1 -1.833078000 -1.621859000 0.845480000
1 -2.648967000 -0.059360000 0.771475000
1 0.338032000 -1.871122000 1.610714000
1 1.466397000 -0.563645000 1.923561000

E = –389.279205
ZPVE = 0.209485

d_2-2,4-Dehydroprotoadamantane (C_1)

6 -1.069612000 -1.099318000 0.000001000
1 -1.747282000 -1.955578000 0.000001000
6 -0.197589000 -1.128209000 1.271888000
6 0.905283000 -0.056597000 1.186028000
1 1.440671000 0.012377000 2.133028000
6 0.354026000 1.320145000 0.759563000
1 0.672293000 2.192551000 1.313843000
6 0.354027000 1.320143000 -0.759564000
6 -0.949128000 1.381761000 -0.000002000
1 -1.433244000 2.351813000 -0.000003000
6 -1.887017000 0.197787000 0.000000000
6 1.829032000 -0.405315000 0.000001000
6 0.905284000 -0.056599000 -1.186028000
1 1.440673000 0.012373000 -2.133026000
6 -0.197588000 -1.128213000 -1.271886000
1 0.265024000 -2.110596000 1.396905000
1 -0.829645000 -0.961022000 2.147793000
1 0.672293000 2.192548000 -1.313846000
1(Iso=2) -2.536962000 0.234603000 -0.878944000
1(Iso=2) -2.536963000 0.234605000 0.878941000
1 2.167289000 -1.444716000 0.000002000
1 2.710168000 0.239161000 0.000001000
1 0.265026000 -2.110599000 -1.396901000
1 -0.829643000 -0.961026000 -2.147792000

E = –389.380965
ZPVE = 0.212146

d_2-Protoadamantane alkene (C_1)

6 -0.195200000 -1.121905000 -1.250053000
6 1.024627000 -1.124609000 -0.282965000
6 -1.335593000 -0.145118000 -0.865436000
1 -0.616474000 -2.131938000 -1.269035000
1 0.148573000 -0.909224000 -2.264997000
6 0.537069000 -1.102769000 1.182693000
6 -1.745417000 -0.369357000 0.595980000
6 -0.455057000 0.061969000 1.317239000
1 1.394764000 -0.988328000 1.846083000
1 0.038735000 -2.037052000 1.452368000
1 -2.026441000 -1.398468000 0.825504000
1 -2.591363000 0.272264000 0.853331000
6 1.915471000 0.091597000 -0.417580000
1 1.607361000 -2.026629000 -0.477938000
6 -0.882095000 1.318293000 -0.778648000
1 -2.165135000 -0.275273000 -1.563784000
6 1.460890000 1.251211000 0.045398000
6 0.025015000 1.335818000 0.495456000
1(Iso=2) -0.617604000 0.315304000 2.364440000
1(Iso=2) -1.757862000 1.956613000 -0.640640000
1 -0.350443000 1.671745000 -1.660990000
1 -0.141375000 2.242792000 1.075544000

1	2.916099000	-0.014648000	-0.818954000
1	2.062894000	2.152059000	0.026574000

E = –389.386135
ZPVE = 0.211951

B3LYP/def2TZVPP

Adamantane diazirine (C_{2v})

6	0.000000000	0.000000000	2.197777000
6	0.000000000	1.256798000	1.314449000
6	0.000000000	-1.256798000	1.314449000
1	-0.878974000	0.000000000	2.847533000
1	0.878974000	0.000000000	2.847533000
6	-1.255300000	1.258606000	0.427538000
6	-1.255300000	-1.258606000	0.427538000
6	-1.261975000	0.000000000	-0.459212000
1	-2.154370000	-1.276237000	1.048201000
1	-1.274463000	-2.154068000	-0.197476000
1	-2.154370000	1.276237000	1.048201000
1	-1.274463000	2.154068000	-0.197476000
6	1.255300000	-1.258606000	0.427538000
1	0.000000000	-2.148703000	1.944502000
6	1.255300000	1.258606000	0.427538000
1	0.000000000	2.148703000	1.944502000
6	0.000000000	0.000000000	-1.287745000
1	-2.134084000	0.000000000	-1.114711000
6	1.261975000	0.000000000	-0.459212000
1	2.154370000	1.276237000	1.048201000
1	1.274463000	2.154068000	-0.197476000
1	1.274463000	-2.154068000	-0.197476000
1	2.154370000	-1.276237000	1.048201000
1	2.134084000	0.000000000	-1.114711000
7	0.000000000	0.613029000	-2.624393000
7	0.000000000	-0.613029000	-2.624393000

E = –498.947862
ZPVE = 0.229215

2-Diazoadamantane (C_{2v})

6	0.000000000	0.000000000	-2.274801000
6	-1.255950000	0.000000000	-1.389963000
6	1.255950000	0.000000000	-1.389963000
1	0.000000000	0.879016000	-2.924392000
1	0.000000000	-0.879016000	-2.924392000
6	-1.256968000	1.261449000	-0.509729000
6	1.256968000	1.261449000	-0.509729000
6	0.000000000	1.271169000	0.383131000
1	1.268346000	2.153771000	-1.141268000
1	2.152867000	1.289053000	0.113539000
1	-1.268346000	2.153771000	-1.141268000
1	-2.152867000	1.289053000	0.113539000
6	1.256968000	-1.261449000	-0.509729000
1	2.148137000	0.000000000	-2.019667000
6	-1.256968000	-1.261449000	-0.509729000
1	-2.148137000	0.000000000	-2.019667000
6	0.000000000	0.000000000	1.198397000
1	0.000000000	2.143423000	1.036669000
6	0.000000000	-1.271169000	0.383131000
1	-1.268346000	-2.153771000	-1.141268000
1	-2.152867000	-1.289053000	0.113539000
1	2.152867000	-1.289053000	0.113539000
1	1.268346000	-2.153771000	-1.141268000
1	0.000000000	-2.143423000	1.036669000
7	0.000000000	0.000000000	2.478210000
7	0.000000000	0.000000000	3.621733000

E = –498.964783
ZPVE = 0.229292

Singlet adamantylidene (C_s)

6	0.000000000	0.000000000	-1.716425000
6	-1.255625000	0.000000000	-0.834336000
6	1.255625000	0.000000000	-0.834336000
1	0.000000000	0.878995000	-2.365992000
1	0.000000000	-0.878995000	-2.365992000
6	-1.263230000	1.235330000	0.065284000
6	1.263230000	1.235330000	0.065284000
6	0.000000000	1.223571000	0.972723000
1	1.257431000	2.159684000	-0.517901000
1	2.164238000	1.250241000	0.681449000
1	-1.257431000	2.159684000	-0.517901000
1	-2.164238000	1.250241000	0.681449000
6	1.263230000	-1.235330000	0.065284000
1	2.148290000	0.000000000	-1.464730000
6	-1.263230000	-1.235330000	0.065284000
1	-2.148290000	0.000000000	-1.464730000
6	0.000000000	0.000000000	1.815555000
1	0.000000000	2.122705000	1.592510000
6	0.000000000	-1.223571000	0.972723000
1	-1.257431000	-2.159684000	-0.517901000
1	-2.164238000	-1.250241000	0.681449000
1	2.164238000	-1.250241000	0.681449000
1	1.257431000	-2.159684000	-0.517901000
1	0.000000000	-2.122705000	1.592510000

E = –389.353457
ZPVE = 0.216449

Triplet adamantylidene (C_1)

6	0.000000000	0.000000000	-1.692488000
6	-1.257394000	0.000000000	-0.809648000
6	1.257394000	0.000000000	-0.809648000
1	0.000000000	0.879179000	-2.342086000
1	0.000000000	-0.879179000	-2.342086000
6	-1.263468000	1.262601000	0.068411000
6	1.263468000	1.262601000	0.068411000
6	0.000000000	1.267043000	0.972225000
1	1.269371000	2.157464000	-0.560736000
1	2.159395000	1.290387000	0.690516000
1	-1.269371000	2.157464000	-0.560736000
1	-2.159395000	1.290387000	0.690516000
6	1.263468000	-1.262601000	0.068411000
1	2.147548000	0.000000000	-1.443128000
6	-1.263468000	-1.262601000	0.068411000
1	-2.147548000	0.000000000	-1.443128000
6	0.000000000	0.000000000	1.729449000
1	0.000000000	2.146427000	1.618382000
6	0.000000000	-1.267043000	0.972225000
1	-1.269371000	-2.157464000	-0.560736000
1	-2.159395000	-1.290387000	0.690516000

1	2.159395000	-1.290387000	0.690516000
1	1.269371000	-2.157464000	-0.560736000
1	0.000000000	-2.146427000	1.618382000

E = –389.348668
ZPVE = 0.217606

2,4-Dehydroadamantane (C_s)

6	-0.601162000	-0.972154000	1.269792000
6	-1.398270000	-0.623127000	0.000000000
6	0.817722000	-0.387644000	1.184226000
1	-0.535131000	-2.055793000	1.393945000
1	-1.126550000	-0.580277000	2.144133000
6	-0.601162000	-0.972154000	-1.269792000
6	1.543968000	-1.054046000	0.000000000
6	0.817722000	-0.387644000	-1.184226000
1	-1.126550000	-0.580277000	-2.144133000
1	-0.535131000	-2.055793000	-1.393945000
1	1.468248000	-2.144177000	0.000000000
1	2.601183000	-0.783109000	0.000000000
6	-1.675278000	0.882086000	0.000000000
1	-2.345153000	-1.166305000	0.000000000
6	0.817722000	1.092486000	0.759008000
1	1.340490000	-0.522957000	2.130743000
6	0.817722000	1.092486000	-0.759008000
1	1.340490000	-0.522957000	-2.130743000
6	-0.367639000	1.632838000	0.000000000
1	-2.264069000	1.156476000	0.879733000
1	-2.264069000	1.156476000	-0.879733000
1	-0.457218000	2.712915000	0.000000000
1	1.437695000	1.783502000	1.312942000
1	1.437695000	1.783502000	-1.312942000

E = −389.438509
ZPVE = 0.219508

Adamantane alkene (C_1)

6	-0.232765000	-0.961118000	1.386891000
6	1.023964000	-0.140929000	1.047174000
6	-1.280287000	-0.818424000	0.269234000
1	-0.646231000	-0.619956000	2.338873000
1	0.026701000	-2.015596000	1.512351000
6	0.588390000	1.334338000	0.886238000
6	-1.682458000	0.650784000	0.053685000
6	-0.454995000	1.493820000	-0.298766000
1	1.451738000	1.976331000	0.707824000
1	0.123158000	1.669909000	1.816866000
1	-2.142891000	1.053976000	0.958962000
1	-2.428633000	0.715466000	-0.740347000
6	1.710641000	-0.716796000	-0.279575000
1	1.750124000	-0.216388000	1.859911000
6	-0.626063000	-1.290771000	-1.035922000
1	-2.164123000	-1.414448000	0.509080000
6	0.594133000	-0.423196000	-1.239276000
1	1.963257000	-1.771852000	-0.146601000
1	2.617427000	-0.148214000	-0.486072000
1	-1.314040000	-1.188131000	-1.874192000
1	-0.340946000	-2.342855000	-0.970184000
6	0.437459000	0.917443000	-1.386183000
1	-0.725008000	2.543236000	-0.426580000
1	1.361353000	1.487612000	-1.480889000

E = −389.381968
ZPVE = 0.217923

Adamantane TSA (C_1)

6	-0.238761000	-0.939719000	1.418141000
6	0.942029000	0.006425000	1.157122000
6	-1.163609000	-0.982748000	0.190991000
1	-0.809736000	-0.613990000	2.291263000
1	0.149135000	-1.935943000	1.643280000
6	0.497892000	1.396298000	0.688753000
6	-1.806310000	0.390545000	0.026081000
6	-0.729368000	1.427117000	-0.234675000
1	-2.378571000	0.663267000	0.916884000
1	-2.508031000	0.384909000	-0.811574000
1	0.573428000	2.245190000	1.362464000
1	1.293538000	1.729360000	-0.139418000
6	-0.379128000	-1.279871000	-1.095213000
1	-1.935029000	-1.740520000	0.341240000
6	1.743466000	-0.529520000	-0.037832000
1	1.563966000	0.097683000	2.048426000
6	0.374561000	1.184871000	-1.216773000
1	-1.146772000	2.430598000	-0.304893000
6	0.798166000	-0.294927000	-1.235128000
1	2.004234000	-1.585490000	0.062291000
1	2.667223000	0.037098000	-0.163951000
1	-1.049968000	-1.200283000	-1.953921000
1	0.010047000	-2.301600000	-1.093023000
1	1.332899000	-0.481102000	-2.167870000

E = –389.335187
ZPVE = 0.215103

Adamantane TSB (C_1)

6	0.150480000	-0.855666000	1.463762000
6	-0.999631000	0.091634000	1.082094000
6	1.170354000	-0.949439000	0.315577000
1	-0.240411000	-1.852578000	1.684239000
1	0.635805000	-0.496051000	2.374254000
6	-1.808899000	-0.474429000	-0.166300000
6	0.419280000	-1.442623000	-0.920675000
6	-0.698845000	-0.447792000	-1.193938000
1	0.006840000	-2.442065000	-0.764269000
1	1.085112000	-1.497588000	-1.783125000
1	-2.215662000	-1.468427000	0.042568000
1	-2.612401000	0.221440000	-0.404942000
6	1.770186000	0.425359000	-0.039609000
1	1.973071000	-1.636519000	0.594117000
6	-0.383390000	1.475196000	0.774748000
1	-1.691995000	0.188995000	1.921745000
6	-0.436136000	0.947177000	-1.336521000
1	-0.941576000	0.346646000	-2.325475000
6	0.666605000	1.406174000	-0.455267000
1	0.190473000	1.814928000	1.640467000
1	-1.150382000	2.216116000	0.564780000
1	2.492609000	0.311349000	-0.850721000
1	2.317800000	0.833949000	0.814328000
1	1.050696000	2.406256000	-0.651194000

E = –389.269783
ZPVE = 0.210986

PCU diazirine (C_1)

6	1.437438000	0.647004000	0.910232000
6	0.193413000	1.565733000	0.700762000
6	0.112033000	1.772197000	-0.811085000
6	0.620691000	0.418463000	-1.321524000
1	0.788617000	2.569444000	-1.125836000
1	-0.888606000	2.024072000	-1.160236000
6	1.905812000	0.172936000	-0.487834000
6	0.506778000	-0.513802000	1.378965000
6	-0.746752000	0.398284000	1.177346000
6	-1.437439000	-0.227751000	0.004051000
6	-0.323711000	-0.765140000	-0.852649000
6	0.560602000	-1.508667000	0.187566000
1	0.674509000	-0.953186000	2.357963000
1	2.225337000	0.978843000	1.580791000
1	0.788687000	0.388861000	-2.396118000
6	1.984512000	-1.348124000	-0.345299000
1	0.223326000	-2.516574000	0.417067000
1	2.149775000	-1.862074000	-1.293452000
1	2.744764000	-1.673489000	0.366538000
1	2.788948000	0.677289000	-0.874624000
1	-1.383275000	0.605978000	2.032767000
1	0.133263000	2.473930000	1.294538000
1	-0.662076000	-1.384124000	-1.680134000
7	-2.742762000	-0.890416000	0.105259000
7	-2.752030000	0.176733000	-0.499893000

E = −535.818690
ZPVE = 0.211683

PCU diazo (C_1)

6	1.533438000	0.796078000	0.748950000
6	0.224292000	1.615742000	0.536905000
6	0.008993000	1.629650000	-0.974891000
6	0.572037000	0.260507000	-1.370321000
1	0.587712000	2.428184000	-1.443301000
1	-1.036929000	1.764083000	-1.254209000
6	1.926786000	0.187310000	-0.619866000
6	0.717563000	-0.352760000	1.418257000
6	-0.607366000	0.458657000	1.221008000
6	-1.334281000	-0.343561000	0.188738000
6	-0.261889000	-0.916192000	-0.693459000
6	0.748568000	-1.475934000	0.350508000
1	0.981220000	-0.662463000	2.425489000
1	2.346187000	1.246049000	1.312389000
1	0.660506000	0.113606000	-2.445184000
6	2.114117000	-1.300102000	-0.314011000
1	0.493849000	-2.466494000	0.718676000
1	2.239255000	-1.912147000	-1.208613000
1	2.946248000	-1.497005000	0.363518000
1	2.745546000	0.690990000	-1.129690000
1	-1.182794000	0.736211000	2.099172000
1	0.148394000	2.584750000	1.024020000
1	-0.612988000	-1.646441000	-1.417828000
7	-2.591436000	-0.328359000	-0.049417000
7	-3.718529000	-0.348168000	-0.235632000

E = –535.837582
ZPVE = 0.211636

PCU singlet carbene (C_1)

6	-0.000171000	0.278538000	-1.375866000
6	1.440063000	0.199626000	-0.786596000
6	1.464489000	1.256512000	0.313504000
6	0.039187000	1.115245000	0.854807000
1	1.583087000	2.244963000	-0.139028000
1	2.246697000	1.118950000	1.055517000
6	-0.832640000	1.176534000	-0.420661000
6	-0.317073000	-1.158705000	-0.872817000
6	1.105449000	-1.285841000	-0.242171000
6	1.029546000	-1.101030000	1.212983000
6	-0.262043000	-0.387925000	1.377696000
6	-1.275620000	-0.910846000	0.310980000
1	-0.632992000	-1.901320000	-1.600394000
1	-0.109706000	0.493602000	-2.435205000
1	-0.228443000	1.837700000	1.621337000
6	-2.064491000	0.330855000	-0.104682000
1	-1.853420000	-1.776566000	0.628002000
1	-2.672127000	0.748644000	0.699497000
1	-2.704601000	0.160231000	-0.972128000
1	-1.010798000	2.191301000	-0.772201000
1	1.789836000	-2.046087000	-0.607435000
1	2.278555000	0.210973000	-1.475816000
1	-0.646266000	-0.360163000	2.394790000

E = −426.228274
ZPVE = 0.199734

PCU triplet carbene (C_1)

6	0.052631000	0.316319000	-1.370048000
6	1.477915000	0.257252000	-0.745113000
6	1.438600000	1.241157000	0.421114000
6	-0.015555000	1.105252000	0.883400000
1	1.632365000	2.259330000	0.075757000
1	2.161832000	1.000297000	1.201241000
6	-0.829800000	1.181261000	-0.432929000
6	-0.249810000	-1.135746000	-0.894953000
6	1.193198000	-1.230721000	-0.253330000
6	0.883916000	-1.220428000	1.179897000
6	-0.317965000	-0.386970000	1.389241000
6	-1.266191000	-0.923151000	0.260621000
1	-0.529755000	-1.881454000	-1.633883000
1	-0.037480000	0.534128000	-2.430976000
1	-0.315092000	1.840322000	1.628147000
6	-2.058798000	0.305830000	-0.181855000
1	-1.828795000	-1.807295000	0.548513000
1	-2.714242000	0.697518000	0.597621000
1	-2.651165000	0.131064000	-1.081869000
1	-1.015241000	2.195479000	-0.782150000
1	1.873880000	-1.988492000	-0.629522000
1	2.329228000	0.359916000	-1.413480000
1	-0.754387000	-0.401144000	2.384338000

E = −426.219023
ZPVE = 0.200109

PCU diradical (C_1)

6	0.350336000	-0.422225000	1.283511000
6	1.748058000	-0.174201000	0.847192000
6	1.885139000	-0.439843000	-0.618205000
6	0.457328000	-0.832390000	-1.041348000

1	2.584854000	-1.260306000	-0.821462000
1	2.260867000	0.428158000	-1.171336000
6	-0.150457000	-1.465162000	0.240862000
6	-0.654583000	0.810595000	1.023100000
6	0.039434000	1.993547000	0.347948000
6	0.071655000	1.718232000	-0.940655000
6	-0.519072000	0.391080000	-1.299919000
6	-1.543149000	0.248957000	-0.122387000
1	-1.203763000	1.068642000	1.927812000
1	0.261664000	-0.752395000	2.318403000
1	0.444832000	-1.506210000	-1.896158000
6	-1.650512000	-1.242841000	0.129280000
1	-2.460900000	0.810228000	-0.279426000
1	-2.106675000	-1.787171000	-0.699247000
1	-2.191356000	-1.483829000	1.046234000
1	0.185678000	-2.481547000	0.438950000
1	0.476333000	2.831370000	0.869521000
1	2.514828000	0.278972000	1.457729000
1	-0.971426000	0.339589000	-2.287301000

E = –426.217700
ZPVE = 0.197065

PCU homopentaprismane (C_{2v})

6	-1.203856000	0.786073000	0.173893000
6	-0.776071000	0.781892000	-1.319165000
6	0.000000000	1.141697000	1.071195000
6	1.203856000	0.786073000	0.173893000
6	0.776071000	0.781892000	-1.319165000
6	-1.203856000	-0.786073000	0.173893000
1	-2.137009000	1.280524000	0.432742000
6	1.203856000	-0.786073000	0.173893000
1	2.137009000	1.280524000	0.432742000
6	0.000000000	-1.141697000	1.071195000
6	-0.776071000	-0.781892000	-1.319165000
1	-1.314070000	1.389226000	-2.041372000
1	-2.137009000	-1.280524000	0.432742000
6	0.776071000	-0.781892000	-1.319165000
1	1.314070000	1.389226000	-2.041372000
1	2.137009000	-1.280524000	0.432742000
1	-1.314070000	-1.389226000	-2.041372000
1	1.314070000	-1.389226000	-2.041372000
6	0.000000000	0.000000000	2.107030000
1	0.000000000	2.155200000	1.468352000
1	-0.886008000	0.000000000	2.743905000
1	0.886008000	0.000000000	2.743905000
1	0.000000000	-2.155200000	1.468352000

E = −426.294063
ZPVE = 0.201342

PCU dialkene_1 (C_{2v})

6	1.172841000	0.804013000	0.080721000
6	1.172841000	-0.804013000	0.080721000
6	0.000000000	1.116482000	1.055130000
6	0.000000000	-1.116482000	1.055130000
6	-1.172841000	-0.804013000	0.080721000
6	-1.172841000	0.804013000	0.080721000
6	0.000000000	0.000000000	2.079551000
1	0.000000000	2.139609000	1.425801000
1	-0.886741000	0.000000000	2.716129000
1	0.886741000	0.000000000	2.716129000
1	0.000000000	-2.139609000	1.425801000
6	0.665554000	1.414136000	-1.204566000
1	2.138754000	1.184166000	0.409096000
6	-0.665554000	1.414136000	-1.204566000
1	-2.138754000	1.184166000	0.409096000
1	1.300427000	1.725933000	-2.021710000
1	-1.300427000	1.725933000	-2.021710000
6	-0.665554000	-1.414136000	-1.204566000
1	-2.138754000	-1.184166000	0.409096000
6	0.665554000	-1.414136000	-1.204566000
1	2.138754000	-1.184166000	0.409096000
1	-1.300427000	-1.725933000	-2.021710000
1	1.300427000	-1.725933000	-2.021710000

E = −426.329686
ZPVE = 0.200397

PCU dialkene_2 (C_{2v})

6	1.315162000	0.788300000	0.211841000
6	1.315162000	-0.788300000	0.211841000
6	0.000000000	1.146138000	0.942387000
6	0.000000000	-1.146138000	0.942387000
6	-1.315162000	-0.788300000	0.211841000
6	-1.315162000	0.788300000	0.211841000
6	0.000000000	0.000000000	1.995839000
1	0.000000000	2.154353000	1.353202000
1	-0.886567000	0.000000000	2.632033000
1	0.886567000	0.000000000	2.632033000
1	0.000000000	-2.154353000	1.353202000
6	1.505810000	-0.666723000	-1.290599000
1	2.157209000	-1.247003000	0.734476000
6	1.505810000	0.666723000	-1.290599000
1	2.157209000	1.247003000	0.734476000
6	-1.505810000	-0.666723000	-1.290599000
1	-2.157209000	-1.247003000	0.734476000
6	-1.505810000	0.666723000	-1.290599000
1	-2.157209000	1.247003000	0.734476000
1	-1.597068000	-1.405818000	-2.075465000
1	-1.597068000	1.405818000	-2.075465000
1	1.597068000	-1.405818000	-2.075465000
1	1.597068000	1.405818000	-2.075465000

E = −426.245913
ZPVE = 0.197615

PCU TSA (C_1)

6	-0.122249000	-0.689509000	-1.257807000
6	1.361383000	-0.340257000	-0.942864000
6	1.350384000	1.110698000	-0.438315000
6	-0.116218000	1.413449000	-0.100381000
1	1.977281000	1.866424000	-0.906566000
1	1.951298000	1.035549000	0.746927000
6	-1.000911000	0.562062000	-1.039967000
6	-0.215649000	-1.438769000	0.117919000
6	1.263399000	-1.069401000	0.419292000
6	1.264049000	0.155960000	1.371065000
6	-0.199686000	0.665711000	1.265045000
6	-1.133232000	-0.526362000	0.953737000
1	-0.489858000	-2.490577000	0.101013000
1	-0.334002000	-1.255430000	-2.160995000
1	-0.378564000	2.468197000	-0.060855000
6	-2.101190000	0.051386000	-0.092830000

1	-1.583219000	-0.996954000	1.825350000
1	-2.733589000	0.849532000	0.298457000
1	-2.738549000	-0.706086000	-0.551217000
1	-1.329217000	1.065024000	-1.947576000
1	1.955629000	-1.867125000	0.677740000
1	2.133477000	-0.609257000	-1.658511000
1	-0.531173000	1.270893000	2.106865000

E = −426.193898
ZPVE = 0.196384

PCU TSB (C_1)

6	0.057240000	-0.401048000	1.326049000
6	1.459426000	-0.600165000	0.911084000
6	1.569373000	-1.123954000	-0.440682000
6	0.126797000	-1.062270000	-0.947998000
1	2.068248000	-2.097225000	-0.504342000
1	2.191311000	-0.402876000	-1.030665000
6	-0.747454000	-1.279961000	0.314587000
6	-0.383673000	1.087181000	0.932290000
6	0.835249000	1.755095000	0.260854000
6	0.949732000	1.318998000	-1.003166000
6	-0.235513000	0.442302000	-1.329277000
6	-1.319942000	0.807689000	-0.263088000
1	-0.858428000	1.623383000	1.756064000
1	-0.123832000	-0.602359000	2.382035000
1	-0.087023000	-1.759010000	-1.755247000
6	-2.032116000	-0.494393000	0.062608000
1	-1.924893000	1.666418000	-0.545647000
1	-2.610763000	-0.890517000	-0.773634000
1	-2.678230000	-0.441670000	0.940005000
1	-0.857407000	-2.323496000	0.607713000
1	1.475990000	2.454070000	0.784802000
1	2.309641000	-0.434394000	1.558550000
1	-0.579329000	0.510832000	-2.359203000

E = −426.185930
ZPVE = 0.195423

Protoadamantane diazirine (C_1)

6	1.556672000	0.951218000	-0.991931000
6	0.436224000	1.572322000	-0.125938000
6	1.775825000	-0.556256000	-0.770028000
1	2.493182000	1.466885000	-0.762922000
1	1.345091000	1.144581000	-2.046632000
6	0.532209000	1.072986000	1.323392000
6	2.011187000	-0.828676000	0.720063000
6	0.637138000	-0.460712000	1.299983000
1	-0.345680000	1.400247000	1.884155000
1	1.406403000	1.488611000	1.827833000
1	2.818458000	-0.235890000	1.152169000
1	2.244387000	-1.883208000	0.881430000
6	-0.988616000	1.255182000	-0.625731000
1	0.563339000	2.655498000	-0.157378000
6	-1.452617000	-0.079797000	-0.094344000
1	-1.032633000	1.269550000	-1.718915000
1	-1.676528000	2.027989000	-0.276129000
6	-0.371908000	-1.062569000	0.255080000
1	0.471849000	-0.871674000	2.294614000
6	0.496401000	-1.366830000	-1.001936000
1	2.597570000	-0.899052000	-1.400329000
1	0.736188000	-2.429568000	-1.044334000
1	-0.017174000	-1.114273000	-1.929479000
1	-0.827309000	-1.972329000	0.641923000
7	-2.768463000	-0.582793000	-0.518143000
7	-2.741855000	-0.135574000	0.621334000

E = –498.933811
ZPVE = 0.228617

Protoadamantane diazo (C_1)

6	1.684360000	0.974934000	-0.887935000
6	0.569115000	1.570439000	0.003773000
6	1.854387000	-0.551992000	-0.779931000
1	2.632594000	1.439570000	-0.604202000
1	1.500345000	1.255437000	-1.928147000
6	0.604883000	0.948398000	1.407121000
6	2.039461000	-0.947030000	0.689876000
6	0.661766000	-0.580613000	1.259974000
1	-0.280492000	1.256679000	1.966738000
1	1.475364000	1.291924000	1.968915000
1	2.851887000	-0.415677000	1.187363000
1	2.236853000	-2.017715000	0.773576000
6	-0.856181000	1.370461000	-0.561700000
1	0.743304000	2.645757000	0.067116000
6	-1.358557000	0.008775000	-0.154186000
1	-0.850177000	1.495693000	-1.650169000
1	-1.514576000	2.142814000	-0.158872000
6	-0.341514000	-1.056836000	0.140031000
1	0.449583000	-1.066030000	2.211543000
6	0.562384000	-1.306049000	-1.107253000
1	2.684993000	-0.867543000	-1.412857000
1	0.774710000	-2.371203000	-1.210675000
1	0.084622000	-0.976458000	-2.029003000
1	-0.846958000	-1.971748000	0.441698000
7	-2.615415000	-0.219127000	-0.030519000
7	-3.736394000	-0.412932000	0.076000000

E = –498.951663
ZPVE = 0.228662

Singlet protoadamantylidene (C_1)

6	-0.047905000	-1.091050000	-1.285490000
6	1.081811000	-1.044487000	-0.236689000
6	-1.218447000	-0.142334000	-0.963140000
1	-0.441308000	-2.109274000	-1.344709000
1	0.361009000	-0.854750000	-2.271519000
6	0.503959000	-1.124858000	1.180778000
6	-1.769510000	-0.455903000	0.429297000
6	-0.577088000	-0.047489000	1.308142000
1	1.301234000	-0.969833000	1.911737000
1	0.070430000	-2.106809000	1.383020000
1	-2.053423000	-1.502003000	0.561170000
1	-2.646874000	0.159520000	0.639812000
6	1.886105000	0.263898000	-0.311031000
1	1.755797000	-1.884418000	-0.421220000
6	1.240814000	1.522211000	0.155154000
1	2.333708000	0.424869000	-1.296877000
1	2.761252000	0.205358000	0.355772000
6	-0.103507000	1.306871000	0.681223000
1	-0.856074000	0.102892000	2.350384000
6	-0.746423000	1.303537000	-0.791475000
1	-1.974435000	-0.213127000	-1.747459000
1	-1.567496000	2.017342000	-0.790586000
1	-0.054371000	1.630731000	-1.571069000

1	-0.488291000	2.157116000	1.240934000

E = –389.346262
ZPVE = 0.216205

Triplet protoadamantylidene (C_1)

6	0.003075000	-1.180811000	-1.166201000
6	1.170136000	-0.955916000	-0.175336000
6	-1.274585000	-0.362431000	-0.884367000
1	-0.268417000	-2.239635000	-1.132781000
1	0.351417000	-0.983617000	-2.183269000
6	0.653217000	-0.876139000	1.268614000
6	-1.705349000	-0.560859000	0.573179000
6	-0.533367000	0.099214000	1.312216000
1	1.459807000	-0.547647000	1.926818000
1	0.327417000	-1.855977000	1.624203000
1	-1.835794000	-1.607413000	0.853227000
1	-2.646509000	-0.041388000	0.764060000
6	1.973919000	0.352003000	-0.446286000
1	1.863132000	-1.792667000	-0.284254000
6	1.209519000	1.471411000	0.125627000
1	2.157329000	0.465847000	-1.523931000
1	2.959726000	0.265389000	0.022844000
6	-0.221563000	1.391398000	0.432863000
1	-0.771784000	0.374567000	2.338210000
6	-1.027269000	1.147112000	-0.893422000
1	-2.047048000	-0.653175000	-1.598274000
1	-1.980109000	1.678776000	-0.861415000
1	-0.480324000	1.498773000	-1.767083000
1	-0.575245000	2.288267000	0.940326000

E = –389.337959
ZPVE = 0.216687

2,4-Dehydroprotoadamantane (C_1)

6	1.067125000	-1.097572000	0.000000000
1	1.744752000	-1.953408000	0.000000000
6	0.197457000	-1.125786000	-1.269803000
6	-0.903239000	-0.056452000	-1.184214000
1	-1.438882000	0.011903000	-2.130734000
6	-0.353878000	1.317948000	-0.758997000
1	-0.673068000	2.189713000	-1.312945000
6	-0.353877000	1.317949000	0.758996000
6	0.947399000	1.379731000	-0.000001000
1	1.431436000	2.349421000	-0.000001000
6	1.883029000	0.197272000	-0.000001000
6	-1.824890000	-0.405793000	0.000001000
6	-0.903238000	-0.056451000	1.184215000
1	-1.438881000	0.011905000	2.130735000
6	0.197458000	-1.125785000	1.269804000
1	-0.265981000	-2.107535000	-1.394064000
1	0.830785000	-0.956751000	-2.144098000
1	-0.673067000	2.189714000	1.312944000
1	2.531597000	0.233534000	0.879738000
1	2.531596000	0.233534000	-0.879740000
1	-2.159069000	-1.446196000	0.000001000
1	-2.706108000	0.238077000	0.000001000
1	-0.265980000	-2.107534000	1.394066000
1	0.830786000	-0.956749000	2.144098000

E = –389.438505
ZPVE = 0.219514

Protoadamantane alkene (C_1)

6	-0.195767000	-1.120922000	-1.247252000
6	1.020098000	-1.125458000	-0.280256000
6	-1.331854000	-0.142960000	-0.865726000
1	-0.619591000	-2.129243000	-1.264794000
1	0.150801000	-0.907832000	-2.260498000
6	0.532127000	-1.100729000	1.182870000
6	-1.743662000	-0.365446000	0.593231000
6	-0.455973000	0.064212000	1.315526000
1	1.389652000	-0.986078000	1.845402000
1	0.030724000	-2.032892000	1.451676000
1	-2.024257000	-1.394252000	0.821864000
1	-2.588121000	0.277924000	0.848539000
6	1.911471000	0.087415000	-0.416635000
1	1.600924000	-2.028375000	-0.473046000
6	-0.874377000	1.316722000	-0.780452000
1	-2.160332000	-0.271281000	-1.564657000
6	1.460103000	1.247069000	0.046965000
6	0.026387000	1.334192000	0.495494000
1	-0.619418000	0.318381000	2.361593000
1	-1.747925000	1.958054000	-0.647376000
1	-0.335789000	1.663724000	-1.660351000
1	-0.140844000	2.241143000	1.073929000
1	2.910283000	-0.020708000	-0.820448000
1	2.062576000	2.146862000	0.025575000

E = –389.445207
ZPVE = 0.219018

Protoadamantane alkene 2 (C_1)

6	-0.007732000	-0.216691000	1.529510000
6	-1.236774000	-0.676856000	0.638127000
6	1.379915000	0.097376000	0.847130000
1	0.189959000	-1.024773000	2.237987000
1	-0.314908000	0.645547000	2.126721000
6	-0.758032000	-1.454315000	-0.588372000
6	1.631427000	-0.954831000	-0.233058000
6	0.420970000	-0.637066000	-1.143662000
1	1.616189000	-1.982349000	0.129017000
1	2.588360000	-0.783988000	-0.726805000
6	-2.037176000	0.504479000	0.044577000
1	-1.893104000	-1.289458000	1.259845000
6	1.375406000	1.365999000	-0.072614000
1	2.151368000	0.150672000	1.617590000
6	-0.985419000	1.395685000	-0.568417000
6	0.204435000	0.869099000	-0.887206000
1	0.602415000	-0.846939000	-2.197562000
1	2.343010000	1.449208000	-0.572729000
1	1.156689000	2.294994000	0.449525000
1	-2.538930000	1.078384000	0.826594000
1	-2.820858000	0.128654000	-0.619134000
1	-1.574827000	-1.555732000	-1.304343000
1	-0.416467000	-2.461504000	-0.345631000
1	-1.011024000	2.440001000	-0.277172000

E = – 389.397887
ZPVE = 0.218131

Protoadamantane TSA (C_1)

6	-0.156976000	-1.046750000	1.328334000
6	-1.130722000	-1.021899000	0.137779000

6	1.030148000	-0.091791000	1.109108000
1	0.239063000	-2.054623000	1.472294000
1	-0.694475000	-0.781320000	2.242422000
6	-0.384012000	-1.170784000	-1.193829000
6	1.785226000	-0.523199000	-0.160540000
6	0.755445000	-0.146382000	-1.243978000
1	-1.082306000	-1.017586000	-2.019957000
1	0.029993000	-2.175970000	-1.305884000
1	2.053969000	-1.583016000	-0.165991000
1	2.701788000	0.058661000	-0.276657000
6	-1.871009000	0.321255000	0.106202000
1	-1.856401000	-1.830067000	0.254673000
6	-1.023756000	1.547654000	-0.160270000
1	-2.459987000	0.463016000	1.014972000
1	-2.593474000	0.319331000	-0.717445000
6	0.303416000	1.270163000	-0.791707000
1	1.194356000	-0.107997000	-2.240178000
6	0.592216000	1.316458000	0.705582000
1	1.660271000	-0.066293000	1.998162000
1	1.183898000	2.161919000	1.041063000
1	-0.500742000	1.810311000	1.068534000
1	0.724189000	2.075287000	-1.386096000

E = – 389.335091
ZPVE = 0.213953

Protoadamantane TSB (C_1)

6	-0.156871000	-1.109219000	-1.263161000
6	1.046108000	-1.082351000	-0.291078000
6	-1.311783000	-0.161162000	-0.878006000
1	-0.550890000	-2.128571000	-1.284508000
1	0.187342000	-0.887260000	-2.276250000
6	0.561395000	-1.099674000	1.170596000
6	-1.734627000	-0.419513000	0.570735000
6	-0.468207000	0.027151000	1.319608000
1	1.413349000	-0.965055000	1.838932000
1	0.099830000	-2.056457000	1.422213000
1	-1.997334000	-1.458875000	0.776130000
1	-2.594958000	0.201237000	0.828058000
6	1.884152000	0.187891000	-0.368040000
1	1.680518000	-1.944200000	-0.503785000
6	1.453804000	1.397333000	0.189511000
1	1.641523000	1.118907000	-1.148337000
1	2.938934000	0.074677000	-0.616149000
6	-0.017322000	1.335861000	0.543364000
1	-0.652145000	0.246094000	2.369951000
6	-0.870461000	1.301268000	-0.768306000
1	-2.129394000	-0.286999000	-1.589854000
1	-1.749523000	1.936824000	-0.657711000
1	-0.323052000	1.668330000	-1.636308000
1	-0.281321000	2.215847000	1.126291000

E = –389.331958
ZPVE = 0.213900

Protoadamantane TSB2 (C_1)

6	-0.143619000	-1.087187000	-1.280499000
6	1.058900000	-1.069510000	-0.301530000
6	-1.309053000	-0.156221000	-0.878190000
1	-0.526380000	-2.110193000	-1.326046000
1	0.200799000	-0.837368000	-2.286655000
6	0.564204000	-1.118148000	1.153239000
6	-1.731678000	-0.441413000	0.565162000
6	-0.467598000	0.001601000	1.320547000
1	1.410245000	-1.002257000	1.833646000
1	0.103488000	-2.081362000	1.379675000
1	-1.989182000	-1.485294000	0.754205000
1	-2.595140000	0.170882000	0.831869000
6	1.858877000	0.217549000	-0.416530000
1	1.702264000	-1.922796000	-0.522788000
6	1.366584000	1.454358000	0.017508000
1	2.340628000	0.712392000	0.626586000
1	2.779103000	0.194727000	-0.999103000
6	-0.031080000	1.327352000	0.569875000
1	-0.652848000	0.203083000	2.374374000
6	-0.880305000	1.308172000	-0.749688000
1	-2.124208000	-0.279529000	-1.593270000
1	-1.756609000	1.947031000	-0.640565000
1	-0.315508000	1.677208000	-1.606047000
1	-0.288047000	2.194151000	1.174754000

E = –389.333729
ZPVE = 0.213777

Protoadamantane TSC (C_1)

6	-0.017816000	-0.273992000	1.521988000
6	-1.266260000	-0.658991000	0.610659000
6	1.379222000	0.029142000	0.848775000
1	0.160644000	-1.126689000	2.181338000
1	-0.294988000	0.563500000	2.164592000
6	-0.800227000	-1.417315000	-0.631847000
6	1.600003000	-0.986161000	-0.273586000
6	0.391869000	-0.607033000	-1.160107000
1	-1.614816000	-1.490570000	-1.352865000
1	-0.475990000	-2.435570000	-0.409781000
1	1.560189000	-2.026388000	0.049733000
1	2.557832000	-0.820401000	-0.766696000
6	-2.041420000	0.561396000	0.049193000
1	-1.936879000	-1.265419000	1.220423000
6	-0.954771000	1.532244000	-0.325927000
1	-2.664407000	1.042351000	0.806677000
1	-2.719831000	0.243314000	-0.747247000
6	0.204504000	0.906647000	-0.802260000
1	0.563690000	-0.748710000	-2.225912000
6	1.422360000	1.337105000	-0.013566000
1	2.150616000	0.030645000	1.619805000
1	2.375179000	1.385396000	-0.543507000
1	1.239409000	2.251636000	0.540676000
1	-0.405428000	1.858658000	-1.477173000

E = –389.287129
ZPVE = 0.211716

d_2-Protoadamantane diazirine (C_1)

6	1.556672000	0.951218000	-0.991931000
6	0.436224000	1.572322000	-0.125938000
6	1.775825000	-0.556256000	-0.770028000
1	2.493182000	1.466885000	-0.762922000
1	1.345091000	1.144581000	-2.046632000
6	0.532209000	1.072986000	1.323392000
6	2.011187000	-0.828676000	0.720063000
6	0.637138000	-0.460712000	1.299983000
1	-0.345680000	1.400247000	1.884155000
1	1.406403000	1.488611000	1.827833000

1 2.818458000 -0.235890000 1.152169000
1 2.244387000 -1.883208000 0.881430000
6 -0.988616000 1.255182000 -0.625731000
1 0.563339000 2.655498000 -0.157378000
6 -1.452617000 -0.079797000 -0.094344000
1(Iso=2) -1.032633000 1.269550000 -1.718915000
1(Iso=2) -1.676528000 2.027989000 -0.276129000
6 -0.371908000 -1.062569000 0.255080000
1 0.471849000 -0.871674000 2.294614000
6 0.496401000 -1.366830000 -1.001936000
1 2.597570000 -0.899052000 -1.400329000
1 0.736188000 -2.429568000 -1.044334000
1 -0.017174000 -1.114273000 -1.929479000
1 -0.827309000 -1.972329000 0.641923000
7 -2.768463000 -0.582793000 -0.518143000
7 -2.741855000 -0.135574000 0.621334000

E = –498.940467
ZPVE = 0.221962

d_2-Protoadamantane diazo (C_1)

6 1.684360000 0.974934000 -0.887935000
6 0.569115000 1.570439000 0.003773000
6 1.854387000 -0.551992000 -0.779931000
1 2.632594000 1.439570000 -0.604202000
1 1.500345000 1.255437000 -1.928147000
6 0.604883000 0.948398000 1.407121000
6 2.039461000 -0.947030000 0.689876000
6 0.661766000 -0.580613000 1.259974000
1 -0.280492000 1.256679000 1.966738000
1 1.475364000 1.291924000 1.968915000
1 2.851887000 -0.415677000 1.187363000
1 2.236853000 -2.017715000 0.773576000
6 -0.856181000 1.370461000 -0.561700000
1 0.743304000 2.645757000 0.067116000
6 -1.358557000 0.008775000 -0.154186000
1(Iso=2) -0.850177000 1.495693000 -1.650169000
1(Iso=2) -1.514576000 2.142814000 -0.158872000
6 -0.341514000 -1.056836000 0.140031000
1 0.449583000 -1.066030000 2.211543000
6 0.562384000 -1.306049000 -1.107253000
1 2.684993000 -0.867543000 -1.412857000
1 0.774710000 -2.371203000 -1.210675000
1 0.084622000 -0.976458000 -2.029003000
1 -0.846958000 -1.971748000 0.441698000
7 -2.615415000 -0.219127000 -0.030519000
7 -3.736394000 -0.412932000 0.076000000

E = –498.958308
ZPVE = 0.222017

d_2-singlet protoadamantylidene (C_1)

6 -0.047905000 -1.091050000 -1.285490000
6 1.081811000 -1.044487000 -0.236689000
6 -1.218447000 -0.142334000 -0.963140000
1 -0.441308000 -2.109274000 -1.344709000
1 0.361009000 -0.854750000 -2.271519000
6 0.503959000 -1.124858000 1.180779000
6 -1.769510000 -0.455903000 0.429297000
6 -0.577088000 -0.047489000 1.308142000
1 1.301234000 -0.969833000 1.911737000
1 0.070430000 -2.106809000 1.383020000
1 -2.053423000 -1.502003000 0.561170000
1 -2.646874000 0.159520000 0.639812000
6 1.886105000 0.263898000 -0.311031000
1 1.755797000 -1.884418000 -0.421220000
6 1.240814000 1.522211000 0.155154000
1(Iso=2) 2.333708000 0.424869000 -1.296877000
1(Iso=2) 2.761252000 0.205358000 0.355772000
6 -0.103507000 1.306871000 0.681223000
1 -0.856074000 0.102892000 2.350384000
6 -0.746423000 1.303537000 -0.791475000
1 -1.974435000 -0.213128000 -1.747459000
1 -1.567496000 2.017342000 -0.790586000
1 -0.054371000 1.630731000 -1.571069000
1 -0.488291000 2.157116000 1.240933000

E = –389.352650
ZPVE = 0.209817

d_2-triplet protoadamantylidene (C_1)

6 0.003075000 -1.180811000 -1.166201000
6 1.170136000 -0.955916000 -0.175336000
6 -1.274585000 -0.362431000 -0.884367000
1 -0.268416000 -2.239635000 -1.132781000
1 0.351417000 -0.983617000 -2.183269000
6 0.653217000 -0.876139000 1.268614000
6 -1.705349000 -0.560859000 0.573179000
6 -0.533367000 0.099214000 1.312216000
1 1.459807000 -0.547646000 1.926818000
1 0.327418000 -1.855977000 1.624203000
1 -1.835793000 -1.607413000 0.853227000
1 -2.646509000 -0.041389000 0.764060000
6 1.973919000 0.352004000 -0.446286000
1 1.863133000 -1.792666000 -0.284254000
6 1.209519000 1.471411000 0.125627000
1(Iso=2) 2.157329000 0.465848000 -1.523931000
1(Iso=2) 2.959726000 0.265390000 0.022844000
6 -0.221563000 1.391398000 0.432863000
1 -0.771784000 0.374567000 2.338210000
6 -1.027269000 1.147112000 -0.893422000
1 -2.047048000 -0.653176000 -1.598274000
1 -1.980109000 1.678775000 -0.861415000
1 -0.480324000 1.498773000 -1.767083000
1 -0.575246000 2.288267000 0.940326000

E = –389.344465
ZPVE = 0.210182

d_2-2,4-Dehydroprotoadamantane (C_1)

6 1.067125000 -1.097572000 0.000000000
1 1.744751000 -1.953408000 0.000000000
6 0.197457000 -1.125786000 -1.269803000
6 -0.903239000 -0.056452000 -1.184214000
1 -1.438883000 0.011904000 -2.130734000
6 -0.353877000 1.317949000 -0.758997000
1 -0.673067000 2.189714000 -1.312944000
6 -0.353876000 1.317949000 0.758996000
6 0.947399000 1.379731000 -0.000001000
1 1.431437000 2.349420000 -0.000001000
6 1.883029000 0.197271000 -0.000001000
6 -1.824890000 -0.405792000 0.000001000
6 -0.903238000 -0.056451000 1.184215000
1 -1.438881000 0.011905000 2.130735000

6 0.197458000 -1.125785000 1.269804000
1 -0.265982000 -2.107535000 -1.394064000
1 0.830784000 -0.956751000 -2.144098000
1 -0.673066000 2.189715000 1.312943000
1(Iso=2) 2.531597000 0.233533000 0.879738000
1(Iso=2) 2.531596000 0.233533000 -0.879740000
1 -2.159070000 -1.446196000 0.000001000
1 -2.706108000 0.238078000 0.000001000
1 -0.265980000 -2.107534000 1.394066000
1 0.830786000 -0.956749000 2.144098000

E = –389,445184
ZPVE = 0,212836

d_2-Protoadamantane alkene (C_1)

6 -0.195766000 -1.120922000 -1.247252000
6 1.020099000 -1.125457000 -0.280256000
6 -1.331854000 -0.142961000 -0.865726000
1 -0.619590000 -2.129243000 -1.264794000
1 0.150802000 -0.907832000 -2.260498000
6 0.532128000 -1.100729000 1.182870000
6 -1.743662000 -0.365447000 0.593231000
6 -0.455973000 0.064212000 1.315526000
1 1.389653000 -0.986077000 1.845402000
1 0.030725000 -2.032892000 1.451676000
1 -2.024256000 -1.394253000 0.821864000
1 -2.588121000 0.277922000 0.848539000
6 1.911471000 0.087416000 -0.416635000
1 1.600925000 -2.028374000 -0.473046000
6 -0.874378000 1.316721000 -0.780452000
1 -2.160332000 -0.271282000 -1.564657000
6 1.460102000 1.247070000 0.046965000
6 0.026386000 1.334192000 0.495494000
1 -0.619418000 0.318381000 2.361593000
1 -1.747926000 1.958053000 -0.647376000
1 -0.335790000 1.663724000 -1.660351000
1 -0.140845000 2.241143000 1.073929000
1(Iso=2) 2.910283000 -0.020706000 -0.820448000
1(Iso=2) 2.062575000 2.146863000 0.025575000

E = –389.451612
ZPVE = 0.212613

d_2-Protoadamantane alkene 2 (C_1)

6 -0.007732000 -0.216691000 1.529510000
6 -1.236774000 -0.676856000 0.638127000
6 1.379915000 0.097376000 0.847130000
1 0.189959000 -1.024773000 2.237987000
1 -0.314908000 0.645547000 2.126721000
6 -0.758032000 -1.454315000 -0.588372000
6 1.631427000 -0.954831000 -0.233058000
6 0.420970000 -0.637066000 -1.143662000
1 1.616189000 -1.982349000 0.129017000
1 2.588360000 -0.783988000 -0.726805000
6 -2.037176000 0.504479000 0.044577000
1 -1.893104000 -1.289458000 1.259845000
6 1.375406000 1.365999000 -0.072614000
1 2.151368000 0.150672000 1.617590000
6 -0.985419000 1.395685000 -0.568417000
6 0.204435000 0.869099000 -0.887206000
1 0.602415000 -0.846939000 -2.197562000
1 2.343010000 1.449208000 -0.572729000
1 1.156689000 2.294994000 0.449525000
1(Iso=2) -2.538930000 1.078384000 0.826594000
1(Iso=2) -2.820858000 0.128654000 -0.619134000
1 -1.574827000 -1.555732000 -1.304343000
1 -0.416467000 -2.461504000 -0.345631000
1 -1.011024000 2.440001000 -0.277172000

E = –389.404519
ZPVE = 0.211499

d_2-Protoadamantane TSA (C_1)

6 -0.156976000 -1.046750000 1.328334000
6 -1.130722000 -1.021899000 0.137779000
6 1.030148000 -0.091791000 1.109108000
1 0.239064000 -2.054623000 1.472294000
1 -0.694475000 -0.781320000 2.242422000
6 -0.384012000 -1.170784000 -1.193829000
6 1.785226000 -0.523199000 -0.160540000
6 0.755445000 -0.146382000 -1.243978000
1 -1.082306000 -1.017586000 -2.019957000
1 0.029994000 -2.175970000 -1.305884000
1 2.053969000 -1.583016000 -0.165991000
1 2.701788000 0.058662000 -0.276657000
6 -1.871009000 0.321254000 0.106202000
1 -1.856401000 -1.830068000 0.254673000
6 -1.023756000 1.547654000 -0.160270000
1 -2.459987000 0.463015000 1.014972000
1 -2.593474000 0.319330000 -0.717445000
6 0.303416000 1.270163000 -0.791707000
1 1.194356000 -0.107997000 -2.240178000
6 0.592216000 1.316458000 0.705582000
1 1.660271000 -0.066293000 1.998162000
1 1.183897000 2.161919000 1.041063000
1 -0.500742000 1.810311000 1.068534000
1 0.724189000 2.075287000 -1.386096000

E = –389.341719
ZPVE = 0.207325

d_2-Protoadamantane TSB (C_1)

6 -0.156871000 -1.109219000 -1.263161000
6 1.046108000 -1.082351000 -0.291078000
6 -1.311783000 -0.161162000 -0.878006000
1 -0.550890000 -2.128571000 -1.284508000
1 0.187342000 -0.887260000 -2.276250000
6 0.561395000 -1.099674000 1.170596000
6 -1.734627000 -0.419513000 0.570735000
6 -0.468207000 0.027151000 1.319608000
1 1.413349000 -0.965055000 1.838932000
1 0.099830000 -2.056457000 1.422213000
1 -1.997334000 -1.458875000 0.776130000
1 -2.594958000 0.201236000 0.828058000
6 1.884152000 0.187891000 -0.368040000
1 1.680518000 -1.944200000 -0.503785000
6 1.453804000 1.397333000 0.189511000
1(Iso=2) 1.641523000 1.118907000 -1.148337000
1(Iso=2) 2.938934000 0.074677000 -0.616149000
6 -0.017322000 1.335861000 0.543364000
1 -0.652145000 0.246094000 2.369951000
6 -0.870461000 1.301268000 -0.768306000
1 -2.129394000 -0.286999000 -1.589854000
1 -1.749523000 1.936824000 -0.657711000
1 -0.323052000 1.668330000 -1.636308000

1	-0.281321000	2.215847000	1.126291000

E = –389.337438
ZPVE = 0.208419

d_2-Protoadamantane TSB2 (C_1)

6	-0.143618000	-1.087187000	-1.280499000
6	1.058901000	-1.069509000	-0.301530000
6	-1.309053000	-0.156222000	-0.878190000
1	-0.526379000	-2.110193000	-1.326046000
1	0.200799000	-0.837368000	-2.286655000
6	0.564205000	-1.118148000	1.153239000
6	-1.731678000	-0.441414000	0.565162000
6	-0.467598000	0.001601000	1.320547000
1	1.410246000	-1.002256000	1.833646000
1	0.103489000	-2.081362000	1.379675000
1	-1.989181000	-1.485295000	0.754205000
1	-2.595140000	0.170881000	0.831869000
6	1.858877000	0.217550000	-0.416530000
1	1.702265000	-1.922795000	-0.522788000
6	1.366583000	1.454359000	0.017508000
1	2.340628000	0.712393000	0.626586000
1	2.779103000	0.194729000	-0.999103000
6	-0.031081000	1.327352000	0.569875000
1	-0.652848000	0.203083000	2.374374000
6	-0.880306000	1.308172000	-0.749688000
1	-2.124208000	-0.279530000	-1.593270000
1	-1.756610000	1.947030000	-0.640565000
1	-0.315509000	1.677208000	-1.606047000
1	-0.288048000	2.194151000	1.174754000

E = –389.339187
ZPVE = 0.208319

d_2-Protoadamantane TSC (C_1)

6	-0.017816000	-0.273992000	1.521988000
6	-1.266260000	-0.658991000	0.610659000
6	1.379222000	0.029142000	0.848775000
1	0.160644000	-1.126689000	2.181338000
1	-0.294988000	0.563500000	2.164592000
6	-0.800227000	-1.417315000	-0.631847000
6	1.600003000	-0.986161000	-0.273586000
6	0.391869000	-0.607033000	-1.160107000
1	-1.614816000	-1.490570000	-1.352865000
1	-0.475990000	-2.435570000	-0.409781000
1	1.560189000	-2.026388000	0.049733000
1	2.557832000	-0.820401000	-0.766696000
6	-2.041420000	0.561396000	0.049193000
1	-1.936879000	-1.265419000	1.220423000
6	-0.954771000	1.532244000	-0.325927000
1	-2.664407000	1.042351000	0.806677000
1	-2.719831000	0.243314000	-0.747247000
6	0.204504000	0.906647000	-0.802260000
1	0.563690000	-0.748710000	-2.225912000
6	1.422360000	1.337105000	-0.013566000
1	2.150616000	0.030645000	1.619805000
1	2.375179000	1.385396000	-0.543507000
1	1.239409000	2.251636000	0.540676000
1	-0.405428000	1.858658000	-1.477173000

E = –389.293688
ZPVE = 0.205157

Dinitrogen N_2 ($D_{\infty h}$)

7	0.000000000	0.000000000	0.545450000
7	0.000000000	0.000000000	-0.545450000

E = −109.568426
ZPVE = 0.005588

Bibliography

1. Nandi, A.; Gerbig, D.; Schreiner, P. R.; Borden, W. T.; Kozuch, S., Isotope-controlled selectivity by quantum tunneling: Hydrogen migration versus ring expansion in cyclopropylmethylcarbenes. *J. Am. Chem. Soc.* **2017**, *139*, 9097-9099.
2. Gano, J. E.; Wettach, R. H.; Platz, M. S.; Senthilnathan, V., Di-*tert*-butylcarbene: the low temperature photochemistry of Di-*tert*-butyldiazomethane. *J. Am. Chem. Soc.* **1982**, *104*, 2326-2327.
3. Myers, D. R.; Senthilnathan, V.; Platz, M. S.; Jones, M., Diadamantylcarbene in solution. *J. Am. Chem. Soc.* **1986**, *108*, 4232-4233.
4. Ammann, J. R.; Subramanian, R.; Sheridan, R. S., Dicyclopropylcarbene: direct characterization of a singlet dialkylcarbene. *J. Am. Chem. Soc.* **1992**, *114*, 7592-7594.
5. Bally, T.; Matzinger, S.; Truttmann, L.; Platz, M. S.; Morgan, S., Matrix Spectroscopy of 2-Adamantylidene, a Dialkylcarbene with Singlet Ground State. *Angew. Chem. Int. Ed.* **1994**, *33*, 1964-1966.
6. Rosenberg, M. G.; Brinker, U. H., Constrained Carbenes. *Eur. J. Org. Chem.* **2006**, *2006*, 5423-5440.
7. Rice, F.; Glasebrook, A., The thermal decomposition of organic compounds from the standpoint of free radicals. VII. The ethylidene radical. *J. Am. Chem. Soc.* **1934**, *56*, 741-743.
8. Bawn, C.; Milsted, J., The stability of hydrocarbon biradicals and their reactions. *J. Trans. Faraday Soc.* **1939**, *35*, 889-896.
9. Volman, D.; Leighton, P.; Blacet, F.; Brinton, R., Free Radical Formation in the Photolysis of Some Aliphatic Aldehydes, Acetone, Azomethane, and Diazoethane. *J. Chem. Phys.* **1950**, *18*, 203-206.
10. Brinton, R.; Volman, D., The Ultraviolet Absorption Spectra of Gaseous Diazomethane and Diazoethane. Evidence for the Existence of Ethylidine Radicals in Diazoethane Photolysis. *J. Chem. Phys.* **1951**, *19*, 1394-1395.
11. Kramer, K.; Wright, A., Ethylidene insertion in phenylsilane. *Tetrahedron Lett.* **1962**, *3*, 1095-1096.
12. Tschuikow-Roux, E.; McNesby, J. R.; Jackson, W. M.; Faris, J. L., Reactions of ethylidene in the vacuum ultraviolet photolysis of ethylene. *J. Phys. Chem.* **1967**, *71*, 1531-1533.
13. Seburg, R. A.; McMahon, R. J., Photochemistry of matrix-isolated diazoethane and methyldiazirine: ethylidene trapping? *J. Am. Chem. Soc.* **1992**, *114*, 7183-7189.
14. Modarelli, D. A.; Platz, M. S., Experimental evidence for ethylidene-d_4. *J. Am. Chem. Soc.* **1993**, *115*, 470-475.
15. O'Gara, J. E.; Dailey, W. P., Matrix-Isolation and ab Initio Molecular Orbital Study of 2,2,2-Trifluoroethylidene. *J. Am. Chem. Soc.* **1994**, *116*, 12016-12021.
16. Brinker, U. H.; Bespokoev, A. A.; Reisenauer, H. P.; Schreiner, P. R., Conformations and Reactions of Bicyclo[3.2.1]oct-6-en-8-ylidene. *J. Org. Chem.* **2012**, *77*, 3800-3807.
17. Sulzbach, H. M.; Platz, M. S.; Schaefer, H. F.; Hadad, C. M., Hydrogen Migration vs Carbon Migration in Dialkylcarbenes. A Study of the Preferred Product in the Carbene Rearrangements of Ethylmethylcarbene, Cyclobutylidene, 2-Norbornylidene, and 2-Bicyclo[2.1.1]hexylidene. *J. Am. Chem. Soc.* **1997**, *119*, 5682-5689.
18. Apeland, I. M.; Rosenberg, M. G.; Arion, V. B.; Kählig, H.; Brinker, U. H., Intermolecular Reactions of a Foiled Carbene with Carbonyl Compounds: The Effects of Trishomocyclopropyl Stabilization. *J. Org. Chem.* **2015**, *80*, 11877-11887.
19. Mieusset, J.-L.; Brinker, U. H., The Nature and Extent of π-Stabilization within Foiled Carbenes. *J. Am. Chem. Soc.* **2006**, *128*, 15843-15850.
20. Mieusset, J.-L.; Brinker, U. H., Foiled Carbenes Revisited: When σ-Stabilization Surpasses π-Stabilization. *J. Org. Chem.* **2007**, *72*, 263-268.
21. Gopinath, J. S.; Parameswaran, P., Pentacycloundecanylidene and pentacycloundecanone – hyperconjugatively stabilized carbene and ketone. *Phys. Chem. Chem. Phys.* **2024**, *26*, 13452-13462.
22. Kozuch, S., The reactivity game: theoretical predictions for heavy atom tunneling in adamantyl and related carbenes. *Phys. Chem. Chem. Phys.* **2014**, *16*, 7718-7727.
23. Moss, R. A.; Sauers, R. R.; Sheridan, R. S.; Tian, J.; Zuev, P. S., Carbon tunneling in the ring expansion of noradamantylchlorocarbene. *J. Am. Chem. Soc.* **2004**, *126*, 10196-10197.
24. Castro, C.; Karney, W. L., Heavy-Atom Tunneling in Organic Reactions. *Angew. Chem. Int. Ed.* **2020**, *59*, 8355-8366.
25. Qiu, G.; Schreiner, P. R., The Intrinsic Barrier Width and Its Role in Chemical Reactivity. *ACS Cent. Sci.* **2023**, *9*, 2129-2137.
26. Carpenter, B. K., Heavy-atom tunneling as the dominant pathway in a solution-phase reaction? Bond shift in antiaromatic annulenes. *J. Am. Chem. Soc.* **1983**, *105*, 1700-1701.
27. Schleif, T.; Tatchen, J.; Rowen, J. F.; Beyer, F.; Sanchez-Garcia, E.; Sander, W., Heavy-Atom Tunneling in Semibullvalenes: How Driving Force, Substituents, and Environment Influence the Tunneling Rates. *Chem. Eur. J.* **2020**, *26*, 10452-10458.
28. Schleif, T.; Mieres-Perez, J.; Henkel, S.; Ertelt, M.; Borden, W. T.; Sander, W., The Cope rearrangement of 1, 5-dimethylsemibullvalene-2 (4)-d_1: Experimental evidence for heavy-atom tunneling. *Angew. Chem. Int. Ed.* **2017**, *56*, 10746-10749.
29. Truhlar, D. G.; Garrett, B. C., Variational Transition State Theory. *Annu. Rev. Phys. Chem* **1984**, *35*, 159-189.

30. Hu, W.-P.; Liu, Y.-P.; Truhlar, D. G., Variational transition-state theory and semiclassical tunnelling calculations with interpolated corrections: a new approach to interfacing electronic structure theory and dynamics for organic reactions. *J. Chem. Soc., Faraday Trans.* **1994**, *90*, 1715-1725.
31. Lee, C.; Yang, W.; Parr, R. G., Development of the Colle-Salvetti correlation-energy formula into a functional of the electron density. *Phys. Rev. B* **1988**, *37*, 785-789.
32. Becke, A. D., Density-functional thermochemistry. III. The role of exact exchange. *J. Chem. Phys.* **1993**, *98*, 5648-5652.
33. Karmakar, S.; Datta, A., Tunneling Control: Competition between 6π-Electrocyclization and [1,5]H-Sigmatropic Shift Reactions in Tetrahydro-1*H*-cyclobuta[*e*]indene Derivatives. *J. Org. Chem.* **2017**, *82*, 1558-1566.
34. Šumanovac, T.; Alešković, M.; Šekutor, M.; Matković, M.; Baron, T.; Mlinarić-Majerski, K.; Bohne, C.; Basarić, N., Photoelimination of nitrogen from adamantane and pentacycloundecane (PCU) diazirines: a spectroscopic study and supramolecular control *Photochem. Photobiol. Sci.* **2019**, *18*, 1806-1822.
35. Moore, C. B.; Pimentel, G. C., Matrix Reaction of Methylene with Nitrogen to Form Diazomethane. *J. Chem. Phys.* **1964**, *41*, 3504-3509.
36. Roque, J. P. L.; Nunes, C. M.; Schreiner, P. R.; Fausto, R., Hydrogen Tunneling Exhibiting Unexpectedly Small Primary Kinetic Isotope Effects. *Chem. Eur. J.* **2024**, *30*, e202401323.
37. Marchand, A. P.; Kumar, K. A.; Mlinarić-Majerski, K.; Veljković, J., Intermolecular vs. Intramolecular carbene reactions of a cage-functionalized cyclopentylcarbene. *Tetrahedron* **1998**, *54*, 15105-15112.
38. Alberts, A. H.; Wynberg, H.; Strating, J., Possible precursors of adamantene. *Tetrahedron Lett.* **1973**, *14*, 543-546.
39. Dubau-Assibat, N.; Baceiredo, A.; Bertrand, G., Synthesis and Reactivity of the First Spectroscopically Observed 1*H*-Diazirine. *J. Am. Chem. Soc.* **1996**, *118*, 5216-5220.
40. Bonneau, R.; Liu, M. T. H., Quantum Yield of Formation of Diazo Compounds from the Photolysis of Diazirines. *J. Am. Chem. Soc.* **1996**, *118*, 7229-7230.
41. Becke, A. D., Density-functional exchange-energy approximation with correct asymptotic behavior. *Phys. Rev. A.* **1988**, *38*, 3098.
42. Becke, A., Density-Functional Thermochemistry. III. The Role of Exact Exchange. J. Chem. Phys., 98: 5648-5652. 1993.
43. Fernandez-Ramos, A.; Ellingson, B. A.; Garrett, B. C.; Truhlar, D. G., Variational Transition State Theory with Multidimensional Tunneling. In *Reviews in Computational Chemistry*, 2007; pp 125-232.
44. Majerski, Z.; Hamersak, Z., Rearrangement of bridgehead alcohols to polycyclic ketones by fragmentation-cyclization: 4-protoadamantanone (tricyclo-[4.3.1.$0^{3,8}$]decan-4-one). *Org. Synth.* **1979**, *59*.
45. Egunlusi, A. O.; Malan, S. F.; Omoruyi, S. I.; Ekpo, O. E.; Palchykov, V. A.; Joubert, J., Open and rearranged norbornane derived polycyclic cage molecules as potential neuroprotective agents through attenuation of MPP+- and calcium overload-induced excitotoxicity in neuroblastoma SH-SY5Y cells. *Eur. J. Med. Chem.* **2020**, *204*, 112617.
46. Gaidai, A. V.; Volochnyuk, D. M.; Shishkin, O. V.; Fokin, A. A.; Levandovskiy, I. A.; Shubina, T. E., *D*3-Trishomocubane-4-carboxylic Acid as a New Chiral Building Block: Synthesis and Absolute Configuration. *Synthesis* **2012**, *44*, 810-816.
47. Guerra-Navarro, N. A.; Palacios-Grijalva, L. N.; Angeles-Beltrán, D.; Negrón-Silva, G. E.; Lomas-Romero, L.; González-Zamora, E.; Gaviño-Ramírez, R.; Navarrete-Bolaños, J., Synthesis of New Pentacyclo[5.4.0.0^{2,6}.0^{3,10}.0^{5,9}]undecane-8,11-dione (PCU) Cyanosilylated Derivatives Using Sulphated Zirconia and Hydrotalcite as Catalysts in Microwave-Assisted Reactions under Solvent Free Conditions. *Molecules* **2011**, *16*, 6561-6576.
48. Eaton, P. E.; Cassar, L.; Hudson, R. A.; Hwang, D. R., Synthesis of homopentaprismane and homohypostrophene and some comments on the mechanism of metal ion catalyzed rearrangements of polycyclic compounds. *J. Org. Chem.* **1976**, *41*, 1445-1448.

Full Citations for Electronic Structure Codes

Gaussian 16

M. J. Frisch, G. W. Trucks, H. B. Schlegel, G. E. Scuseria, M. A. Robb, J. R. Cheeseman, G. Scalmani, V. Barone, G. A. Petersson, H. Nakatsuji, X. Li, M. Caricato, A. V. Marenich, J. Bloino, B. G. Janesko, R. Gomperts, B. Mennucci, H. P. Hratchian, J. V. Ortiz, A. F. Izmaylov, J. L. Sonnenberg, D. Williams-Young, F. Ding, F. Lipparini, F. Egidi, J. Goings, B. Peng, A. Petrone, T. Henderson, D. Ranasinghe, V. G. Zakrzewski, J. Gao, N. Rega, G. Zheng, W. Liang, M. Hada, M. Ehara, K. Toyota, R. Fukuda, J. Hasegawa, M. Ishida, T. Nakajima, Y. Honda, O. Kitao, H. Nakai, T. Vreven, K. Throssell, J. A. Montgomery, Jr., J. E. Peralta, F. Ogliaro, M. J. Bearpark, J. J. Heyd, E. N. Brothers, K. N. Kudin, V. N. Staroverov, T. A. Keith, R. Kobayashi, J. Normand, K. Raghavachari, A. P. Rendell, J. C. Burant, S. S. Iyengar, J. Tomasi, M. Cossi, J. M. Millam, M. Klene, C. Adamo, R. Cammi, J. W. Ochterski, R. L. Martin, K. Morokuma, O. Farkas, J. B. Foresman, D. J. Fox, Gaussian 16 Revision C.01, **2016**, Gaussian Inc., Wallingford.

Polyrate

J. Zheng, J. L. Bao, R. Meana-Pañeda, S. Zhang, B. J. Lynch, J. C. Corchado, Y.-Y. Chuang, P. L. Fast, W.-P. Hu, Y.-P. Liu, G. C. Lynch, K. A. Nguyen, C. F. Jackels, A. Fernandez Ramos, B. A. Ellingson, V. S. Melissas, J. Villà, I. Rossi, E. L. Coitiño, J. Pu, T. V. Albu, A. Ratkiewicz, R. Steckler, B. C. Garrett, A. D. Isaacson, D. G. Truhlar, Polyrate Version 2017-C, **2017**, University of Minnesota, Minneapolis.

4. Acknowledgement

This work would not have been possible without the support of many individuals. I would like to express my heartfelt gratitude to:

- **Prof. Dr. Peter R. Schreiner** for his mentorship and guidance since my bachelor's studies, for granting me the freedom to explore research independently, and for the invaluable knowledge I have gained from him.

- **Dr. Artur Mardyukov** for teaching me the matrix isolation technique, guiding me through my first two projects, and for the enjoyable conversations and memorable poker nights.

- **Dr. Dennis Gerbig** for their invaluable support in my third project, for teaching me so much, and for patiently answering all my questions. I am also deeply grateful for his thorough proofreading of my dissertation.

- **Dr. Raffael Wende** for his support in the lab and for guiding me through challenging questions.

- **Dr. Nikolaos Vagkidis** for proofreading my dissertation and for the great times filled with amazing discussions and many wonderful memories.

- **Oliver Pereira, Marvin Domanski** and **Charlotte E. Lauter** for the pleasant working atmosphere, enjoyable conversations, and their help in the lab.

- **The PRS Group** for three harmonious and enjoyable years.

- **Matay** and **Rania Danho** for sacrificing so much to provide for me and my siblings. Only through their immense effort was it possible for me to study and achieve my doctoral degree.

- **Amanuel** and **Dalia Danho** for being the best siblings one could imagine—for their love, help, and encouragement. I am proud to be their oldest brother.

- **Rony** and **Helanie Malki** for their continuous support, love as well as their encouragement and motivation. They are more than friends; they are my family